Antibiotic uptake in *Pseudomonas aeruginosa* and its consequences on the metabolome

Von der Naturwissenschaftlichen Fakultät der

Gottfried Wilhelm Leibniz Universität Hannover

zur Erlangung des Grades

Doktorin der Naturwissenschaften (Dr. rer. nat.)

genehmigte Dissertation

von

Mariel Anel García Rivera, ing. chim. dipl. EPF (Schweiz)

2021

Referent: Prof. Dr. Mark Brönstrup

Korreferent: Prof. Dr. Andreas Pich

Tag der Promotion: 15.12.2020

ABSTRACT

The permeability barrier of the outer membrane in Gram-negative bacteria possess an inherent defense towards antibiotics and is subject of study using multidisciplinary approaches and cutting-edge techniques. In this study, a medium-high throughput assay based on liquid chromatography coupled to tandem mass spectrometry (LC-MS/MS) was optimized and applied for comparing the degree of uptake of antibiotics with different modes of action into *E. coli* and *P. aeruginosa*. This method allowed the elucidation of time-course profiles of rapidly accumulated compounds and helped to differentiate accumulation profiles of nine antibiotics between the two Gram-negative species. The strain transferability of this assay allows the systematic assessment of the uptake of a broad range of compounds in different microorganisms.

Apart from an increased impermeability, pathogenic bacteria quickly adapt metabolically to cope with a wide variety of environmental stresses, including antibiotic stress. Exposure to sub-lethal but constant concentrations of antibiotics in the environment plays an important role in enabling bacteria to make use of tolerance and resistance traits. In this study, the metabolic profile of wild type *P. aeruginosa* treated with different classes of antibiotics at sub-lethal concentrations showed important differences under a short exposure of two hours, and a long exposure of more than seven hours. *P. aeruginosa* maintained high levels of virulence-related metabolites, such as rhamnolipids, as a quick response to sudden antibiotic stress, indicating the readiness of bacteria to adapt quickly to environmental challenges.

Fluoroquinolones, among the most potent antibiotics to date, are known to propitiate diverse bacterial responses, such as growth inhibition, biofilm production, and increased oxidative-stress response. However, these effects are associated to their potent activity and thought to be due to target interactions. In this study, two *P. aeruginosa* strains, one fluoroquinolone-susceptible with MIC of 0.15 µg/mL and one fluoroquinolone-resistant with MIC of 29.83 µg/mL, were subjected to an LC-MS/MS-based untargeted metabolomics analysis and provided with evidence of indirect responses to increasing concentrations of ciprofloxacin. In spite of the lack of an active target, the resistant mutant showed important off-target effects in response to ciprofloxacin accumulation. Those secondary-target effects were related to the virulence regulation of *P. aeruginosa*, such as the quorum sensing response, and to alterations in lipid metabolism and peptidoglycan assembly, and were correlated with ciprofloxacin accumulation.

Key words: metabolomics, antibiotic uptake, sub-inhibitory concentrations, off-target effects, secondary-target effects, quorum sensing

ZUSAMMENFASSUNG

Die äußeren Membran von Gram-negativen Bakterien stellt eine inhärente Permeabilitätsbarriere gegen Antibiotika dar und ist daher Gegenstand von Untersuchungen mit multidisziplinären Ansätzen und modernsten Techniken. In dieser Studie wurde ein auf Flüssigkeitschromatographie-gekoppelter Tandem-Massenspektrometrie (LC-MS/MS) basierender Assay mit mittlerem Durchsatz optimiert und eingesetzt, um die Aufnahme von Antibiotika mit unterschiedlichen Wirkmechanismen in *E. coli* und *P. aeruginosa* zu untersuchen. Die Methode ermöglichte, den Zeitverlauf der Aufnahme zu verfolgen und die Akkumulationsprofile von neun Antibiotika zwischen beiden Gram-negativen Spezies zu vergleichen. Der Assay erlaubt damit die systematische Bewertung der Aufnahme eines breiten Spektrums von Verbindungen in verschiedenen Mikroorganismen.

Pathogene Bakterien passen ihren Metabolismus schnell an, um auf eine Vielzahl von Umweltbedingungen wie Antibiotikastress zu reagieren. Die Exposition von Bakterien mit subletalen, konstanten Konzentrationen von Antibiotika spielt eine wichtige Rolle bei der Ausbildung von Toleranz- und Resistenzeigenschaften. In dieser Studie zeigte das metabolische Profil eines Wildtypstamms von *P. aeruginosa*, der mit verschiedenen Klassen von Antibiotika in subletalen Konzentrationen behandelt wurde, wichtige Unterschiede zwischen einer kurzen Exposition von zwei Stunden und einer langen Exposition von mehr als sieben Stunden. Als schnelle Reaktion auf plötzlichen Antibiotika-Stress wurden hohe Konzentrationen virulenzbezogener Metabolite, wie z. B. Rhamnolipide, detektiert. Dies belegt die Fähigkeit der Bakterien, schnell auf sich verändernde äußere Umgebungen zu reagieren.

Fluorchinolone, die eine hochwirksame Antibiotikaklasse darstellen, sind dafür bekannt, daß sie verschiedene bakterielle Reaktionen induzieren, wie z.B. verringertes Wachstum, Biofilmproduktion und eine erhöhte oxidative Stressreaktion. Es wird angenommen, dass diese Effekte eine Folge spezifischer Target-Interaktionen sind. In dieser Studie wurden zwei *P. aeruginosa*-Stämme, ein Fluorchinolon-sensitiver mit einer minimalen Hemmkonzentration (MHK) von 0,15 µg/mL und eine Fluorchinolon-resistenten Mutante mit einer MHK von 29,83 µg/mL, einer LC-MS/MS-basierten, ungerichteten Metabolomics-Analyse unterzogen. Trotz der fehlenden Target-Interaktion zeigte die resistente Mutante wichtige Off-Target-Effekte als Reaktion auf die Ciprofloxacin-Akkumulation. Diese Sekundär-Effekte standen im Zusammenhang mit der Virulenzregulation von *P. aeruginosa*, wie z. B. der Quorum-Sensing-Antwort. Weiterhin waren Veränderungen im Lipidstoffwechsel und der Peptidoglykan-Assemblierung mit der Ciprofloxacin-Akkumulation korreliert.

Schlagworte: Metabolomik, Antibiotika-Aufnahme, sub-inhibitorische Konzentrationen, Off-Target-Effekte, Sekundär-Target-Effekte, Quorum Sensing

TABLE OF CONTENTS

LIST OF FIGURES

LIST OF TABLES

ABBREVIATIONS

AA	Amino acid
ADP	adenosine diphosphate
AM	Aminoglycosides
AMP	Adenosine monophosphate
AQ	Alkyl quinolone
AZI	Azitromycin
BLA	β-lactam
BM2	Basal medium 2
BPC	Base peak chromatogram
CE	Capillary electrophoresis
CIPRO	Ciprofloxacin
CLARI	Clarithromycin
CON	Control (untreated)
CV	Coefficient of variation
Cx:y	Acyl chain of x carbons with y double bonds
DANN	Dexoxyribonucleic acid
DHQ	2.4-dihydroxyquinoline
EIC	Extracted ion chromatogram
EID	Emerging infectious diseases
ERY	Erythromycin
ESI	Electrospray ionization
FA	Fatty acid
FAD	Flavin adenine dinucleotide
FC	Fold change
FMN	Flavin mononucleotide
FQ	Fluoroquinolone
GC	Gas chromatography
GENTA	Gentamycin
GlcNac	N-acetylglucosamine
Glu	Glutamate
GMP	Guanosine monophosphate
GNPS	Global Natural Product Social Molecular Networking
-HQ	Congener of 2-alkyl-4-quinolones
HSL	Homoserine lactone
IC10	Inhibitory concentration at 10% reduction in growth
IC50	Inhibitory concentration at 50% reduction in growth
IM	Inner membrane
IR	Infrared spectroscopy
ISTD	Internal standard
LC	Liquid chromatography
LE	Long exposure
LEVO	Levofloxacin
Lip	Lipid
log2-FC	Fold change of log2-transformed data
logn	Logarithm base n
LOME	Lomefloxacin
LPE	Lyso-phophatidylethanolamine
LPG	Lyso-phosphatidylglycol
LPS	Lipopolisaccharide
LSU	Large subunit
MA	Macrolide
MDR	Multi-drug resistant
MERO	Meropenem
MIC	Minimum inhibitory concentration
MOA	Mode of action

MRM	Multiple-reaction monitoring
m-RNA	Messenger ribonucleic acid
MS	Mass spectrometry
MTA	Methylthio adenosine
MurNac	N-acetylmuramic acid
m/z	Mass-to-charge ratio of the molecular ion
NAD	Nicotinamide adenine nucleotide
NADP+	Adenine dinucleotide phosphate
NIC	Non-inhibitory concentration
NMR	Nuclear magnetic resonance spectrometry
Nuc	Nucleotide
OD_{600}	Optical density at l = 600 nm
OM	Outer membrane
PBP	Penicillin binding proteins
PC	Principal component
PCA	Principal component Analysis
PE	Phophytidylethanolamine
PEG	Polyethylene glycol
PG	Phosphatidylglycol
Phen	Phenazine
Phenyl	Phenylalanine
PhosLip	Phospholipid
PLS	Partial-least squares
PQS	Pseudomonas quorum sensing
-PQS	Congener of 2-alkyl-3-hydroxy-4-quinolones
PTC	Peptidyl transferase center
Q	Single quadrupole
Q1, Q2, Q3	First, second and third quadrupole, respectively
-QNO	Congener of 2-alkyl-hydroxyquinoline-N-oxides
QQQ	Triple quadrupole
Rha	Rhamnolipid
RNA	Ribonucleic acid
ROS	Reactive oxigen species
r-RNA	Ribosomal ribonucleic acid
RT	Retention time
SE	Short exposure
SNP	Single nucleotide polymorphism
SRM	Selected-reaction monitoring
SSU	Short subunit
sub-MIC	Concentrations under the minimum inhibitory concentration
TCA	Tricarboxylic acid
TIC	Total ion chromatogram
TOBRA	Tobramycin
ToF	Time of flight
tRNA	Transfer ribonucleic acid
UDP	Uridine diphosphate
UPLC	Ultra-Performance Liquid Chromatography
WT	Wild type

1. INTRODUCTION

1.1 Emerging infectious diseases

Infectious diseases are a major cause of death globally, and a leading cause of death in low-income countries (Tacconelli et al. 2018; World Health Organization 2001). Among the most deadly infectious diseases worldwide are lower respiratory infections, diarrheal diseases, tuberculosis and AIDS. Additionally, emerging infectious diseases (EID) have been increasing with alarming speed, and our ability to find effective therapeutics has been surpassed (Ogden, AbdelMalik, and Pulliam 2017). The difficulty of combating infections lies mostly in the emergence of new infectious agents, the re-emergence of known infectious agents previously under control, the gain in the geographical distribution of known infectious diseases, and the increasing resistance of pathogens to the available antimicrobial drugs (World Health Organization 2001).

Antimicrobial resistance has been unprecedentedly addressed worldwide by national governments and international organizations. In order to support the implementation of the Global Action Plan on Antimicrobial Resistance, in 2016, the World Health Organization (WHO) declared a priority pathogens list of antibiotic-resistant bacteria (see Table 1.1). The WHO prioritization list suggests that drug research and development should focus on new antibiotics specifically active against tuberculosis and multi-drug resistant (MDR) Gram-negative bacteria responsible with high morbidity in both high-income and low- and middle-income countries (Tacconelli et al. 2018).

Table 1.1 Wolrd Health Organization Priority Pathogens List

Level	Pathogens
Priority 1: Critical	*Acinetobacter baumannii*, carbapenem-resistant
	Pseudonomas aeruginosa, carbapenem-resistant
	Enterobacteriaceae, carbapenem-resistant, 3G-cephalosporin resistant
Priority 2: High	*Enterococcus faedium*, vancomycin-resistant
	Helicobacter pylori, clarithromycin-resistant
	Salmonella spp., fluoroquinolone-resistant
	Staphylococcus aureus, vancomycin-resistant, methicillin-resistant
	Campylobacter spp., fluoroquinolone-resistant
	Neisseria gonorrhoeae, 3G-cephalosporin resistant, fluoroquinolone-resistant
Priority 3: Medium	*Streptococcus pneumonia*, penicillin-non-susceptible
	Haemophilus influenza, ampicillin-resistant
	Shigella spp., fluoroquinolone-resistant

3G: 3rd generation

1.2 Antibiotics: mode of action and resistance mechanisms

Among antimicrobial drugs, some compounds target bacteria, viruses, fungi or parasites, and they are designated as antibiotics, antivirals, antifungals and antiparasitic drugs, respectively. Most of antibiotics are low-molecular-weight compounds (<1000 Da) with selective activity against bacteria. Antibiotics are classified into two big groups according to their lethality: they are called bacteriostatic when the growth and proliferation of bacteria are inhibited without killing, and they are called bactericidal when the compound leads to a killing effect. The way that antibiotics act against bacteria lies in their mechanism of action, also known as their mode of action (MOA).

1.2.1 Mode of action of major classes of antibiotics

1.2.1.1 Disruption of membrane integrity

The construction of the cell envelopes of Gram-positive and Gram-negative bacteria are very distinctive. While Gram-positive bacteria possess a bacterial membrane and a complex peptidoglycan layer, Gram-negative bacteria possess an inner membrane (IM), a peptidoglycan layer, and an outer membrane (OM) (see Figure 1.1). Agents that can disrupt the integrity of bacterial membranes are considered bactericidal, and there is a subgroup of molecules with sufficient selectivity to bacterial membranes over eukaryotic, human cell membranes to be considered for therapeutic use.
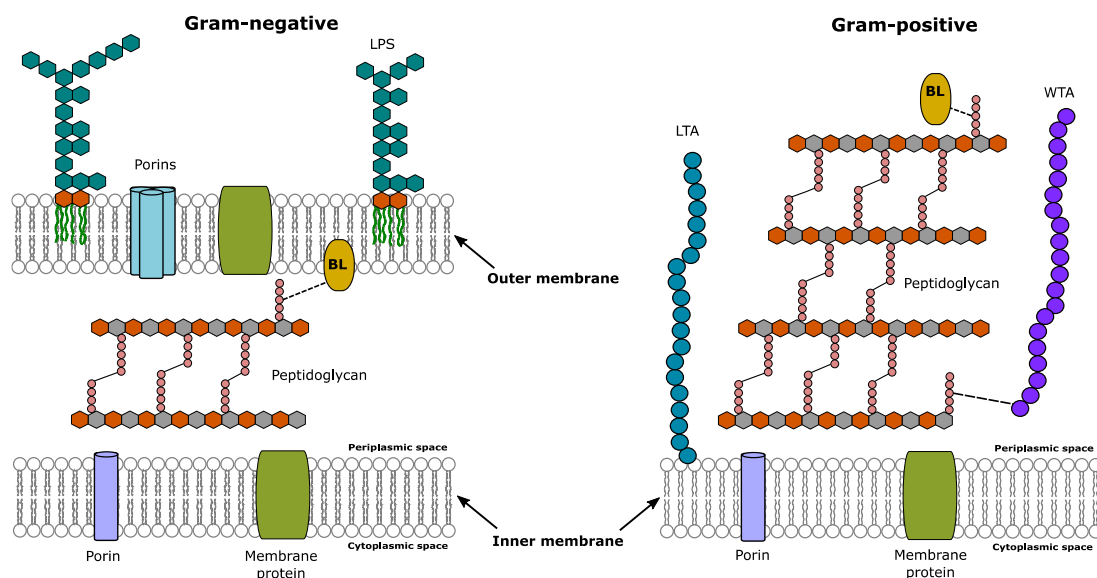
Figure 1.1 Cell envelopes of Gram-negative and Gram-positive bacteria. BL: Braun's lipoprotein, LTA: lipoteichoic acid, LPS: lipopolysaccharide, WTA: wall teichoic acid. From (Walsh and Wencewicz 2016)

Polymyxins, such as colistin and polymyxin B, are last resort antibiotics against Gram-negative bacteria (Kaye et al. 2016). They present electrostatic interaction with lipopolysaccharides (LPS) to disrupt the OM integrity, then passing through the IM to disrupt it as well (Poirel, Jayol, and Nordmann 2017).

For instance, human defensines, produced in different tissues such as skin, small intestine, reproductive tract, kidney, among others, are disulfide-rich small proteins that kill bacteria by their insertion and accumulation in bacterial membranes. Daptomycin is believed to form micelles and insert into bacterial membrane, leading to the formation of pores and depolarization of the membrane (Hojati et al. 2002). Similarly, surfactin can form aggregates in bacterial membranes to make pores that induce potassium ion (K+) efflux (Carrillo et al. 2003). Recently, it was found that daptomycin binds to bactoprenyl-bound precursors in the presence of phosphatidylglycerol (PG) to form a tri-partite complex, interfering with lipid II biosynthesis (Grein et al. 2020).

Other antibiotics are known to have dual mechanisms. For instance, some lantibiotic peptides, such as Nisin, have a high affinity to lipid II (see 1.2.1.2 Blockade of peptidoglycan assemble) and aggregate in the IM in pore-like structures causing membrane perturbation. Similarly, some lipoglycopeptide antibiotics, such as teicoplanin, inhibit the synthesis of cell wall peptidoglycan by interacting with the D-ala-D-ala terminal of the UDP-MurNac-pentapeptide, as their major MoA (Parenti 1986), and also aggregate to disrupt the IM integrity (Kang and Park 2015).

1.2.1.2 Blockade of peptidoglycan assemble

The peptidoglycan layer is a polymeric mesh of repeating units of N-acetylglucosamine (GlcNAc) and N-acetylmuramic acid (MurNAc) croslinked by peptide "bridges." This layer is believed to account for structural rigidity and, at the same time, allow certain fluidity necessary for the bacterial shape in various stages of growth and cell division (Nelson and Cox 2017). Many steps in the formation of the peptidoglycan layer at the different phases of its assembly are targets of inhibition by antimicrobials (see Figure 1.2).

The first phase of assembly occurs in the cytoplasm. Uridine diphosphate- (UDP) GlcNAc, which in turn is formed from fructose-6-P, is converted to UDP-MurNAc through the action of MurA and MurB. UDP-MurNAc is rhen converted to UDP-tripeptide through the action of the ligases MurC-E. Then, MurF adds the dipeptide D-Ala-D-Ala, which is in turn generated by D-Ala-D-Ala ligase, to form UDP-MurNac-pentapeptide. The second phase of the peptidoglycan assemble occurs at the inner face of the cytoplasmic membrane. Lipid I is formed by MraY

from UDP-MurNac-pentapeptide and the membrane-embedded bactoprenol-P. Subsequently, lipid II is formed with the addition of a GlcNAc moiety to lipid I, by MurG. The last step in this phase is the translocation of lipid II from the inner leaflet to the outer leaflet of the cytoplasmic membrane by the action of transmembrane flippases (Nelson and Cox 2017). The final phase occurs at the outer face of the cytoplasmic space, where transmembrane penicillin binding proteins (PBPs) with high molecular weight are located. These PBPs possess both a transglycosylase (TGase) and a transpeptidase (TPase) domain. The translocated lipid II meets with the catalytic TGase domain of PBPs, and its disaccharyl pentapeptide is transferred to the growing chain of peptidoglycan. The released bactoprenol-PP is recycled back to bactoprenol-P and flipped back to the inner face of the cytoplasmic membrane.

The TPase domain of the PBP is responsible for the cross-linking between glycan strands. In Gram-negative bacteria, TPases make a direct 3-4'-peptide cross bridge, resulting in the expulsion of a D-Ala as free amino acid (see Figure 1.2). In Gram-positive bacteria, TPases typically act on a pentaglycine-extended Lys residue, which comes from a modified lipid II (Lipid II 5xGly), generating longer and more flexible cross bridges in the peptidoglycan meshwork (Walsh and Wencewicz 2016).

A great variety of antibiotics target the formation of the peptidoglycan layer from the early steps until the cross-linking of the glycan strands (see Table 1.2). For example, the molecular basis of action of β-lactams is the long lifetime of acyl-enzyme intermediates (or penicilloyl enzymes) that they form with PBPs, particularly with the TPase domain. In a normal cycle, the life times of the natural acyl-enzyme intermediates are in the range of milliseconds, while the penicilloyl enzymes are stable for several hours (Walsh and Wencewicz 2016). The enzymes can no longer keep up with the demand for cross-linking new peptidoglycan strands. On the basis of the same molecular mechanism, some compounds target other types of PBPs responsible for β-lactam resistance: β-lactamases (see 1.2.2 Main resistance mechanisms). In therapeutics, β-lactamases inhibitors are used in combination with other β-lactams. Additionally, the TGase domain of PBPs is inhibited by the moenomycin family.
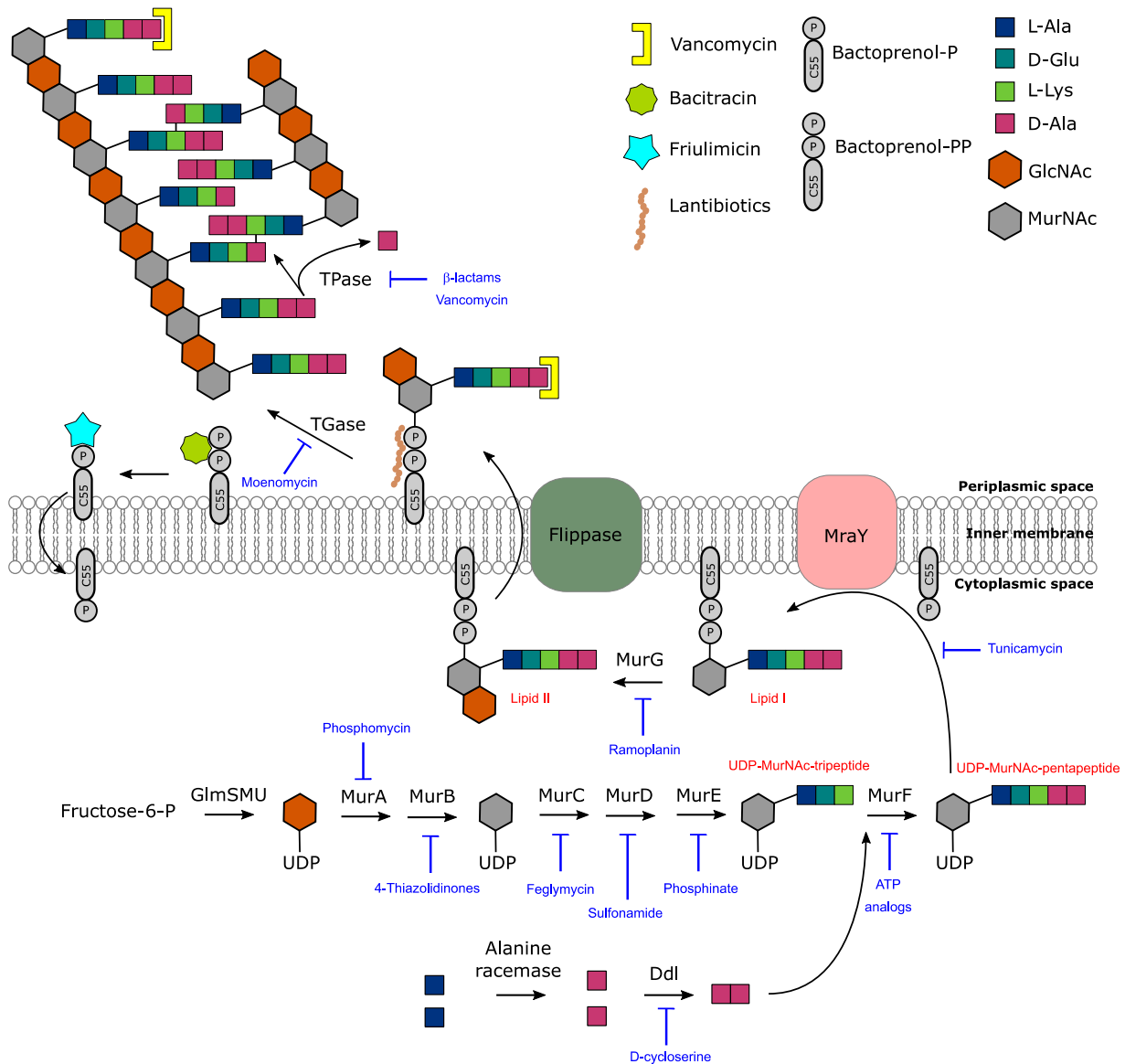
Figure 1.2 Peptidoglycan assembly in Gram-negative bacteria. Antibiotics targeting the peptidoglycan assembly and their molecular target are shown (blue). D-Ala: D-alanine, Ddl: D-alanine-D-alanine ligase, D-Glu: D-glutamic acid, GlcNAc: N-acetylglucosamine, L-Ala: L-alanine, L-Lys: L-lysine, MurA-G: enzymes involved in the biosynthesis steps of peptidoglycan within the cytoplasmic space, MurNAc: N-acetylmuramic acid, TGase: glycosyltransferase, TPase: transpeptidase. Adapted from Lovering et al. 2012 and Waksh & Wencewicz 2016 (Lovering, Safadi, and Strynadka 2012; Walsh and Wencewicz 2016)

Other compounds affect the biosynthesis of lipid II by inhibiting different steps in the formation of UPD-MurNAc-pentapeptide, such as phosphomycin, or by inhibiting MraY, such as tunicamycin. In addition to compounds that have enzymes as molecular targets, there are antibiotics that bind to the substrates of other enzymes. Such is the case of vancomycins and lantibiotics, which bind to lipid II and avoid the subsequent steps of peptidoglycan chain elongation. Other examples are friulimicin, which binds to bactoprenol-P, and bacitracin, which binds to bactoprenol-PP, affecting the bactoprenol recycling.

Table 1.2 Antibiotics targeting the peptidoglycan assembly

Mechanism	Example compounds
Acyl-enzyme intermediates with transpeptidades	Penicillins: ampicillin, carbenicillin, penicillin G, methicillin, piperacillin Cephalosporins: ceftazidime, cefazolin, ceftriaxone, ceftobiprole, ceftarolin Carbapenems: imipenem, meropenem, doripenem, faropenem, ertapenem Monobactams: aztreonam, BAL30072 β-lactamases inhibitors: clavulanate, sulbactam, tazobactam
Inhibition of UDP-MurNAc-tripeptide and UDP-MurNAc-pentapeptide formation	Phosphomycin, 4-Thiazolides, feglymycin, sulfonamide, phosphinate, ATP analogs, D-cycloserine
Inhibition of MraY	Peptidyl nucleoside antibiotics: tunicamycin, mureidomycin, napsamycin, pacidamycin
Inhibition of transglycosylases/ transpeptidases	Moenomycin, vancomycin
Sequestering of lipid II	Glycopeptides: vancomycin telavancin, teicoplanin, dalbavancin, oritavancin Lantibiotics: bacteriocin, nisin, lacticin 3147 Ramoplanin, lysobactin. mannopeptidomycin
Sequestering of bactoprenol-P and bactoprenol-PP	Friulimicin, amphomycin, tsuschimycin, Bacitracin

1.2.1.3 Blockade of protein synthesis

There is also a great variety of compounds that target the ribosomal bacterial protein synthesis. Those compounds affect different steps in any of the phases of the protein chain synthesis (see Figure 1.3).

First, in the initiation phase, the 30S and the 50S ribosomal subunits form a 70S complex together with m-RNA and the first of the aminoacyl-tRNA (aa-tRNA) in the peptidyl (P) site of the ribosome. Then, a second aa-tRNA is accommodated in the aminoacyl (A) site, with the assistance of the elongation factor Tu (EF-Tu). Chain elongation occurs with the amino acid of the first aa-tRNA is transferred to the second aa-tRNA, followed by a translocation of the resulting deacylated tRNA to the exit (E) site with the action of the elongation factor G (EF-G). Simultaneously, the translocation of the peptidyl-tRNA to the P site. In the elongation phase, the cycle from accommodation until translocation repeats itself until the mRNA has been translated, and the peptidyl chain is completed and liberated from the ribosome. The 30S and 50S subunits are uncoupled liberating the mRNA and starting the cycle again (see Figure 1.3).
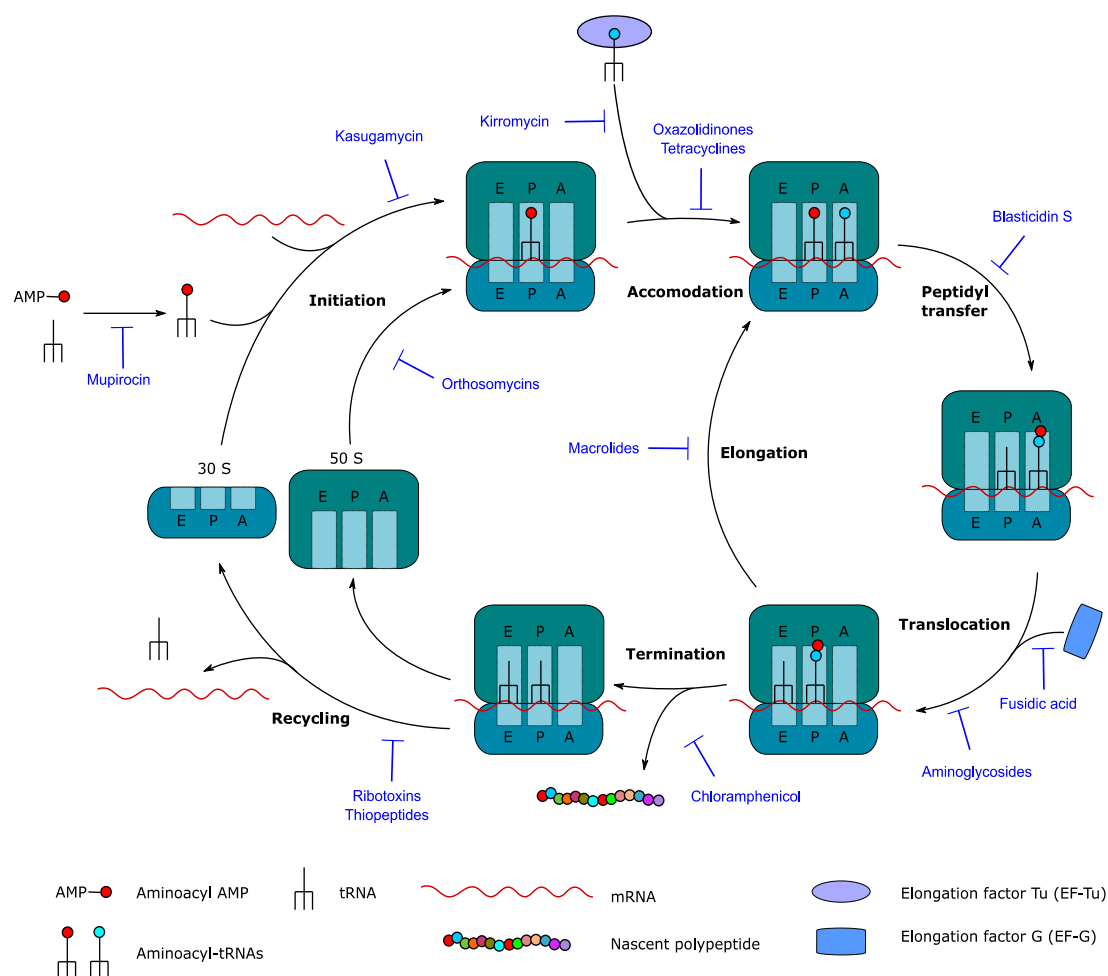
Figure 1.3 Bacterial protein synthesis. A: aminoacyl site, E: exit site, P: peptidyl site. Adapted from Wilson 2012, Arenz & Wilson 2016 and Walsh & Wencewicz 2016 (Arenz and Wilson 2016; Wilson 2013; Walsh and Wencewicz 2016)

Table 1.3 Antibiotics targeting the bacterial protein synthesis and their binding units

Target	Subunit	Example compounds
Ribosome	30S	Tetracyclines: tetracycline. minocycline, doxycycline, tigecycline
Ribosome	30S	Aminoglycosides: gentamycin, amikacin, tobramycin, kanamycin, streptomycin
Ribosome	30S	Kasugamycin, pactamycin, edeine A1
Ribosome	30S	Capreomycins: capreomycin IIA, viomycin
Ribosome / PTC	50S	Oxazolidinones: linezolid, puromycin
Ribosome / PTC	50S	Macrolides: erythromycin, chalithromycin, telithromycin, tylosin, carbomycin
Ribosome / PTC	50S	Lincomycin, clindamycin, tiamulin, chloramphenicol
Ribosome / PTC	50S	Streptogramins A&B: dalfopristin and quinupristin (exit tunnel)
Ribosome	50S	Orthosomycins: everninomicin, avilamycin
Aminoacyl-tRNA synthetase	N.A.	Mupirocin, indolmycin, ochratoxin A, borrelidin, granaticin A, Cis-pentacin
EF-Tu	N.A.	Kirromycin, pulvomycin, GE2270A
EF-G	N.A.	Fusidic acid

N.A. Not applicable

1.2.1.4 Disruption of DNA and RNA information transfer

Unlike the large number and variety of antibiotics that target the bacterial ribosome, there are few compounds that selectively block the bacterial DNA and RNA information transfer. Bacteria have two sets of topo II enzymes, DNA gyrase, with subunits GyrA and GyrB, and topoisomerase IV, with subunits ParC and ParE. Gyrase regulates the supercoiling of double-stranded DNA (dsDNA) that occurs during DNA replication. When gyrase binds to the DNA, the two subunits each break one of the strands of dsDNA forming a covalently bound enzyme-substrate complex. After gyrase pulls the DNA through the cut site enabling topological relaxation, it reseals the two DNA strands before release.

Topoisomerase IV acts similar to DNA gyrase, although its major role seems to be the separation of two daughter chromosomal circles chain-like linked. Topoisomerase IV breaks one of the chromosomes and positions the cut side outside the second chromosome, then reseals the cut resulting in two separated chromosomes (Higgins 2007).

Fluoroquinolones, such as ciprofloxacin, target the GyrA subunit of DNA gyrase, forming tripartite complexes by stabilizing the covalently bound enzyme-substrate complex (see Figure 1.4). The inability to reseal the DNA strands leads eventually to cell death (Aldred, Kerns, and Osheroff 2014). Ciprofloxacin is the most active fluoroquinolone against *P. aeruginosa* (Campoli-Richards et al. 1988; T., BH., and PM. 2020)
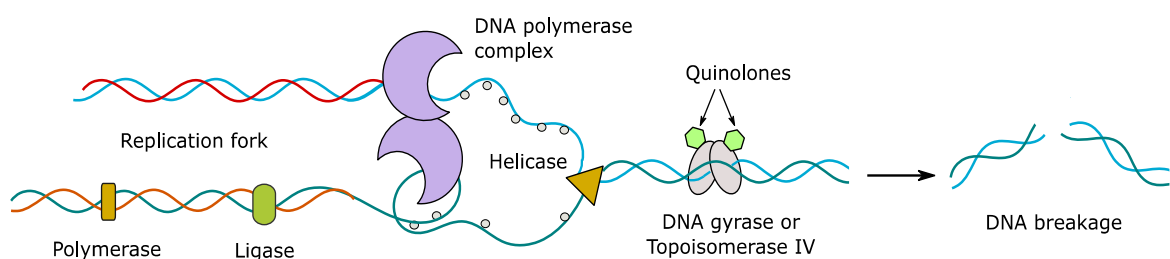
Figure 1.4 Quinolone activity blocking the DNA information transfer. DNA helicase binds to the lagging-strand template at each replication fork and moves the replication fork breaking hydrogen bonds. DNA gyrase and topoisomerase IV relieves strain ahead of the replication fork. When DNA gyrase or topoisomerase IV are inhibited, the extra tension from supercoiling of DNA is not relieved, and the buildup of mechanical strength cause the DNA to break. Adapted from (Kohanski, Dwyer, and Collins 2010; Walsh and Wencewicz 2016)

On the other hand, some compounds, such as novobiocin, target GyrB subunit of gyrase (see Table 1.4) (East et al. 2009). Other antibiotics affect the activity of the bacterial RNA polymerase (RNAP). In general, these compounds bind to the RNAP interrupting the transcription of DNA into mRNA (see Table 1.4).

Table 1.4 Antibiotics targeting bacterial topoisomerases and RNA polymerase

Target	Subunit	Example compounds
DNA gyrase Topoisomerase IV	GyrA ParC	Fluoroquinolones: nalidixic acid, norfloxacin, ciprofloxacin, levofloxacin, lomefloxacin
DNA gyrase	GyrB	Clorobiocin, novobiocin, quinaoline, coumarins
RNA polymerase	N.A.	Rifamycin, rifampicin (rifampin), rifapentine, rifabutin Sorangicin Lipiarmycin (fidaxomycin) Myxopyronin B, crallopyronin A, ripostatin A

N.A. Not applicable

1.2.1.5 Blockade of the folate biosynthesis

As the folate coenzyme is biosynthesized in bacteria but not in humans, any reaction in the folate biosynthesis could be considered an antibiotic target (Pitt 2009). Compounds such as sulfonamide antibiotics, sulfamethoxazole, trimethoprim and abyssomicin C, block the folate pathway, resulting in a shutting off of bacterial DNA synthesis (Kompis, Islam, and Then 2005). Such antibiotics have a slow antimicrobial activity and are considered bacteriostatic.

1.2.2 Main resistance mechanisms

1.2.2.1 Reduction in antibiotic uptake

Gram-negative bacteria are inherently more resistant to many classes of antibiotics than Gram-positive bacteria due to the additional permeability barrier conferred by their OM. Some even more resistant strains have the ability to regulate the entry and accumulation of antibiotics by altering their entry porins or activating their efflux pump machinery (see Figure 1.5). These organisms can alter the OM permeability either by controlling the size and number of their protein porins. For instance, uropathogenic *E. coli* expresses mutated versions of OmpC, reducing the permeability of β-lactams and fluoroquinolones (Lou et al. 2011). Similarly, *Pseudomonas* strains can limit the influx of carbapenems by producing fewer OprD porins, narrower pores or OM without any embedded porins (Fernández and Hancock 2012).
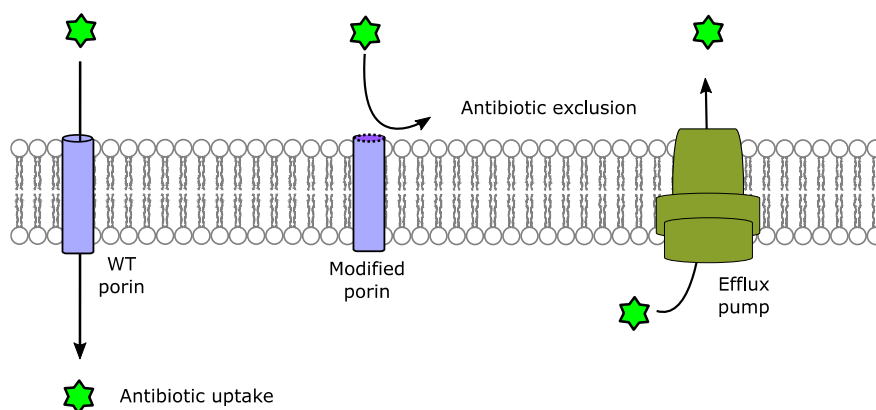
Figure 1.5 Resistance by alteration of porin proteins and activation of efflux pumps

In addition, Gram-negative possess three-protein pump machinery that spans all three components of their cell envelope, or tripartite transenvelope pumps, since they have to pump antibiotics out across two membranes (Opperman and Nguyen 2015; Tegos et al. 2011). Typically, Gram-negative bacteria express multi-drug resistance efflux pumps belonging to the resistance-nodulation-division (RND) family, the major facilitator superfamily (MFS) and the ATP-binding cassette (ABC) superfamily (Sun, Deng, and Yan 2014). These pumps use coupled proton motive force as the source of energy required for pumping out antibiotics against a concentration gradient. Unlike the RNS family, that exports a wide variety of compounds, the ABS superfamily exports macrolides out of the cells, while the MFS exports nalidixic acid and novobiocin (Piddock 2006).

Particularly, *Pseudomonas aeruginosa* (*P. aeruginosa*) has high levels of constitutive and inducible expression of RNS tripartite transenvelope pumps. Most commonly found in *P. aeruginosa* are the constitutively expressed MexAB-OprM and MexXYOprM, and the inducible MexCD-OprJ, MexEF-OprN, and MexJK-OprM (Masuda et al. 2000). These efflux systems have the ability to export a great variety of antibiotics (see Table 1.5) (Fernández and Hancock 2012).

Table 1.5 Multi-drug efflux systems in *P. aeruginosa*

Efflux system	Example compounds
MexAB-OprM	Aminoglycosides, β-lactams, chloramphenicol, macrolides, novobiocin, tetracyclines, trimethoprim
MexCD-OprJ	Chloramphenicol, cationic peptides, fluoroquinolones, tetracyclines
MexEF-OprN	Chloramphenicol, fluoroquinolones
MexJK-OprM	Aminoglycosides, fluoroquinolones, macrolides, tetracyclines
MexXYOprM	Aminoglycosides, fluoroquinolones, macrolides, tetracyclines

1.2.2.2 Modification of the compound

Some resistant bacteria have developed the ability of chemically modifying certain antibiotics, causing them to lose their antimicrobial activity. A classic example of enzymatic modification of antibiotics is the neutralization of β-lactams (Abraham and Chain 1940).

β-lactamases are enzymes with an active site for β-lactams, like PBPs, but with a faster deacylation kinetics. Lactamases decompose the penicilloyl-enzyme intermediate by rapid hydrolytic deacylation, releasing a deactivated, ring-opened penicilloyl and the regeneration of the lactamase active site. There are four classes of β-lactamases, from A to D, and thousands of variants known. Another example of compound modification by ring-opening is the inactivation of the polyketide quinuspristin and related streptogramins, where the macrocyclic ring is acetylated (Rende-Fournier et al. 1993).

Aminoglycosides also suffer deactivation by enzymatic activity. Aminoglycosides can undergo O-adenylation, O-phosphorylation or N-acetylation, or a combination of them (Llano-Sotelo et al. 2002).

1.2.2.3 Modification of the target

Point mutations in genes encoding antibiotic targets, often only by a single base, lead to a change in one amino acid in the encoded protein without affecting essentially its cellular function. Thus, the compound-target interaction is prevented and the uninhibited mutant target mantains its cellular function (see Figure 1.6).
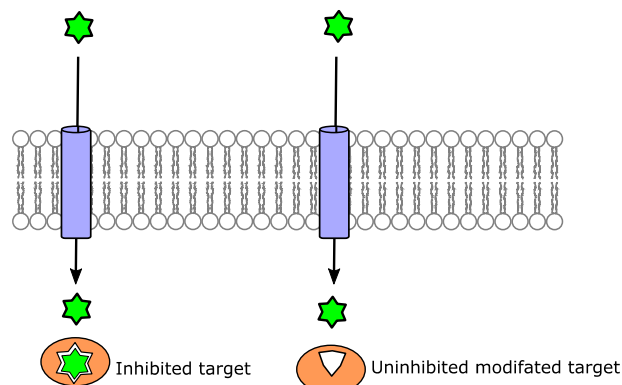
Figure 1.6 Resistance by modification of the molecular target

One type of target modification is given by alterations in protein- and rRNA- encoding genes. Examples of alterations in protein-encoding genes are single nucleotide polymorphisms (SNPs) in GyrA, and in ParC, making the resistant strains less susceptible to fluoroquinolones

(Bruchmann et al. 2013). Another example is novobiocin producers, which often have mutations in GyrB that allow safe antibiotic production. Likewise, point mutations in the rpoB-encoded β subunit of RNAP provide resistance to rifamycins (Ovchinnikov et al. 1983). Trimethoprim resistance is commonly given by dihydrofolate reductase variants due to structural gene mutations (Bergmann et al. 2014).

Similarly, mutations in the 16S and 23S subunits of rRNA, given by alterations in the rRNA-encoding genes, confer resistance to kanamycin and apramycin to *M. tuberculosis.* Streptomycin producers also have protective mutations proximal to the anticodon-codon decoding site in the 30S subunit.

Another type of target modification is given by post-translational methylations of rRNA. The introduction of a methyl group into rRNA is likely to cause minimal perturbation but provides enough disturbance to small ligands, such as antibiotics. Post-translational methylations of rRNA are achieved via 16S rRNA methylases, which modify the small rRNA in the 30S subunit, and via 23S rRNA methylases, which modify the 23S rRNA before incorporation into the 50S subunit.

Aminoglycoside producers make use of methylation of the 16S subunit decoding site. Transferable plasmids have been found in clinical isolates of *P. aeruginosa* and *Klebsiella pneumoniae.* Macrolide producers are capable of methylating the PTC of the 50S subunit, blocking the binding of macrolides, lincosamides, and streptogramin B. Similar methyltransferases have been found in macrolide-resistant strains (Fyfe et al. 2016).

The third type of target modification occurs when bacteria change the net negative charge of the OM by enzymatic acylation or glycosylation of cell envelope components with positively charged amino groups. An example of that is the resistance to polymyxins in Gram-negative bacteria, where the LPS components of the OM are modified by the introduction of either one of two cationic groups, a 4-amino-L-arabinose or a phosphoethanolamine group. As a result, the introduced cationic group provides electrostatic repulsion of cationic antibiotics (Olaitan, Morand, and Rolain 2014).

Similarly, some Gram-positive bacteria increase the expression of the mprf (multiple peptide resistance factors) genes, induced by many cationic peptides, such as lantibiotic nisin, cationic aminoglycosides and by host antimicrobial defensines (Ernst et al. 2009). MprF produces lysyl-phosphatidylglycerols (lysinylation), reaching up to 40% of the total phosphatidylgylcerols. As a result, lysinylation covers up to one phosphate negative charge with two positive ones, causing resistance to cationic peptides and to daptomycin. In the same

way, glycopeptide resistance (e.g., to vancomycin) is achieved by remodeling the pentapeptide end of lipid II. Five contiguous genes vanRSHAX are responsible for the substitution of the D-Ala-D-Ala moiety of lipid II by a D-Ala-D-lactate, decreasing the binding affinity of vancomycin (Walsh et al. 1996).

Finally, methicillin-resistant *S. aureus* (MRSA) strains have achieved to replace the susceptible PBP by a resistant one: PBP2a, with a lower affinity for methicillin, cephalosporins, and carbapenems (Stapleton and Taylor 2002). PBP2a has a half-life for acylation between 3-12 min in comparison with milliseconds required to form penicilloyl-PBPs.

1.3 Antibiotic uptake in Gram-negative bacteria

Overcoming the permeability barrier of Gram-negative bacteria poses a major challenge in the current era of antibiotic development. Attempts to better predict antibiotic uptake are currently gaining popularity in preclinical studies, and so the need to fully understand drug permeability and, even more, antibiotic uptake (Stavenger and Winterhalter 2014; Cama, Henney, and Winterhalter 2019).

Many studies over the last decades have described different methods to evaluate the accumulation of antibiotics in whole bacterial cells (see Table 1.6). Some methods rely on the indirect detection of the compound of interest, e.g. by determining the residual activity of the supernatant of a culture treated with antibiotic, or measuring the expression of a compound-inducible protein by its enzymatic activity (Chopra, Shales, and Ball 1982; Chopra and Hacker 1992). Another example of indirect detection is to monitor the degradation of a blue starch-iodine complex that reacts with the hydrolyzed form of β-lactams, leading to a discoloration of the solution (Zimmermann and Rosselet 1977). The hydrolyzed β-lactam is produced by the activity of β-lactamases forming a penicilloic acid.

Many other methods used in accumulation studies make use of a labeled form of the compound of interest, relying on the detection of radioactive incorporation or fluorescent probes (McMurry and Levy 1978; McMurry, Petrucci, and Levy 1980). Additionally, some fluorogenic probes that exhibit their fluorescence only by their activation through a protein expressed intracellularly provide uptake-specificity (Ferreira et al. 2017). Other, more direct methods detect the intrinsic fluorescence of the original compounds upon their spectrum of excitation and emission (Stone et al. 2019). Most importantly, the direct detection of unlabeled and unmodified compounds is achievable by LC-MS/MS methods.

In recent years, LC-MS/MS-based methods have been successfully applied in uptake studies because of their broad applicability and versatility. Their sensitivity allows for the absolute quantification of compounds in the pmol range, and they have been even used as cross-validation of other methods (Dumont et al. 2018). According to Zgurskaya and Rybenkov, LC-MS/MS could probably be considered the gold standard in efflux and permeation studies at the present (Zgurskaya and Rybenkov 2020).

Table 1.6 Methods used for the determination of antibiotic uptake in whole bacterial cells

Method	Description	Reference
Enzymatic activity	Monitoring the enzymatic activity of tetracycline-inducible β-galactosidase	(Chopra, Shales, and Ball 1982; Chopra and Hacker 1992)
Fluorescence	Autoflourescent compound is directly monitored	(Samra, Krausz-Steinmetz, and Sompolinsky 1978; Leive et al. 1984; Chapman and Georgopapadakou 1988; McCaffrey et al. 1992; Li, Zhang, and Nikaido 2004; Bensikaddour et al. 2008; Cai et al. 2009; Coldham et al. 2010; Kaščáková et al. 2012; Meylan et al. 2017)
Fluorophore	The compound of interest is conjugated to a fluorescent dye, and the fluorescence is monitored	(Benincasa et al. 2009; Ning et al. 2011; Phetsang et al. 2016; Ferreira et al. 2017; Allam et al. 2017)
Fluorogenic dye	Bacteria express a fluorescence activator protein, while the compound of interest is conjugated to a fluorogenic dye	(Ferreira et al. 2017; Stone et al. 2019)
LC-MS/MS	Monitoring the chromatographic signal of the compound of interest, which is detected by a mass spectrometer	(Liu et al. 2003; Schumacher et al. 2006; Cai et al. 2009; Bhat et al. 2013; Davis, Gerry, and Tan 2014; Zhou et al. 2015; Richter et al. 2017; Dumont et al. 2018; Graef et al. 2018; Iyer et al. 2018; Prochnow et al. 2018; Wang et al. 2018; Spangler et al. 2018)
MALDI-MS/MS	The sample is adsorbed in a solid matrix while a projected beam ionizes the compound of interest to be detected by a mass spectrometer	(Tian et al. 2017)
Photometry	The hydrolyzed product of β-lactams is stoichiometrically oxidized by iodine. The degradation of a blue starch-iodine complex is reflected by discoloration of the solution.	(Zimmermann and Rosselet 1977; Malouin et al. 1991; Lei et al. 1991; Kojima and Nikaido 2013)
Radiometry	The compound of interest is modified with a radioactive label. The incorporation of radioactivity is monitored.	(McMurry and Levy 1978; McMurry, Petrucci, and Levy 1980; McMurry, Cullinane, and Levy 1982; Gutmann et al. 1985; Hooper et al. 1989; Bedard et al. 1989; Diver, Piddock, and Wise 1990; Mortimer and Piddock 1991; Li, Livermore, and Nikaido 1994; Williams and Piddock 1998; Williams, Chung, and Piddock 1998; Oethinger et al. 2000; Li, Zhang, and Nikaido 2004; Hasdemir et al. 2004; Cai et al. 2009; Krishnamoorthy et al. 2016)
Residual activity	Determine the antimicrobial activity of the supernatant of a treated culture	(Celesk and Robillard 1989; Bazile et al. 1992; Walters et al. 2003)
Spectrofluorimetry	The compound of interest is monitored within a range of excitation and emission wavelengths	(Chopra, Shales, and Ball 1982; Piddock and Zhu 1991; Piddock et al. 1999; Ricci and Piddock 2003; Cinquin et al. 2015; Vergalli et al. 2017; Vergalli et al. 2018; Westfall et al. 2017; Siriyong et al. 2017; Dumont et al. 2018)

1.4 Bacterial adaptation to antibiotics

The massive and indiscriminate use of antibiotics in humans, animals, aquaculture, and agriculture is the most important component in the development of antibiotic resistance (Carlet et al. 2012). When cycled across different environments, antibiotics concentration gradients exert selective pressure on bacteria, leading to the selection of resistant strains, which also transmit to different environments and mobilize resistant genes and determinants (Andersson and Hughes 2014).

In infections, pathogens adapt to their host's defenses by coping with diverse stresses such as oxidative, acidic, osmotic, temperature, nutrient starvation, and antibiotic stress. All these stresses can impact antibiotic susceptibility (Poole 2012). Additionally, when antibiotic concentrations in body fluids and tissues are lower than the lethal concentrations, bacterial growth is inhibited, but the totality of the cells is not killed, and the infection can resume later (Felden and Cattoir 2018). Efforts in understanding the mechanisms of how pathogens interact with antimicrobial drugs and how they ultimately develop resistance highlight the microbial interaction to sub-lethal levels of those compounds (Andersson and Hughes 2014; Bernier and Surette 2013; Davies, Spiegelman, and Yim 2006; Gullberg et al. 2011; Linares et al. 2006).

1.4.1 Metabolomics approach on the effects of antibiotics in bacteria

A growing body of evidence shows that exposing bacteria to antibiotics induces a specific metabolic response according to the antibiotic's mode of action. This has enabled the prediction of the mode of action of unknown compounds by comparing bacterial metabolic responses to those generated after exposure to reference antibiotics. This approach has been applied in different strains such as *S. aureus*, *E. coli*, and *M. smegmatis* (Dörries, Schlueter, and Lalk 2014; Vincent et al. 2016; Zampieri et al. 2018; Yang et al. 2019), and even in *S. cerevisiae* treated with diverse antifungal compounds (Allen et al. 2004) (see Table 1.7).

Table 1.7 Recent studies on the mode of action of antibiotics

Compounds	Strain	Analytical method	Overview	Reference
Ciprofloxacin, erythromycin, fosfomycin, ampicillin, vancomycin	*S. aureus*	^{1}H-NMR, GC-MS/MS, LC-MS/MS	Antibiotic dependent metabolic regulation	(Dörries, Schlueter, and Lalk 2014)
AZ1, fosmidomycin, AZ7, Triclosan, CCCP, Ceftazidime, CHIR-090, 2-(cyclobutylmethoxy)-5'-deoxyadenosine	*E. coli*	LC-MS/MS	Prediction of MOA	(Vincent et al. 2016)
Ampicillin, carbenicillin, doxycycline, kanamycin, streptomycin, tetracycline, cephalecin, ciprofloxacin, ofloxacin	*E. coli*	^{1}H NMR	Prediction of MOA	(Hoerr et al. 2016)
Kanamycin, spectinomycin, hydrogen peroxide, chloramphenicol, amoxicillin, ampicillin, norfloxacin, nalidixic acid, trimethoprim, sulfamethizole	*E. coli*	MS and MS/MS direct injection	Responsive metabolites: specific to antibiotic, specific to MOA, and promiscuous	(Zampieri et al. 2017)
62 compounds with known MOA 212 new antimycobacterial compounds	*M. segmantis*	MS and MS/MS direct injection	Prediction of MOA	(Zampieri et al. 2018)
Ampicillin, ciprofloxacin, gentamycin	*E. coli*	LC-MS/MS	Prediction of MOA	(Yang et al. 2019)

Although it is well accepted that antibiotics have diverse and specific mechanisms of action, some authors suggest that antibiotics kill bacteria by rather a general mechanism. Antibiotics of different classes with distinct targets are proposed to affect the balance in bacterial metabolism, respiration and iron homeostasis, which leads to an increase in the production of oxidants and radicals, and eventually to bacterial cell death (Dwyer et al. 2014). Reactive oxygen species (ROS) have been found to be generated by hyperactivation of bacterial metabolism and to be important for killing bacteria (Kohanski et al. 2007; Dwyer et al. 2012; Dwyer et al. 2014; Lobritz et al. 2015). Conversely, low levels of ROS induced by sub-inhibitory antibiotic concentrations have a strong influence on the promotion of resistance (Kohanski, DePristo, and Collins 2010).

The elevated antibiotic-induced oxidative stress resulting from disruptions in the cell wall, protein synthesis, and DNA metabolism may propitiate a metabolic imbalance, as well as perturbations in respiration and iron homeostasis (Dwyer et al. 2014). The open question remains on whether bacterial redox imbalance could predict new classes of bactericidal antibiotics, whereas the killing effect of antibiotics goes beyond growth inhibition (Walsh and Wencewicz 2016).

However, cell death as a result of antibiotic treatment is difficult to study due to the diverse cellular mechanisms involved, such as gene expression, growth control, programmed cell death, biofilm formation, and generation of traits involved in resistance as well as in persistence (Van Acker and Coenye 2017). The implication of self-induced cell death as a programmed response to stressful conditions has been extensively studied (Aldsworth, Sharman, and Dodd 1999; Rice and Bayles 2003; Engelberg-Kulka et al. 2006). Antibiotic-induced self-disintegration has also been shown in *P. aeruginosa* (Häussler and Becker 2008).

1.4.2 Sub-lethal concentrations of antibiotics

Diverse studies have found that bacteria respond readily to antibiotics, even when they are exposed to sub-lethal and even sub-inhibitory concentrations, by the analysis of gene expression and mutation rate (Goh et al. 2002; Ishikawa and Horii 2005; Verbrugghe et al. 2016; Kohanski, DePristo, and Collins 2010; Karatuna and Yagci 2010; Breidenstein, Bains, and Hancock 2012; George and Halami 2017) , proteomic studies (Xiong et al. 2017; Jedrey, Lilley, and Welch 2018), as well as metabolomics studies (Phelan, Fang, and Dorrestein 2015; Han et al. 2019).

In many cases, exposure to insufficiently lethal concentrations of antibiotics has conferred bacteria, such as *P. aeruginosa*, with resistance and persistence traits to different antibiotics, mostly by modulating the expression of many genes related with efflux pumps, cell envelope and enzyme production (Breidenstein, de la Fuente-Núñez, and Hancock 2011).

Additionally, there is evidence that bacteria undergo metabolic shifts as an adaptation response when encountering novel environments (Martínez-Solano et al. 2008; Behrends et al. 2013), conferring bacteria with antibiotic resistance. For instance, *P. aeruginosa*'s sensitivity to aminoglycosides can be enhanced by inducing a metabolic shift in the central carbon metabolism (Allison, Brynildsen, and Collins 2011; Meylan et al. 2017). This underlines the important relation between the bacterial metabolism and the antibiotic susceptibility

1.5 Metabolome analysis

1.5.1 Introduction to metabolomics

Over the past decades, the "omics" techniques have been exploited in systems biology applications. Systems biology is the study of complex interactions in biological systems, evaluating the effect of external factors on the genome (genomics), the transcriptome (transcriptomics), the proteome (proteomics) and the metabolome (metabolomics) (see Figure 1.7) (Horgan and Kenny 2011). Very often, an integrated analysis of these "omics" is required to understand the complex function of a large number of different cellular responses.
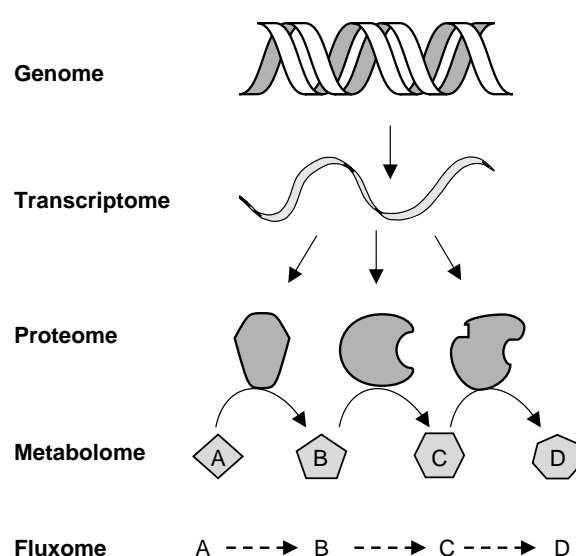
Figure 1.7 "Omics" technologies and the "omes". Genome is the complete nucleotide sequence in the genetic material of a living cell. Transcriptome is the complete set of all mRNA present in the cell. Proteome is the complete set of all proteins present in the cell. Metabolome is the complete set of all metabolites in the cell. Fluxome in the complete set of all fluxes through the different biochemical pathways. Adapted from Vilas-Bôas et al. 2006 (Villas-Bôas et al. 2007)

Particularly, metabolomics is the systematic characterization of the metabolome under very specific conditions (see Table 1.8). Thus, metabolomics involves various steps, from the design of experiment, sampling, sample preparation, sample analysis to data analysis (Dettmer, Aronov, and Hammock 2007). Sampling preparation often brings high variability in the metabolome analysis, and it is highly organism-dependent. A very important step in sample preparation is the rapid quenching of the biochemical processes at the sampling time, as metabolic concentrations change very rapidly under any variation (even unnoticed variations) (Villas-Bôas et al. 2007).

Table 1.8 Basic concepts in metabolomics

Concept	Definition
Metabolism	The sum of all the chemical transformations within a cell or organism
Metabolite	An intermediate or end product in biosynthetic and degradative pathways
Metabolic pathway	A series of enzyme-catalyzed reactions
Metabolome	The complete collection of metabolites produced or used within a cell
Endometabolome	The subset of intracellular metabolites
Exometabolome	The subset of metabolites excreted into the extracellular medium
Metabolomics	An approach to analyzing the metabolome or a fraction of the metabolome
Metabolic fingerprint	Analysis of the endometabolome
Metabolic footprint	Analysis of the exometabolome
Metabolite profiling	Analysis of a group of specific metabolites
Untargeted metabolite analysis	Global analysis of the metabolome (comprehensive)
Targeted metabolite analysis	Analysis of a subset of the metabolome (validation)

Sample preparation for metabolomics studies in microorganisms often requires several steps after quenching the metabolism, including the separation of the biomass from the extracellular medium, extraction of the endometabolome, conditioning the sample before its chemical analysis. The analysis of the metabolome covers the detection and identification of all (or most) intracellular and extracellular small molecules (with molecular mass under 1000 Da), and different analytical techniques are commonly used.

The complexity of the metabolome is so large that it is not possible to detect the complete collection of metabolites in one analysis. For example, metabolic fingerprint and footprint are often analyzed by mass spectrometry (MS), nuclear magnetic resonance spectrometry (NMR), or infrared spectroscopy (IR). In metabolite profiling, as many known and unknown metabolites as possible are detected, and is usually done by chromatography or capillary electrophoresis (CE) in combination with MS. On the other hand, target analyses intend to detect and quantify specific metabolites, and a large number of analytical techniques are available.

MS-based metabolomics allows for quantitative analysis with high sensitivity and the potential to identify metabolites. MS, in combination with a separation technique, such as liquid chromatography (LC) or gas chromatography (GC), provides more information on the physical-chemical properties of the metabolites.

1.5.2 Mass spectrometry and liquid chromatography

Mass spectrometry is a destructive analytical technique that allows for the determination of the nominal mass of an analyte. MS does not directly determine the mass of an analyte, but the mass-to-charge ratio (m/z) of the ions originating from the analyte. One fundamental requirement of mass spectrometers is that the ions must be in the gas phase before they can be detected according to their individual m/z values (Watson and Sparkman 2007).

Among a number of ionization techniques electrospray ionization (ESI) and matrix-assisted laser desorption/ionization (MALDI) have been predominantly used in the analysis of biological samples, where very often the analytes are thermally labile and nonvolatile (Watson and Sparkman 2007). In ESI, a liquid solution containing the analyte is sprayed at the tip of a metal nozzle maintained at a positive potential (positive mode) or at a negative potential (negative mode). The nozzle disperses the solution into a fine spray, while a dry gas at atmospheric pressure reduces the size of the droplets by solvent evaporation (see Figure 1.8).
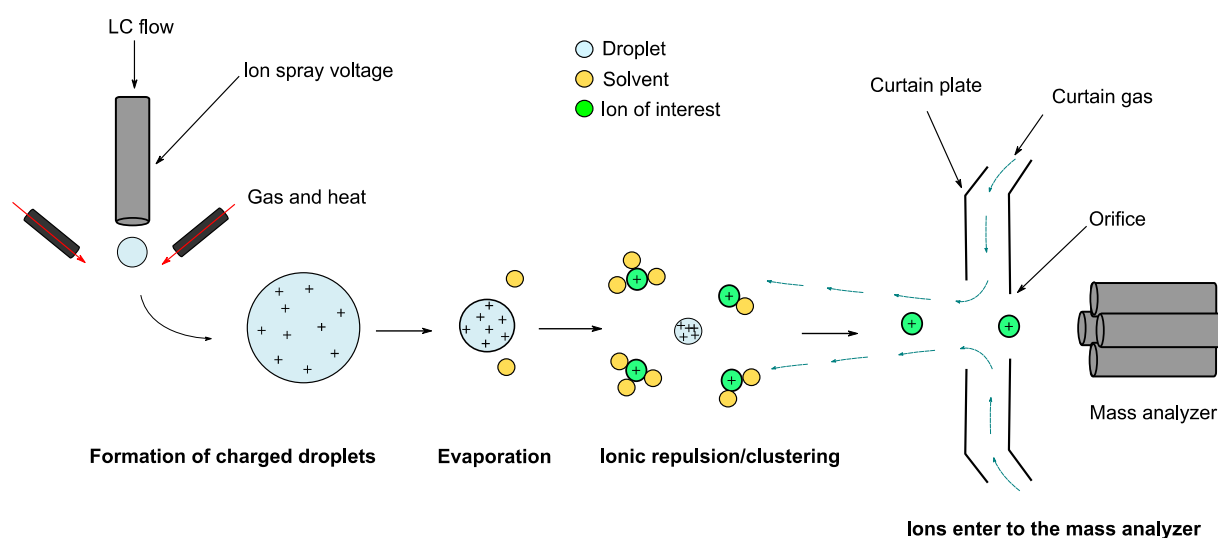
Figure 1.8 Electrospray ionization (ESI) in positive mode Adapted from (Siuzdak 2003). The solution passes through a positively charged nozzle where small, charged droplets are formed and they are dried by applying heat and cross-directional flow of gas. As evaporation occurs, positive charges are concentrated in even smaller droplets, creating an ionic repulsion among the ions of interest before they enter to the mass analyzer. A gas curtain helps minimizing the entry of solvent molecules and neutral species to the mass analyzer (Kang, Schneider, and Covey 2017)

ESI is known for producing singly charged small molecules, and frequently multiply charged species in larger molecules (Siuzdak 2003). In addition to protonation, adduct formation with sodium, potassium and ammonium takes place in the charged nanodroplets produced in positive-mode ESI (Gao, Zhang, and Karnes 2005; Cech and Enke 2001). The resulting charged molecules are the molecular ions to be detected according to their m/z values. In a tandem MS analysis, or MS/MS, different molecular ions are selected and separated, and fragment ions are generated in a collision cell from each molecular ion, or precursor ion (see Figure 1.9). In MS/MS mode, fragments originated from the precursor ion often provide structural information.

Selecton of the   **Fragmentation of the**   **Analyis of fragment ions (MS/MS)**
precursor ion (MS)   **precursor ion**
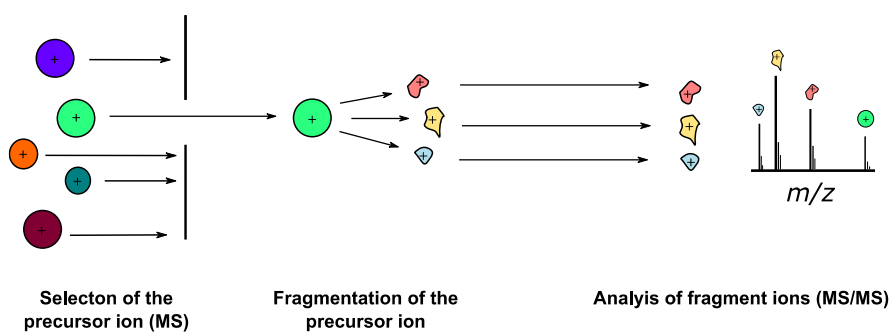
Figure 1.9 Tandem mass spectrometry Adapted from (Siuzdak 2003). The molecular ion of interest is selected according to its m/z value and separated to undergo fragmentation in a collision cell. The generated fragments, and the rest of the precursor ion are detected by the mass analyzer

Due to their good to excellent accuracy, good resolution and high sensitivity, the most commonly used mass analyzers in tandem MS are quadrupoles, time-of-flight (ToF) and Fourier-Transform Mass Spectromety (FTMS) connected in series (Siuzdak 2003). For instance, in triple quadrupoles, the first quadrupole (Q1) scans across an m/z range and selects an ion of interest. The second quadrupole (Q2) serves a collision cell, fragmenting the selected ion along its flight path, while the third quadrupole (Q3) analyzes the fragment ions generated in Q2 (see Figure 1.10). Similarly, in a Q-ToF, the quadrupole selects the ion of interest, and sends it to a collision cell for fragmentation. The resulting fragments travel through an accelerating potential, where the lighter ions reach the detector first, while the heavier ions take longer to reach (see Figure 1.11.).

Tandem MS analyzers are often coupled to a chromatographic separation unit, as good separation of analytes reduces background noise, leading to improved detection limits and data quality (Dettmer, Aronov, and Hammock 2007). Reversed phase (RP) liquid chromatography is widely used in metabolomics analysis, as it is a standard tool for separating medium polar and non-polar metabolites. The applicability of LC-MS/MS has gained ground in the analysis of biological samples in the last decades (Pitt 2009).
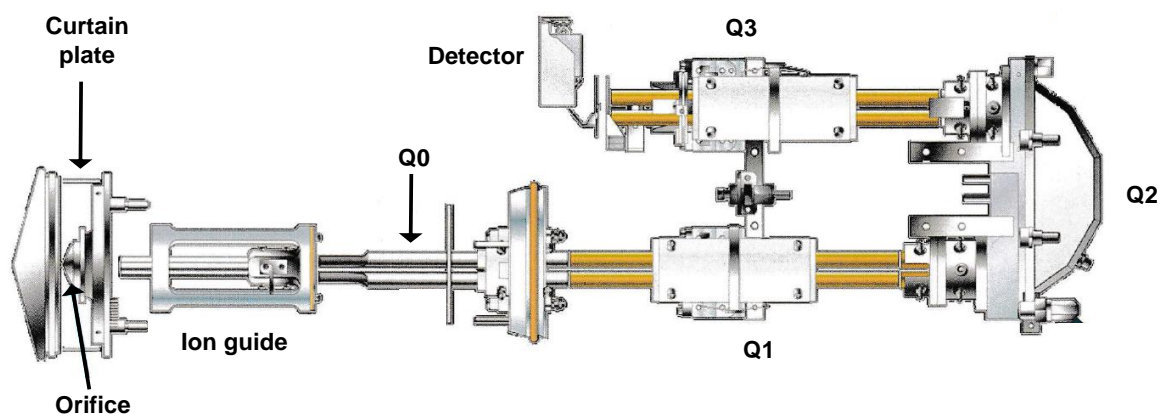
Figure 1.10. Configuration of a triple quadrupole (QQQ). The ions that were produced in the source enter through orifice in the curtain plate, and they are transferred through an ion guide that creates a barrier against neutral molecules and micro droplets. Similarly, an also quadrupole array, Q0, transmits the ions to the first mass resolving quadrupole, Q1. In Q1, the precursor ion of interest is selected by adjusting the ratio of radio frequency (RF) and direct current (DC), RF/DC, so that only one particular m/z ratio have a stable trajectory through the quadrupole. The selected precursor ion undergoes fragmentation in Q2, or collision cell, and the fragments are monitored in the third quadrupole, Q3, which is connected to a continuous electron multiplier as detector. Adapted from (AB Sciex 2015).
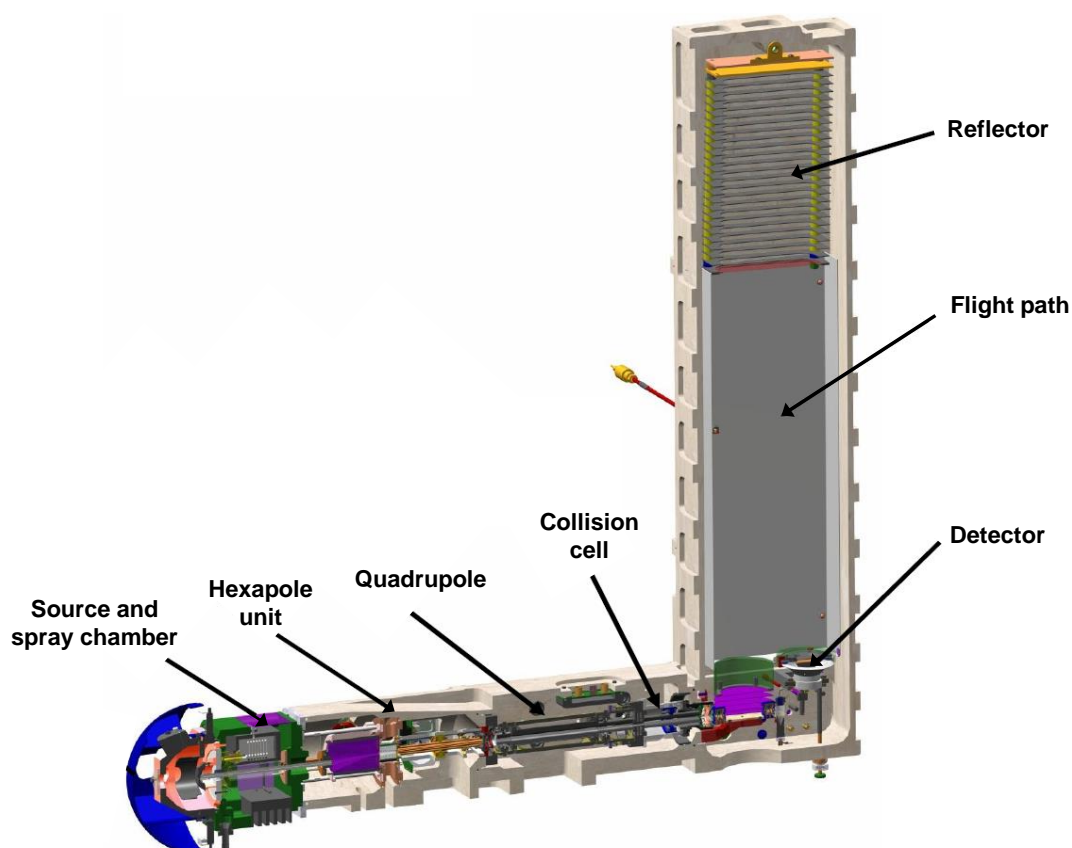
Figure 1.11.Configuration of a quadrupole time-of-flight (Q-TOF) Ions are generated in the source chamber, and transferred through the hexapole unit up to the quadrupole. In MS mode, there is not ion isolation in the quadrupole and the collision cell operates at low collision energy. In MS/MS mode, the precursor ion of interest is isolates in the quadrupole and sent to the collision cell operating at high collision energy for collision-induced dissociation (CID). The ion fragments are accelerated into a flight path, required for the calculation of the velocity of the ions (heavier ions with the same charge reach lower speeds). A reflectron helps ions with the same m/z but different kinetic energies reach the detector at the same time (less energetic ions penetrate less profound into the reflectron, taking a shorter path to the detector). Adapted from (Bruker Daltonics 2012)

1.5.3 Data analysis in metabolomics

Raw data in LC-MS/MS analysis come in the shape of chromatographic peaks with different intensities, where each chromatographic peak is the sum of the intensity of all molecular ions eluting at a particular retention time (RT). In MS level, or MS^1, a mass spectrum is generated, while in MS/MS, or MS^2, each of the precursor ions with a defined m/z value contains information of its fragment ions.

Noise filtering, peak detection, peak deconvolution and retention time alignment are required to identify features, which are pairs with an m/z value, a retention time and, if it is the case, MS/MS information. It is important to note that a feature is not always a metabolite, as related species (e.g. isotopes, adducts or multiply charged ions) of a single metabolite may be present with different m/z values (Schrimpe-Rutledge et al. 2016). Thus, one single chemical species may generate different features in an LC-MS/MS analysis. Similarly, the annotation of isotopic peaks corresponding to a particular molecular ion and its fragment peaks is also required (Cambiaghi, Ferrario, and Masseroli 2016; Dettmer, Aronov, and Hammock 2007).

Metabolite identification remains a big challenge in untargeted metabolomics (Creek et al. 2014). Usually, *in-house* compound libraries are used for the direct comparison of mass spectra to assign metabolite identity to a feature. Apart from that, there are different open databases available such as Human Metabolome Database (HMDB), the Metabolite and Tandem MS Database (METLIN), and organism-specific databases such as the *E. coli* Metabolome Database (ECMDB) or the recent *Pseudomonas aeruginosa* Metabolome Database (PAMDB) (Wishart et al. 2017; Guijas et al. 2018; Guo et al. 2013; Huang et al. 2018).

1.6 *Pseudomonas aeruginosa* as a model organism

P. aeruginosa is a Gram-negative aerobic bacillus that causes severe hospital-acquired infections, especially in immunocompromised hosts (Lyczak, Cannon, and Pier 2000). Among other infections, *P. aeruginosa* causes bacteremia in severe burn victims, chronic lung infections in cystic fibrosis patients, and acute ulcerative keratitis in patients with serious eye disorders (Lyczak, Cannon, and Pier 2000). To worsen the situation, *P. aeruginosa*'s clinical isolates are often antibiotic resistant, hampering the choice of therapy, and they are often associated with a high mortality rate and high hospitalization burden (WHO 2017).

P. aeruginosa exhibits high intrinsic resistance to a wide variety of compounds, such as aminoglycosides, β-lactams, and aminoglycosides. This broad antibiotic resistance is given by low outer membrane permeability, β-lactamase production, efflux pump overexpression, target mutations and the expression of regulatory genes (Behrends et al. 2013; Chalmers 2017; Subedi et al. 2018; Breidenstein, de la Fuente-Núñez, and Hancock 2011; Fraile-Ribot et al. 2017). Antibiotic resistance has been related to bacterial virulence, as virulence genes are often influenced by conditions found in the host environment and help the bacteria to cope with the encountered stresses (Breidenstein, de la Fuente-Núñez, and Hancock 2011).

Some examples of virulence factors are secreted molecules such as elastases, proteases, phospholipase C, hydrogen cyanide, exotoxin A, exoenzyme S, phenazines and rhamnolipids. Other associated factors, like flagella, pili, and LPS also contribute to the pathogenesis of *P. aeruginosa* (Cornelis 2008). Virulence factors in *P. aeruginosa* are known to be regulated by a complex network of quorum sensing (QS) small molecules, also called autoinducers, which serve to regulate gene expression (Moradali, Ghods, and Rehm 2017; Nadal Jimenez et al. 2012; Cornelis 2008). Furthermore, *P. aeruginosa* strains are known to be highly virulent, particularly PA14 is more virulent than PAO1 (Lee et al. 2006).

QS is controlled by an interconnected regulatory network that initiates by the cumulative production of autoinducers in a cell-density dependent manner and results in collective responses (see Figure 1.12). Three linked QS systems, Las, Rhl, and PQS (Pseudomonas Quorum Sensing) rule the production of many of *P. aeruginosa* virulence factors. Las and Rhl systems use N-acyl-homoserine lactones as signal molecules, where the Las system controls the Rhl system. The PQS system has also a hierarchical dependence on Las, and it involves the production of 2-heptyl-3-hydroxy-4-quinolone. Phenazines, such as pyocyanin, depend on the Rhl and the PQS systems. While the production of rhamnolipids is known to be controlled by the Rhl system (Nadal Jimenez et al. 2012; Moradali, Ghods, and Rehm 2017).
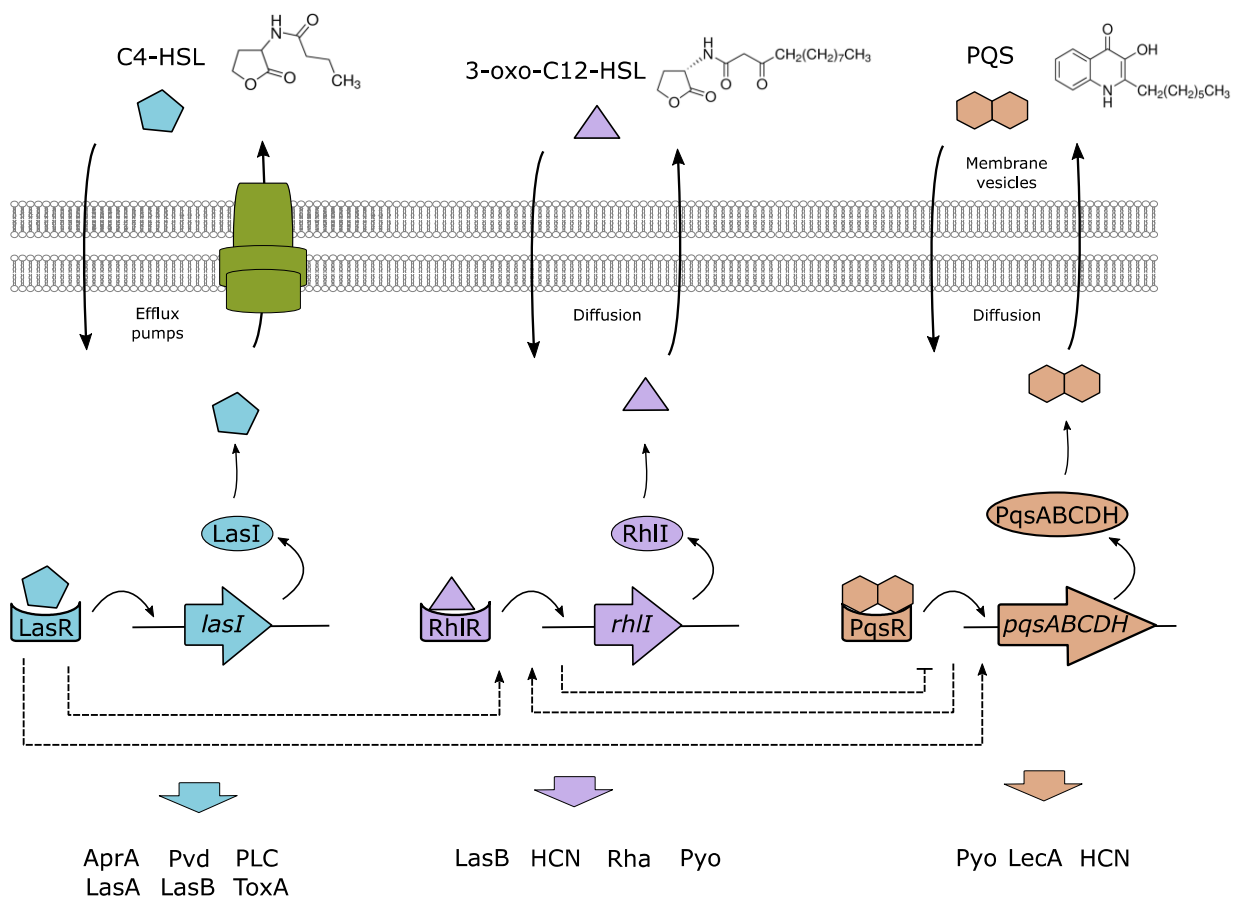
Figure 1.12 Quorum sensing regulatory circuits for *P. aeruginosa*'s virulence factors. *P. aeruginosa* responds to stress and stimuli, producing autoinducers C4-HSL, 3-oxo-C12-HSL, PQS. Export and import of HSL are mediated by the action of the efflux pumps MexAB-OprM and MexEF-OprN. BHL is import and export are achieved by diffusion. PQS translocation is mediated by membrane vesicles. Transcriptional factors LasR, RhlR, and PqsR are activated by autoinducers to upregulate the expression of their synthases, LasI, RhII and PqsABCDH, respectively. Other virulence factors are overexpressed as well, and their secretion is mediated by type1 and type 2 secretion systems, PvdRT-OpmQ efflux pump as well as simple diffusion. 3-oxo-C12-HSL: 3-oxo-C12-homoserine lactone, AprA: alkaline protease, C4-HSL: N-butyrylhomoserine lactone, HCN: hydrogen cyanide, LasA: LasA elastase, LasB: LasB elastase, Lec A: lectin A, PLC: phospholipase C, PQS: 2-heptyl-3-hydroxy-4-quinolone. Pvd: pyoverdin, Pyo: pyocyanin, Rha: rhamnolipids, ToxA: toxin A. Adapted from Moradali *et al.* 2017 and Cornelis 2020 (Moradali, Ghods, and Rehm 2017; Cornelis 2020)

Phenazines are virulence factors with antibiotic activity, as they trigger the formation of reactive oxygen species (ROS), although they also have antifungal and antiparasitic activities (Guttenberger, Blankenfeldt, and Breinbauer 2017). Phenazines have been related to biofilms, as they can maintain the redox homeostasis where oxygen exchange can be compromised (Price-Whelan, Dietrich, and Newman 2007; Guttenberger, Blankenfeldt, and Breinbauer 2017).

Biofilm formation is a major burden in antimicrobial therapy since a biofilm offers physical protection that protects bacteria from adverse environmental conditions (Wu, Cheng, and Cheng 2019). For instance, antibiotic amounts in biofilms can be reduced to sub-lethal concentrations, which can lead to antibiotic resistance (Lebeaux, Ghigo, and Beloin 2014).

Conversely, the overproduction of rhamnolipids inhibits biofilm formation (Davey, Caiazza, and O'Toole 2003). Although the biological function of rhamnolipids is still unclear, rhamnolipids seem to enhance the initial adherence of cells to a surface (Al-Tahhan et al. 2000), and the uptake of hydrophobic compounds (Noordman and Janssen 2002).

2. AIM OF THE DISSERTATION

As noted before, pathogenic bacteria have the ability to cope with a wide variety of environmental stress, and they adapt to their host cell's environment. To accomplish this, bacteria rely on the rapid modification of metabolism and gene expression. The knowledge of how modifications on gene expression provide bacteria with antibiotic resistance has been widely documented, and the understanding of how these alterations influence bacterial responses at the metabolic level is on the rise. However, the knowledge of how metabolism promotes resistance and how it influences the activity of antibiotics and is still limited. herefore, the aim of this study was to obtain a comprehensive picture of the metabolism of *P. aeruginosa* upon antibiotic stress under limited lethality via untargeted analysis based on ultra-performance liquid chromatography and mass spectrometry. First, an evaluation on the metabolic fingerprint of *P. aeruginosa* upon sub-lethal concentrations of selected antibiotics was carried out in order to discern whether with different modes of action exhibit distinctive metabolic responses.

Although there is a body of evidence that shows how bacterial responses to antibiotics depend strongly on the encountered concentrations, little is known on how strongly such responses depend in the exposure times to the antibiotic-induced stress. Hence, one of the aims of this study was to evaluate *P. aeruginosa*'s response to clinically relevant antibiotics classes under short and long exposure times, under the same cultivation conditions.

Furthermore, there are still unknown aspects of the off-target mechanisms that antibiotics exert in bacteria. Since the relation between the degree of accumulation of a compound and its consequent effects on the bacterial response has not been extensively investigated, this study aimed to collect information on the indirect effects of ciprofloxacin in *P. aeruginosa* by comparing the metabolic fingerprints of a susceptible and a resistant strain showing similar compound accumulation. Ultimately, this study aimed to uncover the off-target effects of ciprofloxacin in a *P. aeruginosa* strain with a reduced drug-target interaction.

Additionally, a part of this study was devoted to developing a robust and strain-transferable plate-based assay for the quantification of antibiotic uptake, with the potential to be used in a high-throughput accumulation screening workflow of known and novel compounds. As starting point, the optimization of experimental settings and minimization of the handling volumes were contemplated. One of the ultimate goals of such a development was to measure the amounts of accumulated antibiotic in different strains, most emphatically in Gram-negative bacteria such as *E. coli* and *P. aeruginosa*, and to show the accumulation profiles of a selection of antibiotics in such organisms.

3. MATERIALS AND METHODS

3.1 Materials

3.1.1 Strains

Table 3.1 List of strains used in this study

Strain	Information	Reference
E. coli K-12 MG1655	Wild type, N.S.M.	(Blattner et al. 1997)
P . aeruginosa UCBPP-PA14	Human isolate, N.S.M.	(Rahme et al. 1995)
PA14 *gyrA* Thr83Ile	PA14, *gyrA* Thr83Ile, N.S.M.	(Bruchmann et al. 2013)
PA14 *gyrA* Thr83Ile *parC* Ser87Leu	PA14, *gyrA* Thr83Ile *parC* Ser87Leu, N.S.M.	(Bruchmann et al. 2013)

N.S.M.: No selection marker

3.1.2 Chemicals

Table 3.2 List of chemicals used in this study

Name	Company
Ammonium sulfate ((NH_4)$_2SO_4$)	Sigma-Aldrich
Azithromycin	Sigma-Aldrich
Caffeine	Sigma-Aldrich
Casaminoacids (CasAA)	Roth
Ciprofloxacin	Sigma-Aldrich
Clarithromycin	Sigma-aldrich
Clindamycin	Cayman Chemical Company.
Erythromycin	Sigma-Aldrich
Fosfomycin	Sigma-Aldrich
Gentamycin	Sigma-Aldrich
Glipizide	Acros
Glucose monohydrate	Roth
Iron(II) sulfate (Fe$^{(II)}SO_4$)	Sigma-Aldrich
Levofloxacin	Sigma-Aldrich
Lomefloxacin	Sigma-Aldrich
Lyncomycin	Sigma-Aldrich
Meropenem	Sigma-Aldrich
Magnesium chloride hexahydrate ($MgCl_2 \cdot 6H_2O$)	MP Biomedicals
Magnesium sulfate haptahydrate ($MgSO_4 \cdot 7H_2O$)	Roth
Nalidixic acid	Cayman Chemical Company
(S)-Naproxene	Cayman Chemical Company
Nortriptyline	Sigma-Aldrich
Novobiocin	Sigma-Aldrich
Potassium phosphate dibasic (K_2HPO_4)	Merck
Potassium dihydrogen phosphate (KH_2PO_4)	Merck
Sodium phosphate dibasic (Na_2HPO_4)	Roth
Sodium dihydrogen phosphate (NaH_2PO_4)	Roth
Streptomycin	Sigma-Aldrich
Sulfamethazole	Fluka Analyticals
Tetracycline	Sigma-Aldrich
Tigecycline	LKT Labs
Tobramycin sulfate	Fluka Analyticals
Trimethroprim	Sigma-Aldrich

3.1.3 Equipment and consumables

Table 3.3 List of equipment and consumables used in this study

Name	Company
AB Sciex QTrap 6500 ESI-QQQ	AB Sciex Germany GmbH, Darmstadt, Germany
AcroPrep™ Supor® 96-well filter plate, 2 mL, 0.45 µm pore size	Pall Corporation, NY, USA
Agilent 1290 UHPLC	Agilent Technologies, Santa Clara, CA, USA
Bravo Automated Liquid-Handling Platform	Agilent Technologies, Santa Clara, CA, USA
Centrifugal vacuum concentrator	Labconco Corporation, Kansas, MO, USA
Centrifugation tube filters 0.2 µm Corning® Costar® SPIN-X®	Corning Inc., NY, USA
ChemiDoc XRS	BioRad, Hercules, CA, USA
Cold trap at -50°C	Labconco Corporation, Kansas, MO, USA
Conical bottom receiver plate, 350-µL , clear polypropylene	Greiner Bio-One GmbH, Frickenhausen, Germany
Deep-well rounded-bottom plate, 1 mL	NUNC, Denmark
Dionex Ultimate 3000 UPLC	Thermo Fisher Scientific, Waltham, MA
Eppendorf tubes® 1 mL, 2 mL, and 5 mL	Eppendorf AG, Hamburg, Germany
Falcon™ tubes	Corning Inc., NY, USA
Image Lab software	BioRad, Hercules, CA, USA
Kinetex C18 reverse phase column with 1.7 µm particle size and 2.1 mm	Phenomenex, Aschaffenburg, Germany
maXis™ HD QTOF	Bruker, Bremen, Germany
microtiter plates clear PP, flat bottom, untreated,	NUNC, Denmark
Millipore SteriCup® filter cups	Merck KGaA, Darmstadt, Germany
MultiScreenHTS DV filter plate, transparent, 300 µL, 0.45 µm pore size	Merck Millipore, Tullagreen, IRL
Parafilm platic foil	Bemis CompanyInc, USA
PH meter	Mettler-Toledo, Switzerland
Plate adapter	Self-made
Plate reader	BioTek Instruments, Winooski, Vermont, USA
Square plates with lid,12cm x 12cm	Greiner Bio-One GmbH, Frickenhausen, Germany
ThermoMixer® C	Eppendorf GmbH, Hamburg, Germany
ZORBAX Eclipse Plus C18 reverse-phase column 2.1 x 5.0 mm, 1.8 µm	Agilent Technologies, Santa Clara, CA, USA

3.1.4 Preparation of diverse solutions

3.1.4.1 BM2 medium

Basal Medium 2 (BM2) complemented with 0.01% casaminoacids (CasAA) was freshly prepared for every experiment according to Table 3.4. Every stock was prepared separately and sterilized by filtration through Millipore SteriCup® filter cups, and a 10x concentrated BM2 buffer autoclaved (Table 3.5).

Table 3.4 Stock dilution and medium preparation

Stock solution	Sterilization	Dilution	Final concentration of compound	Volume to prepare 1L of medium (mL)
10x BM2	Autoclaved	1:10	1 x BM2	100
20% (w/v) Glucose	steril filtered	1:50	0.4% Glucose	20
1 M MgSO$_4$	steril filtered	1:500	2 mM MgSO4	2
10 mM FeSO$_4$	steril filtered	1:1000	10 µm FeSO4	1
2,5% (w/v) CasAA	steril filtered	1:250	0.01% CAA	4
Milli-Q® filtered water	steril filtered	N.A.	N.A	873

Table 3.5 BM2 preparation

Compound	Final concentration (M)	Molar mass (g/mol)	Amount for 500 mL of stock (g)
$(NH_4)_2SO_4$	0.07	132.14	4.62
K_2HPO_4	0.4	174.18	34.83
KH_2PO_4	0.22	136.09	14.97
Milli-Q® filtered water	N.A	N.A.	445.58

3.1.4.2 NaPi-MgCl$_2$ buffer

100 mM NaPi buffer + 5 mM MgCl$_2$ buffer for uptake assay was prepared according to Table 3.6. The pH was adjusted with NaOH solution to reach 7.0 before adjusting the final volume with filtered water. The whole solution was sterilized by filtration though Millipore SteriCup® filter cups.

Table 3.6 Preparation of NaPi buffer for uptake assay (100 mM NaPi buffer + 5 mM MgCl$_2$)

Stock solution	Sterilization	Dilution	Final concentration of compound	Volume to prepare 500 mL of buffer (mL)
1 M NaH$_2$PO$_4$	steril filtered	1:20	50 mM NaH$_2$PO$_4$	21.1
1 M Na$_2$HPO$_4$	steril filtered	1:20	50 mM Na$_2$HPO$_4$	28.9
500 mM MgCl$_2$	Autoclaved	1:100	5 mM MgCl$_2$	5
1 N NaOH	N.A.	N.A.	Until pH = 7.0	< 1 mL until pH = 7.0
Milli-Q® filtered water	steril filtered	N.A.	N.A	< 445

3.1.4.3 Antibiotic solutions for uptake experiments

Stocks of antibiotics were prepared by dissolving 1 to 2 mg of compound in solvent according to Table 3.7 to reach a concentration of 1 mg/mL. Further dilutions were carried out with NaPi buffer to reach a final concentration of 1 mM. For uptake assays, 25 µL of antibiotic stock solutions was added to 100 µL of bacterial solution, so that the final concentration of compound was 200 µM.

Table 3.7 Preparation of 1 mM antibiotic stocks for uptake experiments in filter plates

Compound	Solvent for first dilution*	Molar mass (g/mol)	Stock mass concentration (mg/mL)	Stock molar concentration (mM)
Ciprofloxacin	First in 0.1 mL 0.1 N HCl, then dilution with NaPi	331.35	0.331	1
Clindamycin	NaPi	424.98	0.425	1
Phosphomycin	NaPi	182.02	0.182	1
Lyncomycin	NaPi	461.01	0.461	1
Nalidixic acid	First in 0.1 mL 0.1 N NaOH, then dilution with NaPi	232.24	0.232	1
Novobiocin	First in 0.1 mL 0.1 N HCl, then dilution with NaPi	634.61	0.635	1
Streptomycin	First in 0.2 mL H$_2$O, then dilution with NaPi	728.69	0.729	1
Sulfamethazole	NaPi	253.28	0.253	1
Tetracycline	NaPi	480.90	0.481	1
Tigecycline	First in 0.2 mL H$_2$O, then dilution with NaPi	585.65	0.586	1
Tobramycin	First in 0.2 mL H$_2$O, then dilution with NaPi	467.51	0.468	1

* Compounds were first dissolved to 1 mg/mL, then sterilized by filtration, and further dilutions were carried out with NaPi buffer

3.1.4.4 Antibiotic solutions for metabolomics experiments

Stocks of antibiotics were prepared by dissolving 0.7 to 1.0 mg of compound in enough solvent to reach a concentration of 1 or 2 mg/mL, and they were sterilized by filtration though Spin-X® tube filters. Further dilutions were carried out with BM2 medium to reach the stock concentrations listed in Table 3.8. For metabolomics experiments in filter plates, 50 μL of antibiotic stock solutions was added to 1 mL of bacterial solution.

Table 3.8 Preparation of antibiotic stocks for metabolomics experiments in deep-well filter plates

Compound	Solvent for first dilution	Stock concentration (μg/mL)	Final concentration in 1.05 mL (μg/mL)
Azithromycin	First in 0.1 mL DMSO, then dilution with BM2 upto 2 mg/mL	1050	50
Ciprofloxacin	First in 0.1 mL 0.1 N HCl, then dilution with BM2 upto 1 mg/mL	4.2	0.2
Clarithromycin	First in 0.1 mL DMSO, then dilution with BM2 upto 2 mg/mL	1050	50
Erythromycin	First in 0.5 mL H$_2$O, then dilution with BM2 upto 2 mg/mL	1050	50
Levofloxacin	First in 0.1 mL 0.1 N HCl, then dilution with BM2 upto 1 mg/mL	4.2	0.2
Lomefloxacin	First in 0.2 mL H$_2$O, then dilution with BM2 upto 1 mg/mL	4.2	0.2
Meropenem	First in 0.2 mL H$_2$O, then dilution with BM2 upto 1 mg/mL	210	10

For metabolomics experiments in test tubes, the stock solutions were prepared similarly. 50 μL of antibiotic stock solutions was added to 1 mL of bacterial solution, following the concentrations listed in Table 3.9.

Table 3.9 Preparation of antibiotic stocks for metabolomics experiments in test tubes

Compound	Solvent for first dilution	Stock concentration (µg/mL)	Final concentration in 3.1 mL (µg/mL)
Azithromycin	First in 0.1 mL DMSO, then dilution with BM2 to 2 mg/mL	124	4
Ciprofloxacin	First in 0.1 mL 0.1 N HCl, then dilution with BM2 to 1 mg/mL	1.55	0.05
Erythromycin	First in 0.5 mL H_2O, then dilution with BM2 to 2 mg/mL	124	4
Gentamycin	First in 0.5 mL H_2O, then dilution with BM2 to 1 mg/mL	6.2	0.2
Levofloxacin	First in 0.1 mL 0.1 N HCl, then dilution with BM2 to 1 mg/mL	1.55	0.05
Tobramycin	First in 0.5 mL H_2O, then dilution with BM2 to 1 mg/mL	6.2	0.2

For metabolomics experiments upon sub-inhibitory concentrations of ciprofloxacin, the stock solutions were prepared from a common stock of ciprofloxacin at 1 mg/mL.

Table 3.10 Preparation of antibiotic stocks for metabolomics experiments in test tubes

Treatment	Stock concentration (µg/mL)	Final concentration in 3.1 mL (µg/mL)
Control	0.00	0.000
NIC	0.50	0.016
IC10	0.72	0.023
IC50	1.83	0.059
MIC	4.67	0.151

3.1.4.5 Internal standards

In addition, internal standards stocks (ISTDs) were prepared by solubilizing approx. 0.7 mg of compound in solvent according to Table 3.11.

Table 3.11 Preparation of internal standards stocks for metabolomics studies

Compound	Solvent	Stock concentrations	Dilution	Final concentration in 80% v/v MeOH
Trimethroprim	MeOH	0.1 mg/mL	1:1000	0.1 µg/mL
Nortriptyline	MeOH	0.1 mg/mL	1:1000	0.1 µg/mL
Glipizide	MeOH	0.1 mg/mL	1:1000	0.1 µg/mL
Naproxene	MeOH	0.1 mg/mL	1:100	1 µg/mL
Caffeine	MeOH	0.1 mg/mL	1:100	1 µg/mL

3.2 Microbiological methods

3.2.1 Determination of colony-forming units (CFUs)

Bacterial solutions were serially diluted in a microtiter plate. 100 µL of the corresponding dilutions 1:10^6 and 1:10^7 were distributed in plain LB (Luria Bertani broth) agar plates and incubated at 37 °C for 24 h. CFUs were determined for the dilution that showed less than 100 colonies.

3.2.2 Spot-plating

For each sample of interest, 10 µL was serially diluted in 90 µl of PBS in a 96-well microtiter plate. From each well, 2 µL were carefully dropped onto 12cm x 12cm square LB agar plates with a Bravo Automated Liquid-Handling Platform. The plates were incubated at 37°C for 24 h. Images were taken with a ChemiDoc XRS and processed with the Image Lab software.

3.2.3 Determination of inhibitory concentrations

Overnight cultures were prepared with 5 mL of BM2 + 0.01% CasAA inoculated with the corresponding strain and incubated overnight at 37 °C and 150 rpm. 20 mL of fresh BM2 were inoculated with 0.7 mL of overnight culture (starting OD$_{600}$ ≈ 0.1) and incubated at 37 °C and 150 rpm until an OD$_{600}$ = 1.0 was reached. 1 mL culture was centrifuged in 2-mL Eppendorf tubes (9 min, 4500xg, 20°C) and the supernatant was discarded. The pellet was resuspended in fresh BM2 to reach an OD$_{600}$ = 0.1. Compounds were first dissolved in water to reach 1 mg/mL (for ciprofloxacin, approx. 0.7 mg first dissolved in 100 µL 0.1 N HCl and further diluted in water), and further dilutions in BM2 were carried out to reach the required stock concentration. 100 µL of stock solution (4 µg/mL for ciprofloxacin) were given to the first column of a microtiter plate and 1:2 serial dilutions followed, leaving 50 µL in each well. 50 µL of bacterial solution were mixed in every well of the microtiter plate containing 50 µL of antibiotic solution (OD$_{600}$ = 0.05, max concentration 2 µg/mL). The plate was incubated at 37°C for 24 h and the OD$_{600}$ was measured in a plate reader. OD$_{600}$ values were analyzed with the R Shiny App (Ebner 2016) to determine the non-inhibitory concentration (NIC), the concentration at 10% growth loss (IC10), the concentration at 50% growth loss (IC50) and the minimum inhibitory concentration (MIC), where a Gompertz function is fitted to the data (sigmoid curve) (Lambert and Pearson 2000).

3.3 Targeted analysis for uptake quantification

3.3.1 Medium throughput method

3.3.1.1 Uptake assay in 96-well filter plates

Overnight cultures of *P. aeruginosa* or *E. coli* were prepared with 5 mL of LB medium inoculated with one-single colony of the corresponding strain from a day-old LB-agar plate, and incubated overnight at 37 °C and 150 rpm. 2 x 60 mL of fresh LB broth was inoculated with 1 mL of overnight culture and incubated at 37 °C and 150 rpm (starting $OD_{600} \approx 0.1$) until reaching an $OD_{600} = 1.0$ for *P. aeruginosa*, or $OD_{600} = 0.6$ for *E. coli*. The bacterial cultures were centrifuged in 50-mL Falcon® tubes (9 min, 4500 x g, 20°C), the supernatant was removed, and the pellet was resuspended in 5 mL NaPi buffer to be again centrifuged under the same conditions. The supernatant was discarded and the pellet was resuspended in enough warm NaPi buffer to reach $OD_{600}= 5.0$. 100 µL of bacterial suspension was given per well into a MultiScreenHTS DV filter plate (transparent, pore size 0.45 µm) dampened with 2 µL NaPi buffer and the plate was incubated at 37°C for 5 min. At time points 0, 10, 20, 30, 40, 45, 48, and 50 min (which become 50, 40, 30, 20, 10, 5, 2 and 0 min incubation times, respectively), 25 µL of the respective antibiotic solution was added in the corresponding wells and mixed by pipetting three times up and down to give a final volume of 125 µL and a concentration of 200 µM. The filter plate was shaken at 350 rpm and 37°C in a ThermoMixer® C during antibiotic addition.

For the 50 min time point (0 min incubation time), 25 µL of antibiotic solution was added right before filtration The incubation was stopped by fast removal of the supernatant with a vacuum manifold (~15s) and the cells were washed twice with 100 µL of ice-cold NaPi buffer with the help of a Bravo Automated Liquid-Handling Platform. After every filtration, the filter plate was pressed against absorbent paper to remove the remaining liquid. The filter plate was placed on top of a 350-µL conical bottom receiver plate, and the pellets were resuspended in 100 µL of ice-cold 80% methanol-water. After that, the suspension was incubated for 30 min at 25°C and 450 rpm while sealed with Parafilm® and closed with a plate lid. Following the incubation step, the filter plate was centrifuged at 2250 x g for 5 min and the filtrate was collected in the receiver plate.

The cell debris was further extracted by resuspension in 100 µL of ice-cold acetonitrile before it was incubated for 30 min at 25°C and 400 rpm. The filtrate was then collected by centrifugation at 2250 x g for 15 min and then followed by evaporation using a centrifugal vacuum concentrator at 20°C coupled to a cold trap at -50°C. The dry remnants were

reconstituted in 100 µL of 50% acetonitrile-water containing 0.1% v/v formic acid and 10 ng/mL caffeine (for positive mode) and 50 ng/mL glipizide (for negative mode) as internal standards. The samples were subsequently measured with LC-MS/MS methods specific for each compound, were 1 µL of sample was injected to an UPLC-ESI-QQQ.

3.3.1.2 Uptake assay in round-bottom 96-well plates

Overnight cultures of *P. aeruginosa* or *E. coli* were prepared with 5 mL of LB medium inoculated with one-single colony of the corresponding strain from a day-old LB-agar plate, and incubated overnight at 37 °C and 150 rpm. 2 x 60 mL of fresh LB broth was inoculated with 1 mL of overnight culture and incubated at 37 °C and 150 rpm (starting $OD_{600} \approx 0.1$) until reaching an OD_{600} = 1.0 for *P. aeruginosa*, or OD_{600} = 0.6 for *E. coli*. The bacterial cultures were centrifuged in 50-mL Falcon® tubes (9 min, 4500xg, 20°C), the supernatant was removed, and the pellet was resuspended in 5 mL NaPi-MgCl$_2$ buffer to be again centrifuged under the same conditions. The supernatant was discarded and the pellet was resuspended in enough warm NaPi buffer to reach OD_{600}= 5.0. 600 µL of bacterial solution were distributed in a 1-mL round-bottom plate, and 50 µL of antibiotic solution were added at fixed times, and the plate was kept shaking at room temperature and 400 rpm. The plate was centrifuged at 2250 x *g* (maximum speed for the swinging-plate rotor centrifuge) and 4°C on a plate adapter to distribute the pellets closer to the wall than the bottom. With the help of a Bravo pipetting robot, the removal of the supernatant was carried out by introducing the tips from the opposite side of the wall to avoid disruption of the pellets. The bacterial pellets were washed once and centrifuged again for 15 min at 4°C to remove the supernatant. Right after, bacterial cells were disrupted with 200 µL of ice-cold 80% v/v MeOH in H$_2$O for 30 min at room temperature and 400 rpm, followed by a second extraction with 200 µL of ice-cold ACN for 30 min (total volume = 400 µL).

To remove cell debris and precipitated proteins, the plate was centrifuged for 45 min at 4 °C, and 200 µL of the supernatant was transferred to a clean, conical-bottom receiver plate. The solution was dried overnight in a centrifugal vacuum concentrator at 20°C coupled to a cold trap at -50°C. The remaining dried solids were reconstituted in 100 µL of LC-MS compatible solution (ACN:H$_2$O 1:1 + 0.1% v/v formic acid + 10 ng/mL of caffeine as internal standard) and analysed using the appropriate LC-MS/MS methods. The antibiotic concentration was calculated from standard curves.

3.3.2 LC-MS/MS compound-specific MRM methods

Multi-reaction monitoring methods (MRM) were developed for each of the analyzed compounds (see Table 3.12). The selected compounds were dissolved in MeOH to reach a concentration of 10 μg/mL and directly injected to an AB Sciex QTrap 6500 ESI-QQQ mass spectrometer at a constant flow rate of 10 or 20 μL/min.

Table 3.12 Optimized parameters of multi-reaction monitoring methods (MRM)

Compound	Retention time, RT (min)	Column temperature (°C)	Precursor ion m/z (Da)	Fragment ions m/z (Da)	Declustering potential,DP (V)	Entering potential, EP (V)	Collision energy, CE (V)	Cell exit potential, CXP (V)
Caffeine	2.14	30	195.116	138.1	66	10	27	10
				110.1	66	10	31	6
Ciprofloxacin	2.64	30	332.040	314.2	111	10	27	16
				231.2	111	10	49	12
Clindamycin	3.67	30	425.188	126.1	80	10	40	11
				377.3	80	10	20	11
Glipizide	5.19	30	443.900	319.1	-66	-10	-30	-21
				170.1	-66	-10	-40	-7
Lincomycin	1.86	30	407.222	126.2	80	10	31	6
				82.1	80	10	109.5	9.3
Nalidixic acid	4.92	30	233.200	215.1	80	10	19	14
				187.2	80	10	33	13
Novobiocin	5.49	30	613.200	189.3	80	10	45	13
				218.2	80	10	18	11
Phosphomycin	0.28	30	137.000	79.0	-80	-10	-35	-9
				62.9	-80	-10	-19	-9
Sulfamethoxazole	3.35	30	254.000	156.0	76	10	21	10
				108.0	76	10	29	8
Streptomycin	0.22	30	582.274	263.2	248	10	42.7	15
				246.2	248	10	50.6	12
Tetracycline	2.77	30	445.148	410.1	66	10	25	22
				427.1	66	10	15	30
Tigecycline	1.56	30	586.288	569.2	80	10	24	11
				513.3	80	10	64	11
Tobramycin	0.39	30	468.261	163.1	101	10	31	10
				324.3	101	10	19	24

A full scan in Q1 was performed to identify the molecular ion of each compound by manually optimizing the declustering potential (DP) in the orifice plate and keeping an entering potential (EP) of 10 V in positive mode, and -10 V in negative mode. The molecular ion (also precursor ion) was selected in the first quadrupole (Q1) for further ion fragmentation in the second quadrupole (Q2), and the resulting ions were scanned in the third quadrupole (Q3). To identify the two most abundant fragment ions, the collision energy (CE) and the cell exit potential (CXP) in Q2 were optimized for best sensitivity. The transition (Q1 → Q3) from the precursor ion to the first fragment ion is considered as the quantifier (used for calculations of peak area against concentration), and the transition to second fragment ion is considered as the qualifier (confirmation of the original analyte).

Samples and standard curves were injected (1 µL per sample) to a ZORBAX Eclipse Plus C18 reverse-phase column on an Agilent 1290 UPLC. The corresponding ion transitions, two for each compound and two for the internal standard, were monitored simultaneously (4 transitions in total) in AB Sciex QTrap 6500 ESI-QQQ mass spectrometer. Each run was recorded over 6 min with a constant flow rate of 700 µL/min and a gradient elution with eluent A (water with 0.1% v/v formic acid) and eluent B (acetonitrile with 0.1% v/v formic acid) as follows: 1% B for t = 0 min to t = 0.3 min, linear gradient from 1% B to 99% B from t = 0.1 min to t = 6 min, hold 99% B until t = 6.2 min and linear gradient from 99% B to 1% B from t = 6.2 min to t = 8 min.

3.3.3 Standard curves for antibiotic quantification

Standard curves were obtained by measuring predefined concentrations of antibiotics (see *Appendix I. Standard curves for uptake studies***Error! Reference source not found.**). The integrated peak area was then plotted over antibiotic concentration in µM or ng/mL, and a linear regression curve was performed by least squares regression. The amount of antibiotic in bacterial samples was determined on the basis of the regression curve and the sample volume (100 µL).

3.4 Untargeted metabolomics studies

3.4.1 Preparation of overnight culture and working culture

For overnight culture, 20 mL of freshly prepared BM2 in a non-baffled 50-mL flask was inoculated with a PA14 WT single-colony from a day-old LB agar plate. The culture was incubated overnight at 37°C shaking at 150 rpm. Before the preparation of working cultures, 10 mL of the overnight culture was transferred to a 50-mL Falcon™ tube and centrifuged at 5000 x g for 5 min. The supernatant was discarded and the pellet was washed with 1 mL of medium, and centrifuged again. The final pellet was resuspended in 10 mL of fresh BM2 medium reaching an optical density between 2.0 and 3.0.

Working cultures were prepared by transferring the required volume of BM2 to a clean, non-baffled 250-mL flask and inoculating it with medium to reach an $OD_{600} = 0.05$. For example, to prepare 100 mL of working culture, 97.5 mL of BM2 medium was mixed with 2.5 mL of bacterial solution with an $OD_{600} = 2.0$.

3.4.2 Metabolomics in deep-well filter plates

A non-baffled 250-mL flask containing 100 mL of working culture (initial $OD_{600} = 0.05$) was incubated at 37°C at 150 rpm until an $OD_{600} = 1.0$. Rapidly, 1 mL of a working culture was transferred to every well of a 96-well filter plate previously incubated at 37°C and with the bottom sealed with Parafilm plastic foil. 50 µL of antibiotic stocks dissolved in BM2 (see Table 3.8) was added to each well and mixed by pipetting up and down. In total, each condition had 9 replicates, including untreated controls with no antibiotics, and blank samples without bacteria as listed in Table 3.13. Blank samples were prepared by adding 1.05 mL of clean BM2.

Table 3.13 Samples for metabolomics studies in deep-well plates

Sample	Treatment	Replicates for analysis
CON	Untreated	6
CIPRO	Ciprofloxacin	6
LEVO	Levofloxacin	6
LOME	Lomefloxacin	6
AZI	Azithromycin	6
ERY	Erythromycin	6
CLARI	Clarithromycin	6
MERO	Meropenem	6
BLK	No bacteria	3

The plate was covered with a plate lid and located on a plate shaker at 400 rpm and 37°C. After 2 hours of incubation, the plate was filtered onto a vacuum manifold until no liquid remained (~ 3 min). Supernatants are not recovered with this method. The bacterial cells were washed immediately in 200 µL of ice-cold 0.9% m/v NaCl with an automated pipetting robot. The filter plate was pressed onto absorbent paper after every filtration to remove the excess of solution. Before cell lysis, the plate was placed onto a 300-µL conical-bottom receiver plate and its borders were sealed with Parafim. Both plates were kept on ice at all times.

Cells were lysed by resuspending them in 200 µL of ice-cold extraction solution (80% v/v MeOH with 0.1 µg/mL trimethoprim, 0.1 µg/mL glipizide and 0.1 µg/mL nortriptyline, as internal standards) with the pipetting robot. The solution was further homogenized twice by shaking for 1 min at 600 rpm in a plate shaker, followed by 10 min sonication (100% intensity and 0°C) in an ice-cold water bath. To collect the extract, the plates were centrifuged at 2250 x g and 4°C for 20 min, the filter plate was discarded and the contents of the receiver plate were dried overnight in a centrifugal vacuum concentrator at 20°C coupled to a cold trap at -50°C. The remaining dried solids were reconstituted in 30 µL of LC-MS compatible solution (80% v/v MeOH with 1 µg/mL caffeine and 1 µg/mL naproxen, as internal standards), and the plate was centrifuged at 2250 x g and 4°C for 20 min. 25 µL was transferred to brown glass vials with inserts for LC-MS/MS untargeted analysis.

3.4.3 Metabolomics in test tubes

3.4.3.1 Short and long exposure to antibiotic concentrations

Both short- and long-exposure treatments were carried out under the same experimental configuration (see Table 3.14). 150 mL of working culture with initial OD_{600} = 0.05 was prepared in a non-baffled 250-mL flask. 3 mL of the working culture were transferred to 10-mL glass test tubes, previously labeled for short and long exposure. For the long-exposure samples, 100 µL of the antibiotic stocks dissolved in BM2 (see Table 3.9) were added to the test tubes in triplicates at an initial OD_{600} = 0.05. Immediately after, all the tubes were incubated in an inclined rack at θ = 60°, 150 rpm and 37°C indistinctively of the label. When an OD_{600} = 0.5 was reached in the tubes labeled as short exposure, 100 µL of the antibiotic stocks dissolved in BM2 were added to the test tubes in triplicates. All the tubes continued shaking until an OD_{600} = 1.0. Untreated controls were prepared by incubating 3 mL of the working culture without addition of any solution. Blank samples were prepared by adding 3-mL of fresh BM2 medium to the tubes.

Table 3.14 Samples short and long exposure to antibiotics in test tubes

Sample	Treatment	Replicates for long exposure	Replicates for short exposure
CON	Untreated	3 for both long and short exposure	
CIPRO	Ciprofloxacin	3	3
LEVO	Levofloxacin	3	3
AZI	Azithromycin	3	3
ERY	Erythromycin	3	3
GENTA	Gentamycin	3	3
TOBRA	Tobramycin	3	3
BLK	No bacteria	3 for both long and short exposure	

3.4.3.2 Sub-inhibitory concentrations

For each strain, PA14 WT and PA14 gyrAparC, 100 mL of working culture with initial OD_{600} = 0.05 was prepared in a non-baffled 250-mL flask. 3 mL of the working culture were transferred to 10-mL glass test tubes. 100 µL of the antibiotic stocks dissolved in BM2 were added to the test tubes at an initial OD_{600} = 0.05 to reach the desired concentration (see Table 3.10). One blank sample for each antibiotic was generated by adding 3-mL of fresh BM2 medium to 3 tubes. All the tubes were incubated in an inclined rack at θ = 60°, 150 rpm and 37°C until an OD_{600} = 1.0.

Table 3.15 Samples for metabolomics studies upon sub-inhibitory concentrations

Sample	Treatment	Replicates for PA14 WT	Replicates for PA14 gyrAparC
CON	Untreated	3	3
NIC	Non-inhibitory	3	3
IC10	10% inhibition	3	3
IC50	50% inhibition	3	3
MIC	No growth (in plates)	3	3
BLK	No bacteria	3	3

3.4.3.3 Harvest and storage

From every test tube, 2 mL of bacterial solution were transferred to 2-mL Eppendorf tubes, previously labeled and kept on an ice bath. The tubes were centrifuged at 9000 x g for 5 min at 4 °C, transporting them in an ice bath at all times. 1 mL of the supernatants was transferred to labeled, clean Eppendorf tubes and the rest was discarded. The supernatants were submerged in liquid nitrogen and stored at -70°C until needed. The pellets were washed once in 1 mL ice-cold 0.9% NaCl by adding the solution to the tube and vortexing for 1 min (maximum speed). Pipetting up and down was avoided, so that fractions of the pellet did not stick to the

tips. The tubes were centrifuged again (9000 x g, 5 min, 4°C), and the supernatant was discarded. The tubes containing the washed pellets were submerged in liquid nitrogen and stored at -70°C until needed for metabolite extraction.

3.4.3.4 Intrametabolome extraction

Cells were lysed by adding 1 mL of ice-cold extraction solution (80% v/v MeOH with 0.1 μg/mL trimethoprim, 0.1 μg/mL glipizide and 0.1 μg/mL nortriptyline, as internal standards) in every sample. Pipetting up and down was avoided, so that fractions of the pellet did not stick to the tips. The solution was further homogenized twice by vortexing for 1 min (maximum speed), followed by 10 min sonication (100% intensity and 0°C) in an ice-cold water bath.

The tubes were centrifuged at 9000 x g for 5 min at 4 °C, transporting them in an ice bath at all times. 900 μL from each tubes was transferred to labeled, clean Eppendorf tubes and the rest was discarded. The contents of the tubes were dried overnight in a centrifugal vacuum concentrator at 20°C coupled to a cold trap at -50°C. The remaining dried solids were reconstituted in 100 μL of LC-MS compatible solution (50% v/v ACN in water with 1 μg/mL caffeine and 1 μg/mL naproxen, as internal standards), and the tubes were centrifuged at 10000 x g, and 4°C for 20 min. 50 μL was transferred to brown glass vials with inserts for LC-MS/MS untargeted analysis.

3.4.3.5 LC-MS/MS untargeted analysis

Replicates were analyzed on a Dionex Ultimate 3000 UPLC using a 150 mm Kinetex C18 reverse phase column with 1.7 μm particle size and 2.1 mm inner diameter coupled to a maXis™ HD QTOF mass spectrometer.

Full scans (50–1500 Da) were recorded in positive mode ESI, data-dependent MS/MS was performed by collision-induced dissociation of the five most abundant ions. Each run was recorded over 30 min with a constant flow rate of 300 μL/min and a gradient elution with eluent A (water with 0.1% v/v formic acid) and eluent B (acetonitrile with 0.1% v/v formic acid) as follows: 1% B for t = 0 min to t = 2 min, linear gradient from 1% B to 100% B from t = 2 min to t = 20 min, hold 100% B until t = 25 min and linear gradient from 100% B to 1% B from t = 25 min to t = 30 min.

3.5 Data processing and analysis

3.5.1 Uptake data

The analysis of chromatogram peaks from samples and standard curves was performed automatically in MultiQuant™ 2.0 for each MRM. Manual determination of the peak area was performed when required. The peak table was exported and the scatter plots for antibiotic uptake and dose-response curves were plotted in SigmaPlot 14.0.

3.5.2 LC-MS/MS data processing with XCMS Online

Raw data in mzXML format were processed in positive mode and negative mode with XCMS Online for feature detection and retention time alignment across samples. XCMS Online built-in CAMERA algorithm was selected to annotate isotopic features and adducts formations, dimers, trimers, neutral losses (for the settings, refer to Table 3.16). The generated feature tables were further processed with R (3.6.1) in RStudio.

Table 3.16 XCMS Online settings for raw data processing

Description	Name	Value
Maximal tolerated m/z deviation in consecutive scans (parts per million)	ppm	8
Minimum chromatographic peak width (s)	minimum peak width	5
Maximum chromatographic peak width (s)	maximum peak width	25
Minimum difference in m/z for peaks with overlapping retention time	mzdiff	0.0155
Signal-to-noise threshold	Signal/Noise threshold	30
Peak integration method	Integration method	1 (Mexican hat filter)
Minimum number of peaks for retention of mass traces	prefilter peaks	3
Peak intensity threshold	prefilter intensity	400
Noise threshold	Noise filter	100
Step size for profile generation of raw data	profStep	1
Retention time deviation (s)	bw	20
Minimum fraction of samples necessary in a group for it to be a valid group	minfrac	0.4
Width of overlapping m/z slices for grouping peak areas across samples	mzwid	0.026
Minimum number of samples in one of the sample groups for it to be a valid group	minsamp	1
Maximum number of groups to identify in a single m/z slice	max	50
Isotopic peak annotation and adduct formations		
Ppm error	ppm	8
Absolute error	m/z abs error	0.015
Identification with online database	Biosource	PAMBD
Pathway deviation		5
Significant list p-value cutoff		0

3.5.3 LC-MS/MS data processing with XCMS R package

Raw data in mzXML format were processed with the R-package for XCMS, and a feature table with MS1 information was generated (for the settings, refer to Table 3.17).

Table 3.17 Parameters for raw data processing with R-based XCMS

Function	Parameter	Value
readMSData()	centroided	TRUE
findChromPeaks() / CentWaveParam()	ppm	8
	peakwidth	c(5,25)
	noise	400
	snthresh	30
	integrate	1
	mzdiff	0.0155
	prefilter	c(2,1000)
	fitgauss	FALSE
adjustRtime() / ObiwarpParam()	binSize	0.1
peakDensityParam()	minFraction	0.6
	binSize	0.1
	bw	20
peakGroupsParam()	minFraction	0.6
	span	1
	smooth	loess
fillChromPeaks() / FillChromPeaksParam()	fixedRT	medwidth_rt
featureValues()	value	into

3.5.4 Feature table processing

3.5.4.1 Isotope filtering

Feature filtering was carried out by refining isotopic ion peaks annotated by CAMERA from the feature list. The features with isotopic labels and their multiple charges were filtered out, i.e. [M+1]+ to [M+4]+, [M+1]2+ to [M+4]2+, and [M+1]3+ to [M+4]3+. The resulting filtered feature table contained singly- and multiply-charged molecular ions [M], including dimers, trimers and multiple adduct formation, as well as not annotated isotopic ions.

3.5.4.2 Retention time cutoff

Retention time (RT) cutoff was applied to filter features coming from the injection peak (first minute of each run) and features coming from the column washing (last 5 min of each run). Therefore, a filter of $0.3 \leq RT \leq 28$ min was applied.

3.5.4.3 Normalization by internal standards

Signal normalization by internal standards (ISTDs) in positive mode was applied by calculating two consecutive normalization factors, one for injection standards (caffeine and naproxen) and

the other for extraction standards (trimethoprim and glipizide, but not for nortriptyline as it is better ionized in negative mode). First, a normalization factor for caffeine and naproxen was calculated for each feature *i* (*rows*) with the formulas:

$$norm\_factor_{caffeine,i} = \frac{max\ intensity_{caffeine}}{intensity_i}$$

$$norm\_factor_{naproxen,i} = \frac{max\ intensity_{naproxen}}{intensity_i}$$

A normalization factor for the injection standards was calculated as follows:

$$norm\_injection_i = \frac{norm\_factor_{caffeine,i} + norm\_factor_{naproxen,i}}{2}$$

Then, the intensity matrix with *n* features and *m* samples was processed as follows, for every feature in *i = 1* to *n*, and sample in *j = 1* to *m*:

$$norm\_feature\ intensity_{i,j} = feature\ intensity_{i,j} * norm\_injection_i$$

Subsequently, a norm factor for trimethoprim, glipizide was calculated as follows:

$$norm\_factor_{trimethoprim,i} = \frac{max\ intensity_{trimetoprim}}{intensity_i}$$

$$norm\_factor_{glipizide,i} = \frac{max\ intensity_{glipizide}}{intensity_i}$$

And a normalization factor for the extraction standards was calculated as follows:

$$norm\_extraction_i = \frac{norm\_factor_{trimethoprim,i} + norm\_factor_{glipizide,i}}{2}$$

Finally, the intensity matrix with *n* features and *m* samples was processed as follows, for every feature in *i = 1* to *n*, and sample in *j = 1* to *m*:

$$norm\_feature\ intensity_{i,j} = feature\ intensity_{i,j} * norm\_extraction_i$$

3.5.4.4 Normalization by optical density

Similarly, normalization by the OD_{600} value at harvest of each sample *j* (columns) was performed for every strain as follows:

$$ODnorm\_factor_{strain,j} = \frac{max\ OD_{strain}}{OD_j}$$

Where $max\ OD_{strain}$ is the maximum OD_{600} value at harvest of the respective strain: WT or gyrAparC. The intensity matrix with *n* features and *m* samples was processed as follows, for every feature in i = 1 to n, and sample in j = 1 to m:

$$norm\_feature\ intensity_{i,j} = feature\ intensity_{i,j} * ODnorm\_factor_{strain,j}$$

3.5.4.5 Quantile normalization

Only for the metabolomics experiments in filter plates, a quantile normalization was carried out by using function normalizeBetweenArrays() with the method "quantile" from the R package "limma". The feature table used for quantile normalization was not subjected to any other precedent or subsequent normalization.

3.5.4.6 Addition of an offset value

After signal normalization, the data were log2 transformed. However, log2 cannot be applied to zero values. Therefore, a value of 50 was added up to all the intensity values from *n* to *m*, as a rule of thumb. By increasing the offset to 50 total counts, the zero values were filled up, and the natural distribution of the data was not modified.

3.5.4.7 Removal of internal standard intensities

After the previous steps of feature table processing were carried out, the intensities of all five features corresponding to the ISTDs were deleted from the feature table within the same R script. The rest of identified m/z adducts from the ISTDs were removed manually (see 3.5.5.5 Manual refinement).

3.5.4.8 Fold change and p-value calculation

The mean values of the log2-transformed intensity were calculated for each sample group. For fold change calculation, the mean value of the untreated control samples was subtracted from each of the mean value of the remaining groups, so that a positive value is attributed to up-regulation and a negative value is attributed to down-regulation. For p-value calculation, pairwise comparisons between sample groups were performed through T-tests in R with the function pairwise.t.test().

3.5.5 Feature identification

3.5.5.1 MS/MS annotation

Bruker MetaboScape 4.0 was used to process raw data and generate an MS/MS identified feature table with the use of two *in-house* libraries, one specific for *P. aeruginosa* (with 45 entries) and a general one (with 559 entries), as well as commercial libraries such as LipidBlast (with 14048 entries) and MetaboBase (with 482025 entries). For this purpose, a bucket table in positive mode was generated from the raw data files of all the samples of the experiment (for settings, refer to Table 3.18).

The resulting bucket table was exported. To combine the newly generated bucket table with the preprocessed XCMS Online feature table, they were matched by retention time and m/z. Firstly, the values for maximum and minimum retention time and m/z values were calculated for every MetaboScape bucket k, using an m/z tolerance of ± 8 ppm, and a retention time constrain of ± 25 s:

$$max\ m/z_k = (1 + ppm) * m/z_k$$

$$min\ m/z_k = (1 - ppm) * m/z_k$$

$$max\ RT_k = RT_k + 25$$

$$min\ RT_k = RT_k - 25$$

Then, every row of the processed feature table i was compared against the maximum and minimum values of each MetaboScape feature k, and the MetaboScape identification label was copied to the feature table only when:

$$min\ m/z_k \leq m/z_i \leq\ max\ m/z_k$$

and

$$min\ RT_k \leq RT_i \leq\ max\ RT_k$$

Table 3.18 Parameters for the generation of bucket table with MetaboScape 4.0

Parameter	Value	Parameter	Value
ferraWorkflow_minCorrelation	0.8	ferraWorkflow_enableMsmsExtraction	true
ferraWorkflow_lockMass	622.02896	ferraWorkflow_minNumClusters	1
ferraWorkflow_GroupFeatures_rtDelta	10	ferraWorkflow_uffMinClusterSize	2
ferraWorkflow_chargeMax	3	processingWorkflowId	Ferra3d
ferraWorkflow_rtMaxInSeconds	1680	polarity	POSITIVE
ferraWorkflow_ForeachAnalysisMsms_MsmsExtractionWorkflow_ConsolidateMsmsPeaklists_method	average	exclusionMassList	[622.02896]
msmsExtractionCompassResult_fillNonDeconvolutedValue	0	exclusionMassListTolerance	5
ferraWorkflow_substanceClass	small molecules	exclusionMassListToleranceUnit	mDa
ferraWorkflow_rtMinInSeconds	21	Deconvolution.eicCorrelation	0.8
ferraWorkflow_ForeachAnalysis_FeatureFinder_ClusterDeisotoping_featureIntervalMethod	FWHM	persistOnlyConsensusIsotopePattern	false
ferraWorkflow_seedIntensityThreshold	400	Deconvolution.primaryIon	[M+H]+
ferraWorkflow_enableLockMass	true	sampleGroupFilter	Treatment
ferraWorkflow_useIsotopePatternCoverage	false	sampleGroupFilterType	ABSOLUTE
ferraWorkflow_ForeachAnalysisMsms_MsmsExtractionWorkflow_MsmsDeisotoping_relativeAbundanceThreshold	0.005	sampleGroupPresenceFilterValue	2
ferraWorkflow_targetedExtractionMinClusterSize	4	nupfParameterProviderId	processing-results-mcube-ferra-parameter-provider
ferraWorkflow_maxClusterOverlap	0.1	nupfTimeStamp	1.565E+12
ferraWorkflow_ForeachAnalysisMsms_MsmsExtractionWorkflow_ConsolidateMsmsPeaklists_groupByCollisionEnergy	true	nupfWorkflowVersion	3.4
ferraWorkflow_mzMin	50	nupfOriginId	78259a3c-3940-4e21-b56a-2015489d1365
ferraWorkflow_ForeachAnalysis_FeatureFinder_ClusterDeisotoping_areaCalculationScale	0.2	nupfOriginType	bruker.bsf.mcube.server.entity.BucketTable
ferraWorkflow_minExistFraction	0.55	Deconvolution.seedIons	[M+Na]+, [M+K]+, [M+NH4]+
ferraWorkflow_CreateRecursiveTargets_threshold	15	Deconvolution.commonIons	[M-H2O+H]+, [M-H2O+Na]+, [M-CO2+H]+, [M-NH3+H]+
ferraWorkflow_ForeachAnalysisMsms_MsmsExtractionWorkflow_MsmsDeisotoping_proteomics	true	ferraWorkflow_CreateBatchFeatures_minGroupSize	24
msmsExtractionCompassResult_fillStrategy	topN	ferraWorkflow_minCorrelatedFraction	0.55
ferraWorkflow_uffMinSeedClusterSize	9	ferraWorkflow_mzMax	1500
ferraWorkflow_maxIsotopePatternError	0.2	ferraWorkflow_areaIntensity	true

3.5.5.2 Exact mass identification by XCMS Online

XCMS Online provides a preliminary feature identification by matching the exact mass of the feature table with a predefined database (*biosource*, see Table 3.16). As a result, a tentative match table is generated with m/z values, compound ID, m/z difference, matched adduct, and the corresponding pathway. This matching list contains several doubles, meaning that the same exact mass matched with more than one metabolite in the database.

The XCMS Online tentative matches were compared against the processed feature table fitting their exact masses. Firstly, the values for maximum and minimum m/z values were calculated for every tentative match *l*, using an m/z tolerance of ± 8 ppm:

$$max\ m/z_l = (1 + ppm) * m/z_l$$

$$min\ m/z_l = (1 - ppm) * m/z_l$$

Then, every row of the processed feature table *i* was compared against the maximum and minimum values of each tentative match *l*, and the tentative identification label was copied to the feature table only when:

$$min\ m/z_l \leq m/z_i \leq max\ m/z_l$$

Several matches in the tentative matching for the same feature *i* were expected. So the value with the lowest mass difference was preferred. For this reason, systematic manual validation of exact mass matching was later carried out for the features of interest.

3.5.5.3 Spectral similarity clustering with GNPS

Spectral similarity among the features was found via an online-based GNPS Molecular Networking tool. This tool detects sets of spectra from related molecules (molecular networks), even when the spectra themselves are not matched to any known compounds in the built-in libraries.

The mzXML files for the triplicates of WT_CON, WT_IC50, gyrAparC_CON and parC_IC50 were processed with the following parameters: precursor ion mass tolerance = 0.01 Da, and fragment ion mass tolerance = 0.05 Da. The option for filtering peaks in 50 Da was not applied. The rest of the settings were kept as default. The processed data was visualized with Cytoscape (3.7.2), and an identified feature table was obtained.

The GNPS features where matched against the processed feature table by retention time and exact mass. Firstly, the values for maximum and minimum retention time and m/z values were

calculated for every GNPS feature g, using an m/z tolerance of ± 8 ppm, and a retention time constrain of ± 25 s:

$$max\ m/z_g = (1 + ppm) * m/z_g$$

$$min\ m/z_g = (1 - ppm) * m/z_g$$

$$max\ RT_g = RT_g + 25$$

$$min\ RT_g = RT_g - 25$$

Then, every row of the processed feature table i was compared to the maximum and minimum values of each GNPS feature g, and the GNPS identification label was copied to the feature table only when:

$$min\ m/z_g \leq m/z_i \leq max\ m/z_g$$

and

$$min\ RT_g \leq RT_i \leq max\ RT_g$$

3.5.5.4 Spectral similarity clustering with CluMSID

Spectral similarity was performed with the R package CluMSID. CluMSID computes the cosine distance among MS/MS spectra and determines the spectral similarity of features within one single sample. Therefore, a convenient pooled (gyrAparC_CON or gyrAparC_IC50) sample was used for the analysis.

The CluMSID features were matched against the processed feature table by retention time and exact mass. Firstly, the values for maximum and minimum retention time and m/z values were calculated for every CluMSID feature h, using an m/z tolerance of ± 8 ppm, and a retention time constraint of ± 25 s.

$$max\ m/z_h = (1 + ppm) * m/z_h$$

$$min\ m/z_h = (1 - ppm) * m/z_h$$

$$max\ RT_h = RT_h + 25$$

$$min\ RT_h = RT_h - 25$$

Then, every row of the processed feature table i was compared to the maximum and minimum values of each CluMSID feature h, and the CIMSID identification label was copied to the feature table only when:

$$min\ m/z_h\ \leq m/z_i \leq\ max\ m/z_h$$

and

$$min\ RT_h\ \leq RT_i \leq\ max\ RT_h$$

3.5.5.5 Manual refinement

Manual identification refinement was performed to fully integrate the described identification tools. The exported MetaboScape feature table did not contain the MS/MS annotated adducts that were otherwise visible in MetaboScape software. Additionally, spectral data were visualized with Bruker Compass DataAnalysis 4.2, and theoretical isotope distributions for proposed sum formulas were simulated with Bruker Compass IsotopePattern.

3.5.6 Data visualization methods

3.5.6.1 PCA

An eigendecomposition of the scaled and log2-transformed data was carried out by the function prcomp() in R . The scores (eigenvalues) of the first two principal components (eigenvectors) were projected for every sample in a PCA plot. The explained variance for each principal component is a measure that represents how much information (variance) can be attributed to each principal component.

3.5.6.2 Correlation matrix and heat maps

The correlation matrix was generated by calculating the correlation of the scaled and log2-transformed data with cor() in R. For visualization purposes, the values of 1-cor() were plotted instead of the correlation values.

3.5.6.3 U-plots

The feature table was separated in WT samples and gyrAparC samples. For each new data set, a correlation test was performed with the function cor.test() in R by comparing every row against the corresponding to ciprofloxacin. The method used for the correlation test was

"*spearman"* and the data were previously center scaled. The correlation of each feature was plotted against their respective p-value. For visualization purposes, the p-values from the correlation test were log10-transformed.

3.5.6.4 Bar plots and box plots

Bar plots were generated in R Studio by plotting features with Spearman correlation higher than 0.5 and lower than -0.5. Box plots were also generated in R Studio. The significance with respect to the control samples was plotted on the top of each box plot as follows: *** for p-value ≤ 0.001, ** for 0.001 < p-value ≤ 0.01, * for 0.01 < p-value ≤ 0.05, no asterisk for p-value > 0.05.

4. ANTIBIOTIC UPTAKE

4.1 Medium-high throughput assay for antibiotic uptake

The present work describes the implementation of a medium-high throughput assay for the screening of compound accumulation in bacteria. In its current state, the assay is transferable to different strains, including Gram-negative bacteria, such as *P. aeruginosa* or *E. coli*, and Gram-positive bacteria, such as *S. aureus*.

Until recently, experimental setups in LC-MS/MS-based uptake studies have always been carried out in the common lab-scale of approx. 20-50 mL (Bhat et al. 2013; Heumann 2015). Some approaches have reduced the working volumes in order to handle more samples at a time (Schumacher et al. 2006; Richter et al. 2017; Prochnow et al. 2018; Iyer et al. 2018). Few studies have implemented higher throughput assays in this direction (Cai et al. 2009; Widya et al. 2019).

In order to increase the throughput of a previously described assay for ciprofloxacin (Heumann 2015), the working volumes were reduced from 20 mL to 100 μL. Reducing working volumes of the bacterial solution implies that the amount of cells is also reduced, decreasing the signal of the compound after the workflow. Thus, cell density was necessarily increased to compensate for the miniaturization of the geometry (Figure 4.1).
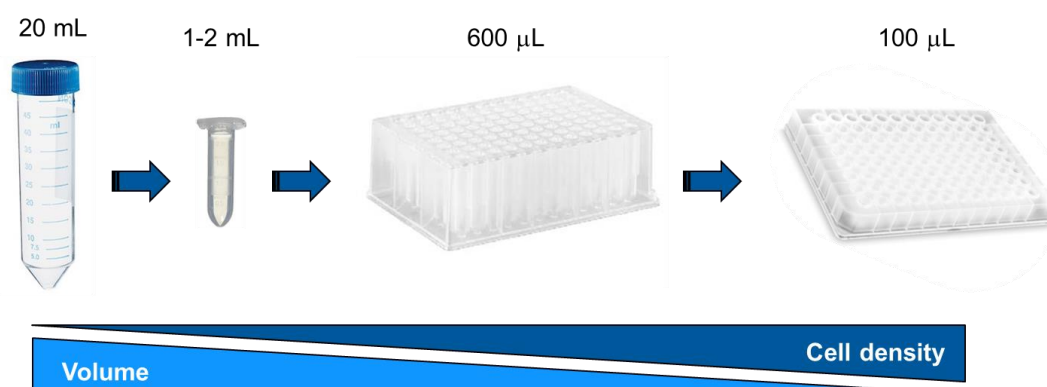
Figure 4.1 Scheme of volume reduction needed to increase the throughput in the uptake assay

4.1.1 Uptake assay in deep-well plates

In the first attempts to achieve a higher throughput assay, the configuration of a 96-well plate with a capacity of 1 mL per well was chosen. In brief, 600 µL of bacterial solution at $OD_{600} =$ 5.0 was distributed in each well of the plate. Bacterial cells were incubated with antibiotics for 10 min before centrifugation and removal of supernatant with a pipetting robot. To remove the totality of the supernatant and to avoid pellet disruption, the plate was centrifuged onto an adapter to force the bacterial cells to pellet far from the well bottom and closer to the wall, so that the pipetting robot aspirates the supernatant from the opposite side of the well (Figure 4.2). The pellets were washed once with buffer and lysed with an organic solvent mixture, to extract the internalized compound. The solution was then further processed to measure the amount of accumulated compound (see 3.3.1.2 Uptake assay in round-bottom 96-well plates).
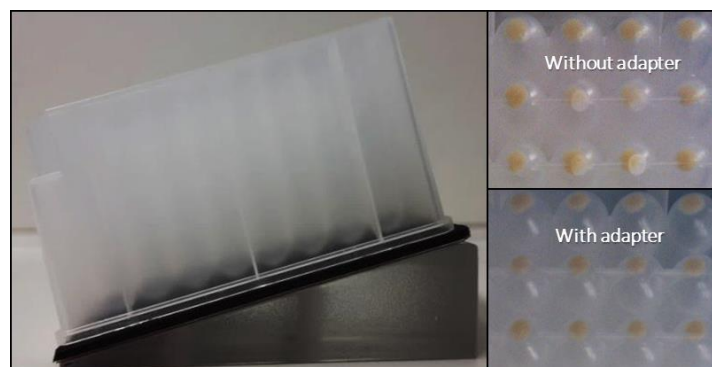
Figure 4.2 Plate adapter for the uptake assay in deep-well round-bottom plates.The plate is centrifuged onto the adapter at an angle of 15° in a bucket centrifuge

One limitation of this procedure is the extended centrifugation times to achieve stable bacterial pellets that are not easily disturbed when aspirating the supernatant. Several trials to reduce the centrifugation times were performed (from 10 to 5 min), but the pellets were partially disturbed with the pipetting robot even at low aspiration speeds (100 µL/min), or by decanting the contents of the plate upside down and removing the excess of liquid with absorbent paper.

The optimal centrifugation time was 15 min for *E. coli*, and 25 min for *P. aeruginosa*, resulting in dead times of 30 to 50 min before the extraction of the internalized compound. Therefore, the time-resolved accumulation of compounds during the first minutes of the incubation is not possible to determine.

In principle, the protocol in deep-well plates allows for the determination of the steady-state concentration of the accumulated compound. However, some results in β-lactam accumulation

show that the measured accumulation after 10 min incubation was lower than the proposed control at 0 min before centrifugation (Figure 4.3). This is an indication that, for some compounds, the concept of steady-state concentration might not hold true.
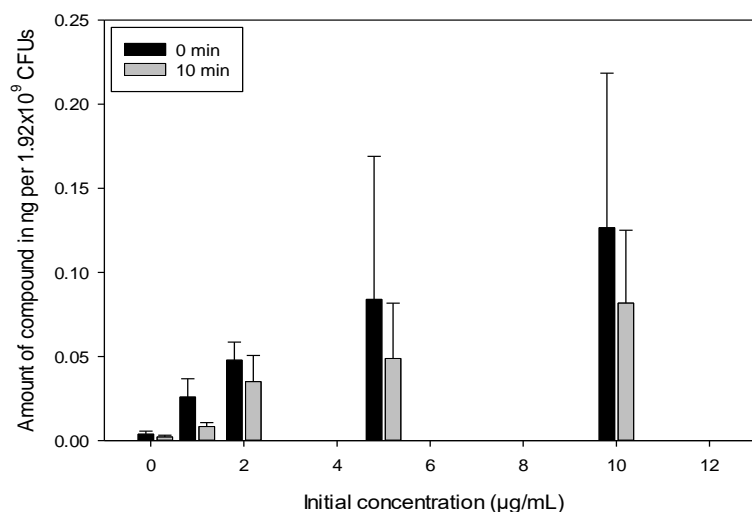
Figure 4.3 Meropenem uptake in *E. coli* BW25113 wild type after 0 and 10 min incubation at 37°C in NaPi buffer, and washed once with Napi buffer (2x15 min centrifugation at 2250 rpm and 4°C).The bars represent the average values of the three replicates and the standard deviation is represented with the error bars

Although this protocol allows the observation of the steady-state concentration of antibiotics, it will not be useful for time-resolved assays. Thus, a filter plate assay was developed for depicting time-course accumulation profiles.

4.1.2 Uptake assay in filter plates

In order to improve the dead times in the uptake assay, a workflow optimized for filter plates was developed. In brief, 100 µL of bacterial solution at OD_{600} = 5.0 was distributed in each well of the filter plate. Antibiotic solutions were added at different time points, and the incubation was stopped by the fast filtration of the solution (~15 s). The filtered bacteria were washed twice with fresh buffer with a pipetting robot. To extract the internalized compound, the pellets were lysed with an organic solvent mixture. The solution was then further processed to measure the amount of accumulated compound (see 3.3.1.1 Uptake assay in 96-well filter plates).

4.1.2.1 Selection of filter plates

In order to optimize the assay outcome, the appropriate pore size of the filter plate was selected to optimize the filtration time, while keeping the number of bacteria passing through the filter low. Table 4.1 lists some commercially available filter plates, and the experimentally determined filtration times required to filtrate 100 - 600 µL of cultures of *P. aeruginosa* at OD = 5.0. In this selection, a filter plate with a pore size of 1.2 µm was included to compare the efficiency of filtration, although it was considered as too large because bacteria may pass through it.

Table 4.1 Comparison of filtration performance among a set of filter plates

Plate description	Pore size (µm)	Vacuum pressure (inHg)	Filtered volume (µL)	Cells per well (CFU)	Filtration time
Millipore GV, hydrophilic low protein binding Durapore®	0.22	5 - 10	100	3.5×10^8	> 5 min
Millipore HTS hydrophobic high protein binding Immobilion P®	0.45	5 -10	100	3.5×10^8	> 5 min
AcroPrep™ Supor®	0.45	20-25	100	3.5×10^8	1-3 min
AcroPrep™ Supor®	0.45	20-25	600	1.3×10^9	> 5 min
AcroPrep™ Advance PTFE solvent resistant membrane	0.45	20-25	100	3.5×10^8	N.A.
MultiScreen$_{HTS}$-DV	0.45	20-25	100	3.5×10^8	~ 15 s
MultiScreen$_{HTS}$-DV	0.65	20-25	100	3.5×10^8	~ 10 s
AcroPrep™ Supor®	1.2	20-25	100	3.5×10^8	35 s
AcroPrep™ Supor®	1.2	20-25	200	3.5×10^8	2 min

The plate with the smallest pore size of 0.22 µm took the longest, more than 5 min, to filtrate 100 µL of solution, while the plate with the largest pore size of 1.2 µm took 35 s to filtrate the same volume. The best filtration times were achieved by filtrating 100 µL with MultiScreen$_{HTS}$-DV filter plates with pore sizes of 0.45 and 0.65 µm.

To check whether the filters effectively retained bacteria, a plate containing 100 µL of the bacterial solution at OD_{600} = 5.0 without antibiotics was centrifuged for 30 min, and the filtrate was collected onto a receiver plate. The filtrated solutions were spot-plated onto an LB-agar plate. As shown in Figure 4.4, the number of *P. aeruginosa*'s CFUs after filtration though a 0.45-µm filter plate reduced drastically as compared to a 0.65-µm filter plate. The CFUs after filtration of *E. coli* and *S. aureus* were also reduced. Thus, the filter plate of choice of the HT screening was the MultiScreen$_{HTS}$ DV 0.45 µm filter plate, as it allowed the fastest filtration and better cell retention, providing the assay with strain transferability for further screening studies.

	P. aeruginosa	*E. coli*	*S. aureus*
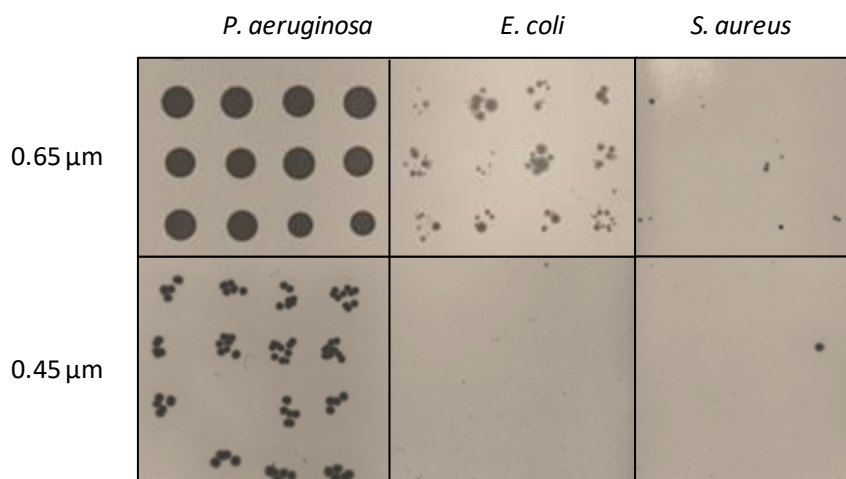
Figure 4.4 Remaining colonies in the filtrated solution after centrifugation of 100 µL of bacterial solutions at OD_{600}= 5.0 onto a receiver plate through MultiScreenHTS DV filter plates with a pore size of 0.65 µm and with 0.45 µm
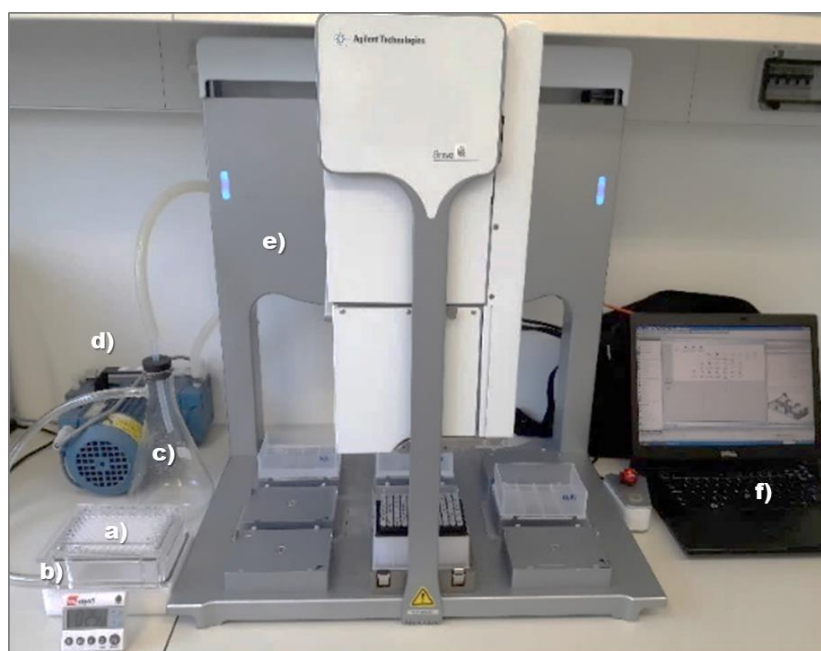
Figure 4.5 Experimental setup for fast filtration and efficient washing of bacterial cells after incubation: a) filter plate, b) vacuum manifold, c) filtrate trap, d) vacuum pump, e) automatic pipetting robot, f) PC to control the automated pipetting workflow.

Figure 4.5 displays the experimental setup used for fast filtration assisted by a Bravo pipetting robot. The physical proximity of the vacuum manifold to the pipetting robot enables the user to stop the incubation and to add the lysis solvent in approx. two minutes, including the time for removing the supernatant and washing the cells twice. As a result, the dead times before extraction of the internalized compound reduced drastically from 30-50 min with deep-well plates, to 1-2 min with filter plates.

4.1.2.2 Assurance of bacterial cells intactness

Another important aspect of the assay is to guarantee that the concentration used for uptake measurements does not compromise the intactness of the bacterial cells throughout the workflow – especially if potent, bactericidal antibiotics are tested. Determining bacterial viability gives an indication of their survival to antibiotic treatment after the exposure.

For this purpose, bacterial cells were incubated for one hour with a gradient of antibiotic concentrations under the same conditions as for uptake studies, serially diluted with fresh buffer and spot-platted on LB-agar plates to assay viability (Figure 4.6). Thus, the highest antibiotic concentration for uptake studies is the one that does not decrease the number of CFUs. In this example, *P. aeruginosa* at an OD = 5.0 tolerates a concentration up to 0.8 µg/mL of ciprofloxacin without compromising viability, while meropenem concentrations could go up to 100 µg/mL.
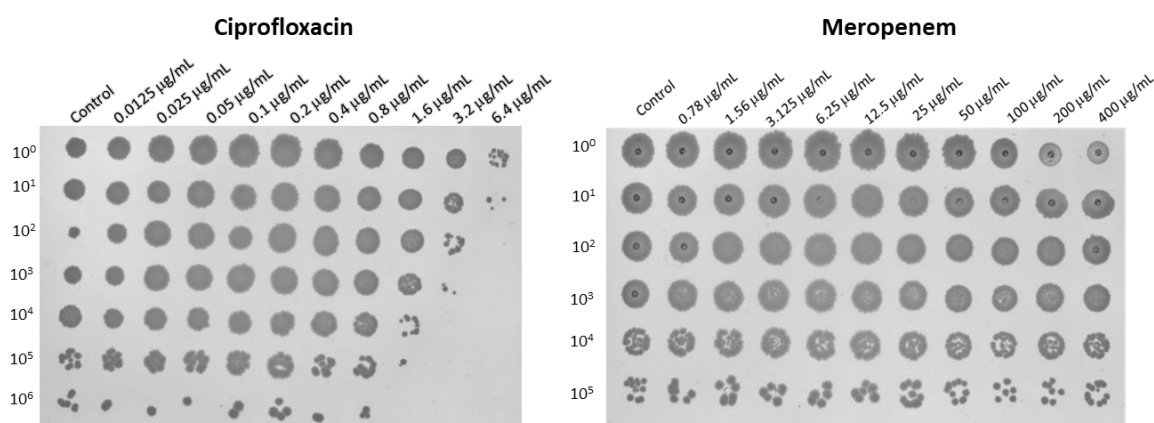
Figure 4.6 Colonies of *P. aeruginosa* after being treated for 1 h with a gradient concentration of ciprofloxacin (left) and meropenem (right). The first row was serially diluted downwards in a plate, and 2 µL of each well was spot-plated in an LB agar plate and incubated for 24 h at 37°C

4.1.2.3 Time-course accumulation profiles

Monitoring the compound accumulation over exposure time poses a dynamic advantage over fixed-time analysis. Unlike single time-point analysis, time-course accumulation studies provide information on the first cell-compound interactions, the possible saturation points and the possible modifications of the compound once internalized.

This assay seems capable of showing the dynamic process of antibiotic accumulation (depicted in Figure 4.7). When exposed to an initial concentration of 100 ng/mL, *P. aeruginosa* accumulates ciprofloxacin increasingly during the first 10 min, reaching a plateau at 0.05 ng per well containing 2.1×10^8 CFUs. When bacterial cells were incubated with CCCP for 5 min

before incubation with ciprofloxacin, the accumulated amounts of ciprofloxacin increased drastically by more than 5-fold (see Figure 4.7a). The depolarization of the membrane by CCCP has been previously employed as a control for enhanced uptake (Piddock and Johnson 2002). This increased accumulation is comparable to the profile of 200 ng/mL as initial concentration (Figure 4.7b). This curved profile is characteristic of ciprofloxacin and it was described extensively before (Piddock 1991; Piddock and Johnson 2002).
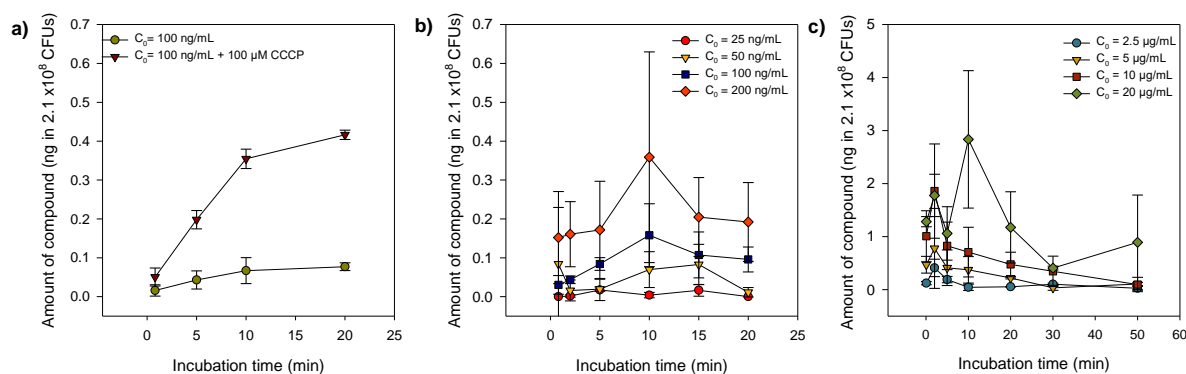
Figure 4.7 Time-course profiles for antibiotic uptake in *P. aeruginosa*. a) Ciprofloxacin uptake with and without pre-incubation with 100 μM CCCP for 5 min. b) Ciprofloxacin uptake at different initial concentrations. C) Meropenem uptake at different concentrations. Error bars are the standard deviation of three replicates (n=3) for ciprofloxacin and two replicates for meropenem (n=2)

Meropenem accumulation profiles show a different trend, as shown in Figure 4.7c. For all initial concentrations, there is an accumulation of compound during the first 5 min, and then it continuously decreases until a value close to zero. This behavior has not been reported earlier in accumulation studies. This profile could be characteristic of active efflux, induced by the rapid uptake of the compound, leading to a resistant phenotype. To prove that *P. aeruginosa* PA14 wild type was not resistant to meropenem, a susceptibility test was performed, showing that the strain has a MIC of 1 μg/mL (Figure 4.8).
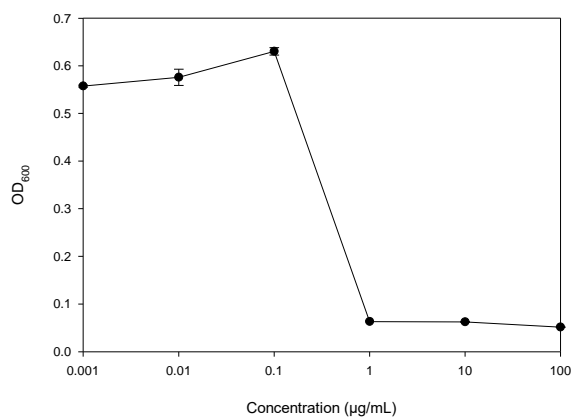
Figure 4.8 Susceptibility test of *P. aeruginosa* PA14 wild type to meropenem. Dots are the average value of duplicates and the standard deviation is represented by the error bars

4.2 Uptake of antibiotics in Gram-negative bacteria: *E. coli* and *P. aeruginosa*
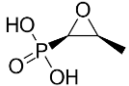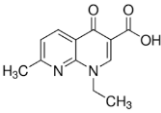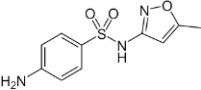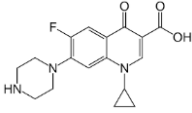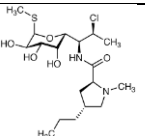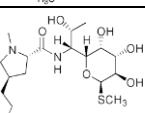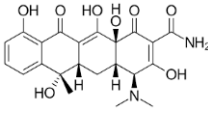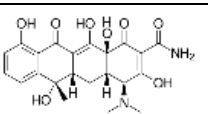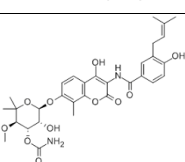
To prove the applicability of the described assay, the accumulation profiles for a panel of antibiotics were determined for *E. coli* and *P. aeruginosa* when treated at the same molar concentrations of 200 µM. These compounds are listed and ordered by mass concentration in Table 4.2. The advantage of plotting the accumulation of a determined compound in both strains upon the same initial concentration is that their accumulation can be directly compared without the need for correcting for unspecific binding. However, despite having both the same OD_{600} = 5.0 for antibiotic incubation, PA14 WT and *E. coli* MG1655 had different CFU count. Therefore, the values in µmol obtained were normalized to 10^{12} CFU for a direct comparison between both strains and shown as time-course accumulation curves (Figure 4.9).

Overall, the quantities of compounds tend to increase over incubation time, and many of the accumulation profiles reach a plateau after 20 min (ciprofloxacin, tetracycline, tigecycline, and sulfamethoxazole). Nalidixic acid was the compound that accumulated the most in *P. aeruginosa*, reaching 120 µmol per 10^{12} CFU after 40 min, showing a higher accumulation than in *E. coli*. Another compound that presented better accumulation in *P. aeruginosa* is phosphomycin. It is important to note that these two compounds had the lowest molar masses compared to the others tested, and therefore, the lowest mass concentrations in the assay. Similarly, clindamycin showed a noticeable higher accumulation in *P. aeruginosa*.

The antibiotics that accumulated to the same extent in both strains were sulfamethoxazole and lincomycin. Ciprofloxacin accumulated less in *P. aeruginosa*, its uptake in *E. coli* after 10 min was 8.15 µmol per 10^{12} CFU, while in *P. aeruginosa* it was 1.38 µmol per 10^{12} CFU. In contrast to *E. coli*, *P. aeruginosa* did not accumulate tetracycline and tigecycline. Similarly, novobiocin showed higher accumulation in *E. coli*, reaching 2.33 µmol per 10^{12} CFU after 50 min, while *P. aeruginosa* showed 0.46 µmol per 10^{12} CFU over the total incubation period.

Although there is no direct relationship, compounds with higher molar mass tend to accumulate better in *E. coli*, and those with a lower molar mass accumulated better in *P. aeruginosa*. This is not a rule since ciprofloxacin should accumulate more in *P. aeruginosa* based on the same principle.

Table 4.2 Compounds used in uptake assays with *P. aeruginosa* and *E. coli*

Compound	Structure	Inhibited cellular function	Molecular weight (g/mol)	Molar concentration (µM)	Mass concentration (µg/mL)
Phosphomycin		Peptidoglycan synthesis	182.02	200	36.40
Nalidixic acid		DNA replication	232.24	200	46.45
Sulfamethoxazole		Folate pathway	253.28	200	50.66
Ciprofloxacin		DNA replication	331.35	200	66.27
Clindamycin		Peptide formation	424.98	200	85.00
Lincomycin		Peptide formation	461.01	200	92.20
Tetracycline		Translation of m-RNA	480.9	200	96.18
Tigecycline		Translation of m-RNA	585.65	200	117.13
Novobiocin		DNA replication	634.61	200	126.92
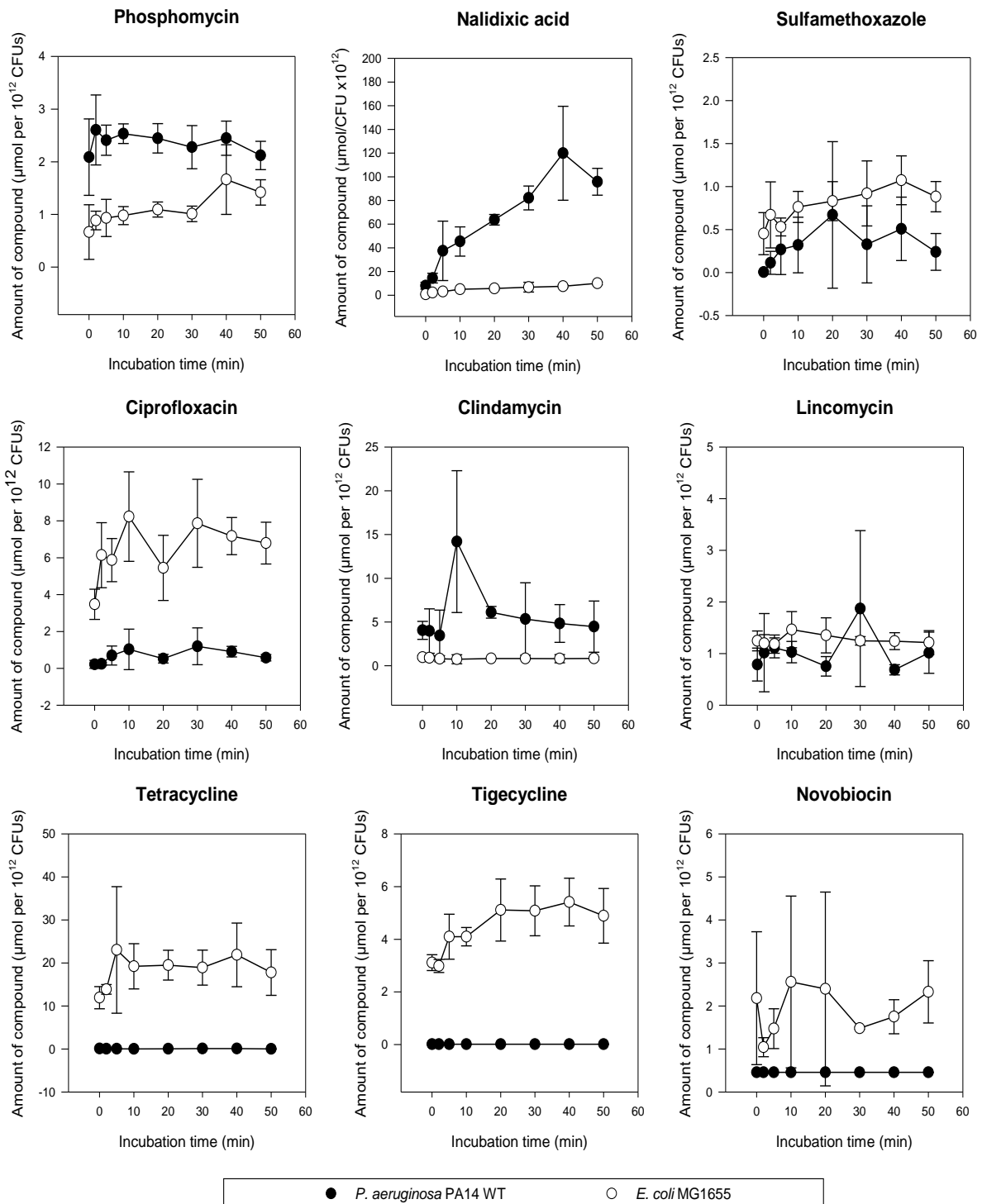
Figure 4.9 Time-course accumulation curves for a selected set of antibiotics incubated in 100 µL of bacterial solution at an OD_{600} = 5.0 in NaPi buffer and at an initial concentration of 200 µM for all compounds. Error bars are the standard deviation of two biological replicates and two technical replicates (n=4)

4.3 Discussion

Antibiotic uptake in Gram-negative bacteria is species-specific

In spite of possessing an outer membrane with similar properties that hamper penetration, various Gram-negative organisms often present different susceptibility to antibiotics. Thus, it is not surprising that Gram-negative species present different rates of compound accumulation. Examples of this are tetracyclines, as they accumulated substantially in *E. coli* but not in *P. aeruginosa*, contrary to what was previously reported for radio-labeled tetracycline in *P. aeruginosa* (Li, Livermore, and Nikaido 1994).

Another example is nalidixic acid, which accumulated greatly in *E. coli*, and showed a remarkable accumulation in *P. aeruginosa*. These results are in agreement with Piddock et al. (1999), who reported that the accumulation kinetics of nalidixic acid in *P. aeruginosa* was notably faster than in *E. coli* (Piddock et al. 1999). With an artificial membrane approach, Graef et al. (2018) reported nalidixic acid to be the compound with the highest permeation rate among other gyrase inhibitors such as ciprofloxacin, norfloxacin and pipemidic acid (Graef et al. 2018), and the authors inferred that this effect was likely an effect of the molecular size. However, the results reported here paint a different picture (Figure 4.9), as phosphomycin, the smallest molecule of the set, and sulfamethoxazole was not among the highly accumulating compounds.

Recent studies postulated a set of accumulation rules in Gram-negative bacteria based on the inherent physicochemical properties of different compounds. Broadly, the proposed rules establish numeric thresholds related to the shape and rigidity of the molecules, as well as the degree of substitution of their amines (Richter et al. 2017; Richter and Hergenrother 2019). Although many compounds seem to be in agreement with the proposed rules, among them tetracycline and ciprofloxacin in *E. coli*, the present study shows that two Gram-negative species may show very different accumulation profiles of the same compound under identical incubation conditions.

Thus, in order to avoid an over-generalization of such accumulation rules in Gram-negative species, further data on antibiotic uptake in diverse species are still required. Comparing actual accumulation amounts across studies with different experimental setups is difficult, underlining the need for high throughput and easily strain-transferable uptake assay. The present medium-high throughput method allows for the systematic generation of data on antibiotic accumulation across species, which can be worthwhile for further in-depth structure-accumulation relationship studies.

Detection of unlabeled and unmodified compounds

Several factors may lead to uptake misinterpretation in LC-MS/MS-based studies (Zgurskaya and Rybenkov 2020): first, the compound may be lost due to unspecific binding to the labware. In addition, the workup procedure that aims at removing residual compounds from the wells by washing may lead to a washout of compounds from the cells. Other factors may lead to a reduced signal, such as strong (noncovalent) interactions with e.g. proteins or cellular membranes due to imperfect protein denaturation or precipitation steps, making the compound unavailable for detection. Finally, compounds may undergo possible covalent modifications once they enter the cell (Rende-Fournier et al. 1993; Ramirez and Tolmasky 2010).

Monitoring the uptake of β-lactams via LC-MS/MS in bacterial cells is still challenging. After incubation with whole cells, β-lactams either a) are rapidly hydrolyzed by β-lactamases; or b) rapidly form long-lived covalent acyl-enzyme intermediates with their target PBPs. In both cases, the compounds are covalently modified and thus undetectable by the original, molecular ion-specific MRMs. Despite these challenges, meropenem was detected and quantified using the medium-high throughput assay, showing a rapid accumulation in the first minutes, and the amount dropped over time (Figure 4.7). This observation was possible due to the fast removal of the supernatant with an optimized filtration time (about 15 s). These results prove that it is incorrect to assume that β-lactams might serve as a negative control for LC-MS/MS-based accumulation studies (Richter and Hergenrother 2019).

For a complete picture of the uptake of β-lactams, a study that determines the accumulation of unmodified compound, its rate of hydrolysis and the formation of the corresponding covalent acyl-enzyme intermediate is still needed. In this regard, in 2017, Allam *et al.* monitored the accumulation of fluorophore-labeled ceftazidime conjugates in *E. coli*. After 30 min incubation and a subsequent wash, conjugated ceftazidime was found intracellularly. However, a such designed probe does not differentiate between the fluorescent signal coming from the hydrolyzed product and the one coming from the original compound. In the same study, a second ceftazidime conjugate was designed in such a way that it released its fluorophore after the cleavage of the β-lactam ring by the action of β-lactamases. This is an elegant approach to provide an overall insight into the uptake and transformation of β-lactams, by making use of two different conjugates for the same compound.

The herein proposed medium-high throughput assay could allow for direct detection of the hydrolyzed products of β-lactams by LC-MS/MS, although further development is required to obtain a purified hydrolyzed compound to develop MRMs and to perform standard curves. Similarly, other compounds that may undergo modification once intracellularly translocated are

suitable to be detected, such as aminoglycoside modification by N-acetylation, O-phosphorylation, or O-adenylation (Ramirez and Tolmasky 2010).

Moreover, since their lifetime is rather long, acyl-protein intermediates are good candidates for LC-MS/MS detection through PBP-targeted proteomics analyses. In targeted proteomics, the protein of interest undergoes proteolytic digestion, and the generated peptides are detected by selected reaction monitoring (SRM) (Chen and Liu 2019). In this way, an MRM could detect the formation of the surrogate peptide-acyl conjugate, as well as the free peptide from the same sample. However, in the current assay, the acyl-enzyme intermediates are likely precipitated together with other cell debris during the solvent-based lysis of bacteria. Thus, further optimization of this protocol might require lysing bacteria without compromising protein integrity, e.g. by sonication in an appropriate buffer with a multi-tip horn, in order to keep the assay throughput.

In summary, the present study provides a method to systematically evaluate the accumulation of different classes of antibiotics in bacteria. It was possible to detect and quantify label-free compounds accumulating in bacteria in small quantities, underlining the versatility and further applicability of LC-MS/MS-based methods. The development of a medium-high throughput method allowed the elucidation of time-course profiles of rapidly accumulated compounds and helped to differentiate the accumulation profiles between two Gram-negative species. Furthermore, the transferability of the assay to other species allows for reliable, robust and direct screening of accumulation of compounds, an increasingly important step in the development of novel antimicrobials to combat drug-resistant bacteria.

5. EFFECT OF ANTIBIOTICS IN *P. AERUGINOSA*

Antibiotics are known to have multiple effects on bacterial cells depending on the exposure concentrations (Davies, Spiegelman, and Yim 2006; Bernier and Surette 2013). At inhibitory concentrations, bacteria has been shown to exhibit metabolic responses that are associated with the compound's mode of action (Allen et al. 2004; Currie et al. 2016; Dörries, Schlueter, and Lalk 2014; Vincent et al. 2016; Yang et al. 2019; Zampieri et al. 2018; Zampieri et al. 2017). These studies have allowed the prediction of the mode of action of unknown compounds by comparing bacterial metabolic responses to those generated after exposure to reference antibiotics.

In the present work, a set of experiments was designed to elucidate the effects of exposure to sub-lethal concentrations of antibiotics on *P. aeruginosa*'s metabolic phenotype. Firstly, as a proof of concept, a medium high-throughput metabolomics workflow was carried out in order to assess whether sub-lethal concentrations of antibiotics with different modes of action exhibit distinctive metabolic fingerprints in *P. aeruginosa*. Secondly, the metabolic fingerprint of *P. aeruginosa* was evaluated under short and long exposure of clinically relevant antibiotics classes.

5.1 Metabolic phenotype under antibiotic perturbation

In order to investigate the phenotypic response of *P. aeruginosa* under antibiotic perturbation at non-lethal concentrations, three members of the fluoroquinolone class, three members of the macrolide class, and one β-lactam were selected (see Table 5.1). This allowed for the evaluation of inter- as well as intra-group variability. The treatment concentrations were selected as the highest at which the bacterial cells were still intact during the exposure time (see 4.1.2.2 Assurance of bacterial cells intactness).

As shown before, ciprofloxacin's concentration applicability went up to 0.8 µg/mL and meropenem's concentration applicability reached 100 µg/mL (see Figure 4.6), while for erythromycin, 1 mg/mL did not decrease cell viability in 1 hour of treatment (see Figure 5.1). Thus, the exposure concentrations (hereon called non-killing concentrations) were selected by choosing an intermediate point from the gradient concentration used in these analyses, i.e., 0.2 mg/mL for ciprofloxacin, 10 µg/mL for meropenem and 50 µg/mL for erythromycin.

Table 5.1 Experimental conditions to study the phenotypic response of PA14 WT to antibiotic perturbation in filter plates

Treatment	Antibiotic class	Concentration (µg/mL)	Initial OD_{600}	Total incubation time (h)
Control (CON)	N.A.	0	1.0	2.0
Ciprofloxacin (CIPRO)	FQ	0.2	1.0	2.0
Levofloxacin (LEVO)	FQ	0.2	1.0	2.0
Lomefloxacin (LOME)	FQ	0.2	1.0	2.0
Azithromycin (AZI)	MA	50	1.0	2.0
Erythromycin (ERI)	MA	50	1.0	2.0
Clarithromycin (CLARI)	MA	50	1.0	2.0
Meropenem (MERO)	BLA	10	1.0	2.0

N.A. not applicable, FQ: fluoroquinolones, MA: macrolides, BLA: β-lactam.
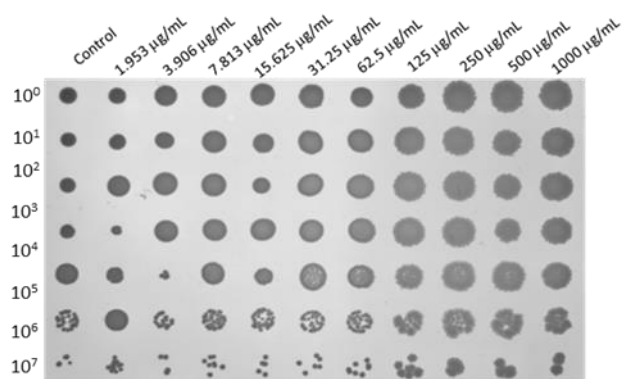
Figure 5.1 Colonies of *P. aeruginosa* after being treated for 1 h with a gradient concentration of erythromycin. The first row was serially diluted downwards in a plate, and 2 µL of each well was spot-plated in an LB agar plate and incubated for 24 h at 37°C

For consistency, the selected concentrations were applied to all the compounds within the same class. The experimental conditions were adjusted to a medium-high-throughput format in 96-deep well filter plates, since six replicates per condition were carried out simultaneously (see 3.4.2 Metabolomics in deep-well filter plates). Briefly, antibiotic solutions were added to a filter plate containing 1 mL of bacterial solution at OD_{600} =1.0 per well, and it was incubated at 37°C and 400 rpm for 2 hours. Samples were harvested simultaneously by fast filtration in a vacuum manifold. Filtered bacterial cells were washed and lysed and the extracted intracellular metabolome was analyzed in positive mode in a UPLC-ESI-QToF.

Untargeted metabolomics was performed by processing mzXML-formated raw data with the XCMS R-based package for peak picking and feature detection, resulting in a table with 2376 features. After retention time cutoff of 0.3 min ≤ RT ≤ 28 min (to discard the injection peak and the column wash), the number of features was reduced to 2110. As a quality control procedure, the coefficient of variation (CV) of the intensity of the internal standards (ISTDs) from all samples was calculated. For this data set, the intensity of all ISTDs was within an acceptable range of CV ≤ 20% (Table 5.2). In general, ISTDs account for variations in sample preparation,

elution time, and in the response of the detector (Wieling 2002). The use of a set of ISTDs for the intrametabolome extraction step (trimethoprim and glipizide, and nortriptyline) allows for correction in case of loses in sample preparation. On the other hand, the ISTDs for injection into the UPLC unit (caffeine and naproxen) help identifying variation in the device's functioning.

Table 5.2 Coefficient of variation (CV) of the internal standards for quality control of metabolomics in filter plates

Glipizide	Trimethoprim	Nortriptyline	Caffeine	Naproxen
5.99 %	4.13 %	15.37 %	4.45 %	4.63 %

The feature table was further analyzed to find the principal components (PC) that bring the most diversity among groups, without removing the intensity of the ISTDs and neither was a normalization carried out. The first two components with the highest explained variance are plotted in Figure 5.2a. Meropenem samples were the samples with better separation from the rest of the samples. At the same time, there is no perceptible separation among fluoroquinolone-treated samples from macrolide-treated samples nor untreated samples along PC2 (Figure 5.2a).

After a visual inspection on the pre-processed data, a series of highly intense peaks were found in all samples, including the blank samples (Figure 5.3). All samples were incubated and extracted with organic solvent identically. Since the metabolite extraction step carried out in the filter plates, the observed peaks likely are extractable compounds from the polymeric materials of plate. In total, 19 adjacent peaks with a difference in m/z value of 44.026 m/z were detected between 6.5 and 11 min, showing a typical polyethylene glycol (PEG) mass distribution where the mass of the repeat unit ethylene oxide is 44 Da (Chen, Yu, and Li 2002) (for more details, see *Appendix II. Extractables from filter-plate-based metabolomics workflow***Error! Reference source not found.**).

The high intensity of such peaks could bring more similarity among the samples and the groups, which might hinder the separation among them in the principal component analysis (PCA). Therefore, a total of 84 features, including singly- and doubly-charged protonated ions and adducts, showed a CV ≤ 15% and were removed from the feature table. Similarly, the features corresponding to the five internal standards were removed from the feature table, as they appear in all the samples as well.
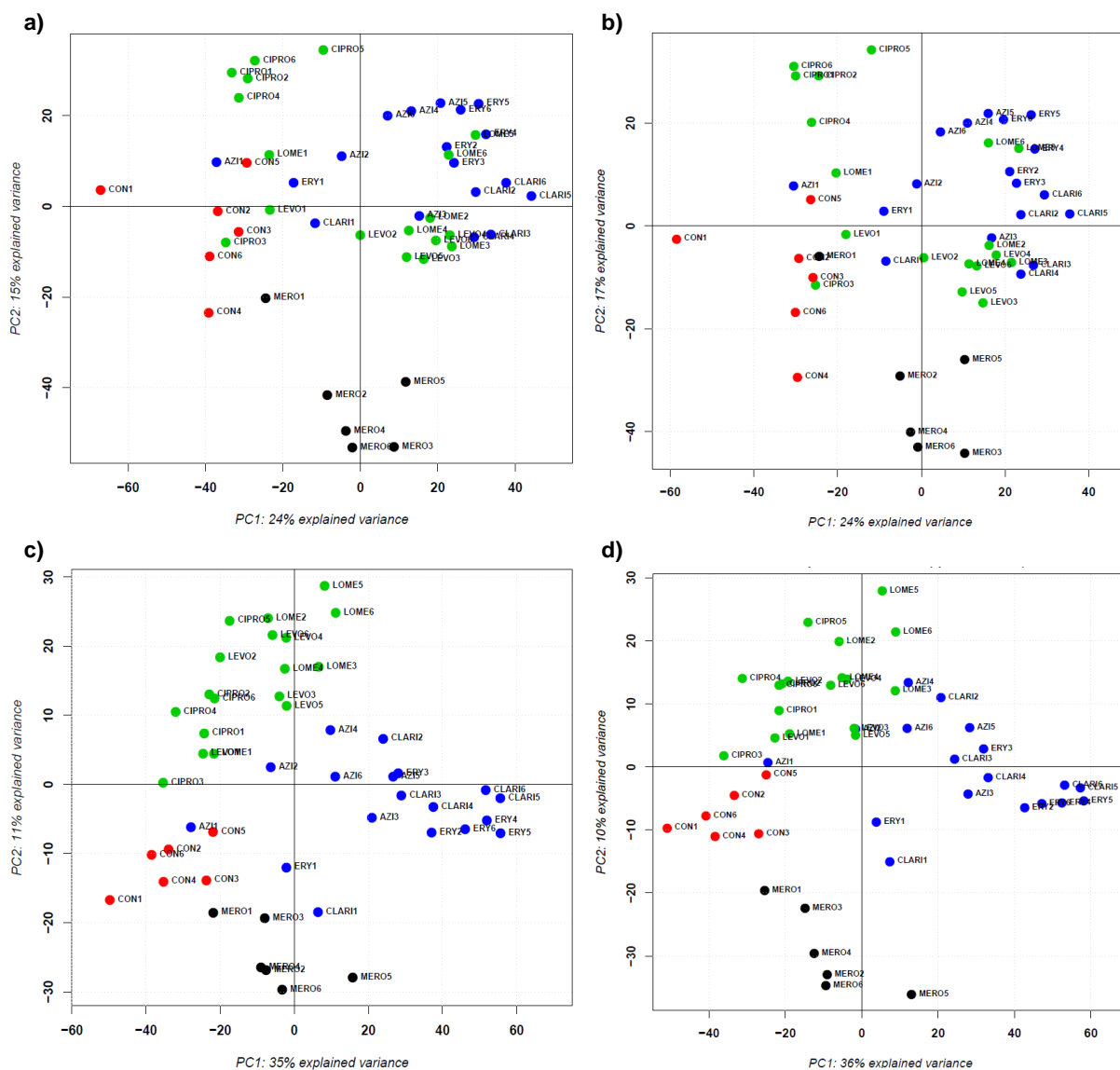
Figure 5.2 Principal component analysis for samples treated with four classes of antibiotics: fluoroquinolones (green), macrolides (blue), one β-lactam (black) and controls with no antibiotic addition (red). The preprocessed data were filtered by a retention time cutoff of $0.3 \leq RT \leq 28$ min, and no normalization by the intensity of internal standards was carried out. a) Data before removing the PEG and ISTDs peaks, b) after removing the PEG and ISTDs peaks. Quantile normalization was carried out in order to better display the separation of the groups c) before and d) after removing the PEG and ISTDs peaks.

A second PCA was performed after removal of the common 89 features (Figure 5.2b), showing a light increase in the explained variance of PC2, from 15 to 17%, while the explained variance in PC1 remained unchanged. Generally, there was not a noticeable improvement on the separation among classes after the removal of the identified PEG and ISTDs features.
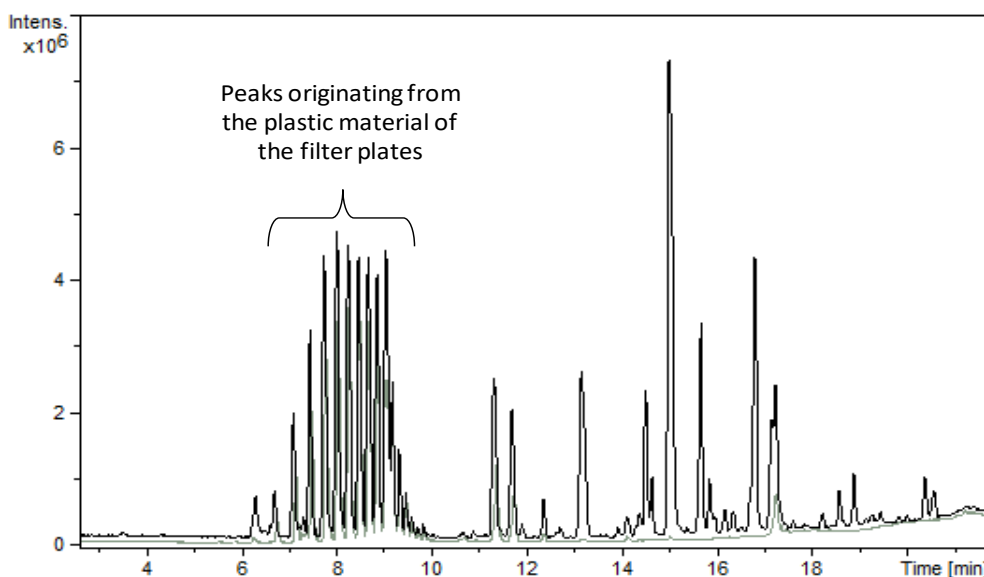
Figure 5.3 Total ion chromatograms (TIC) two metabolomics samples coming from the filter plate experimental set up showing a series of 19 peaks corresponding to PEG, likely coming from the plastic labware. Pooled sample in black and blank sample in grey. All the peaks appear in the blank samples, which were extracted with organic solvents identically to the rest of the samples.

In order to evaluate whether the treatments by antibiotic class could be better separated, quantile normalization was performed to the feature table, before and after removing the PEG as well as the ISTDs features. In a quantile normalization, the features of each sample keep their ordered position from the most intense to the least intense, but their intensity values are substituted by the mean value of the features in the same position across samples (Peterson and Cavanaugh 2019). Thus, samples belonging to groups with different distributions will have identical quantiles (therefore the name). Quantile normalization has been widely used in the analysis of large data sets coming from gene expression microarrays (Qiu, Wu, and Hu 2013), and it is applicable e.g. when only a minority of genes are expected to be differentially expressed (Hicks and Irizarry 2014).

The resulting feature table was further analyzed to find the principal components, and the first three components with the highest explained variance are plotted in Figure 5.2c-d. This time, a separation among antibiotic class was better detected along PC2. In general, replicates of the same treatment clustered together according to their antibiotic class. Only one replicate of each macrolide (AZI1, ERY1, and CLARI1) remained farther from the macrolide cluster and closer to the untreated controls and the β-lactam. The fluoroquinolone-treated samples were located mainly in the second quadrant of the scores plot for PC1 vs. PC2, while the untreated samples clustered within the third quadrant. Macrolide-treated samples were primarily located within the first and fourth quadrant, while β-lactam-treated samples were located in the lower-middle of the plot, mainly within the third quadrant (Figure 5.2c). It important to notice that, in

all cases, the distinction of individual antibiotic members within a class was not possible, as the variability within replicates was as large as between members of a class.

Although there was no sharp separation found among the groups, the distancing among classes showed in the PCA analysis is an indication of a class-specific phenotype of PA14 WT upon antibiotic perturbation. However, the experimental setup of this study showed an important drawback: the medium-high-throughput configuration prevented the measurement of OD_{600} at the time of harvest, leading to the inability to measure any difference in growth due to the antibiotic activity. This aspect may have a strong influence on the available metabolite pool due to different biomasses at the harvest point. In order to account for any deviation in growth rate, a measure of biomass is needed; therefore, OD_{600} was monitored in further experiments.

With the first insights of a class-specific phenotype for antibiotic treatment, additional questions were posed to interrogate whether the specific phenotype remains present at non-inhibitory concentrations instead of non-killing concentrations. For this purpose, both the immediate response to the treatment, as well as the long-term response were investigated.

Short- and long-term responses were investigated by exposing PA14 WT to antibiotics from three different classes at concentrations that did not show growth inhibition in a plate assay. The compounds selection for this analysis was in accordance with the antibiotic class most frequently used to treat *P. aeruginosa* (Pang et al. 2018). Aminoglycosides, such as tobramycin and gentamycin, and fluoroquinolones, such as ciprofloxacin and levofloxacin, are among the effective treatment against *P. aeruginosa*. Similarly, the treatment with macrolides such as azithromycin and erythromycin has been effective in patients with *P. aeruginosa* despite their high MIC values (Chalmers 2017).

5.2 Short and long exposure to non-inhibitory antibiotic concentrations

5.2.1 Determination of non-inhibitory concentrations

Unlike minimum inhibitory concentrations (MICs) assays, where bacterial cells are incubated at an initial OD_{600} = 0.05, non-inhibitory concentrations were determined by exposing a bacterial solution in the mid-log phase (OD_{600} = 0.5) to different antibiotic concentrations overnight. The non-inhibitory concentrations per antibiotic class were selected so that no reduction in growth was observed in both members of the class (Figure 5.4).
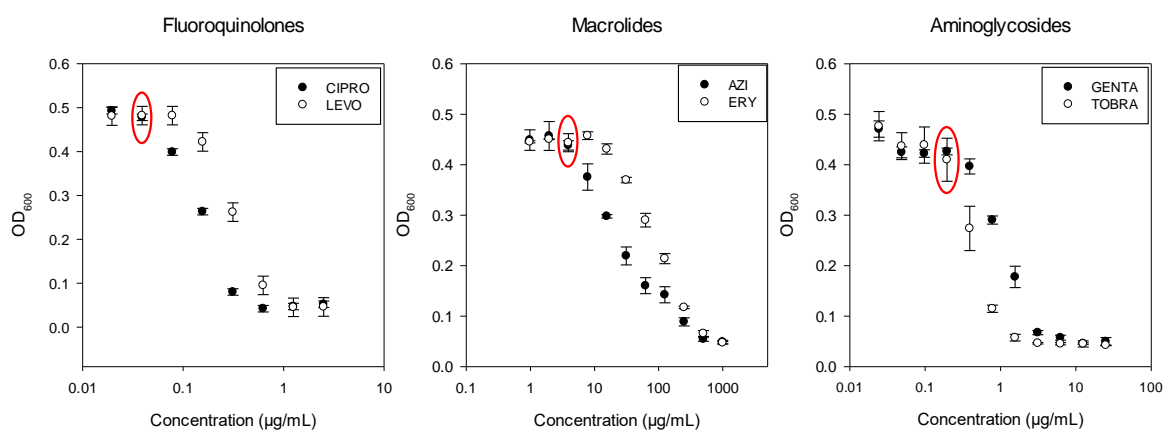
Figure 5.4 Growth inhibition after 24 h at 37°C of incubation under antibiotic stress in BM2 medium starting with an initial OD_{600}=0.50 in a cuvette with a path length *l* = 1cm. Red circles show the selected concentration for short- and long-term exposure experiments. The y-axis is the OD_{600} of 100 μL in a microplate. Error bars are the standard deviation of three replicates (n=3)

5.2.2 Design of experiment

The immediate responses of bacteria to antibiotic treatment was evaluated by the short exposure of bacterial cells to the non-inhibitory concentrations of the selected compounds. In contrast, the long-term responses to antibiotic treatment were evaluated by the long exposure to the same non-inhibitory concentration of compounds. In order to avoid undesired deviation in the metabolomics samples due to batch effects, both the short- and long-exposure treatment was carried out in one experiment.

Briefly, 3-mL cultures with an initial OD_{600} = 0.05 were incubated in test tubes on an inclined rack to favor aeration. The long exposure was achieved by adding the antibiotic solutions at the beginning of the incubation and harvesting the bacterial cells at OD_{600} = 1.0 (see Table 5.3). Short exposure samples were grown in the medium until OD_{600} = 0.5 and incubated with antibiotic solutions until the OD_{600} = 1.0 (see Table 5.4). As the number of samples to handle went to 48, OD_{600} monitoring was carried out by removing 100 μL of solution from each tube and transfer them to clear, flat bottom 96-well plates to be measured in a plate reader. Thus,

the equivalent of a final $OD_{600} = 1.0$ measured in cuvettes with 1-cm path length is $OD_{600} = 0.4$ measured in plates with 100 µL of solution.

Table 5.3 Experimental conditions in the long exposure of PA14 WT to non-inhibitory concentration of selected antibiotics

Treatment	Concentration (µg/mL)	Antibiotic class	Initial OD$_{600}$[a]	Final OD$_{600}$[b] per replicate			Exposure time (h)
				1	2	3	
Control (CON)	0	N.A.	0.05	0.390	0.383	0.383	7.0
Ciprofloxacin (LE_CIPRO)	0.05	FQ	0.05	0.117	0.144	0.128	7.5
Levofloxacin (LE_LEVO)	0.05	FQ	0.05	0.288	0.358	0.34	7.5
Azithromycin (LE_AZI)	4.00	MA	0.05	0.496	0.424	0.481	7.5
Erythromycin (LE_ERY)	4.00	MA	0.05	0.437	0.444	0.395	7.5
Gentamycin (LE_GENTA)	0.20	AM	0.05	0.396	0.354	0.413	8.0
Tobramycin (LE_TOBRA)	0.20	AM	0.05	0.393	0.416	0.417	8.0

N.A. not applicable, FQ: fluoroquinolones, MA: macrolides, AM: aminoglycosides
[a] measured in cuvettes with a path length of 1.0 cm
[b] measured in a plate reader with 100 µL of solution

Table 5.4 Experimental conditions in the short exposure of PA14 WT to non-inhibitory concentration of selected antibiotics

Treatment	Concentration (µg/mL)	Antibiotic class	Initial OD$_{600}$[a]	Final OD$_{600}$[b] per replicate			Exposure time (h)
				1	2	3	
Control (CON)	0	N.A.	0.5	0.390	0.383	0.383	0
Ciprofloxacin (SE_CIPRO)	0.05	FQ	0.5	0.351	0.340	0.373	2
Levofloxacin (SE_LEVO)	0.05	FQ	0.5	0.412	0.421	0.498	2
Azithromycin (SE_AZI)	4.00	MA	0.5	0.420	0.448	0.445	2
Erythromycin (SE_ERY)	4.00	MA	0.5	0.455	0.455	0.424	2
Gentamycin (SE_GENTA)	0.20	AM	0.5	0.424	0.451	0.451	2
Tobramycin (SE_TOBRA)	0.20	AM	0.5	0.387	0.407	0.496	2

N.A. not applicable, FQ: fluoroquinolones, MA: macrolides, AM: aminoglycosides
[a] measured in cuvettes with path length of 1.0 cm
[b] measured in a plate reader with 100 µL of solution

Samples of PA14 WT were harvested at different incubation times in order to reach comparable OD_{600} values, while all samples of PA14 gyrAparC were harvested simultaneously. Harvested bacterial cells were washed and lysed and the extracted intracellular metabolome was analyzed in positive mode in a UPLC-ESI-QToF.

5.2.3 Data analysis

Untargeted metabolomics was performed by processing mzXML-formated raw data with XCMS Online for peak picking and feature detection, resulting in a table with 2786 features. From them, 640 features (22.97%) were identified by XCMS Online as first, second, third, and fourth isotope peaks, with single, double, and triple charges (Table 5.5). These features were removed for further analysis, leaving 2146 monoisotopic ions.

Table 5.5 Number of features identified as ion isotopes in short and long exposure to non-inhibitory concentrations of antibiotics

Isotopic peak	Ion charge		
	1+	**2+**	**3+**
[M+1]	350	76	37
[M+2]	112	6	21
[M+3]	32	1	1
[M+4]	2	0	2

After retention time cutoff of 0.3 min ≤ RT ≤ 28 min (to discard the injection peak and the column wash), the number of features was reduced to 1744. The quality control for ISTDs showed that one replicate of ciprofloxacin at short exposure (SE_CIPRO1) presented highly deviated ISTDs intensities and it was removed from the analysis (see Figure 5.5). After this depuration, normalization based on the intensities of ISTDs was carried out within an acceptable range of CV before and after normalization (Table 5.6).
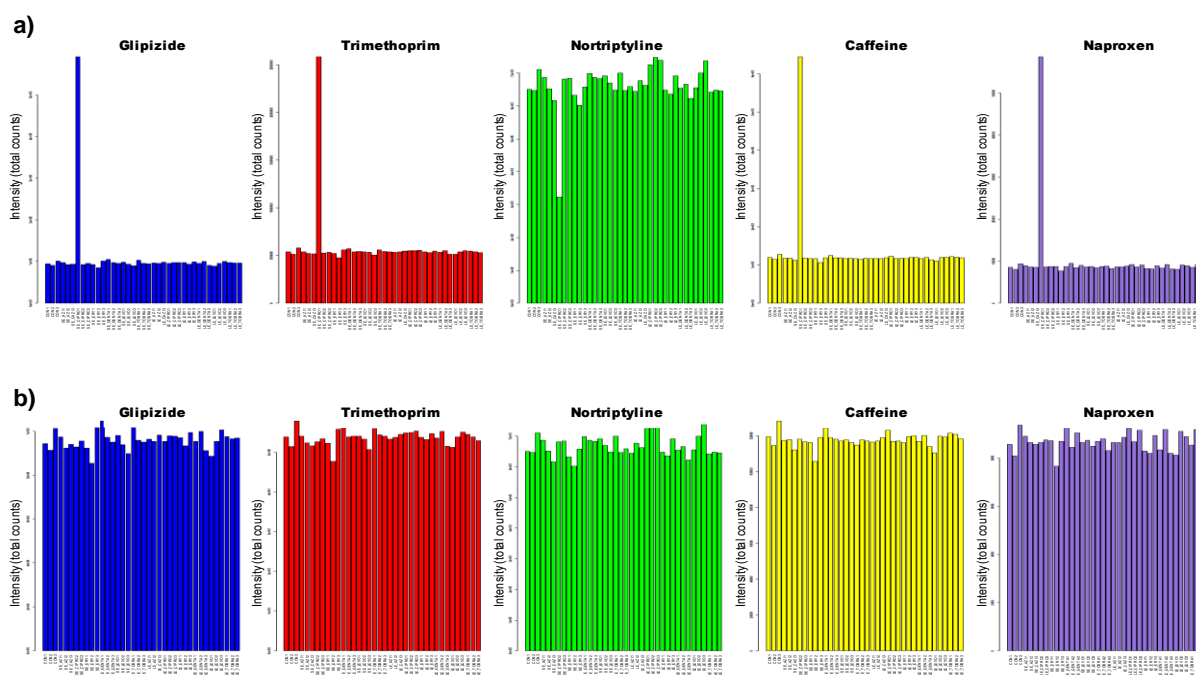
Figure 5.5 Intensities of the internal standards for short and long exposure to antibiotics a) before and b) after removal of sample SE_CIPRO_1

Table 5.6 Coefficient of variation (CV) of the internal standards for quality control of metabolomics in filter plates

	Glipizide	**Trimethoprim**	**Nortriptyline**	**Caffeine**	**Naproxen**
Before normalization	4.10 %	3.42 %	5.11 %	3.16 %	4.45 %
After ISDTs normalization	3.59 %	3.36 %	4.27 %	3.82 %	3.75 %
After OD$_{600}$ normalization	48.94 %	50.00 %	54.85 %	49.26 %	51.24 %

To account for differences in optical density across treatments, a normalization based on OD_{600} values was carried out. As the long exposure treatment with ciprofloxacin presented the lowest OD_{600} values, the intensity of all the features from these samples was substantially compensated after the OD_{600} normalization, bringing the CV of ISTDs around 50%. Although this variation was no longer within the acceptance range, the normalized data set was subjected to PCA, expecting only the replicates of LE_CIPRO to be overcompensated.

Before PCA analysis, the intensities of the five ISTDs, as well as their adducts identified manually by retention time (RT) and MS information, were discarded from the data set. Additionally, macrolides and their adducts were identified by RT, MS, and MS/MS information and removed from the analysis. Neither fluoroquinolones nor aminoglycosides were identified by their exact mass or spectral information. In addition, the data set was separated into two subsets, one for short-exposure treatment and one for long-exposure treatment, including the respective untreated controls.

As shown in Figure 5.6, fluoroquinolone-treated samples mostly remain separated from the rest of the treated and untreated samples for both short and long exposure. Moreover, macrolide-treated samples and aminoglycoside-treated samples were clustered together in both cases. In the short exposure, untreated control samples formed an independent cluster separated from the rest of the treatments Figure 5.6a. Ciprofloxacin-treated samples remained farther from the rest of the samples, and they did not cluster together with levofloxacin-treated samples.

In the long exposure, the samples of ciprofloxacin and levofloxacin treatment clustered together among replicates, but they did not form a fluoroquinolone-treatment cluster Figure 5.6b. In this analysis, replicates from LE_CIPRO were expected to distant from the rest of the samples as the OD_{600} normalization compensated greatly the intensity of all their features. Surprisingly, also LE_LEVO formed a distant cluster away from the rest of the samples. Besides, there was no separation of the untreated controls from the macrolide-treated samples.
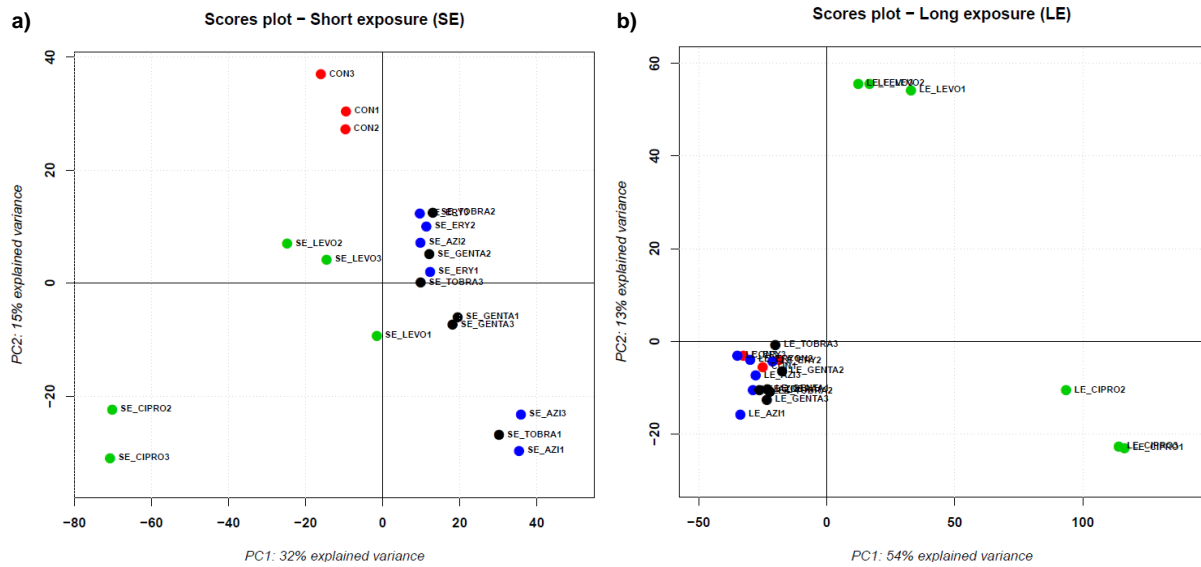
Figure 5.6 Principal component analysis for samples treated with sub-inhibitory concentrations of antibiotics upon a) short exposure (SE) and b) long exposure (LE). Color code for treatment: untreated controls (red), fluoroquinolones (green), macrolides (blue), aminoglycosides (black).

In order to compare short- and long-exposure treatments, a correlation matrix was performed including all samples from all the groups (Figure 5.7). Four main clusters were identified: I) all ciprofloxacin-treated samples and LE_LEVO samples, II) all levofloxacin-treated samples and SE_CIPRO, III) all short-exposure samples (except for SE_CIPRO), and IV) all long-exposure samples (except LE_LEVO) and untreated controls.

Together with Figure 5.6, the correlation matrix in Figure 5.7 shows that the response of PA14 WT to fluoroquinolone treatment is distinctive from the other treatments and the untreated controls, as cluster I and II form a larger fluoroquinolone cluster. Additionally, long exposure to macrolides and aminoglycosides did not exhibit a distinct response, in comparison with the untreated controls. It is important to note that PA14 WT responded more readily to a short exposure to all antibiotic classes, and even more, to fluoroquinolone treatment.
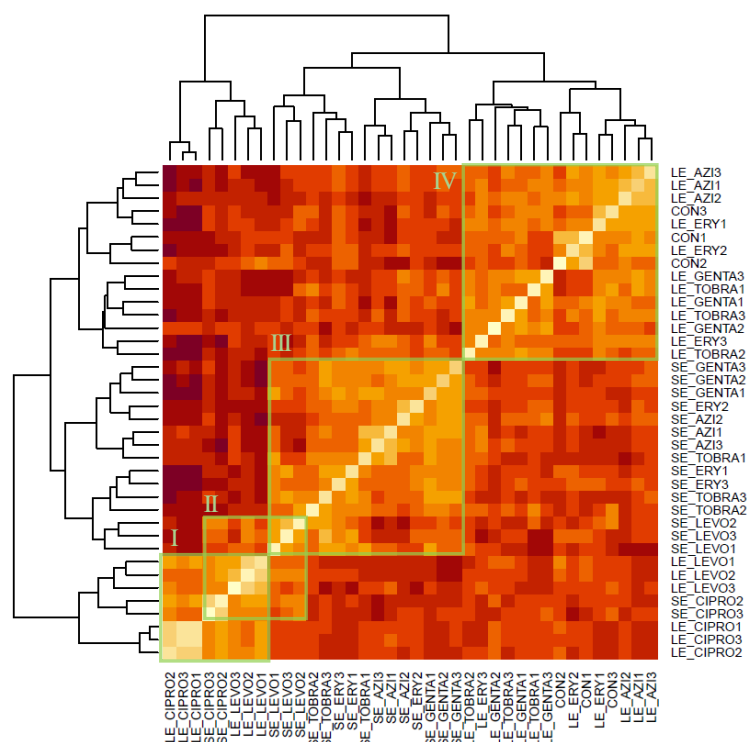
Figure 5.7 Correlation matrix of short- and long-exposure treated samples to non-inhibitory concentrations of antibiotics. Four clusters are highlighted: I) and II) fluoroquinolone treatment, III) short-exposure treatment (excluding ciprofloxacin), and IV) long-exposure treatment and untreated controls. SE: short exposure, LE: long exposure.

Additionally, a heatmap with hierarchical clustering was performed to detect similarities and differences in short- and long-exposure treatments (Figure 5.8). For this, log2-transformed fold changes (log2-FC) were calculated by subtracting the log2-mean values of the untreated controls from the log2-mean values of each treatment group; thus, over-produced features had a positive log2-FC, while under-produced metabolites had a negative log2-FC.

Indistinctly of the exposure time, fluoroquinolone-treated samples formed a group separated from the rest of the treatments, as shown in the column-wise hierarchical cluster in Figure 5.8. LE_CIPRO presented the most marked changes in feature abundance with respect to the controls, which could not be associated with a distinctive biological phenotype, but rather to artifacts due to the OD_{600} normalization step. On the one hand, the intensity of all the features in LE_CIPRO replicates was substantially compensated because of their low OD_{600} values. On the other hand, low OD_{600} values in these replicates resulted in many features with lower intensity than the detection threshold of 400 total counts, showing a strong negative log2FC (after correction for missing values).
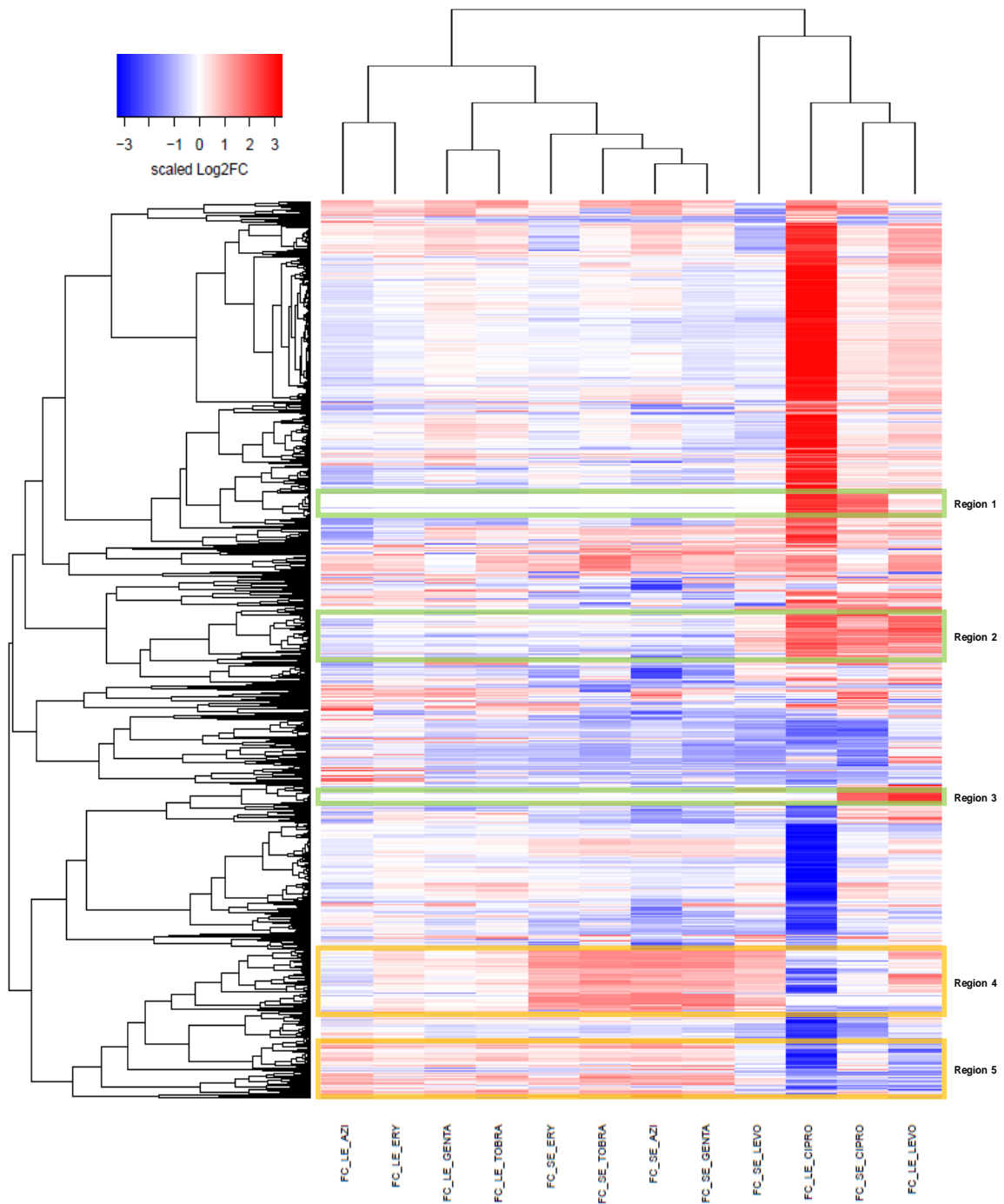
Figure 5.8 Heat map of feature fold-changes for samples treated with non-inhibitory concentrations of antibiotics upon short exposure (SE) and long exposure (LE). Four regions of interest are highlighted: 1), 2) and 3) over-produced features in samples treated with fluroquinolones, 4) over-produced features in samples upon short-exposure treatment, and 5) over-produced features in samples treated with aminoglycosides and macrolides. Log2-transformed fold change (Log2FC) was calculated from the mean values of triplicates, by subtracting the log2 values of each condition from the untreated control samples. Scaled Log2FC was performed as a default function in R Studio for visualization of over-produced metabolites (in red) and under-produced metabolites (in blue) with respect to the untreated controls.

The row-wise hierarchical clustering allowed for the detection of four regions of interest, which were detected visually and highlighted on the heat map (Figure 5.8). The highlighted regions 1, 2, and 3 correspond to two subsets of features that were found to be uniquely over-produced under fluoroquinolone treatment. The highlighted region 4 corresponds to a subset of features that were found to be over-produced particularly under short exposure to antibiotics. Finally, the highlighted region 5 corresponds to a subset of features over-produced under macrolide and aminoglycoside treatment (see *Appendix III. Feature table - comparison between short and long exposure*).

To identify the nature of these features, a general feature identification procedure was applied to the whole data set first. MS/MS identification of a pooled sample (a sample containing the same volume of each replicate from all groups) was carried out in Bruker Compass DataAnalysis 4.2 by finding the molecular features and performing a comparison with an *in-house* library. The search was refined manually to detect unidentified adducts and *in-source* fragments of the matching features, labeled with a preceding asterisk (putative annotation). In total, 85 features were structurally assigned to 54 metabolites (for more details, see *Appendix III. Feature table - comparison between short and long exposure*).

The features belonging to regions 1, 2, 3, 4, and 5 of the heat map were filtered out visually. Region 1, 2 and 3 together accounted for 171 features, from which only 11 belonging to region 2 were annotated (see Table 5.7). Region 4 consisted of 117 features, from which only 11 were annotated (see Table 5.8). Region 5 consisted of 113 features, from which none were identified (see *Appendix III. Feature table - comparison between short and long exposure*).

Table 5.7 Identified features that showed a distinct fold-change pattern under treatment to fluoroquinolones

Feature name	Retention time (min)	m/z value	Annotation	CIPRO		LEVO	
				SE	LE	SE	LE
M272T14	13.55	272.1646	C8:1-QNO	↑	↓*	↑	↑*
M274T14	14.03	274.1806	C8-QNO	↑	↑**	↑	↑
M313T17	16.68	313.2740	†LPG (16:0) (fragment)	↑***	↑***	↑*	↑***
M339T17_2	17.04	339.2896	†LPE (18:1) (fragment)	↑	↑***	↑	↑***
M436T17	16.70	436.2826	†LPE (16:0) [M-H2O+H]+	↑***	↑***	↑***	↑***
M454T17	16.68	454.2938	LPE (16:0)	↑***	↑***	↑***	↑***
M466T16	16.32	466.2930	LPE (17:1)	↑**	↑**	↑	↑***
M474T15	15.32	474.2594	†LPE (16:1) [M+Na]+	↑	↑	↑	↑
M476T17	16.69	476.2754	†LPE (16:0) [M+Na]+	↑***	↑***	↑***	↑***
M480T17	17.05	480.3094	LPE (18:1)	↑	↑***	↑	↑***
M502T17	17.05	502.2912	†LPE (18:1) [M+Na]+	↑	↑***	↑	↑***

†: Putative annotation, SE: short exposure, LE: long exposure, ↑: log2FC > 0, ↓: log2FC < 0, *** for p-value ≤ 0.001, ** for 0.001 < p-value ≤ 0.01, * for 0.01 < p-value ≤ 0.05

Table 5.8 Identified features that showed a distinct fold-change pattern in the short-exposure treatment to antibiotics

Feature name	Retention time (min)	m/z value	Annotation	AZI	ERY	GENTA	TOBRA	LEVO	CIPRO
M359T17_3	16.66	359.2798	†Rha-C10-C10 (fragment)	↑***	↑***	↑***	↑***	↑	↑**
M387T17	17.23	387.3108	†Rha-C10-C12 (fragment)	↑	↑	↑	↑**	↑	↓
M387T18	18.04	387.3111	†Rha-C10-C12 (fragment)	↑	↑	↑	↑	↑	↑
M505T17	16.64	505.3374	†Rha-C10-C10 [M+H]+	↑*	↑	↑**	↑	↑	↑
M553T18_2	17.73	553.3395	Rha-C10-C12:1+Na	↑	↑	↓	↑	↓	↑
M575T17	17.44	575.3170	†Rha-C10-C12:1 [M+Na]+	↑	↑	↑	↑	↑	↑
M673T16_1	15.87	673.3777	Rha-Rha-C10-C10+Na	↑	↑	↑	↑	↑	↓
M679T17_1	17.23	679.4270	Rha-Rha-C10-C12	↑	↑	↑	↑**	↑	↑
M699T17_2	16.64	699.3933	Rha-Rha-C10-C12:1+Na	↑*	↑	↑*	↑**	↑	↓
M701T17_3	17.23	701.4094	Rha-Rha-C10-C12+Na	↑	↑	↑	↑*	↑	↓
M1032T17	16.66	1031.6504	†Rha-C10-C10+Na [2M+H]+	↑***	↑***	↑***	↑***	↑	↓*

†: Putative annotation, ↑: log2FC > 0, ↓: log2FC < 0, *** for p-value ≤ 0.001, ** for 0.001 < p-value ≤ 0.01, * for 0.01 < p-value ≤ 0.05

Fluoroquinolone treatment enhanced the production of the identified lyso-phosphatidyl ethanolamines significantly in both exposures (Table 5.7). Additionally, two identified 2-alkyl-hydroxyquinoline-N-oxides (-QNO) were also over-produced, although not as significant. It is important to note that these identified features were found in region 2 of the heat map, where the fluoroquinolone treatment showed over-production. In contrast, treatment with macrolides and aminoglycosides showed under-production (Figure 5.8). On the contrary, rhamnolipids found in region 4 of the heat map were significantly over-produced under short exposure of all treatments, except for ciprofloxacin (Table 5.8).

Other important identified features did not cluster in any of the mentioned regions of interest, such as secondary metabolites associated with virulence factors: a) quorum sensing molecules HHQ and PQS, and b) phenazines and pyocyanin (Figure 5.9). PQS did not show any significant change in abundance under any treatment. However, HHQ presented a significative reduction in abundance under short and long exposure to ciprofloxacin, as well as under short exposure to levofloxacin, but not under long exposure to it. Additionally, HHQ was significantly less abundant under short exposure to aminoglycosides.

Without exception, the abundance of the identified phenazines (pyocyanin, phenazine-1-carboxilic acid, phenazine-1-carboxamide, and 1-hydroxyphenazine) did not change significantly under any treatment, except for the long exposure to ciprofloxacin (Figure 5.9). However, since these features showed missing values in LE_CIPRO replicates, the significant changes are most likely an artifact of reduced OD_{600} values.
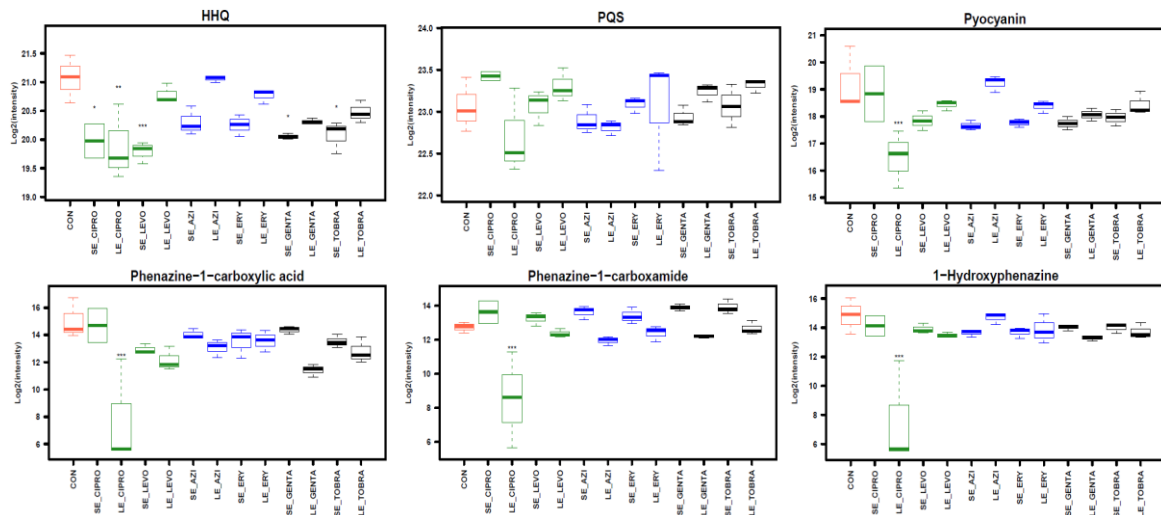
Figure 5.9 Box plots of identified virulence factors in samples of PA14 WT treated under short (SE) and long exposure (LE) to non-inhibitory concentrations of antibiotics: fluoroquinolones (green), macrolides (blue) and aminoglycosides (black) The first box plot correspond to the untreated control (red). *** for p-value ≤ 0.001, ** for 0.001 < p-value ≤ 0.01, * for 0.01 < p-value ≤ 0.05, with respect to the untreated control

In summary, PA14 WT treated with non-inhibitory concentrations of antibiotics presented distinctive phenotypes upon short- and long-exposure treatment. Remarkably, responses to fluoroquinolone-treatment were differentiated from the treatment with macrolides and aminoglycosides. The responses to the treatment with these last two classes of antibiotics were impossible to differentiate under the conditions applied (non-inhibitory concentrations under short and long exposure).

Although important for a matter of comparison between the two experiments, the selected concentrations might have had different inhibitory effects upon short and long exposure. Proved by different harvest points under low exposure, the bacterial growth was impaired at the selected concentrations meaning that the assumption of non-inhibitory concentrations is no longer valid at those conditions.

Most importantly, the strong response to fluoroquinolones at sub-lethal concentrations poses the question of whether this response originates from the inhibitory effect of target-compound specific interactions or due to off-target effects. To solve this question, an experiment to study the direct effects caused by gyrase/topoisomerase inhibition was designed (see 6. Direct and indirect responses upon antibiotic exposure).

5.3 Discussion

Antibiotics cause specific responses according to their mode of action

In this study, a metabolomics approach to evaluate the metabolic response of PA14 WT upon treatment with different classes of antibiotics was undertaken. Differentiated metabolic profiles were observed when using compounds within classes with very distinctive molecular targets: fluoroquinolones (targeting the topoisomerases type II and IV in *P. aeruginosa*), macrolides (with high affinity to the bacterial ribosome) and β-lactams (with high affinity to PBPs).

Nevertheless, no clear distinction was found between antibiotics that inhibit protein synthesis as a mechanism of action, such as macrolides and aminoglycosides, even when the exposure concentrations varied greatly from class to class (20x higher for macrolides). This was observation was consistent with previous reports on the study of the mode of action of antimicrobials (Zampieri et al. 2018; Zampieri et al. 2017).

As protein synthesis inhibitors, macrolides block peptidyl-tRNAs chain elongation by binding to the peptidyl transferase center (PTC) located in the large subunit (LSU) of the bacterial ribosome. Aminoglycosides, however, increase the error rates during the elongation chain of peptidyl-tRNAs by binding to the 16S rRNA as their primary target in the small subunit (SSU), but they also bind to the 23S rRNA as their secondary target in the LSU (Romanowska, Reuter, and Trylska 2013; O'Sullivan et al. 2018). These differences seem to have similar alterations in the metabolic profile, regardless of the ribosomal subunit affected. Bacterial metabolic responses associated to protein synthesis inhibitor have been reported before, using concentrations close to the IC50 and the MIC (Zampieri et al. 2018; Zampieri et al. 2017), where the affected pathways were principally the biosynthesis and metabolism of amino acids, and the biosynthesis of aminoacyl-tRNAs (Dörries, Schlueter, and Lalk 2014; Zampieri et al. 2017). However, under the experimental conditions in the present study, no significant changes in the abundance of the identified amino acids were found, presumably due to the absence of growth inhibition.

Non-inhibitory concentrations of antibiotics cause immediate metabolic changes

PA14 WT responded readily to sudden exposure to antibiotics, where the perturbing agent was introduced while cells were exponentially growing. Signature profiles were identified for groups treated upon short exposure to non-inhibitory concentrations, in comparison with groups treated under long exposure to the same concentrations. Rapid changes induced by

short exposure to aminoglycosides and macrolides were rather heterogeneous, while the treatment with fluoroquinolones exhibits a different profile.

Rhamnolipids were found to be significantly increased under short exposure to non-inhibitory concentrations of aminoglycosides, and macrolides, and less significantly to fluoroquinolones. Rhamnolipids have a complex regulation circuitry in *P. aeruginosa*, and they are widely considered as virulence factors, as well as important contributors to the formation and maturation of biofilm (Chrzanowski, Ławniczak, and Czaczyk 2012). In agreement with previous reports, aminoglycosides contribute to the biofilm generation at sub-inhibitory concentrations (Hoffman et al. 2005; Linares et al. 2006). Conversely, *P. aeruginosa* treated with azithromycin has shown delays in biofilm formation (Nalca et al. 2006) and reduced production of rhamnolipids (Tateda et al. 2001). A possible explanation for the diversity of the result may rely on the difference of experimental setups used in the studies.

Since rhamnolipids biosynthetic pathway shares steps in common with lipid metabolism, alginate production, and AQs biosynthesis, their difference in abundance might be the result of a set of adaptations towards antibiotic stress.

Fluoroquinolones cause a strong metabolic response even at sub-inhibitory concentrations

Both ciprofloxacin and levofloxacin presented a better antimicrobial efficacy in terms of inhibitory concentrations than the rest of the compounds. This was observable also at the non-inhibitory level, as the applied concentrations for fluoroquinolones were 80x lower than for macrolides and 4x lower than for aminoglycosides.Immediate and long-term responses of *P. aeruginosa* treated with fluoroquinolones were stronger and more distinctive than those under other antibiotic class treatment, even by trying to ensure the comparison of harvested cultures at the same cell density.

Treatment with fluoroquinolones showed some unidentified features that responded more readily than in any other of the treatments. Additional work on the identification of some of these features is needed. There were also identified features that responded more strongly to fluoroquinolone treatment, mainly LPEs and some 2-alkyl-4hydroxyquinoline N-oxides (QNO) analogs. These metabolites showed significantly increased intensity in samples treated under short and long exposure of both ciprofloxacin and levofloxacin. LPE is evidence of alterations in lipid metabolism, while AQNOs themselves have been found to present antimicrobial properties (Heeb et al. 2011). Previous reports found that sub-MIC concentrations of fluoroquinolones in *P. aeruginosa*, specifically ciprofloxacin, induce biofilm formation and

reduce swimming and swarming (Linares et al. 2006), decrease siderophore production (Trancassini et al. 1992), enhance the mutation frequency (Wolter et al. 2007; Tanimoto et al. 2008), and induce the general SOS bacterial response (Brazas and Hancock 2005; Breidenstein, Bains, and Hancock 2012).

Although the disturbance in lipid metabolism due to fluoroquinolones is not yet understood, some studies highlight the interactions of fluoroquinolones across lipid layers (Cramariuc et al. 2012; Bensikaddour et al. 2008) and it has been shown that alteration in the LPS structure lead to a reduced compound translocation (Mingeot-Leclercq and Décout 2016), e.g. reduced fluoroquinolones accumulation (Everett et al. 1996). The present study shows that fluoroquinolones have an effect on *P. aeruginosa*'s lipid metabolism, even when treated at sub-lethal concentrations.

Antibiotic concentrations for metabolomics studies are not standardized

Treatment concentrations vary greatly in studies that aim to profile the response of microorganisms to antimicrobials. Some authors select sub-MIC concentrations based on the plate-assay determined measured MIC value, e.g. 0.1xMIC, 0.5xMIC or 0.8xMIC. Others make their selection based on the concentrations that do not affect bacterial growth. This shows that the selection of sub-inhibitory, sub-MIC, non-inhibitory, sub-lethal or non-killing concentrations is not yet standardized. Even the term "sub-inhibitory" often is confused with "sub-MIC".

Yet, treatment concentrations can cause a strong inhibitory effect even when they are lower than the MIC values. For instance, Zampieri et al. analyzed the response of *E. coli* to a set of 10 antibiotics with a nontargeted metabolomics approach (Zampieri et al. 2017). For their study, they chose concentrations "close to" the concentration that inhibits 50% of the growth (IC50), and one concentration "close to" the MIC value. When compared to both "low" and "high" dosages, they found little deviations in the metabolic response, indicating that IC50 concentrations influence metabolic changes to an extent comparable to bacterial cell death.

Logically, non-inhibitory concentrations do not affect bacterial growth when compared with the untreated control. However, the growth conditions vary also from study to study, being unable to compare the effects of punctual concentrations across experiments with e.g. different carbon sources or different nutrient availability. Therefore, a complete study of antibiotic effects upon a range of concentrations, both sub-inhibitory and inhibitory, is still needed.

6. DIRECT AND INDIRECT RESPONSES UPON ANTIBIOTIC EXPOSURE

According to their concentrations, antibiotics my act as toxins at high concentrations, stress inducers at sub-lethal concentrations, or as cues or coercions at low, sub-inhibitory concentrations (Bernier and Surette 2013). One major challenge is to differentiate whether the effects induced by antibiotics at low concentrations are due to on-target effects as an adaptive response of the organism to partial inhibition of the target, or whether secondary, unknown targets induce additional responses. Under this scenario, the following hypothesis was posed: a target mutation that prevents compound binding should completely evade all effects caused by the primary target. Therefore, all responses of the organism should be triggered by interactions with other, secondary components (see Figure 6.1).
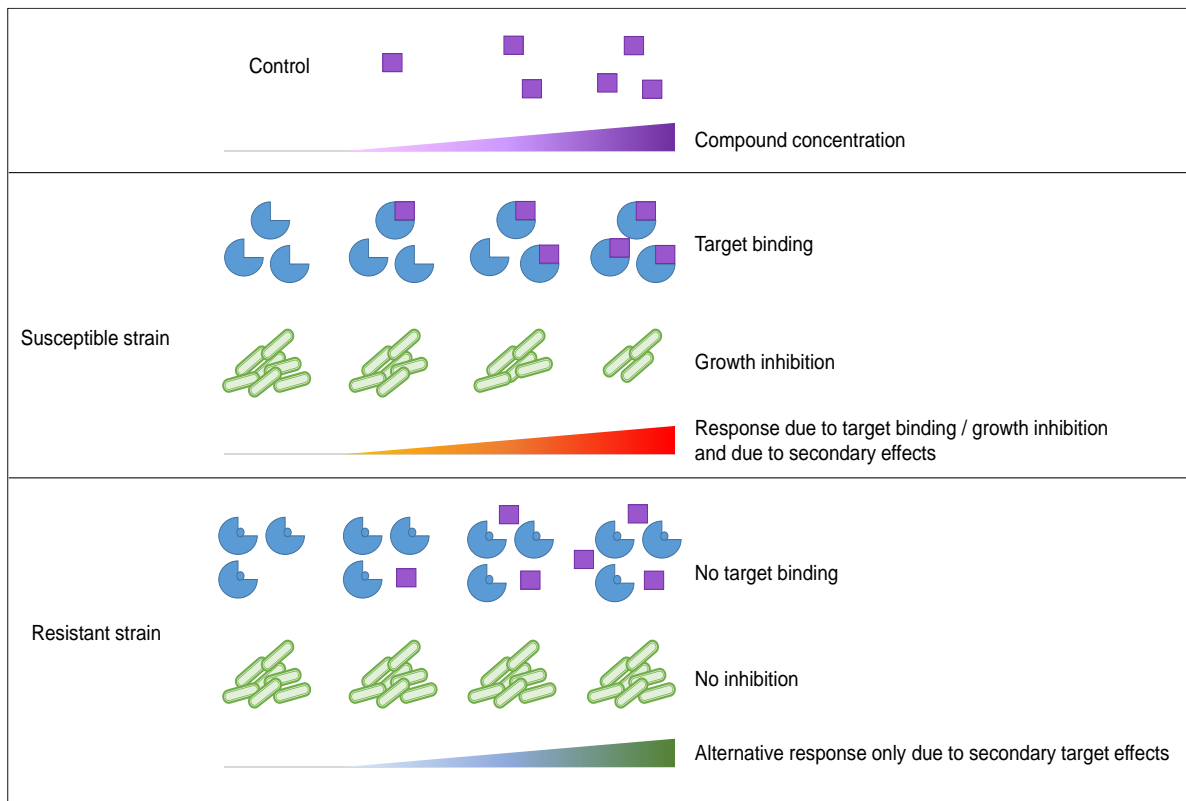
Figure 6.1 Experimental design to study the direct and indirect consequences of antibiotic exposure

6.1 Characterization of fluoroquinolone resistant strains

Two fluoroquinolone-resistant mutants were evaluated to select the most resistant to ciprofloxacin. The mutants were constructed with the introduction of one or two single nucleotide polymorphisms (SPN) in *gyr*A Thr83Ile and *par*C Ser87Leu to the ciprofloxacin-susceptible reference strain PA14 WT (Bruchmann et al. 2013), and were kindly donated by Prof. Dr. Susanne Häußler. The extent of resistance was evaluated by growth inhibition assays, and the sub-inhibitory concentrations were determined for PA14 WT, PA14 *gyrA* Thr83Ile (hereon PA14 gyrA) and PA14 *gyrA* Thr83Ile *parC* Ser87Leu (hereon PA14 gyrAparC). The values for their inhibitory concentrations are listed in Table 6.1. The calculation of sub- and inhibitory concentrations NIC, IC10, IC50, and MIC was based on the method previously reported by Lambert *et al*. 2000, where NIC is defined as the concentration above which growth inhibition starts (Lambert and Pearson 2000).

Table 6.1 Inhibitory concentrations of ciprofloxacin in susceptible and resistant *P. aeruginosa* strains in µg/mL

Strain	NIC	IC10	IC50	MIC
PA14 WT (WT)	0.016 ± 0.003	0.023 ± 0.000	0.059 ± 0.001	0.151 ± 0.005
PA14 *gyrA* T83I (gyrA)	0.053 ± 0.026	0.127 ± 0.052	1.073 ± 0.068	12.983 ± 0.827
PA14 *gyrA* T83I *parC* S87L (gyrAparC)	8.501 ± 0.598	10.440 ± 0.691	17.597 ± 0.985	29.833 ± 1.360

These results are consistent with previous data showing that GyrA is not the only target affected by ciprofloxacin in *P. aeruginosa* (Bruchmann et al. 2013). Inhibition of the DNA topoisomerase IV complex also accounts for the activity of this compound. By inserting a point mutation in *gyrA*, PA14 WT increased its tolerance to ciprofloxacin by 6.4 log2-units in MIC. Inserting a second mutation, but now in *parC* to the PA14 gyrA mutant, increased its resistance by only 1.2 log2-units in its MIC value. However, the rest of the sub-MIC concentrations (NIC, IC10 and IC50) changed substantially upon this second point mutation, as seen in Figure 6.2a.
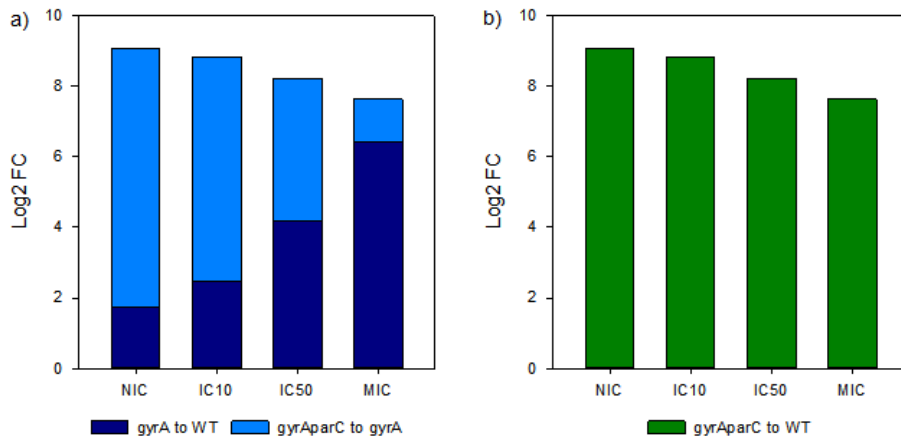
Figure 6.2 Log2 fold-changes respect to the WT at MIC and sub-MIC concentrations, a) fold-change given by a point mutation in gyrA compared to the WT (dark blue), fold change given by point mutations in gyrA and parC compared to the gyrA mutant (light blue), b) global fold-change given by both mutations in gyrA and parC compared to the WT (green).

When compared with the WT, PA14 gyrAparC increased the tolerance to the whole range of inhibitory concentrations more homogenously (Figure 6.2b). This analysis shows how the contribution of each individual mutation to the overall resistance is distributed over a range of concentrations. While the point mutation in *gyrA* provides resistance to highly inhibitory concentrations, the additional mutation in *parC* extends the tolerance toward the low range of inhibitory concentrations.To account for a minimal drug-target interaction, the PA14 gyrAparC mutant was selected for studying the metabolic response upon ciprofloxacin treatment. This because its range of inhibition does not overlap with the reference WT strain as shown in Figure 6.3, and the exposure to WT sub-inhibitory concentrations (sub-MIC$_{WT}$) does not affect the growth of gyrAparC.
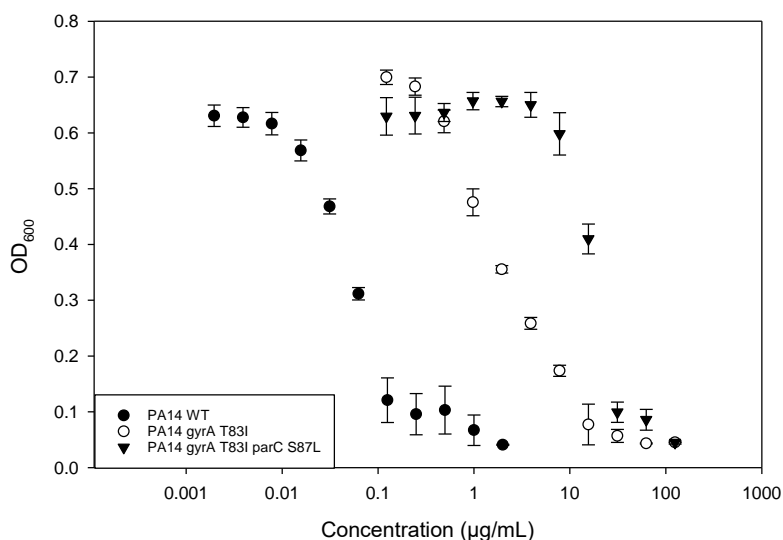
Figure 6.3 Growth inhibition of resistant and reference strains under ciprofloxacin stress after 24 h at 37°C of incubation in BM2 medium. The y-axis is the OD$_{600}$ of 200 μL in a microplate. Error bars are the standard deviation of two independent experiments with two replicates (n=4)

6.2 Selection of antibiotic concentrations for metabolome experiments

In order to select the appropriate concentrations for metabolomics experiments, the growth inhibition of ciprofloxacin in both strains, PA14 WT and PA14 gyrAparC, was monitored over 12 hours. Briefly, 3-mL cultures, inoculated with the respective strain to an OD_{600} = 0.05, were incubated at 37° and 150 rpm under the inhibitory concentrations for WT listed in Table 6.1. Exposure to inhibitory concentrations affected growth in PA14 WT, while PA14 gyrAparC treated with WT inhibitory concentrations showed no effect in growth, even at MIC_{WT} (Figure 6.4). Although ciprofloxacin at MIC_{WT} inhibited the growth of PA14 WT over the first 12 h, the cultures reached visibly high turbidity after been left incubating overnight at 37°C (not shown); contrary to what was expected, since the treatment of PA14 WT with MIC should inhibit the growth after 24 h.
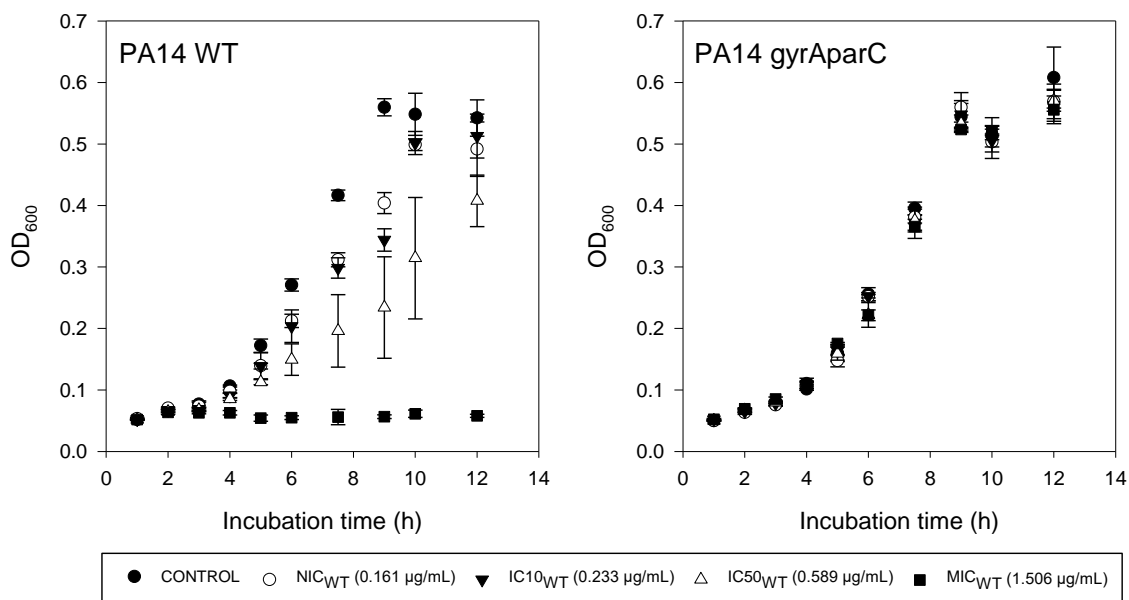
Figure 6.4 Growth curves for PA14 WT and PA14 gyrAparC under ciprofloxacin treatment at MIC and sub-MIC concentrations. Cultures were incubated at 37° and 150 rpm in 10-mL test tubes inclined at 60°. Aliquots of 100 µL were taken at a fixed time from all the replicates of both strains and transferred to the wells of a microtiter plate to measure the OD_{600}. Error bars are the standard deviation of three replicates (n=3)

As a comparison, PA14 WT growth assays in microtiter-plate format and in test-tube format were carried out. As shown in Figure 6.5, the curve from the test-tubes format resulted in being shifted to the right, increasing the concentration required for different degrees of inhibition when compared to the plate format. Furthermore, the calculation of sub- and inhibitory concentrations was carried out and listed in Table 6.2. The MIC in tubes was about 9-fold

higher than MIC in plates, while IC50 in tubes was over 4-fold higher than in plates. NIC and IC10 in tubes were about 1.5- and 2-fold higher than in plates, respectively.
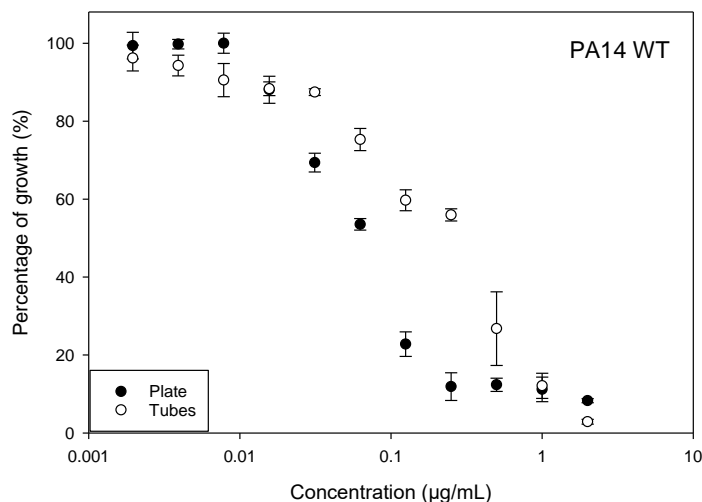
Figure 6.5 Comparison of PA14 growth inhibition assay in a plate (96-well microtiter plates containing 200 µL of culture) and in tubes (test tubes containing 3.1 mL of culture) under ciprofloxacin stress after 24 h at 37°C of incubation in BM2 medium. The antibiotic solutions were freshly prepared, and all the dilutions were performed from the same stock. The y-axis shows the percentage of growth for each format calculated based on the OD_{600} measured for the untreated controls (not shown). Error bars are the standard deviation of 3 replicates (n=3)

Table 6.2 Sub- and inhibitory concentrations for PA14 WT in a plate and tubes in µg/mL

Format	Culture volume (mL)	NIC	IC10	IC50	MIC
Plate	0.2	0.016	0.023	0.059	0.151
Tubes	3.1	0.025	0.048	0.255	1.364

For metabolomics experiments, PA14 WT and PA14 gyrAparC were cultivated in tubes and exposed to the whole range of sub- and inhibitory concentrations determined in plates for WT, including the value for MIC_{WT}. Briefly, 3-mL cultures were incubated at 37°C and 150 rpm under the inhibitory concentrations for WT and harvested when the OD_{600} value was close to 1.0 (Table 6.3). Samples of PA14 WT were harvested at different incubation times in order to reach comparable OD_{600} values, while all samples of PA14 gyrAparC were harvested simultaneously. PA14 WT samples treated with MIC_{WT} reached an OD_{600} close to 1.0 after 28 h of incubation.

Table 6.3 Harvest information of samples un- and treated with ciprofloxacin concentration for metabolomics experiments

Treatment	Initial concentration (µg/mL)	Incubation time (h)	Final OD$_{600}$ per replicate		
			1	2	3
WT_CON	0	6.5	1.28	1.08	1.24
WT_NIC	0.016	7.0	0.97	1.07	0.94
WT_IC10	0.023	7.0	1.01	1.01	0.97
WT_IC50	0.059	9.0	0.99	1.07	0.94
WT_MIC	0.151	28.0	1.39	1.44	1.24
gyrAparC_CON	0	7.0	1.23	1.14	1.34
gyrAparC_NIC	0.016	7.0	1.06	1.03	1.12
gyrAparC_IC10	0.023	7.0	1.19	1.2	1.17
gyrAparC_IC50	0.059	7.0	1.18	1.19	1.14
gyrAparC_MIC	0.151	7.0	1.00	1.00	1.13

6.3 Data analysis and feature identification

An untargeted analysis was applied for the samples of PA14 WT and PA14 gyrAparC treated with ciprofloxacin. Briefly, harvested bacterial cells were washed and lysed; the extracted intracellular metabolome was analyzed in positive mode in a UPLC-ESI-QToF.

6.3.1 Data filtering

Raw metabolomics data were pre-processed in XCMS Online for peak picking and feature detection. The complete pre-processed metabolomics data consisted of a total of 7344 features. Out of them, 1334 features (18.16%) were identified by XCMS as first, second, third, and fourth isotope peaks, with single, double and triple charges (Table 6.4). These features were removed for further analysis, leaving 6010 monoisotopic ions.

Additionally, a retention time cutoff of 0.3 min ≤ RT ≤ 28 min was applied, so 770 features were filtered out. Five compounds were used as internal standards: glipizide, trimethoprim, and nortriptyline as extraction standards, and caffeine and naproxen as injection standards. The data were normalized by the intensity of the internal standards (ISTDs) and OD$_{600}$, and the intensity of these ISTDs and their adducts were filtered out, resulting in a feature table with 5216 candidates to be identified as metabolites, as shown later in Figure 6.8.

Table 6.4 Number of features identified as ion isotopes in metabolomics data

Isotopic peak	Ion charge		
	1+	2+	3+
[M+1]	768	173	29
[M+2]	215	25	18
[M+3]	81	6	2
[M+4]	13	4	0

6.3.2 Feature identification in positive mode

With the use of two MS/MS *in-house* and two commercial compound libraries (*in-silico* generated MS/MS spectra from MetaboBase Personal Library and LipidBlast), 193 features were successfully annotated, corresponding to 87 unique metabolites. One of the libraries is *P. aeruginosa*-specific and contains spectral information from representative secondary metabolites. Direct MS/MS library matching accounted for an identification yield of 3.70%, including in-source fragments, adducts, and multiple-charged ions. As it is shown later in Table 6.5, this yield of identification was improved by another two means of spectral clustering, as well as putative annotation by manual scrutiny.

Followed by the library matching identification, mzXML-formatted data for PA14 WT treated and untreated samples with triplicates was submitted to analysis via on-line GNPS (Global Natural Product Social Molecular Networking) library-based molecular networking, which performs a spectral alignment among samples and creates clusters of features with spectral similarity (Wang et al. 2016). GNPS molecular networking resulted in 938 features grouped in 51 clusters, from which nine were the most prominent and those with MS/MS matching with the GNPS library (Figure 6.6). The most representative classes of secondary metabolites in *P. aeruginosa*, alkyl-quinolones, phenazines, and rhamnolipids were grouped in three respective clusters. The cluster corresponding to alkyl-quinolones congeners consisted of 96 features, including HQ-, PQS- and QNO- related compounds, while the rhamnolipids cluster contained 57 features. The phenazine cluster contained only four features. A crowded cluster containing phenylalanine-related compounds but also pyocyanin was found with 40 features. A cluster containing phospholipids was generated with 20 features. Similarly, 12 glutamate-related features were clustered together, and seven features related to spermidine formed a separated cluster. A cluster containing glutathione was found with four features. Clusters for three of the internal standards were found as well: a cluster of nortriptyline with eight features, a cluster of glipizide with two features, and a cluster of trimethoprim with two features (for the complete cluster table, see *Appendix V. GNPS clustering*).
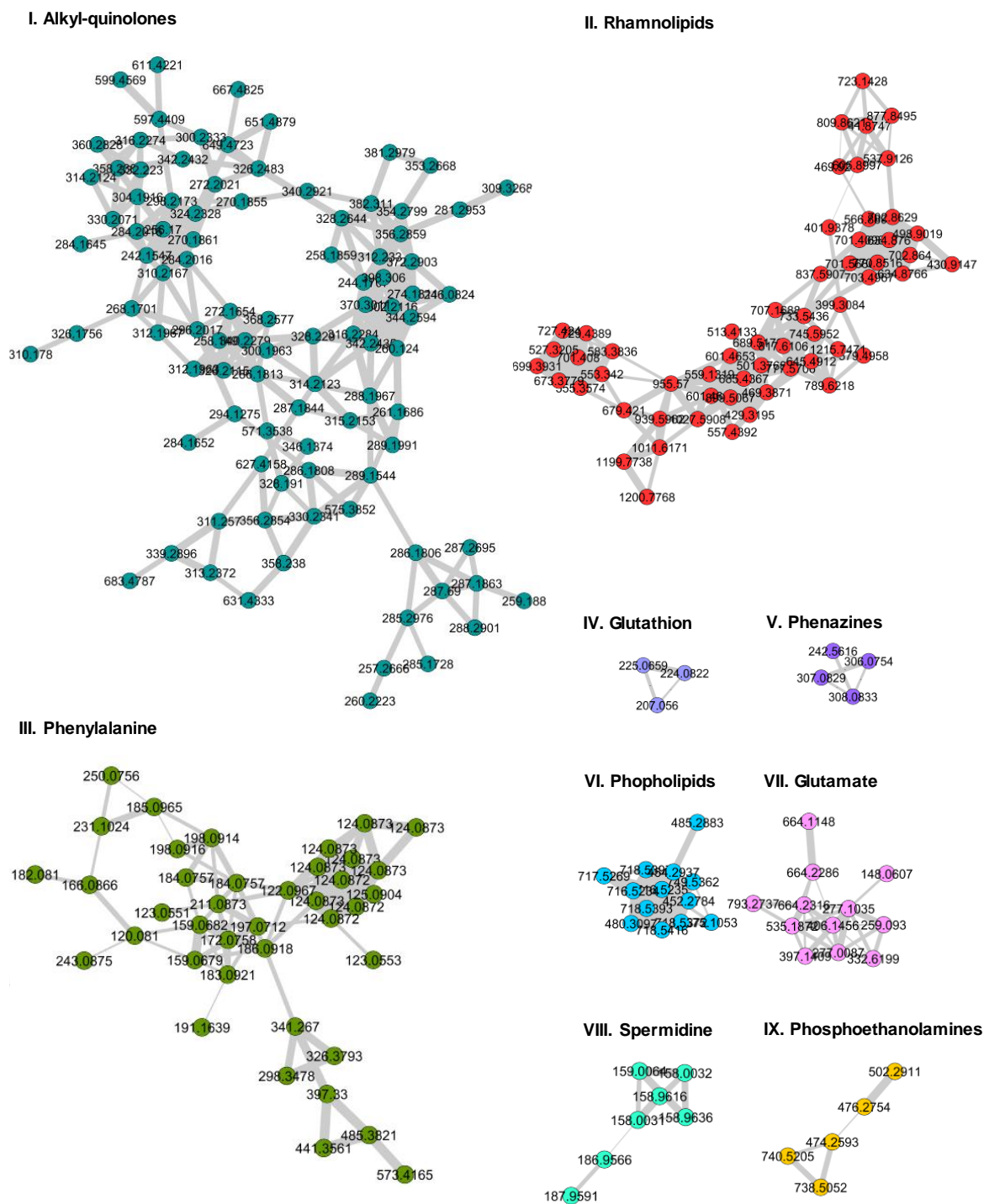
Figure 6.6 Molecular networking of the identified features found by the GNPS algorithm. Every node corresponds to a feature with a defined m/z value (shown) and an RT (not shown). The width of the edges (in grey) corresponds to the cosine score as a measure of spectral similarity, the thicker the edge, the more spectral similarity among the features

Furthermore, a pooled sample of gyrAparC untreated samples (controls) was analyzed with CluMSID (Depke, Franke, and Brönstrup 2017, 2019), an R-based package that performs clustering of features with spectral similarity. Figure 6.7 depicts the resulting circular hierarchical clustering of 1172 features, grouped in 120 clusters, where the most populated clusters are highlighted. These data were analyzed manually to identify three of the most prominent clusters. Cluster #35 with 240 features corresponds to alkyl-quinolones congeners, cluster #8 with 186 features corresponds to rhamnolipids, and cluster #1 with 106 features contains glutamate-related compounds. For cluster #2 with 94 features and cluster #3 with 140, there were no identified features (for the complete cluster table, see *Appendix VI. CluMSID clustering*).
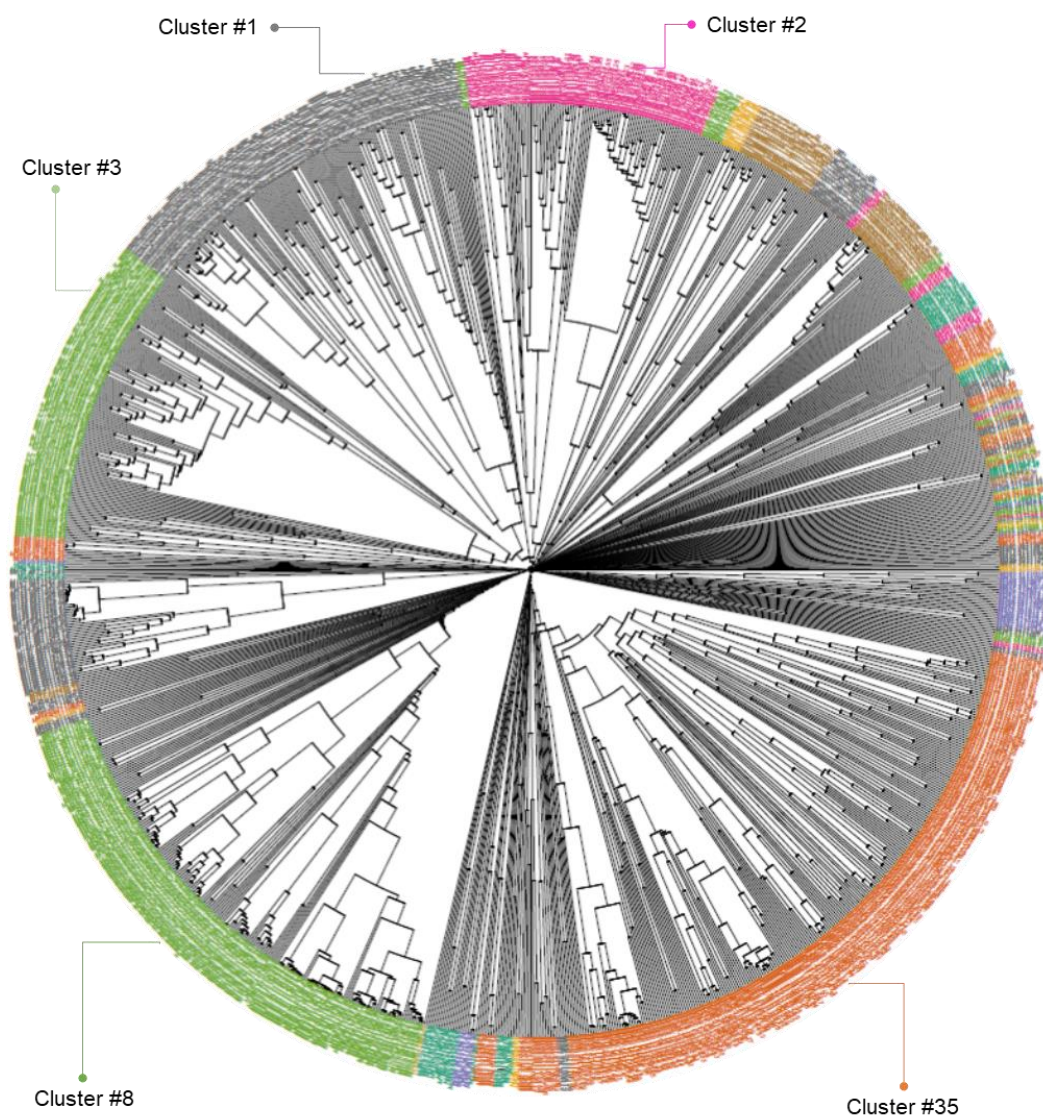
Figure 6.7 CluMSID circular hierarchical clustering of 1172 features in a pooled sample of gyrAparC untreated control. Cluster #1: glutamate-related compounds, Cluster #8: rhamnolipids, Cluster #35: alkyl-quinolones, Cluster #2 and #3: not identified features

So far, three metabolite identification tools were applied: direct matching with MS/MS *in-house* and commercial libraries, feature clustering by GNPS-generated molecular network, and feature clustering by CluMSID. The last two resulted in two different tables with independent features that do not necessarily match with the original data set (feature table from XCMS Online). By comparing the exact mass and retention time of the features in the original data set with those in the cluster table (see 3.5.5 Feature identification), 763 features were matched with the GNPS cluster numeration, and 442 features were matched with the CluMSID cluster numeration. However, not all the cluster numbers could be identified, only 336 features with GNPS numeration and 293 features with CluMSID numeration were assigned an identification label (see Figure 6.8).

Identification labels were assigned according to the compound class: "AA" for aminoacids, "AQ" for alkyl-quinolones, "FA" for fatty acids, "Glu" for glutamic containing features, "Glutathion" for the glutathione-related features, "HSL" for homoserine-lactones, "Lip" for unidentified lipids, "Nuc" for nucleotides, "Phen" for phenazines, "Phenyl" for phenylalanine-related features, "PhosLip" for phospholipids, "Rha" for rhamnolipids, and "UDP" for features containing uridine diphosphate (see *Appendix VII. Annotation table - sub-MIC ciprolfoxacin concentrations*). When a cluster contained one or more identified features, a label of the compound class was assigned; when a cluster contained only unidentified features, the complete cluster remained unlabeled. In total, 539 features were assigned with a class label.

Additional manual identification was carried out based on the RT, the exact mass of the molecular ion for each feature, and with the help of the assigned class labels, resulting in another 152 features with a putative label preceded by an asterisk (*). The spectral information of features with putative labels was examined in Data Analysis to corroborate their exact mass and isotope distribution (for more details, see *Appendix IV. MS and MS/MS identification).*

Table 6.5 summarizes the feature identification strategy and the tools used. After feature filtering and identification, only 70.96% (5211 of 7344) of the features were considered candidates for being metabolites (Figure 6.8). With 564 features assigned with an annotation by means of any of the identification tools (539 with a class label and 25 without), the yield of identification raised to 10.82%, in comparison with a search strategy that is limited to direct matching with spectral libraries with 3.70%.
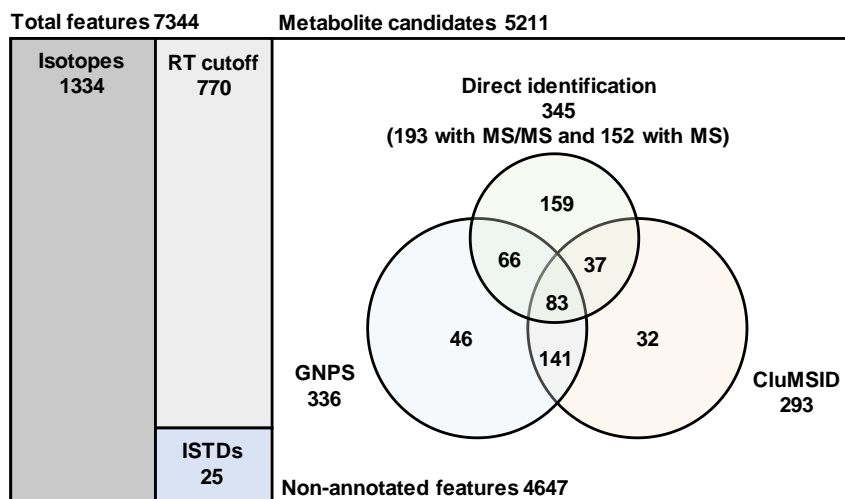
Figure 6.8 Feature filtering and identification after preprocessing with XCMS Online. 1334 features were filtered by monoisotopic signals with CAMERA, and 770 by retention time (0.3≤RT≤28 min). 25 features related to ISTDs were filtered out. Out of the original 7344 features, 5211 were selected as effective metabolite candidates, from which, 193 features were identified by MS/MS libraries, 293 grouped by spectral similarity by CluMSID, and 336 by GNPS molecular networking. The colored Venn diagram shows the distribution of the 564 annotated/identified features, while the remaining 4647 features were not annotated.

Table 6.5 Feature identification based on spectral information

Identification tool	Level of information	Matches	In labeled clusters	Effective annotations[a]
in-house general	RT, MS, MS/MS	61[b]		
in-house (P. aeruginosa)	RT, MS, MS/MS	100[b]	193	159[b] (87 identified metabolites)
MetaboBase	*in-silico* MS/MS	15		
LipidBlast	*in-silico* MS/MS	17		
Putative	RT, MS	152[b]	152	
GNPS	Experimental MS/MS	764	336	46
CluMSID	Experimental MS/MS	443	293	32

[a] Not sharing annotation with other identification tools
[b] Including manual annotation of fragments, adducts and multiply charged ions

6.3.3 Feature identification in negative mode

Apart from the feature filtering and identification in positive mode, a similar approach was used with data coming from the same samples analyzed in negative mode. XCMS Online and GNPS parameters were adjusted for negative mode, and the resulting data was processed in the same way as for positive mode.

From this analysis, nine features were identified by the direct match with MS/MS libraries, so their retention times, as well as m/z and intensity values were added to the feature table. The annotation label was proceeded by "(neg)" for negative mode. As seven of them were identified as phospholipids, the corresponding class label "PhosLip" was assigned. Similarly, one feature corresponded to an alkylquinolone, therefore the class label "AQ" was assigned. However, no matches were found with the cluster analysis from GNPS and CluMSID, and no additional

putative labels were possible to assign. The annotation information is listed in Appendix VII. *Annotation table - sub-MIC ciprolfoxacin concentrations*.

6.4 Effects of ciprofloxacin on the metabolome in fluoroquinolone-resistant and susceptible strains

6.4.1 Phenotype characterization

The feature table was further analyzed to find the principal components that bring the most diversity among groups. The two components with the highest explained variance are plotted in Figure 6.9a. All samples from gyrAparC remain close forming a big cluster that also contains the WT untreated controls, with the exception of one replicate of the WT untreated controls, which remains far from this cluster, which can be due to experimental deviation. As expected, gyrAparC responded similarly to the untreated controls, as the concentrations used for the mutant have no inhibitory effect at all.

In the case of the treated WT samples, the replicates remain close to each other, but the groups with increasing antibiotic concentration are distributed along the PC1 and PC2. Since PCA is a mathematical decomposition of the possibly correlated variables within a dataset, in order to reduce its dimensionality, there is no certain way to attribute a physical variable to each component.

Additionally, a loadings plot shows what features contribute the most to the separation among the groups seen in Figure 6.9a. As shown in Figure 6.9b, rhamnolipids (in red) have the largest effect on both components, as they are located at the most distant points over both PC1 and PC2. Similarly, phenylalanine-related features (in gray) and homoserine-lactones (in purple) are gathered towards the extreme points in PC1. Alkyl-quinolones have an important effect as they are located mostly around the negative extreme of PC1; however, they are also widely distributed across the cloud of points in the plot, meaning that they have a moderate contribution to differentiate among the separated groups.
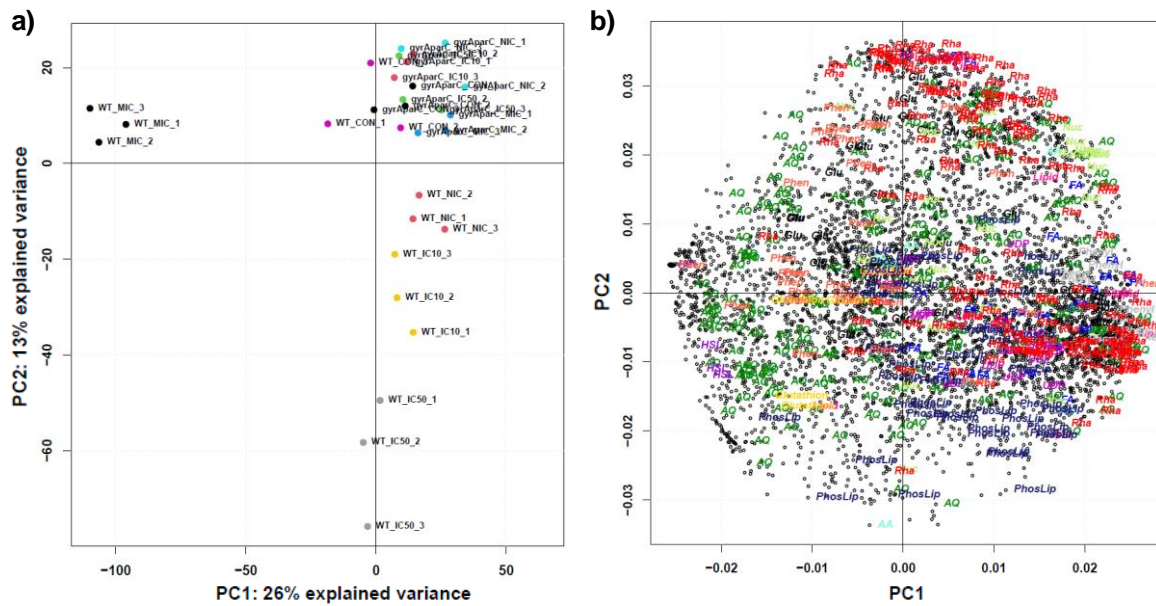
Figure 6.9 Principal component analysis of WT and gyrAparC samples treated with sub-MIC$_{WT}$ concentrations. a) Scores plot of PC1 and PC2 for every sample, b) loadings plot of PC1 and PC2 for every feature showing the cluster label if available. Aminoacids (AA) in aquamarine, alkyl-quinolones (AQ) in green, fatty acids (FA) in blue, glutamate (Glu) in black, glutathione (Glutathion) in yellow, homoserine-lactones (HSL) in purple, lipids (Lipid) in pink, nucleotides (Nuc) in lightgreen, phenazines (Phen) in orange, phenylalanine (Phenyl) in grey, phospholipids (PhosLip) in darkblue, rhamnolipids (Rha) in red, uridine diphosphate (UDP) in magenta.

Another method to evaluate how closely related the samples are, a correlation matrix was built with the processed and normalized data. As shown in Figure 6.7, two main clusters are indicated by the dendrogram, the first contains all the treated samples from PA14, while the second contains all the samples (treated and untreated) from PA1a gyrAparC and the untreated PA14 WT. Additionally, MIC$_{WT}$-treated samples for PA14 WT form a sub-cluster, indicated by the height of the dendrogram of this group. Therefore, three main clusters are observed from left to right: I) a "high-inhibition" cluster, II) a "medium-inhibition" cluster, and III) a "non-inhibition" cluster. Furthermore, both strains PA14 WT and gyrAparC are metabolically similar, as the untreated controls are clustered together.

No surprisingly, even NIC-treated samples were included in the "inhibition" cluster, since they were delayed up to 30 min for the harvest at OD$_{600}$ ≈ 1.0 when compared with the untreated samples. (Table 6.3). This was previously found in the short- and long-term experiments where treatment with fluoroquinolones at NIC depicted strong responses (Figure 5.8).
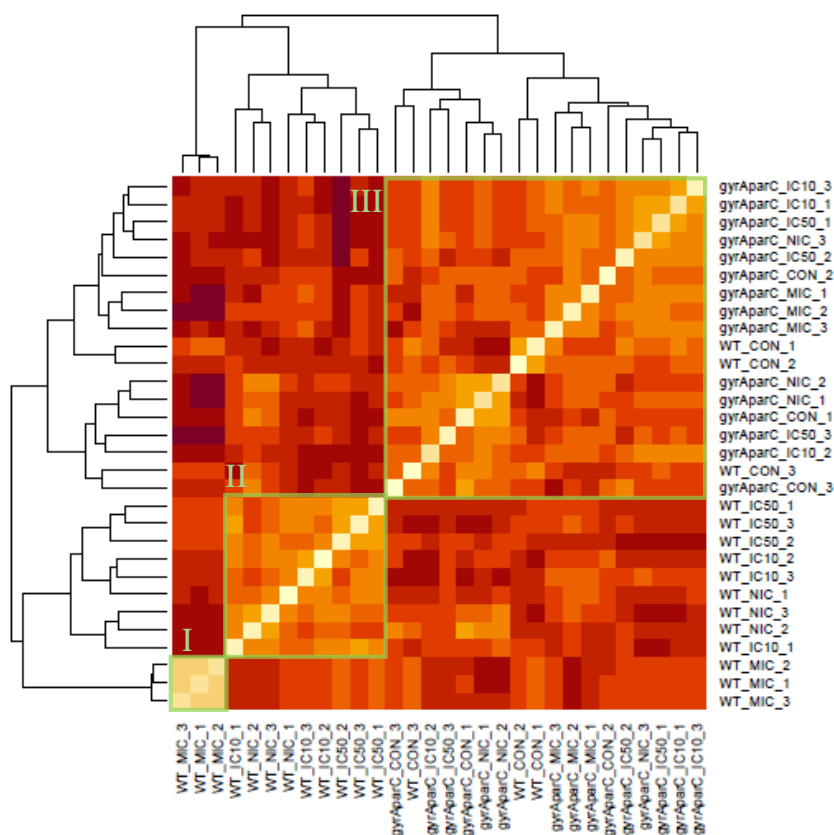
Figure 6.10 Correlation matrix for PA14 WT and gyrAparC samples treated with MIC_{WT} and sub-MIC_{WT} concentrations. Three clusters are highlighted: I) a "high-inhibition" cluster, II) a "medium-inhibition" cluster, and III) a "non-inhibition" cluster.

To this point, PA14 WT and gyrAparC presented different responses when treated with sub-MIC_{WT} concentrations, supporting the hypothesis that the resistant strain does not respond to ciprofloxacin due to lack of binding to the target as proposed in Figure 6.1. Yet, differences in the gyrAparC mutant across treatment concentrations have not been identified. For this, the treated samples were compared against the respective untreated controls to find changes in abundance throughout their metabolic profiles. The log2-transformed fold changes (relative to the respective untreated controls) of identified metabolites are depicted as heat maps in Figure 6.11. A comparison between untreated samples of PA14 WT and gyrAparC was not carried out because both strains presented similar metabolic profiles at the harvest point.
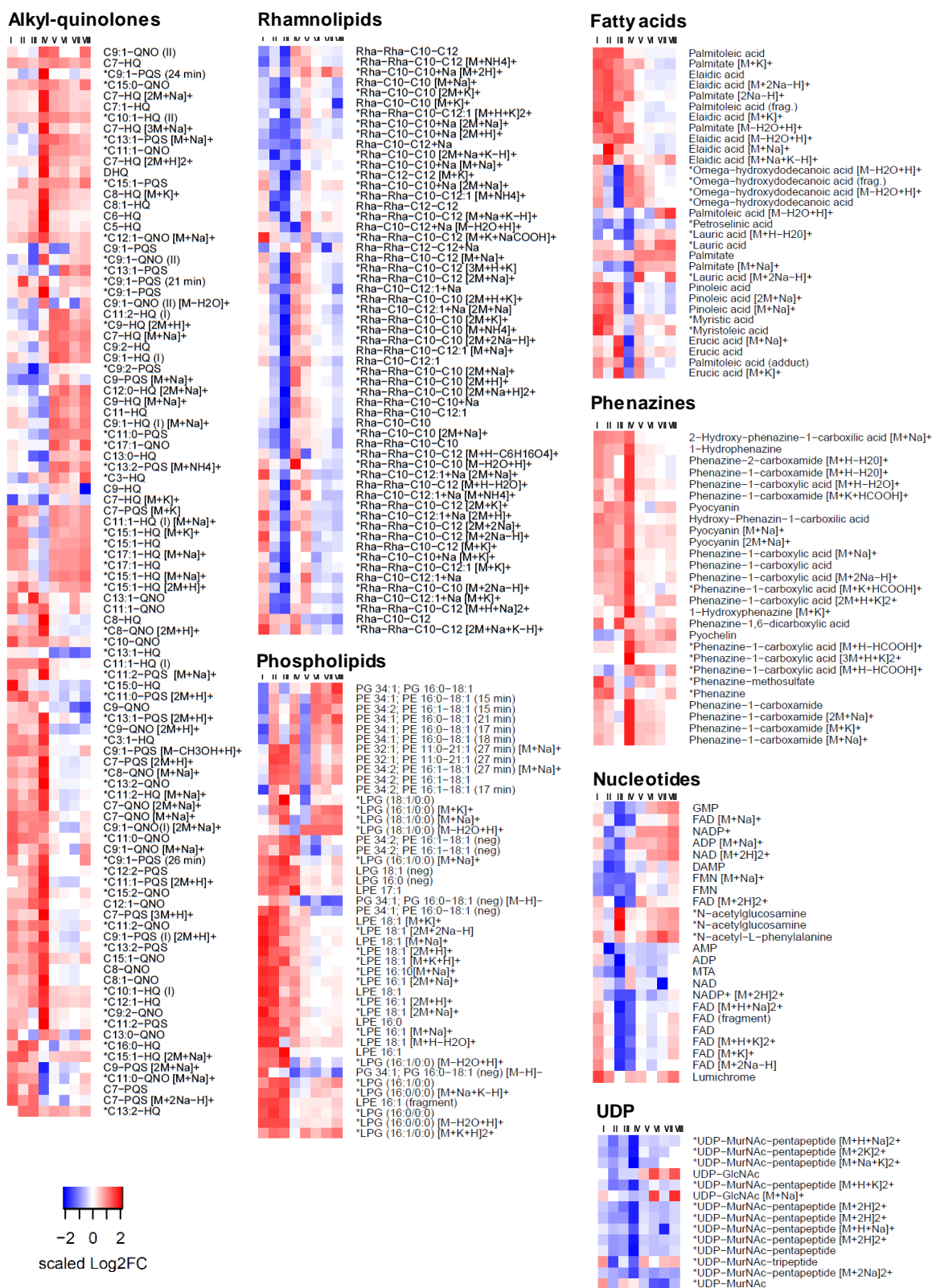
Figure 6.11 Heat maps of identified features including their adducts (*: putative annotation). Log2-transformed fold change (Log2FC) was calculated from the mean values of triplicates, by subtracting the log2 values of each condition (I: WT_NIC, II: WT_IC10, III: WT_IC50, IV: WT_MIC, V: gyrAparC_NIC, VI: gyrAparC_IC10, VII: gyrAparC_IC50, VIII: gyrAparC_MIC) from the untreated control samples of the respective strain (WT_CON and gyrAparC_CON). Scaled Log2FC was performed as a default function in R Studio for visualization of over-produced metabolites (in red) and under-produced metabolites (in blue)

Generally, rhamnolipids and UDP-related metabolites showed a decrease in their intracellular abundance in both strains, indicated visually with intense blue shades in the heat maps. In the case of nucleotides, most of the decreased levels were present in PA14 WT, while gyrAparC presented a slight increase in their levels, indicated by light red shades. For example, WT treated samples showed less abundance of flavin adenine dinucleotide (FAD) and its precursor flavin mononucleotide (FMN), while gyrAparC showed slight increases. Furthermore, phenazines were consistently over-produced in both strains, and more strongly in PA14 WT treated with MIC_{WT}, although the gyrAparC mutant presented slight increases in those compounds.

The panel of identified phospholipids primarily shows increased levels in PA14 WT, with particular cases for gyrAparC. Three phosphoethanolamines identified as PE 32:1 with 16:0 and 16:1 fatty acid chains, PE 34:1 with 16:0 and 18:1 fatty acid chains, and PE 34:2 with 16:1 and 18:1 fatty acid chains, generally increased their levels in PA14 WT, while in gyrAparC showed a slight increase. The levels of lyso-phosphatidylethanolamines, such as LPE 16:0, LPE 16:1 and LPE 18:1, were increased in PA14 WT, while they remained unchanged in gyrAparC. Additionally, the levels of the only identified phosphatidylglycerol, PG 34:2 with 16:0 and 18:1 fatty acid chains, decreased in both strains, but mainly in gyrAparC. Lyso-phophatidylglycerols, such as LPG 16:0, LPG 16:1, LPG 18:1, presented higher levels in PA14 WT, while their increment in gyrAparC was less pronounced.

The panel of alkyl-quinolones shows great variation in the abundance of these metabolites. For instance, many PQS and QNO congeners were over-produced by PA14 WT, showing their largest change with MIC_{WT} treatment. While the response of PA14 gyrAparC is less pronounced. The most abundant alkyl-quinolones C9-HQ and C9-PQS presented mild fold changes, due to the saturation in their detection, making their semi-quantitative analysis difficult. Moreover, the levels of a group of glutamate-containing metabolites, consisting mainly of glutamic acid and related peptides, were found to increase in gyrAparC. Finally, the levels of some fatty acids were increased in PA14 WT, while in gyrAparC their levels remained mostly unmodified.

Comparing the effect on WT with the effect on gyrAparC should disclose the target-mediated effects. From the analysis of the relative abundance of the identified features, there is evidence that some of them respond accordingly to the initial concentration used for the treatment, indicating that the intracellular metabolic response to the antibiotic exposure relates to the degree of antibiotic accumulation. The accumulation of ciprofloxacin was evaluated by the untargeted analysis and corroborated by its quantification by a targeted analysis.

6.4.2 Intracellular accumulation of ciprofloxacin

MS/MS identification of ciprofloxacin was carried out by direct comparison with the *in-house* library. As shown in Figure 6.12a, PA14 WT and PA14 gyrAparC presented a similar abundance of ciprofloxacin at NIC_{WT} and $IC10_{WT}$; however, the signalwas lower for PA14 WT at $IC50_{WT}$ and MIC_{WT} compared to the mutant. Ciprofloxacin accumulation was determined by measuring the samples with the MRM targeted method for ciprofloxacin as described before for the high-throughput uptake assay (3.3.2 LC-MS/MS compound-specific MRM methods).
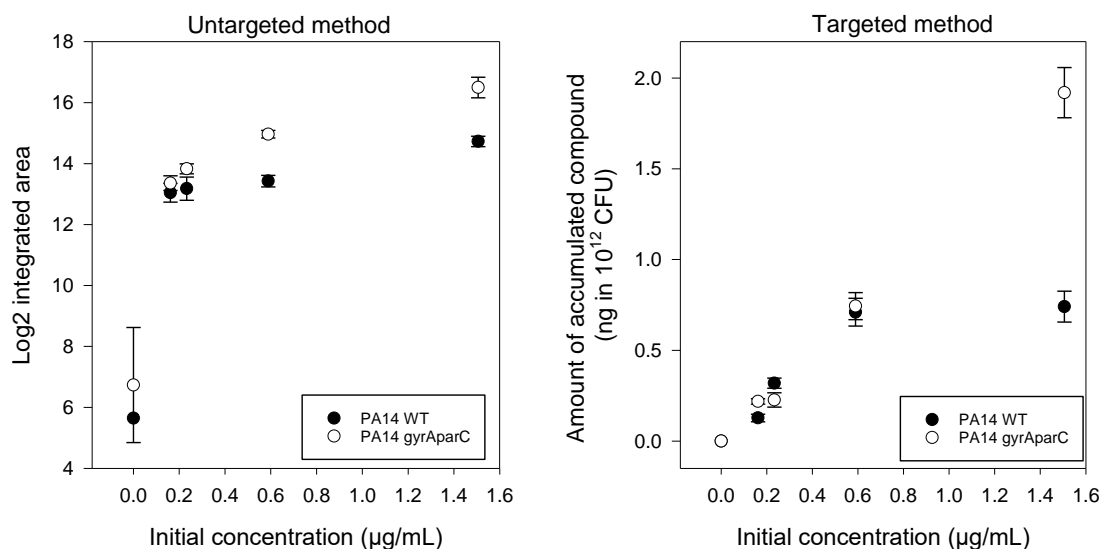
Figure 6.12 Ciprofloxacin accumulation determined by untargeted mode in log2-transformed area (left) and targeted mode in ng of compound in 10^{12} CFU (right). In the untargeted method, an offset value of 50 total counts is added to all features before a logarithmic transformation, making the blank ciprofloxacin intensity in the control samples equal to 50, whose log2 value is in turn equal to 5.64. In the targeted method, a blank ciprofloxacin intensity is interpolated within a standard curve, giving an actual value of 0 µg/mL

The normalized amount of accumulated ciprofloxacin to 10^{12} CFU is shown in Figure 6.12b, the resistant mutant gyrAparC exhibits a linear ciprofloxacin accumulation profile over the treatment, while the susceptible WT exhibits a logarithmic curve, reaching a plateau at $IC50_{WT}$. Both strains exhibit very similar accumulation profiles until $IC50_{WT}$ concentrations, where ciprofloxacin uptake was 0.71 and 0.74 ng in 10^{12} CFU for PA14 WT and gyrAparC, respectively. The picture changes for PA14 WT treated at MIC_{WT}, where ciprofloxacin uptake was 0.74 ng in 10^{12} CFU, while in gyrAparC it reached 1.91 ng in 10^{12} CFU.

During the incubation with $IC50_{WT}$, PA14 WT presented clump formation, indicating that *P. aeruginosa* initiates the production of biofilm even in planktonic cultures, as shown in Figure 6.13a. The optical density was measured after resuspending the bacterial clumps into the solution, but the registered values might have been affected by the biofilm formation. Thus,

information on viable cells was required. In a separate experiment, the viability of each culture at the harvest point was determined for all concentrations except for MIC_{WT}-treated samples, since no clump formation was observed at harvest time (28 h). The determination of CFUs after antibiotic exposure revealed that the amount of viable WT bacteria is reduced across antibiotic treatment, even when bacteria were harvested at the same optical density (Figure 6.13c).
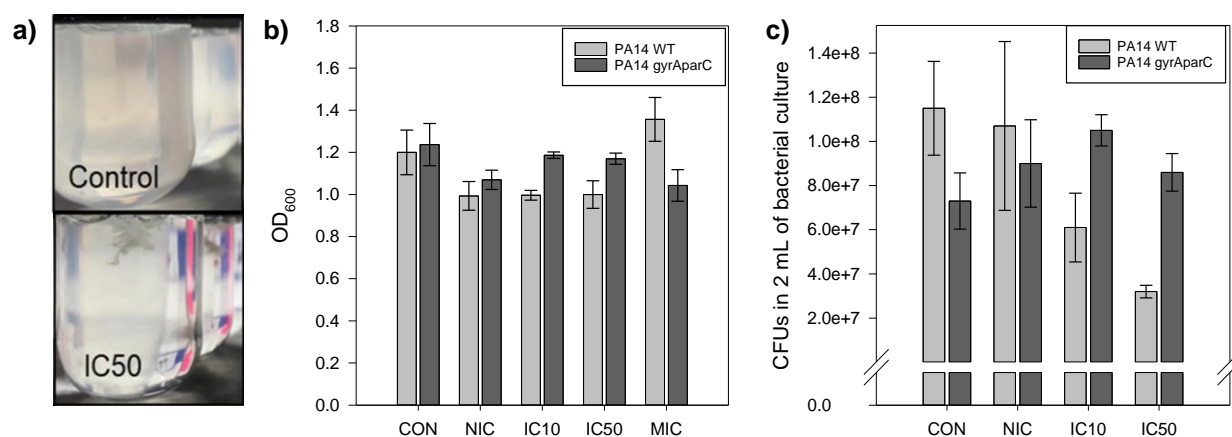
Figure 6.13 a) Visual phenotyping of PA14 WT control and after exposure to IC50WT of ciprofloxacin, b) optical density to the harvest point, c) viable bacteria harvested at OD600 = 1.0 under treatment with sub-MIC concentrations

6.4.3 Responsive features to ciprofloxacin accumulation

As shown before in Figure 6.11, some of the features from the untargeted analysis respond accordingly with the initial concentration used for the treatment. To investigate which features respond to the treatment in each strain, a Spearman correlation between the corresponding ciprofloxacin feature and each of the rest of the features was computed independently for PA14 WT and PA14 gyrAparC. In 2017, Zampieri *et al.* proposed a procedure where metabolites showing responses that change proportionally (or inverse proportionally) to a low and a high concentration of antibiotic were selected as responsive metabolites (Zampieri et al. 2017). A similar concept is proposed in this study, where the features that respond similarly to the degree of antibiotic exposure were selected as responsive features.

Each strain exhibits a different correlation profile as shown in the U-plots in Figure 6.14, where the compound class identified by clustering tools is displayed. PA14 WT generates a broader U-plot with more significantly correlated points compared with gyrAparC, indicating that the susceptible WT responds more readily to the presence of the antibiotic, although the nature of the responsive features in WT and gyrAparC varies greatly. To provide a better view of the responsive features to ciprofloxacin treatment, Figure 6.15 depicts bar plots of only identified features that show a significant correlation with ciprofloxacin uptake.
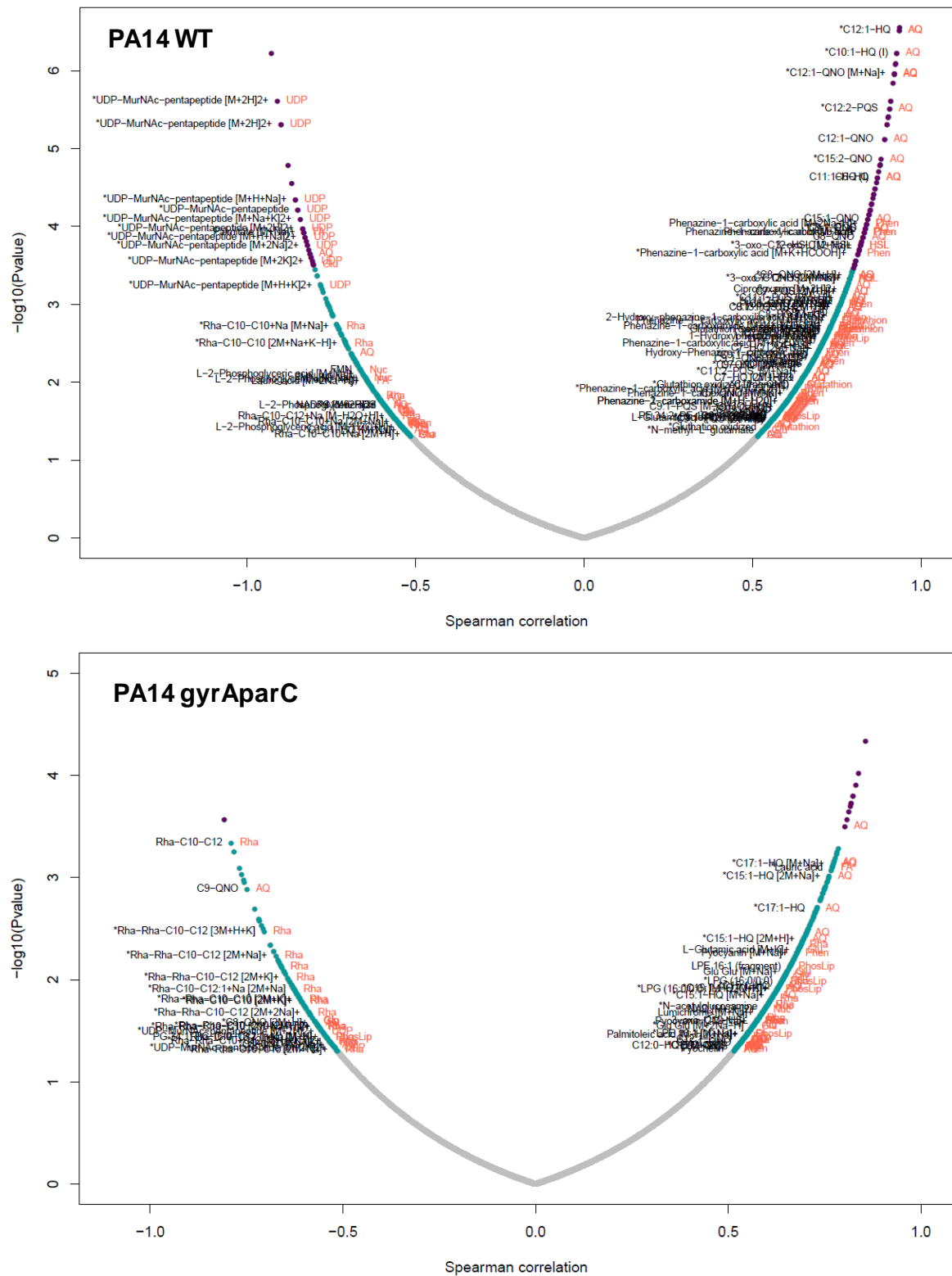
Figure 6.14 U-plots of feature correlation with ciprofloxacin accumulation in PA14 WT and in PA14 gyrAparC. Annotation of the identified features (*: putative annotation) is shown in black, and the compound class identified by clustering tools is shown in red. For each feature, the Spearman correlation with ciprofloxacin levels in all conditions was performed and the corresponding p-value was calculated. Dots in green: 0.5 ≤ correlation ≤ -0.5 & p-value ≤ 0.05, dots in purple: 0.8 ≤ correlation ≤ -0.8 & p-value ≤ 0.01

PA14 WT

*C12:1-HQ
*C10:1-HQ (I)
*C12:1-QNO [M+Na]+
*C12:2-PQS
C12:1-QNO
*C15:2-QNO
C6-HQ
C11:1-HQ (I)
C15:1-QNO
Phenazine-1-carboxylic acid [M+2Na-H]+
C8:1-QNO
*C9:1-PQS
Phenazine-1-carboxylic acid [M+Na]+
Phenazine-1-carboxylic acid
C8-QNO
3-oxo-C12-HSL
*3-oxo-C12-HSL
*Phenazine-1-carboxylic acid [M+K+HCOOH]+
*C8-QNO [2M+Na]+
C7-QNO [2M+Na]+
*3-oxo-C12-HSL [M+K]+
Ciprofloxacin [M+2H]2+
C7-PQS [3M+H]+
C7-PQS [2M+H]+
*C11:1-PQS [2M+H]+
C5-HQ
*C11:2-HQ [M+Na]+
Pyocyanin [2M+Na]+
*C8-QNO [M+Na]+
C9:1-PQS (I) [2M+H]+
*C13:1-PQS [2M+H]+
*C3:1-HQ
C8-HQ [M+K]+
2-Hydroxy-phenazine-1-carboxilic acid [M+Na]+
Phenazine-1-carboxylic acid [2M+H+K]2+
Phenazine-1-carboxamide [M+K+HCOOH]+
LPE 17:1
Pyocyanin [M+Na]+
Glutathion oxidized [M+2H]2+
*C10:1-HQ (II)
*C13:2-QNO
C7-HQ [M+Na]+
1-Hydroxyphenazine [M+K]+
1-Hydrophenazine
LPG 18:1 (neg)
Phenazine-1-carboxylic acid [M+H-H2O]+
*C4-HSL
C7-HQ [2M+Na]+
Hydroxy-Phenazin-1-carboxilic acid
C8:1-HQ
*C9:1-PQS (26 min)
C9:1-QNO [M+Na]+
Pyocyanin
*C13:2-PQS
C7-HQ [3M+Na]+
*C9-QNO [2M+H]+
*C11:2-PQS [M+Na]+
C7-HQ [2M+H]2+
C7:1-HQ
*Glutathion oxidized (fragment)
*C11:2-QNO
*Phenazine-1-carboxylic acid [M+H-HCOOH]+
Phenazine-1-carboxamide [M+K]+
C7-QNO [M+Na]+
Phenazine-2-carboxamide [M+H-H2O]+
Phenazine-1-carboxamide [M+H-H2O]+
C9:1-PQS [M-CH3OH+H]+
*C11:2-PQS
C13:1-QNO
*C9:2-QNO
DHQ
PE 34:2; PE 16:1-18:1 (neg)
C9:1-QNO (II)
C7-HQ
L-Glutamic acid [M-H2O+H]+
*C9:1-PQS (21 min)
*C11:1-QNO
C8-HQ
*C9:1-PQS (24 min)
*Gluthation oxidized
*N-methyl-L-glutamate
*Rha-C10-C10+Na [2M+H]+
*C15:1-HQ [M+Na]+
L-2-Phosphoglyceric acid [M-H2O+H]+
*Rha-C10-C10+Na [2M+Na]+
Rha-C10-C12+Na [M-H2O+H]+
NADP+ [M+2H]2+
L-2-Phosphoglyceric acid
*C11:0-PQS
*Lauric acid [M+2Na-H]+
L-2-Phosphoglyceric acid (neg)
FMN [M+Na]+
L-2-Phosphoglyceric acid [M+Na]+
FMN
*Rha-C10-C10 [2M+Na+K-H]+
*Rha-C10-C10+Na [M+Na]+
*UDP-MurNAc-pentapeptide [M+H+K]2+
*UDP-MurNAc-pentapeptide [M+2K]2+
*UDP-MurNAc-pentapeptide [M+2Na]2+
*UDP-MurNAc-pentapeptide [M+H+Na]2+
Palmitate [M+Na]+
*UDP-MurNAc-pentapeptide [M+2H]2+
*UDP-MurNAc-pentapeptide [M+Na+K]2+
*UDP-MurNAc-pentapeptide
*UDP-MurNAc-pentapeptide [M+H+Na]+
*UDP-MurNAc-pentapeptide [M+2H]2+
*UDP-MurNAc-pentapeptide [M+2H]2+

-1.0 -0.5 0.0 0.5 1.0
Spearman correlation

PA14 gyrAparC

*C17:1-HQ [M+Na]+
*Lauric acid
*C15:1-HQ [2M+Na]+
*C17:1-HQ
*C15:1-HQ [2M+H]+
L-Glutamic acid [M+K]+
Pyocyanin [M+Na]+
LPE 16:1 (fragment)
Glu Glu [M+Na]+
*LPG (16:0/0:0)
*C15:1-HQ
*C15:1-HQ [M+K]+
*LPG (16:0/0:0) [M-H2O+H]+
*C15:1-HQ [M+Na]+
*N-acetylglucosamine
NAD [M+2H]2+
Lumichrome [M+Na]+
3-oxo-C12-HSL
Pyocyanin [2M+Na]+
*Glu Glu [M+2Na-H]
*LPE 16:1 [M+Na]+
Palmitoleic acid [M-H2O+H]+
C12:1-QNO
C15:1-QNO
C12:0-HQ [2M+Na]+
*C15:0-QNO
C9:1-PQS
Pyochelin
*Rha-Rha-C10-C10 [2M+Na]+
*UDP-MurNAc-pentapeptide [M+2H]2+
*C8-QNO [M+Na]+
Rha-C10-C12:1
*Rha-Rha-C10-C12 [M+H+Na]2+
Rha-C10-C12:1+Na [M+K]+
PG 34:1; PG 16:0-18:1 (neg) [M-H]−
*UDP-MurNAc-pentapeptide [M+2H]2+
*Rha-Rha-C10-C10 [2M+Na+H]2+
*Rha-Rha-C10-C10 [2M+H]+
*C8-QNO [2M+H]+
*Rha-Rha-C10-C12 [2M+2Na]+
*Rha-C10-C10 [2M+K]+
*Rha-Rha-C10-C10 [2M+K]+
*Rha-C10-C12:1+Na [2M+Na]
*Rha-Rha-C10-C12 [2M+K]+
*Rha-Rha-C10-C12 [2M+Na]+
*Rha-Rha-C10-C12 [3M+H+K]
C9-QNO
Rha-C10-C12

-1.0 -0.5 0.0 0.5 1.0
Spearman correlation

Figure 6.15 Bar plots of identified features (*: putative annotation) showing a significant correlation (0.5 ≤ correlation ≤ -0.5 & p-value ≤ 0.05) with ciprofloxacin uptake in PA14 WT (left), in PA14 gyrAparC (right). Alkyl-quinolones in green, fatty acids in blue, glutamate in black, glutathione in yellow, homoserine-lactones in purple, nucleotides in lightgreen, phenazines in orange, phospholipids in darkblue, rhamnolipids in red, uridine diphosphate in magenta.

6.4.3.1 Commonly responsive features

As shown in Figure 6.15, some features responded similarly in both strains, indicating that the alteration of their abundance is not a result of growth inhibition, but rather a general response due to diverse interactions with the compound.

Metabolites involved in the quorum-sensing mechanisms of *P. aeruginosa* responded positively to ciprofloxacin treatment. The identified homoserine lactones N-butanoyl-homoserine lactone (C4-HSL) and N-(3-Oxododecanoyl)-L-homoserine lactone (3-oxo-C12-HSL) correlated strongly positively to ciprofloxacin in PA14 WT, while in PA14 gyrAparC 3-oxo-C12-HSL showed a moderate correlation with a significant fold-change at MIC_{WT} (Figure 6.16).
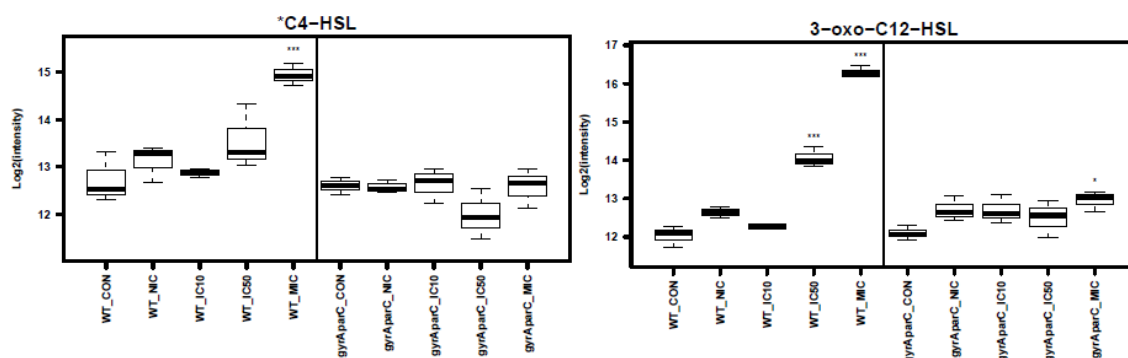
Figure 6.16 Box plots of identified homoserine lactones C4-HSL and 3-oxo-C12-HSL. Significance was calculated by Student's T-tests of each condition against the untreated control: *** for p-value ≤ 0.001, ** for 0.001 < p-value ≤ 0.01, * for 0.01 < p-value ≤ 0.05

Alkyl-quinolones responded positively in both PA14 WT and PA14 gyrAparC (Figure 6.15). In WT, 2-alkyl-4-quinolones (-HQ), 2-alkyl-3-hydroxy-4-quinolones (-PQS) and 2-alkyl-hydroxyquinoline-N-oxides (-QNO) followed a direct correlation with ciprofloxacin, while in PA14 gyrAparC the most directly correlated features where identified as long-chain-HQ congeners (C11-C17). As shown in Figure 6.17a, the levels of DHQ, C7-HQ and C7-PQS also showed an increase in PA14 gyrAparC.
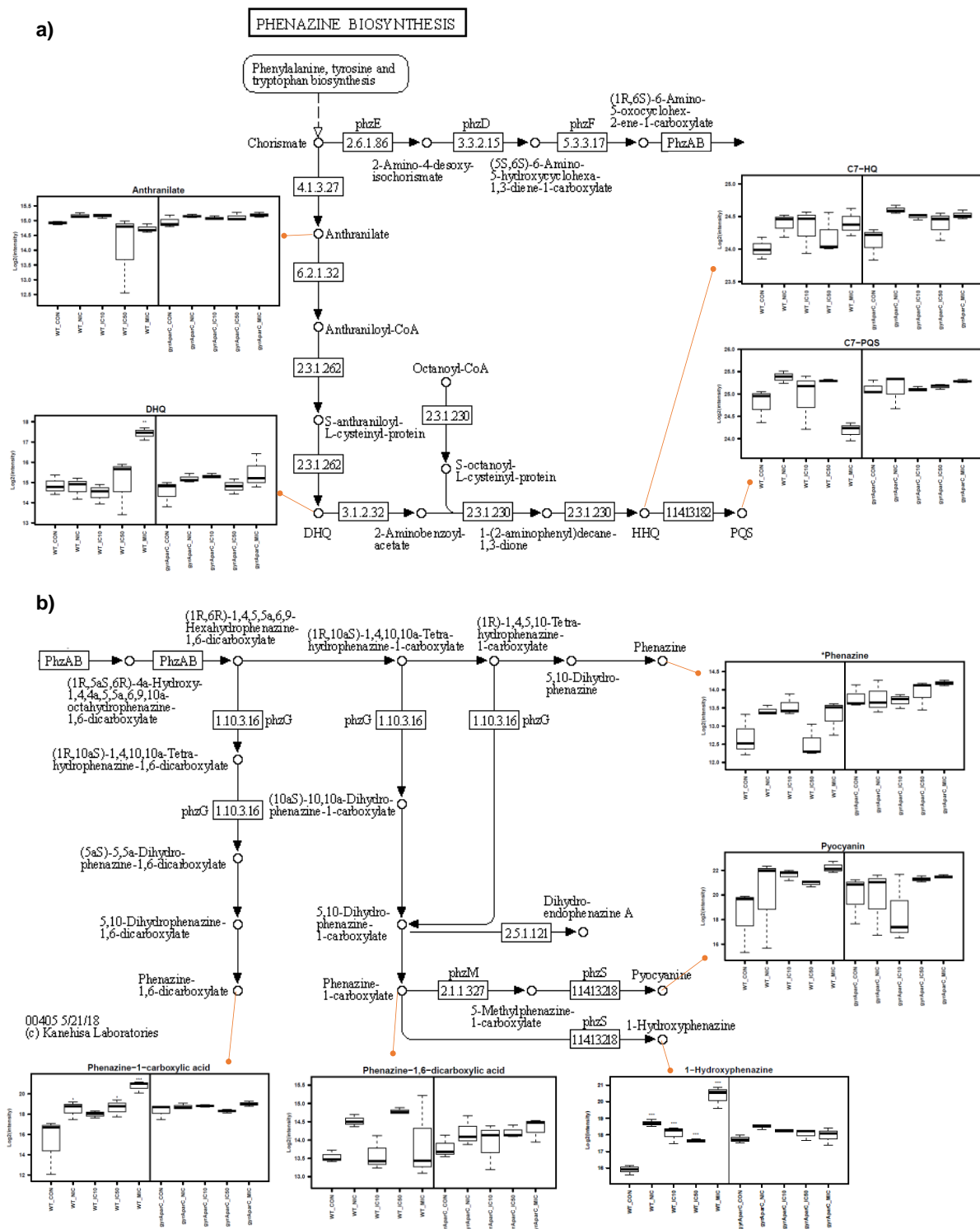
Figure 6.17 Box plots of identified intermediates and final products in the phenazine and PQS biosynthetic pathway: a) anthranilate, DHQ, HHQ (C7-HQ) and PQS (C7-PQS), b) phenazine-1,6-dicarboxylic acid, phenazine-1-carboxilc acid, phenazine, pyocyanin and 1-hydrophenazine. Significance was calculated by Student's T-tests of each condition against the untreated control: *** for p-value ≤ 0.001, ** for 0.001 < p-value ≤ 0.01, * for 0.01 < p-value ≤ 0.05. PQS pathway starts from chorismate towards the conversion to anthranilate, while phenazine pathway starts from chorismate towards the conversion to 2-amino-4-desoxyisochorismate by phzE (https://www.genome.jp/kegg/kegg1.html)

Phenazines levels correlated directly to ciprofloxacin accumulation, although the intermediates showed to be more responsive to PA14 WT. As shown in Figure 6.17b, the end products of the biosynthetic pathway were increased in both strains according to ciprofloxacin treatment, but PA14 WT showed the most significant changes when compared with the untreated controls. Particularly, the levels of phenazine-1-carboxylic acid, pyocyanin and 1-hydroxyphenazine showed significant changes in WT even when treated at NIC_{WT}.

Conversely, rhamnolipids correlated negatively to ciprofloxacin uptake in both strains. In Figure 6.15, mono-rhamnolipids showed a negative correlation in PA14 but not di-rhamnolipids. However, the box plots in Figure 6.18 show that the abundance of mono- and di-rhamnolipids increased back substantially when PA14 WT was treated with MIC_{WT}, in converse order to the concentration-dependent reduction of abundance at sub-MIC_{WT} concentrations. On the other hand, in PA14 gyrAparC, rhamnolipids followed a decreased abundance along with ciprofloxacin treatment.
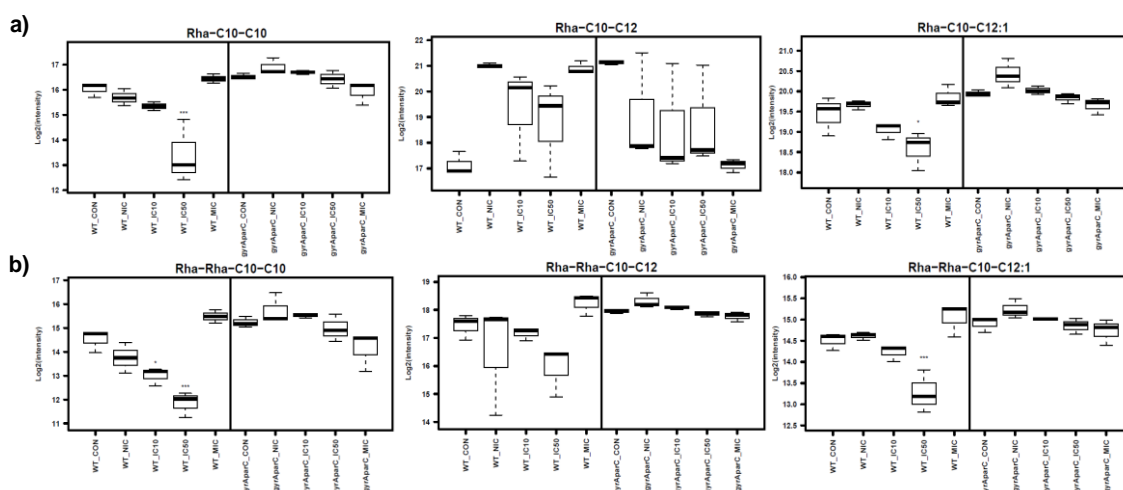
Figure 6.18 Box plots of identified rhamnolipids a) mono-rhamnolipids, b) di-rhamnolipids. Significance was calculated by Student's T-tests of each condition against the untreated control: *** for p-value ≤ 0.001, ** for 0.001 < p-value ≤ 0.01, * for 0.01 < p-value ≤ 0.05

Furthermore, the levels of identified lipids and phospholipids were responsive to ciprofloxacin uptake in both strains (Figure 6.15). Specifically, lyso-phosphatidylglycerols LPG (16:0) and LPG (18:1), and lyso-phosphatidylethanolamines LPE 16:0, LPE 16:1, LPE 17:1 and LPE 18:1 responded positively to ciprofloxacin uptake. Conversely, phosphatidylglycerol PG 34:1 correlated inversely, while phosphoethanolamine PE 34:1 did not have a clear trend and PE 34:2 increased in WT. Some fatty acids such as lauric acid (C12:0), elaidic acid (C16:1), palmitate (C16:0) and palmitoleic acid (C16:1) were also directly correlated with ciprofloxacin

uptake. Generally, PA14 WT showed the most significant changes when compared with the untreated controls. Additionally, pyochelin and glutamic acid correlated directly to ciprofloxacin uptake. Moreover, L-2-phosphoric acid correlated inversely in PA14 WT, while in PA14 gyrAparC it showed a generally decreased abundance.

UDP-MurNAc-pentapeptide adducts were the most inversely correlated features in PA14 WT, although they also showed a correlation in PA14 gyrAparC (see Figure 6.15). UDP-MurNAc-pentapeptide is the last intermediate of the reaction that is still unbound to a membrane-embedded scaffold, and it is still free in the cytoplasm (for details, see Figure 1.2). Because the metabolomics workflow was optimized for the extraction of metabolites with medium polarity, none of the subsequent intermediates of peptidoglycan assembly were available for LC-MS/MS detection.
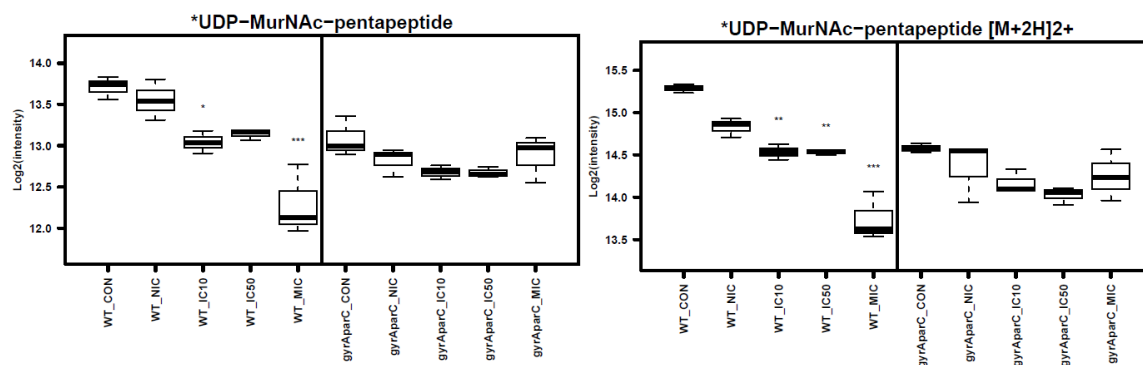
Figure 6.19 Box plots of UDP-MurNAc-pentapeptide. The doubly protonated molecular ion [M+2H]+ was presented higher abundance than the singly protonated ion. Significance was calculated by Student's T-tests of each condition against the untreated control: *** for p-value ≤ 0.001, ** for 0.001 < p-value ≤ 0.01, * for 0.01 < p-value ≤ 0.05

6.4.3.2 Responsive features in PA14 WT

Furthermore, some nucleotides such as adenosine monophosphate (AMP), adenosine diphosphate (ADP), flavine mononucleotide (FMN), flavine adenine dinucleotide (FAD), and nicotidamide adenine dinucleotide phosphate (NADP+) correlated inversely (Figure 6.15). Conversely, the levels of glutathione in PA14 WT correlated positively with ciprofloxacin uptake. Additionally, 86 unidentified features showed a strong correlation with ciprofloxacin uptake (0.8 ≤ correlation ≤ -0.8). Three of the unidentified correlated features were assigned with a label for alkyl-quinolones, and one for glutamate-related compounds, but they were not identified manually by exact mass nor MS/MS spectral information (Table 6.6).

Table 6.6 Features with high correlation to ciprofloxacin uptake in PA14 WT

Feature name	Retention time	m/z value	Correlation	Compound class	Feature name	Retention time	m/z value	Correlation	Compound class
M308T7	7.02	308.0697	0.9363		M489T11	11.31	489.2370	0.8381	
M310T16	16.40	310.2168	0.9355	AQ	M241T10_2	10.12	241.2042	0.8351	
M354T20	20.04	354.2795	0.9283		M577T21	21.10	577.4082	0.8351	
M496T14_2	13.65	496.2445	0.9247		M282T27_2	26.97	282.1461	0.8315	
M301T15_1	14.69	300.6054	0.9245		M291T16_1	15.74	291.1426	0.8280	
M300T15_6	14.69	300.4329	0.9212		M341T20_2	20.43	341.2426	0.8280	
M287T11_2	11.47	287.2694	0.9209	AQ	M340T16_2	16.48	340.4790	0.8244	
M300T15_5	14.69	300.3676	0.9176		M317T10	10.45	317.1330	0.8228	
M275T14_1	14.01	274.5712	0.9104		M586T15	14.67	586.3726	0.8213	
M380T20_2	20.25	380.2952	0.9104		M238T15_2	15.23	238.1231	0.8208	
M301T15_2	14.70	301.1998	0.9068		M418T1_1	1.31	417.6951	0.8174	
M340T14	13.93	340.2286	0.9032		M318T14	13.85	318.2067	0.8172	
M631T12	12.24	631.2402	0.9032		M263T15	14.53	263.0821	0.8165	
M312T16_2	16.31	312.4700	0.9029		M173T11_1	11.44	173.0418	0.8123	
M316T15_4	15.08	316.1916	0.8996		M188T13	13.16	188.0708	0.8065	
M352T19_2	18.58	352.2640	0.8996		M267T1_2	1.31	267.1313	0.8065	
M626T16	15.54	626.4033	0.8925		M313T15_3	15.23	312.8214	0.8065	
M384T16	15.70	384.2534	0.8789		M494T19_2	18.97	494.3246	0.8065	
M338T18	17.97	338.2481	0.8781		M260T13_6	13.17	260.3848	0.8029	
M354T17	17.36	354.2428	0.8781		M305T15_1	14.69	305.1096	0.8029	
M322T15	14.69	322.1776	0.8746		M313T15_1	15.23	312.6136	0.8029	
M611T15_2	15.21	611.3845	0.8710		M328T16_3	16.30	328.3290	0.8029	
M455T9_1	8.94	454.6435	0.8681		M392T18_1	18.48	392.2559	0.8029	
M238T17_2	16.50	238.1222	0.8638		M303T1_1	1.33	302.8125	0.8000	
M274T14_3	14.03	274.3439	0.8638		M811T1	1.33	811.2705	-0.8029	Glu
M289T16	16.43	289.1998	0.8638		M705T6	6.17	704.7580	-0.8029	
M328T16_4	16.28	328.4066	0.8602		M893T1	1.18	893.2545	-0.8047	
M355T17	17.30	355.2466	0.8602		M625T5	5.43	624.6356	-0.8100	
M356T15	15.25	356.1604	0.8602		M642T3	3.43	642.1536	-0.8101	
M366T16_2	16.06	366.1865	0.8574		M279T19_2	19.08	279.1904	-0.8136	AQ
M665T11	10.76	665.2460	0.8539		M695T6	6.18	694.7686	-0.8136	
M337T14_2	14.11	337.1609	0.8538		M558T19	19.10	558.3767	-0.8172	
M488T11	11.33	488.2339	0.8531		M476T6_2	6.34	476.1880	-0.8208	
M474T17_3	17.21	474.3224	0.8495		M816T1	1.28	816.2490	-0.8244	
M524T15	15.08	524.2761	0.8495		M1235T1	1.31	1235.3880	-0.8280	
M279T1_2	1.32	278.7990	0.8489		M1267T1	1.32	1267.3320	-0.8315	
M116T13	13.15	116.0493	0.8459		M803T1	1.26	803.2195	-0.8315	
M173T13	13.18	173.0806	0.8459		M911T1	1.30	911.2848	-0.8351	
M186T13_1	12.66	186.0552	0.8459		M644T5	5.43	643.6115	-0.8495	
M200T13_1	13.16	200.1069	0.8459		M694T6_2	6.19	694.2672	-0.8566	
M807T19	19.46	807.4643	0.8423		M1073T1	1.27	1073.3364	-0.8674	
M430T18_1	17.92	429.7391	0.8387		M476T6_1	6.19	476.1643	-0.8781	

The fact that two of the AQ-labeled features have an odd m/z value indicates that they do not correspond to an alkyl quinolone structure (containing one nitrogen atom), as their nominal mass is an even number as a protonated species, and that would violate the "nitrogen rule" (Watson and Sparkman 2007). On the contrary, the Glu-labeled feature seems to be in agreement with the nitrogen rule, as its odd m/z value could correspond to a dipeptide (containing two nitrogen atoms).

6.4.3.3 Responsive features in PA14 gyrAparC

In general, most of the responsive features in PA14 gyrAparC were also found to respond to PA14 WT, although to a different extent. As shown before in Figure 6.18, rhamnolipids were found to correlate more strongly in PA14 gyrAparC than in WT. Additionally, some nucleotides such as N-acetylglucosamine and NAD were found to correlate positively only in PA14 gyrAparC. However, 12 additional features showed a strong correlation with ciprofloxacin uptake ($0.8 \leq$ correlation ≤ -0.8) only in PA14 gyrAparC but not in WT (Table 6.7). One of the unidentified correlated features was assigned as an alkyl-quinolone, but it was not identified manually by exact mass nor MS/MS spectral information. Again, the AQ-labeled feature has an odd m/z value, which indicates that it does not correspond to an alkyl quinolone structure.

Table 6.7 Features with high correlation to ciprofloxacin uptake in PA14 gyrAparC

Feature name	Retention time	m/z value	Correlation	Compound class	Feature name	Retention time	m/z value	Correlation	Compound class
M150T1	1.16	150.1126	0.8561		M458T25	25.42	458.3534	0.8186	
M282T15_2	15.36	282.2799	0.8382		M227T1_1	1.31	227.0545	0.8168	
M783T22	22.09	783.1846	0.8311		M328T13_1	12.97	328.1426	0.8132	
M310T17_2	16.83	310.3104	0.8240		M310T17_3	17.41	310.3301	0.8079	
M635T23	23.20	634.8760	0.8240		M309T17_2	17.41	309.3268	0.8025	AQ
M423T1_2	1.22	423.0650	0.8190		M298T11_2	11.00	298.2018	-0.8079	

While PA14 WT showed significant changes in many of the analyzed features with respect to the untreated control, PA14 gyrAparC showed modest log2-fold changes visually perceptible, but marginally significant with respect to the untreated control. The fact that the correlation of the described identified features to ciprofloxacin accumulation is significant (p-value ≤ 0.05) does not necessary guarantee that the levels of those features were significantly changed at each treatment concentrations with respect to the untreated controls. Therefore, in order to find the most responsive features to ciprofloxacin treatment, a volcano plot of gyrAparC treated with MIC_{WT} compared with the untreated control is shown in Figure 6.20.
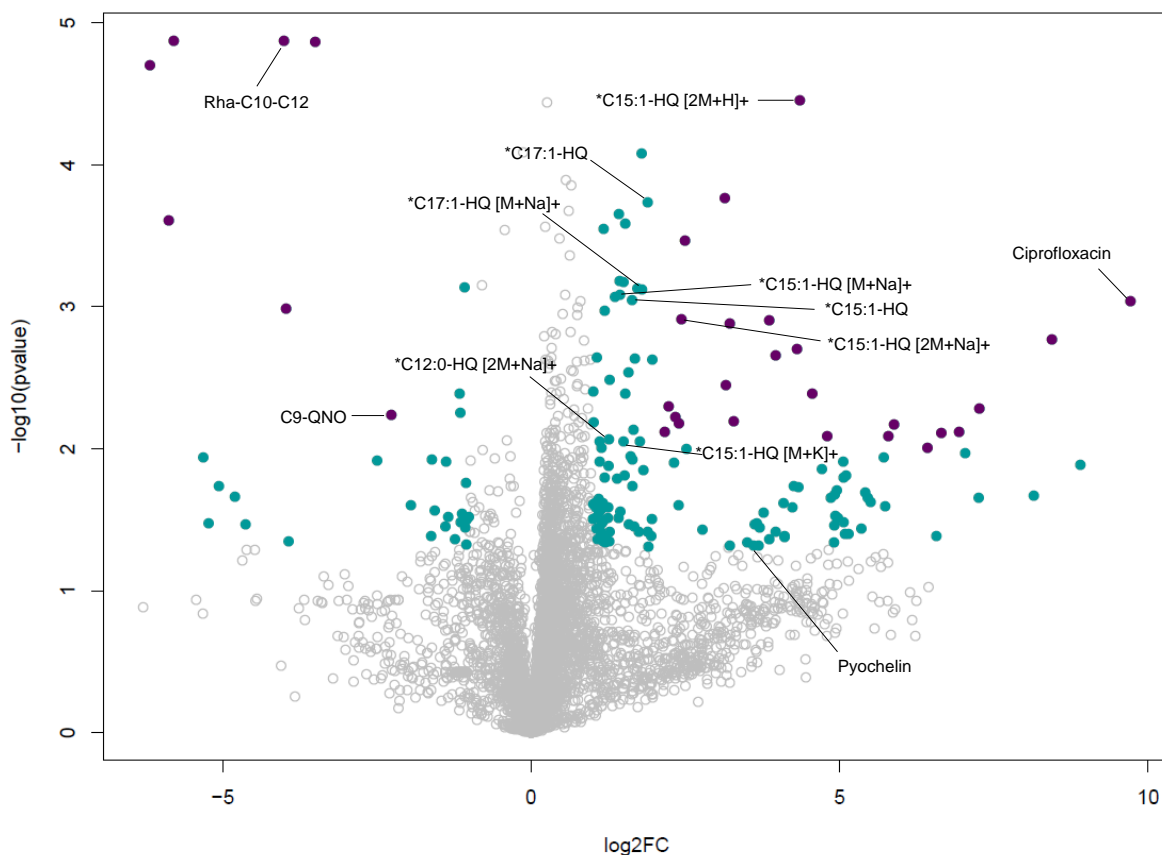
Figure 6.20 Volcano plot of gyrAparC treated at MIC_{WT} compared with the untreated control, showing the identified features (*: putative annotation). Significance: purple dots: $-2 \leq log2FC \leq 2$ and p-value ≤ 0.01, green dots: $-1 \leq log2FC \leq 1$ and p-value ≤ 0.05.

The gyrAparC mutant treated with the highest concentration of 0.151 µg/mL presented mainly over-produced metabolites when compared to the untreated control. The volcano plot revealed 135 over-produced features, and 32 less produced features (Figure 6.20). In consistency with the correlation analysis in Figure 6.14 and Figure 6.15, long-chain alkyl-quinolones were over-produced significantly upon treatment with MIC_{WT}. The protonated ions of C15:1-HQ, C17:1-HQ and C12:0-HQ, as well as their adducts, were significantly over-produced.

The difference in abundance of the most significantly regulated metabolites is better displayed as box plots in Figure 6.21, even if not all of them were highlighted in the volcano plot. Five of the identified long-chain alkyl-quinolones from C11 to C17 presented a significant increase in abundance. Interestingly, the longer the alkyl-chain of these metabolites, the most significant their over-production.
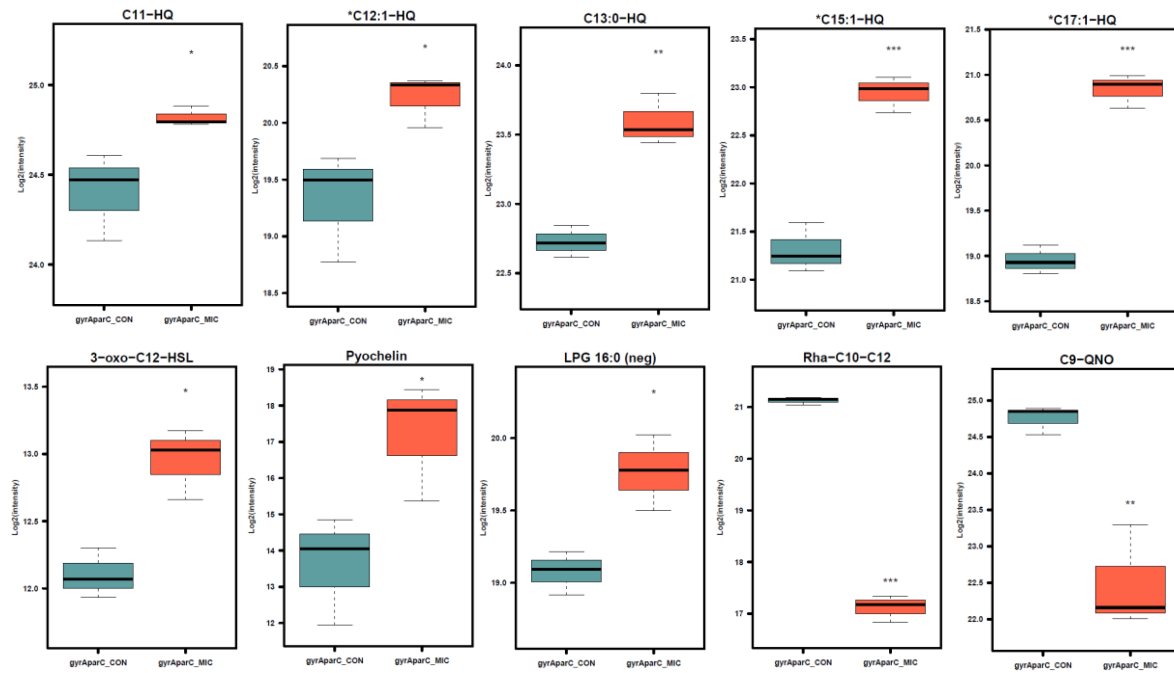
Figure 6.21 Box plots of most significantly regulated features in gyrAparC treated at MIC_WT compared with the untreated control, showing only the singly-protonated species and not their adducts. Significance was calculated by Student's T-tests of each condition against the untreated control: *** for p-value ≤ 0.001, ** for 0.001 < p-value ≤ 0.01, * for 0.01 < p-value ≤ 0.05

Additionally, other metabolites such as pyochelin, 3-oxo-C12-HSL, and LPG (identified in negative mode) were found to be significantly over-produced in MIC_WT treated samples (Figure 6.21). On the other hand, Rha-C10-C12 and C9-QNO were less produced after the treatment.

As a summary, the responses of WT and gyrAparC mutant, listed in Table 6.8, differentiate the secondary effects of ciprofloxacin accumulation. PA14 WT treated with sub-MIC and MIC concentrations of ciprofloxacin showed growth inhibition, biofilm production, and an increased oxidative-stress response, attributed to the effect of ciprofloxacin acting on its main target gyrA. In contrast, the gyrAparC mutant did not show any growth inhibition nor biofilm production, even though ciprofloxacin accumulated to the same and higher extent than in PA14 WT, indicating that the main target gyrA was unaffected. Up to a different extend, both strains produced less rhamnolipids when exposed to ciprofloxacin, and they both showed higher levels of QS molecules, such as alkyl-quinolones and homoserine lactones. In general, the pepdidoglycan assembly of both strains was affected, as well as the lipid metabolism.

Table 6.8 The response of *P. aeruginosa* WT and gyrAparC mutant to ciprofloxacin treatment at sub-MIC and MIC concentrations

Response	WT	gyrAparC
Growth inhibition	Yes	No
Biofilm formation	Yes	No
Target binding	Yes	No
Compound accumulation	Yes	Yes
Oxidative-stress response	Increased	No change
Rhamnolipid production	Decreased	Decreased
Lipid metabolism	Altered	Altered
Peptidoglycan assembly	Altered	Altered
QS response	Increased	Increased

The previous analysis verifies the hypothesis formulated in Figure 6.1, demonstrating that *P. aeruginosa* presents an alternative response to the accumulation of ciprofloxacin, attributed only to secondary target effects.

6.5 Discussion

Ciprofloxacin accumulates to the same extent in resistant and sensitive *P. aeruginosa* at sub-MIC concentrations, but not at MIC

The fact that introducing two-single mutations in *gyr*A T83I and *par*C S87L confers PA14 with substantial resistance to ciprofloxacin does not affect intracellular compound accumulation. In fact, the accumulation of ciprofloxacin in the resistant and susceptible strains does not correlate with their fold change of inhibitory concentrations. Although the point mutations increase the values of sub-MIC concentrations by more than 8 log2-units, ciprofloxacin accumulated to the same extent in both the sensitive WT and the resistant strain PA14 gyrAparC.

Ciprofloxacin has been reported to induce biofilm formation at concentrations below MIC (Linares et al. 2006; Morita, Tomida, and Kawamura 2014). Consistent with the literature, at IC50 PA14 WT started biofilm production and clump formation, which was also observed at MIC. The effects of biofilm-based antibiotic resistance and tolerance have been extensively studied and a complete revision has recently been published (Hall and Mah 2017). The literature suggests that the reduced susceptibility to certain antibiotics may be influenced by the diffusion limitation through biofilms. In particular, ciprofloxacin has been found to successfully penetrate experimental biofilms setups (Hall and Mah 2017). In the present study, the values of accumulated ciprofloxacin increased along with the increasing concentration until reaching a plateau at the concentration when biofilm was observed. The same levels of intracellular ciprofloxacin were found at IC50 and MIC, indicating that clump formation could act as a protective measure to restrict the surface contact of bacteria with the solubilized compound. It is important to note that biofilm formation was not observed in the untreated controls after 7h of incubation in BM2 medium with casaminoacids, in agreement with previous reports where biofilms are developed after 24 h in tryptic soy broth (Pericolini et al. 2018) or after three days in Muller Hinton medium (Al-kafaween et al. 2019).

Nevertheless, the stationary compound accumulation cannot be attributed to biofilm formation alone. The coordinated response of bacteria to decrease porin expression and increase the efflux capability is known to reduce the net permeability in the outer membrane (Fernández and Hancock 2012). But although *P. aeruginosa* is capable of exporting fluoroquinolones by four of its known efflux pumps: MexCD-OprJ, MexEF-OprN, MexAB-OprM, and MexXY-OprM (Nakajima et al. 2002; Fernández and Hancock 2012), there is no evidence that ciprofloxacin itself acts as a regulator for their over-expression. However, ciprofloxacin does promote the formation of ROS in susceptible *P. aeruginosa*'s strains (but not in *gyrA* resistant mutant)

(Jensen et al. 2014), and oxidative stress has been found to induce the genes that code for MexXY in *P. aeruginosa* (Fraud and Poole 2011).

The fact that PA14 maintains the same levels of ciprofloxacin accumulation in both the sensitive and the resistant strain under sub-MIC$_{WT}$ concentrations suggests that the synergistic effect of active compound efflux and biofilm production in the susceptible WT occurs at a certain compound concentration threshold (IC50$_{WT}$ in the present study). However, more studies are required to differentiate the compound concentration dependence of both biofilm and ROS production, e.g. the study of the transcriptome in a concentration-dependent manner, while monitoring the formation of hydroxyl radicals may give insights into the expression levels of efflux genes and biofilm production genes.

On-target metabolic effects of ciprofloxacin

Fluoroquinolones are known to propitiate bacterial responses in *P. aeruginosa*, such as biofilm formation, diminished swimming and swarming, induction of SOS response, up-regulation of the bacteriophage-like pyocins (Morita, Tomida, and Kawamura 2014). Most of these responses are associated with the result of the compound's interaction with the protein target.

Since ciprofloxacin is known to produce oxidative stress in bacteria (Becerra and Albesa 2002; Wu et al. 2012), it is not surprising to find elevated levels of oxidized glutathione, which serves as a preventive antioxidant in the presence of ROS. Similarly, phenazine production increased with ciprofloxacin uptake in PA14 WT. Phenazines are redox-active molecules, and among other functions, they modify the cellular redox state (Pierson and Pierson 2010). However, their over-production would be deleterious for the bacterial cells because they induce the generation of ROS. Therefore, phenazines should have a different role than keeping the redox intracellular homeostasis in PA14 WT. Phenazines have an important impact on biofilm architecture and cell adhesion (Pierson and Pierson 2010), and the results of this study suggest that biofilm is enhanced at increasing concentrations of ciprofloxacin.

One metabolite that showed the most dependence with ciprofloxacin uptake was UDP-MurNac-pentapeptide. At first glance, its decreasing amount indicates a compromised turnover of the peptidoglycan wall. However, Jedrey *et al.* recently found that PAO1 WT treated with sub-MIC concentrations (50 and 75 ng/mL) of ciprofloxacin increased its modulation of the UDP-MurNac-tripeptide synthetase *murE*, but not its *gyrA* resistant strain (Jedrey, Lilley, and Welch 2018). Furthermore, when Lipid II is modified and then translocated to the outer leaflet of the cytoplasmic membrane, a driving force in the cytoplasm is generated to favor its biosynthesis, accelerating the substrate consumption in the up-stream cascade. Together,

these observations suggest that the peptidoglycan assembly is generally enhanced as an effect of ciprofloxacin activity.

Induction of the SOS response has been shown to induce persister cells under sub-MIC treatment with ciprofloxacin (Dörr, Lewis, and Vulić 2009; Andersson and Hughes 2014; Johnson and Levin 2013). Persisters tend to grow very slowly or tend to emerge stochastically after non-growing conditions, providing them with a low metabolic state though to be responsible for surviving to antibiotic exposure (Brauner et al. 2016).

In this study, PA14 WT was incubated for 28 hours at MIC, having enough time to develop a drug-tolerant phenotype of persister cells. Although the study of the persister phenotype was not among the goals of this project, it was found that the levels of some metabolites in PA14 WT treated at MIC responded in a different manner than the rest of the treatment concentrations.

Off-target metabolic effects of ciprofloxacin

Quorum sensing molecules were found to be highly responsive in both the susceptible and the resistant strain, posing a great interest as many virulence factors in *P. aeruginosa* are regulated by quorum sensing. PA14 gyrAparC showed a ciprofloxacin-dependent increase in long-chain AQs. The diversity of the acyl chain of AQs depends on the available pool of acyl-CoA for AQ biosynthesis, and in turn, on the available pool of fatty acids (Witzgall et al. 2018). The over-production of long-chain AQs suggests that the pool of fatty acids that is available for AQ biosynthesis was unbalanced by the presence of the antibiotic.

More evidence supports the idea of an alteration in the lipid pool. On the one hand, the rhamnolipid biosynthetic pathway shares one acyl-CoA substrate (octanoyl-CoA) with the AQ pathway, and their abundance decreased along with ciprofloxacin uptake. On the other hand, LPEs and LPGs, which are involved in lipid metabolism, were responsive in PA14 gyrAparC and their abundance increase along with ciprofloxacin concentration.

Although, additional efforts to identify important responsive features are still required to conceive a complete picture of the indirect effects of compound accumulation, the analysis of the identified features gives already valuable information on the off-target interactions of ciprofloxacin in *P. aeruginosa* (see Table 6.9).

Table 6.9 On- and off-target effects of ciprofloxacin accumulation in *P. aeruginosa*

On-target effects	Off-target effects
Growth inhibition	Intracellular antibiotic accumulation
Target binding	Decrease in rhamnolipid production (Rha ↓)
Biofilm formation	Elevated QS response (AQs ↑, HSL ↑)
Elevated oxidative-stress response	Alteration in lipid metabolism (PG ↓, LPG ↑, LPE ↑, LC-AQs ↑)
(GHS ↑, Phen ↑)	Affected peptidoglycan assembly
	(UDP-MurNac-pentapeptide ↓)

AQs: alkyl-quinolones, GHS: glutathione, HSL: homoserine lactones, LC: long chain, LPE: lyso-phosphatidylethanolamines, LPG: lyso-phosphatidylglycerols, PG: phophatydylglycerol, QS: quorum sensing, Rha: rhamnolipids.

The results in this study support the theory that antibiotics act as stress inducers when growth inhibition is achieved, and they act as cues in the absence of inhibition (Bernier and Surette 2013). While it is true that fluoroquinolones are "sensed" by *P. aeruginosa* and they exert a preparatory bacterial response, they do not act as signaling molecules as they are not considered autoinducers (Diggle et al. 2007). However, fluoroquinolones enhanced the QS system in an intracellular concentration-dependent manner, leaving the open question of a possible secondary target, or targets, until now unknown.

CONCLUDING REMARKS AND OUTLOOK

This study tackled two of the main aspects in the struggle against the increasingly frequent antibiotic resistance: the capability of bacteria to accumulate antibiotics and their response to insufficient amounts of compound needed to arrest growth.

Detecting and quantifying the small amounts of antibiotics accumulated in susceptible bacterial cells is challenging, and powerful analytical techniques are required. Here, an LC-MS/MS-based assay was developed, optimized and applied to measure the absolute and dynamic accumulation of antibiotics with different modes of action into *E. coli* and *P. aeruginosa*, showing different accumulation profiles in spite of both being Gram-negative. One advantage of the assay is its strain transferability and its medium-high throughput, since it allows the systematic assessment of the accumulation of a broad range of compounds in different microorganisms. As it is a compound-specific LC-MS/MS method, it could allow the direct detection of possible intracellular modifications occurring on the compounds after their uptake, e.g. hydrolyzed β-lactams or modified aminoglycosides.

With respect to the response to sub-lethal concentrations of antibiotics, the metabolic profile of wild type *P. aeruginosa* treated with different classes of antibiotics showed important differences in the response profiles under short and long exposure. As a quick response to sudden antibiotic stress, *P. aeruginosa* maintained high levels of virulence-related metabolites, such as rhamnolipids.

Additionally, this study provided new insights into the off-target effects of *P. aeruginosa* treated with sub-lethal concentrations of ciprofloxacin. The metabolic profiles of a susceptible and a resistant strain, with MIC values of 0.15 µg/mL and 29.83 µg/mL, respectively, provided evidence of indirect responses to increasing concentrations of ciprofloxacin. The resistant mutant showed important off-target effects in response to ciprofloxacin accumulation, despite the lack of activity of the compound to the target.

An open question remains about the behavior of sensitive strain incubated at MIC (determined on a plate assay), where the trend on the response of certain metabolites to compound accumulation was disrupted. A methodological evaluation of the presence and behavior of persister cells at such conditions is still needed, as persister cells are likely to emerge under the culture conditions (28h at 37°), and they are metabolically different from the otherwise susceptible cells, and the current analysis is suited for homologous cultures.

The use of untargeted metabolomics studies provided information on the nature of the found off-target effects, which were related to the complex quorum sensing network in *P. aeruginosa*. The study of small sensing molecules is a good example of the applicability of metabolomics, although the effects on the regulatory system can be reconstructed at the transcriptome level. It is common to make use of more than one of the "omics" technologies for comprehensive analyses, where efforts must be made to preserving the experimental conditions across the different workflows. On the same basis, analyzing the transcriptome response can enable identifying possible secondary targets of fluoroquinolones in *P. aeruginosa*'s resistant strains, in order to complement the current knowledge on sensitive strains.

Furthermore, alterations in lipid metabolism were consistently found as a result of fluoroquinolone treatment. Lipid metabolites were dysregulated not only during under short or long exposure of wild type *P. aeruginosa* to ciprofloxacin and levofloxacin, but also under the exposure of the resistant mutant to increasing concentrations of ciprofloxacin. Further studies on lipidomic analysis could contribute to clarify the extent of such alterations as a result of antibiotic activity in the wild type, and off- target-related response in the resistant mutant.

REFERENCES

AB Sciex. 2015. "QTRAP 6500 LC/MS/MS System. Basic Training." In. Darmstadt, Germany: AB SCIEX Germany GmbH.

Abraham, E. P., and E. Chain. 1940. 'An Enzyme from Bacteria able to Destroy Penicillin', *Nature*, 146: 837-37.

Al-kafaween, Mohammad Abdulraheem, Abu Bakar Mohd Hilmi, Norzawani Jaffar, Hamid Ali Nagi Al-Jamal, and Mohd Khairi Zahri. 2019. 'Determination of optimum incubation time for formation of Pseudomonas aeruginosa and Streptococcus pyogenes biofilms in microtiter plate', *Bulletin of the National Research Centre*, 43: 100.

Al-Tahhan, R. A., T. R. Sandrin, A. A. Bodour, and R. M. Maier. 2000. 'Rhamnolipid-induced removal of lipopolysaccharide from Pseudomonas aeruginosa: effect on cell surface properties and interaction with hydrophobic substrates', *Applied and Environmental Microbiology*, 66: 3262-68.

Aldred, Katie J., Robert J. Kerns, and Neil Osheroff. 2014. 'Mechanism of quinolone action and resistance', *Biochemistry*, 53: 1565-74.

Aldsworth, T. G., R. L. Sharman, and C. E. R. Dodd. 1999. 'Bacterial suicide through stress', *Cellular and Molecular Life Sciences CMLS*, 56: 378-83.

Allam, Anas, Laure Maigre, Julia Vergalli, Estelle Dumont, Bertrand Cinquin, Rodolphe Alves de Sousa, Jelena Pajovic, Elizabeth Pinet, Nikaia Smith, Jean-Philippe Herbeuval, Matthieu Réfrégiers, Isabelle Artaud, and Jean-Marie Pagès. 2017. 'Microspectrofluorimetry to dissect the permeation of ceftazidime in Gram-negative bacteria', *Scientific Reports*, 7: 986-86.

Allen, Jess, Hazel M. Davey, David Broadhurst, Jem J. Rowland, Stephen G. Oliver, and Douglas B. Kell. 2004. 'Discrimination of Modes of Action of Antifungal Substances by Use of Metabolic Footprinting', *Applied and Environmental Microbiology*, 70: 6157-65.

Allison, Kyle R., Mark P. Brynildsen, and James J. Collins. 2011. 'Metabolite-enabled eradication of bacterial persisters by aminoglycosides', *Nature*, 473: 216-20.

Andersson, D. I., and D. Hughes. 2014. 'Microbiological effects of sublethal levels of antibiotics', *Nat. Rev. Microbiol.*, 12: 465.

Arenz, Stefan, and Daniel N. Wilson. 2016. 'Bacterial Protein Synthesis as a Target for Antibiotic Inhibition', *Cold Spring Harbor perspectives in medicine*, 6: a025361.

Bazile, S, N Moreau, D Bouzard, and M Essiz. 1992. 'Relationships among antibacterial activity, inhibition of DNA gyrase, and intracellular accumulation of 11 fluoroquinolones', *Antimicrobial Agents and Chemotherapy*, 36: 2622-27.

Becerra, M. C., and I. Albesa. 2002. 'Oxidative stress induced by ciprofloxacin in Staphylococcus aureus', *Biochemical and Biophysical Research Communications*, 297: 1003-07.

Bedard, J., S. Chamberland, S. Wong, T. Schollaardt, and L. E. Bryan. 1989. 'Contribution of permeability and sensitivity to inhibition of DNA synthesis in determining susceptibilities of Escherichia coli, Pseudomonas aeruginosa, and Alcaligenes faecalis to ciprofloxacin', *Antimicrob. Agents Chemother.*, 33: 1457.

Behrends, V., B. Ryall, J. E. A. Zlosnik, D. P. Speert, J. G. Bundy, and H. D. Williams. 2013. 'Metabolic adaptations of Pseudomonas aeruginosa during cystic fibrosis chronic lung infections', 15: 398-408.

Benincasa, Monica, Sabrina Pacor, Renato Gennaro, and Marco Scocchi. 2009. 'Rapid and reliable detection of antimicrobial peptide penetration into gram-negative bacteria based on fluorescence quenching', *Antimicrobial agents and chemotherapy*, 53: 3501-04.

Bensikaddour, Hayet, Nathalie Fa, Ingrid Burton, Magali Deleu, Laurence Lins, André Schanck, Robert Brasseur, Yves F. Dufrêne, Erik Goormaghtigh, and Marie-Paule Mingeot-Leclercq. 2008. 'Characterization of the Interactions between Fluoroquinolone Antibiotics and Lipids: a Multitechnique Approach', *Biophysical Journal*, 94: 3035-46.

Bergmann, René, Mark van der Linden, Gursharan S. Chhatwal, and D. Patric Nitsche-Schmitz. 2014. 'Factors That Cause Trimethoprim Resistance in Streptococcus pyogenes', *Antimicrobial agents and chemotherapy*, 58: 2281.

Bernier, Steve, and Michael Surette. 2013. 'Concentration-dependent activity of antibiotics in natural environments', 4.

Bhat, Jyothi, Ashwini Narayan, Janani Venkatraman, and Monalisa Chatterji. 2013. 'LC–MS based assay to measure intracellular compound levels in Mycobacterium smegmatis: Linking compound levels to cellular potency', *Journal of Microbiological Methods*, 94: 152-58.

Blattner, Frederick R., Guy Plunkett, Craig A. Bloch, Nicole T. Perna, Valerie Burland, Monica Riley, Julio Collado-Vides, Jeremy D. Glasner, Christopher K. Rode, George F. Mayhew, Jason Gregor, Nelson Wayne Davis, Heather A. Kirkpatrick, Michael A. Goeden, Debra J. Rose, Bob Mau, and Ying Shao. 1997. 'The Complete Genome Sequence of Escherichia coli K-12', 277: 1453-62.

Brauner, Asher, Ofer Fridman, Orit Gefen, and Nathalie Q. Balaban. 2016. 'Distinguishing between resistance, tolerance and persistence to antibiotic treatment', *Nat Rev Micro*, 14: 320-30.

Brazas, M. D., and R. E. Hancock. 2005. 'Ciprofloxacin induction of a susceptibility determinant in Pseudomonas aeruginosa', *Antimicrob Agents Chemother*, 49: 3222-7.

Breidenstein, Elena B. M., César de la Fuente-Núñez, and Robert E. W. Hancock. 2011. 'Pseudomonas aeruginosa: all roads lead to resistance', *Trends in Microbiology*, 19: 419-26.

Breidenstein, Elena B. M., Manjeet Bains, and Robert E. W. Hancock. 2012. 'Involvement of the Lon Protease in the SOS Response Triggered by Ciprofloxacin in Pseudomonas aeruginosa PAO1', 56: 2879-87.

Bruchmann, Sebastian, Andreas Dötsch, Bianka Nouri, Iris F. Chaberny, and Susanne Häussler. 2013. 'Quantitative Contributions of Target Alteration and Decreased Drug Accumulation to Pseudomonas aeruginosa Fluoroquinolone Resistance', *Antimicrobial agents and chemotherapy*, 57: 1361-68.

Bruker Daltonics. 2012. "A presentation to support the customer familiarization." In. Bremen, Germany: Bruker Daltonics,.

Cai, Hongliang, Kelly Rose, Lan-Hsin Liang, Steve Dunham, and Charles Stover. 2009. 'Development of a liquid chromatography/mass spectrometry-based drug accumulation assay in Pseudomonas aeruginosa', *Analytical biochemistry*, 385: 321-25.

Cama, Jehangir, Abby Mae Henney, and Mathias Winterhalter. 2019. 'Breaching the Barrier: Quantifying Antibiotic Permeability across Gram-negative Bacterial Membranes', *Journal of Molecular Biology*, 431: 3531-46.

Cambiaghi, Alice, Manuela Ferrario, and Marco Masseroli. 2016. 'Analysis of metabolomic data: tools, current strategies and future challenges for omics data integration', *Briefings in Bioinformatics*, 18: 498-510.

Campoli-Richards, Deborah M., Jon P. Monk, Allan Price, Paul Benfield, Peter A. Todd, and Alan Ward. 1988. 'Ciprofloxacin', *Drugs*, 35: 373-447.

Carlet, Jean, Vincent Jarlier, Stephan Harbarth, Andreas Voss, Herman Goossens, Didier Pittet, and Forum Participants of the 3rd World Healthcare-Associated Infections. 2012. 'Ready for a world without antibiotics? The Pensières Antibiotic Resistance Call to Action', *Antimicrobial resistance and infection control*, 1: 11-11.

Carrillo, Carmen, José A. Teruel, Francisco J. Aranda, and Antonio Ortiz. 2003. 'Molecular mechanism of membrane permeabilization by the peptide antibiotic surfactin', *Biochimica et Biophysica Acta (BBA) - Biomembranes*, 1611: 91-97.

Cech, Nadja B., and Christie G. Enke. 2001. 'Practical implications of some recent studies in electrospray ionization fundamentals', 20: 362-87.

Celesk, R. A., and N. J. Robillard. 1989. 'Factors influencing the accumulation of ciprofloxacin in Pseudomonas aeruginosa', *Antimicrob. Agents Chemother.*, 33: 1921.

Chalmers, James D. 2017. 'Macrolide resistance in Pseudomonas aeruginosa: implications for practice', *European Respiratory Journal*, 49: 1700689.

Chapman, J. S., and N. H. Georgopapadakou. 1988. 'Routes of quinolone permeation in Escherichia coli', *Antimicrob. Agents Chemother.*, 32: 438.

Chen, Rui, Xinlei Yu, and Liang Li. 2002. 'Characterization of poly(ethylene glycol) esters using low energy collision-induced dissociation in electrospray ionization mass spectrometry', *Journal of the American Society for Mass Spectrometry*, 13: 888-97.

Chen, Yun, and Liang Liu. 2019. 'Targeted Proteomics.' in Xing Wang and Matthew Kuruc (eds.), *Functional Proteomics: Methods and Protocols* (Springer New York: New York, NY).

Chopra, I., S. Shales, and P. Ball. 1982. 'Tetracycline resistance determinants from groups A to D vary in their ability to confer decreased accumulation of tetracycline derivatives by Escherichia coli', *Microbiology*, 128: 689.

Chopra, I., and K. Hacker. 1992. 'Uptake of minocycline by Escherichia coli', *J. Antimicrob. Chemother.*, 29: 19.

Chrzanowski, Łukasz, Łukasz Ławniczak, and Katarzyna Czaczyk. 2012. 'Why do microorganisms produce rhamnolipids?', *World Journal of Microbiology and Biotechnology*, 28: 401-19.

Cinquin, Bertrand, Laure Maigre, Elizabeth Pinet, Jacqueline Chevalier, Robert A. Stavenger, Scott Mills, Matthieu Réfrégiers, and Jean-Marie Pagès. 2015. 'Microspectrometric insights on the uptake of antibiotics at the single bacterial cell level', *Scientific Reports*, 5: 17968.

Coldham, Nick G., Mark Webber, Martin J. Woodward, and Laura J. V. Piddock. 2010. 'A 96-well plate fluorescence assay for assessment of cellular permeability and active efflux in Salmonella enterica serovar Typhimurium and Escherichia coli', *Journal of Antimicrobial Chemotherapy*, 65: 1655-63.

Cornelis, Pierre. 2020. 'Putting an end to the Pseudomonas aeruginosa IQS controversy', 9: e962.

Cornelis, Pierre 2008. *Pseudomonas: Genomics and Molecular Biology* (Caister Academic Press: Great Britain).

Cramariuc, Oana, Tomasz Rog, Matti Javanainen, Luca Monticelli, Anna V. Polishchuk, and Ilpo Vattulainen. 2012. 'Mechanism for translocation of fluoroquinolones across lipid membranes', *Biochimica et Biophysica Acta (BBA) - Biomembranes*, 1818: 2563-71.

Creek, Darren J., Warwick B. Dunn, Oliver Fiehn, Julian L. Griffin, Robert D. Hall, Zhentian Lei, Robert Mistrik, Steffen Neumann, Emma L. Schymanski, Lloyd W. Sumner, Robert Trengove, and Jean-Luc Wolfender. 2014. 'Metabolite identification: are you sure? And how do your peers gauge your confidence?', *Metabolomics*, 10: 350-53.

Currie, Felicity, David I. Broadhurst, Warwick B. Dunn, Christopher A. Sellick, and Royston Goodacre. 2016. 'Metabolomics reveals the physiological response of Pseudomonas putida KT2440 (UWC1) after pharmaceutical exposure', *Molecular BioSystems*, 12: 1367-77.

Davey, Mary E., Nicky C. Caiazza, and George A. O'Toole. 2003. 'Rhamnolipid surfactant production affects biofilm architecture in Pseudomonas aeruginosa PAO1', *Journal of bacteriology*, 185: 1027-36.

Davies, J., G. B. Spiegelman, and G. Yim. 2006. 'The world of subinhibitory antibiotic concentrations', *Curr. Opin. Microbiol.*, 9: 445.

Davis, Tony D., Christopher J. Gerry, and Derek S. Tan. 2014. 'General platform for systematic quantitative evaluation of small-molecule permeability in bacteria', *ACS chemical biology*, 9: 2535-44.

Depke, Tobias, Raimo Franke, and Mark Brönstrup. 2017. 'Clustering of MS2 spectra using unsupervised methods to aid the identification of secondary metabolites from Pseudomonas aeruginosa', *Journal of Chromatography B*, 1071: 19-28.

Depke, Tobias, Raimo Franke, and Mark Brönstrup. 2019. 'CluMSID: an R package for similarity-based clustering of tandem mass spectra to aid feature annotation in metabolomics', *Bioinformatics*, 35: 3196-98.

Dettmer, Katja, Pavel A. Aronov, and Bruce D. Hammock. 2007. 'Mass spectrometry-based metabolomics', 26: 51-78.

Diggle, Stephen P., Andy Gardner, Stuart A. West, and Ashleigh S. Griffin. 2007. 'Evolutionary theory of bacterial quorum sensing: when is a signal not a signal?', *Philosophical transactions of the Royal Society of London. Series B, Biological sciences*, 362: 1241-49.

Diver, J. M., L. J. V. Piddock, and R. Wise. 1990. 'The accumulation of five quinolone antibacterial agents by Escherichia coli', *Journal of Antimicrobial Chemotherapy*, 25: 319-33.

Dörr, Tobias, Kim Lewis, and Marin Vulić. 2009. 'SOS Response Induces Persistence to Fluoroquinolones in Escherichia coli', *PLOS Genetics*, 5: e1000760.

Dörries, Kirsten, Rabea Schlueter, and Michael Lalk. 2014. 'Impact of antibiotics with various target sites on the metabolome of Staphylococcus aureus', *Antimicrobial agents and chemotherapy*, 58: 7151-63.

Dumont, Estelle, Julia Vergalli, Laurence Conraux, Carine Taillier, Aurélie Vassort, Jelena Pajović, Matthieu Réfrégiers, Michael Mourez, and Jean-Marie Pagès. 2018. 'Antibiotics and efflux: combined spectrofluorimetry and mass spectrometry to evaluate the involvement of concentration and efflux activity in antibiotic intracellular accumulation', *Journal of Antimicrobial Chemotherapy*: dky396-dky96.

Dwyer, Daniel J., Peter A. Belenky, Jason H. Yang, I. Cody MacDonald, Jeffrey D. Martell, Noriko Takahashi, Clement T. Y. Chan, Michael A. Lobritz, Dana Braff, Eric G. Schwarz, Jonathan D. Ye, Mekhala Pati, Maarten Vercruysse, Paul S. Ralifo, Kyle R. Allison, Ahmad S. Khalil, Alice Y. Ting, Graham C. Walker, and James J. Collins. 2014. 'Antibiotics induce redox-related physiological alterations as part of their lethality', *Proceedings of the National Academy of Sciences*, 111: E2100-E09.

Dwyer, Daniel J, Diogo M Camacho, Michael A Kohanski, Jarred M Callura, and James J Collins. 2012. 'Antibiotic-Induced Bacterial Cell Death Exhibits Physiological and Biochemical Hallmarks of Apoptosis', *Molecular Cell*, 46: 561-72.

East, Stephen P., Clara Bantry White, Oliver Barker, Stephanie Barker, James Bennett, David Brown, E. Andrew Boyd, Christopher Brennan, Chandana Chowdhury, Ian Collins, Emmanuelle Convers-Reignier, Brian W. Dymock, Rowena Fletcher, David J. Haydon, Mihaly Gardiner, Stuart Hatcher, Peter Ingram, Paul Lancett, Paul Mortenson, Konstantinos Papadopoulos, Carol Smee, Helena B. Thomaides-Brears, Heather Tye, James Workman, and Lloyd G. Czaplewski. 2009. 'DNA gyrase (GyrB)/topoisomerase IV (ParE) inhibitors: Synthesis and antibacterial activity', *Bioorganic & Medicinal Chemistry Letters*, 19: 894-99.

Ebner, Björn. 2016. 'Bestimmung von Kurvenparametern und deren statistischen Unsicherheiten für biologische Inhibitions-Assays', Ostfalia Hochschule für angewandte Wissenschaften.

Engelberg-Kulka, Hanna, Shahar Amitai, Ilana Kolodkin-Gal, and Ronen Hazan. 2006. 'Bacterial Programmed Cell Death and Multicellular Behavior in Bacteria', *PLOS Genetics*, 2: e135.

Ernst, Christoph M., Petra Staubitz, Nagendra N. Mishra, Soo-Jin Yang, Gabriele Hornig, Hubert Kalbacher, Arnold S. Bayer, Dirk Kraus, and Andreas Peschel. 2009. 'The bacterial defensin resistance protein MprF consists of separable domains for lipid lysinylation and antimicrobial peptide repulsion', *PLOS Pathogens*, 5: e1000660-e60.

Everett, M. J., Y. F. Jin, V. Ricci, and L. J. Piddock. 1996. 'Contributions of individual mechanisms to fluoroquinolone resistance in 36 Escherichia coli strains isolated from humans and animals', *Antimicrobial agents and chemotherapy*, 40: 2380-86.

Felden, Brice, and Vincent Cattoir. 2018. 'Bacterial Adaptation to Antibiotics through Regulatory RNAs', 62: e02503-17.

Fernández, Lucía, and Robert E. W. Hancock. 2012. 'Adaptive and Mutational Resistance: Role of Porins and Efflux Pumps in Drug Resistance', *Clinical Microbiology Reviews*, 25: 661.

Ferreira, Kevin, Hai-Yu Hu, Verena Fetz, Hans Prochnow, Bushra Rais, Peter P. Müller, and Mark Brönstrup. 2017. 'Multivalent Siderophore–DOTAM Conjugates as Theranostics for Imaging and Treatment of Bacterial Infections', 56: 8272-76.

Fraile-Ribot, Pablo A., Xavier Mulet, Gabriel Cabot, Ester del Barrio-Tofiño, Carlos Juan, José L. Pérez, and Antonio Oliver. 2017. 'In Vivo Emergence of Resistance to Novel Cephalosporin–β-Lactamase Inhibitor Combinations through the Duplication of Amino Acid D149 from OXA-2 β-Lactamase (OXA-539) in Sequence Type 235 Pseudomonas aeruginosa', 61: e01117-17.

Fraud, Sebastien, and Keith Poole. 2011. 'Oxidative Stress Induction of the MexXY Multidrug Efflux Genes and Promotion of Aminoglycoside Resistance Development in Pseudomonas aeruginosa', *Antimicrobial agents and chemotherapy*, 55: 1068.

Fyfe, Corey, Trudy H. Grossman, Kathy Kerstein, and Joyce Sutcliffe. 2016. 'Resistance to Macrolide Antibiotics in Public Health Pathogens', *Cold Spring Harbor perspectives in medicine*, 6: a025395.

Gao, Songmei, Zong-Ping Zhang, and H. T. Karnes. 2005. 'Sensitivity enhancement in liquid chromatography/atmospheric pressure ionization mass spectrometry using derivatization and mobile phase additives', *Journal of Chromatography B*, 825: 98-110.

George, Jaimee, and Prakash Motiram Halami. 2017. 'Sub-inhibitory concentrations of gentamicin triggers the expression of aac(6′)Ie-aph(2″)Ia, chaperons and biofilm related genes in Lactobacillus plantarum MCC 3011', *Research in Microbiology*, 168: 722-31.

Goh, Ee-Been, Grace Yim, Wayne Tsui, JoAnn McClure, Michael G. Surette, and Julian Davies. 2002. 'Transcriptional modulation of bacterial gene expression by subinhibitory concentrations of antibiotics', *Proceedings of the National Academy of Sciences*, 99: 17025.

Graef, F., R. Richter, V. Fetz, X. Murgia, C. De Rossi, N. Schneider-Daum, G. Allegretta, W. A. M. Elgaher, J. Haupenthal, M. Empting, F. Beckmann, M. Brönstrup, R. W. Hartmann, S. Gordon, and C. M. Lehr. 2018. 'An in vitro model of the gram-negative bacterial cell envelope for investigation of anti-infective permeation kinetics', *ACS Infect. Dis.*

Grein, Fabian, Anna Müller, Katharina M. Scherer, Xinliang Liu, Kevin C. Ludwig, Anna Klöckner, Manuel Strach, Hans-Georg Sahl, Ulrich Kubitscheck, and Tanja Schneider. 2020. 'Ca2+-Daptomycin targets cell wall biosynthesis by forming a tripartite complex with undecaprenyl-coupled intermediates and membrane lipids', *Nature Communications*, 11: 1455.

Guijas, Carlos, J. Rafael Montenegro-Burke, Xavier Domingo-Almenara, Amelia Palermo, Benedikt Warth, Gerrit Hermann, Gunda Koellensperger, Tao Huan, Winnie Uritboonthai, Aries E. Aisporna, Dennis W. Wolan, Mary E. Spilker, H. Paul Benton, and Gary Siuzdak. 2018. 'METLIN: A Technology Platform for Identifying Knowns and Unknowns', *Analytical Chemistry*, 90: 3156-64.

Gullberg, Erik, Sha Cao, Otto G. Berg, Carolina Ilbäck, Linus Sandegren, Diarmaid Hughes, and Dan I. Andersson. 2011. 'Selection of Resistant Bacteria at Very Low Antibiotic Concentrations', *PLOS Pathogens*, 7: e1002158.

Guo, An Chi, Timothy Jewison, Michael Wilson, Yifeng Liu, Craig Knox, Yannick Djoumbou, Patrick Lo, Rupasri Mandal, Ram Krishnamurthy, and David S. Wishart. 2013. 'ECMDB: the E. coli Metabolome Database', *Nucleic acids research*, 41: D625-D30.

Gutmann, L., R. Williamson, N. Moreau, M. D. Kitzis, E. Collatz, J. F. Acar, and F. W. Goldstein. 1985. 'Cross-resistance to nalidixic acid, trimethoprim, and chloramphenicol associated with alterations in outer membrane proteins of Klebsiella, Enterobacter, and Serratia', *J. Infect. Dis.*, 151: 501.

Guttenberger, Nikolaus, Wulf Blankenfeldt, and Rolf Breinbauer. 2017. 'Recent developments in the isolation, biological function, biosynthesis, and synthesis of phenazine natural products', *Bioorganic & Medicinal Chemistry*, 25: 6149-66.

Hall, Clayton W., and Thien-Fah Mah. 2017. 'Molecular mechanisms of biofilm-based antibiotic resistance and tolerance in pathogenic bacteria', *FEMS Microbiology Reviews*, 41: 276-301.

Han, Mei-Ling, Yan Zhu, Darren J. Creek, Yu-Wei Lin, Alina D. Gutu, Paul Hertzog, Tony Purcell, Hsin-Hui Shen, Samuel M. Moskowitz, Tony Velkov, and Jian Li. 2019. 'Comparative Metabolomics and Transcriptomics Reveal Multiple Pathways Associated with Polymyxin Killing in Pseudomonas aeruginosa', 4: e00149-18.

Hasdemir, Ufuk Over, Jacqueline Chevalier, Patrice Nordmann, and Jean-Marie Pagès. 2004. 'Detection and Prevalence of Active Drug Efflux Mechanism in Various Multidrug-Resistant Klebsiella pneumoniae Strains from Turkey', *Journal of Clinical Microbiology*, 42: 2701-06.

Häussler, Susanne, and Tanja Becker. 2008. 'The Pseudomonas Quinolone Signal (PQS) Balances Life and Death in Pseudomonas aeruginosa Populations', *PLOS Pathogens*, 4: e1000166.

Heeb, Stephan, Matthew P. Fletcher, Siri Ram Chhabra, Stephen P. Diggle, Paul Williams, and Miguel Cámara. 2011. 'Quinolones: from antibiotics to autoinducers', *FEMS Microbiology Reviews*, 35: 247-74.

Heumann, Axel. 2015. 'Quantifizierung der Aufnahme niedermolekularer Substanzen in Gram-negative Bakterien unter Verwendung von Zellfraktionierung und LC-MS', Master Thesis, Technische Universität Braunschweig, Institut für Biochemie, Biotechnologie und Bioinformatik.

Hicks, Stephanie C., and Rafael A. Irizarry. 2014. 'When to use Quantile Normalization?', *bioRxiv*: 012203.

Higgins, N. Patrick. 2007. 'Under DNA stress, gyrase makes the sign of the cross', *Nature Structural & Molecular Biology*, 14: 256-58.

Hoerr, Verena, Gavin E. Duggan, Lori Zbytnuik, Karen K. H. Poon, Christina Große, Ute Neugebauer, Karen Methling, Bettina Löffler, and Hans J. Vogel. 2016. 'Characterization and prediction of the mechanism of action of antibiotics through NMR metabolomics', *BMC Microbiology*, 16: 82.

Hoffman, Lucas R., David A. D'Argenio, Michael J. MacCoss, Zhaoying Zhang, Roger A. Jones, and Samuel I. Miller. 2005. 'Aminoglycoside antibiotics induce bacterial biofilm formation', *Nature*, 436: 1171.

Hojati, Zohreh, Claire Milne, Barbara Harvey, Lyndsey Gordon, Matthew Borg, Fiona Flett, Barrie Wilkinson, Philip J. Sidebottom, Brian A. M. Rudd, Martin A. Hayes, Colin P. Smith, and Jason Micklefield. 2002. 'Structure, Biosynthetic Origin, and Engineered Biosynthesis of Calcium-Dependent Antibiotics from Streptomyces coelicolor', *Chemistry & Biology*, 9: 1175-87.

Hooper, D. C., J. S. Wolfson, K. S. Souza, E. Y. Ng, G. L. McHugh, and M. N. Swartz. 1989. 'Mechanisms of quinolone resistance in Escherichia coli: characterization of nfxB and cfxB, two mutant resistance loci decreasing norfloxacin accumulation', *Antimicrob. Agents Chemother.*, 33: 283.

Horgan, Richard P, and Louise C Kenny. 2011. ''Omic' technologies: genomics, transcriptomics, proteomics and metabolomics', 13: 189-95.

Huang, W., L. K. Brewer, J. W. Jones, A. T. Nguyen, A. Marcu, D. S. Wishart, A. G. Oglesby-Sherrouse, M. A. Kane, and A. Wilks. 2018. 'PAMDB: a comprehensive Pseudomonas aeruginosa metabolome database', *Nucleic Acids Res*, 46: D575-d80.

Ishikawa, J., and T. Horii. 2005. 'Effects of Mupirocin at Subinhibitory Concentrations on Biofilm Formation in Pseudomonas aeruginosa', *Chemotherapy*, 51: 361-62.

Iyer, Ramkumar, Zhengqi Ye, Annette Ferrari, Leonard Duncan, M. Angela Tanudra, Hong Tsao, Tiansheng Wang, Hong Gao, Christopher L. Brummel, and Alice L. Erwin. 2018.

'Evaluating LC–MS/MS To Measure Accumulation of Compounds within Bacteria', *ACS Infectious Diseases*, 4: 1336-45.

Jedrey, Hannah, Kathryn S. Lilley, and Martin Welch. 2018. 'Ciprofloxacin binding to GyrA causes global changes in the proteome of Pseudomonas aeruginosa', *FEMS Microbiology Letters*, 365: fny134.

Jensen, Peter Ø, Alejandra Briales, Rikke P. Brochmann, Hengzhuang Wang, Kasper N. Kragh, Mette Kolpen, Casper Hempel, Thomas Bjarnsholt, Niels Høiby, and Oana Ciofu. 2014. 'Formation of hydroxyl radicals contributes to the bactericidal activity of ciprofloxacin against Pseudomonas aeruginosa biofilms', *Pathogens and Disease*, 70: 440-43.

Johnson, Paul J. T., and Bruce R. Levin. 2013. 'Pharmacodynamics, Population Dynamics, and the Evolution of Persistence in Staphylococcus aureus', *PLOS Genetics*, 9: e1003123.

Kang, Hee-Kyoung, and Yoonkyung Park. 2015. 'Glycopeptide Antibiotics: Structure and Mechanisms of Action', *J Bacteriol Virol*, 45: 67-78.

Kang, Yang, Bradley B. Schneider, and Thomas R. Covey. 2017. 'On the Nature of Mass Spectrometer Analyzer Contamination', *Journal of the American Society for Mass Spectrometry*, 28: 2384-92.

Karatuna, O., and A. Yagci. 2010. 'Analysis of quorum sensing-dependent virulence factor production and its relationship with antimicrobial susceptibility in Pseudomonas aeruginosa respiratory isolates', *Clin Microbiol Infect*, 16: 1770-5.

Kaščáková, Slávka, Laure Maigre, Jacqueline Chevalier, Matthieu Réfrégiers, and Jean-Marie Pagès. 2012. 'Antibiotic Transport in Resistant Bacteria: Synchrotron UV Fluorescence Microscopy to Determine Antibiotic Accumulation with Single Cell Resolution', *PLOS ONE*, 7: e38624.

Kaye, Keith S., Jason M. Pogue, Thien B. Tran, Roger L. Nation, and Jian Li. 2016. 'Agents of Last Resort: Polymyxin Resistance', *Infectious Disease Clinics of North America*, 30: 391-414.

Kohanski, Michael A., Daniel J. Dwyer, Boris Hayete, Carolyn A. Lawrence, and James J. Collins. 2007. 'A Common Mechanism of Cellular Death Induced by Bactericidal Antibiotics', *Cell*, 130: 797-810.

Kohanski, Michael A., Mark A. DePristo, and James J. Collins. 2010. 'Sublethal Antibiotic Treatment Leads to Multidrug Resistance via Radical-Induced Mutagenesis', *Molecular Cell*, 37: 311-20.

Kohanski, Michael A., Daniel J. Dwyer, and James J. Collins. 2010. 'How antibiotics kill bacteria: from targets to networks', *Nature Reviews Microbiology*, 8: 423-35.

Kojima, Seiji, and Hiroshi Nikaido. 2013. 'Permeation rates of penicillins indicate that Escherichia coli porins function principally as nonspecific channels', *Proceedings of the National Academy of Sciences*, 110: E2629-E34.

Kompis, Ivan M., Khalid Islam, and Rudolf L. Then. 2005. 'DNA and RNA Synthesis: Antifolates', *Chemical Reviews*, 105: 593-620.

Krishnamoorthy, Ganesh, David Wolloscheck, Jon W. Weeks, Cameron Croft, Valentin V. Rybenkov, and Helen I. Zgurskaya. 2016. 'Breaking the Permeability Barrier of Escherichia coli by Controlled Hyperporination of the Outer Membrane', *Antimicrobial agents and chemotherapy*, 60: 7372-81.

Lambert, R.J.W., and J. Pearson. 2000. 'Susceptibility testing: accurate and reproducible minimum inhibitory concentration (MIC) and non-inhibitory concentration (NIC) values', 88: 784-90.

Lebeaux, David, Jean-Marc Ghigo, and Christophe Beloin. 2014. 'Biofilm-Related Infections: Bridging the Gap between Clinical Management and Fundamental Aspects of Recalcitrance toward Antibiotics', *Microbiology and Molecular Biology Reviews*, 78: 510.

Lee, Daniel G., Jonathan M. Urbach, Gang Wu, Nicole T. Liberati, Rhonda L. Feinbaum, Sachiko Miyata, Lenard T. Diggins, Jianxin He, Maude Saucier, Eric Déziel, Lisa

Friedman, Li Li, George Grills, Kate Montgomery, Raju Kucherlapati, Laurence G. Rahme, and Frederick M. Ausubel. 2006. 'Genomic analysis reveals that Pseudomonas aeruginosa virulence is combinatorial', *Genome Biology*, 7: R90.

Lei, Y., S. Satake, J. Ishii, and T. Nakae. 1991. 'Factors that influence the permeability assay of the outer membrane of Pseudomonas aeruginosa', *FEMS Microbiol. Lett.*, 80: 337.

Leive, L., S. Telesetsky, W. G. Coleman, and D. Carr. 1984. 'Tetracyclines of various hydrophobicities as a probe for permeability of Escherichia coli outer membranes', *Antimicrob. Agents Chemother.*, 25: 539.

Li, X. Z., D. M. Livermore, and H. Nikaido. 1994. 'Role of efflux pump(s) in intrinsic resistance of Pseudomonas aeruginosa: resistance to tetracycline, chloramphenicol, and norfloxacin', *Antimicrobial agents and chemotherapy*, 38: 1732-41.

Li, Xian-Zhi, Li Zhang, and Hiroshi Nikaido. 2004. 'Efflux Pump-Mediated Intrinsic Drug Resistance in Mycobacterium smegmatis', *Antimicrobial agents and chemotherapy*, 48: 2415-23.

Linares, J. F., I. Gustafsson, F. Baquero, and J. L. Martinez. 2006. 'Antibiotics as intermicrobial signaling agents instead of weapons', *Proc Natl Acad Sci U S A*, 103: 19484-9.

Liu, Hanlan, Chantel Sabus, Guy T. Carter, Chao Du, Alex Avdeef, and Mark Tischler. 2003. 'In Vitro Permeability of Poorly Aqueous Soluble Compounds Using Different Solubilizers in the PAMPA Assay with Liquid Chromatography/Mass Spectrometry Detection', *Pharmaceutical Research*, 20: 1820-26.

Llano-Sotelo, Beatriz, Eduardo F. Azucena, Lakshmi P. Kotra, Shahriar Mobashery, and Christine S. Chow. 2002. 'Aminoglycosides Modified by Resistance Enzymes Display Diminished Binding to the Bacterial Ribosomal Aminoacyl-tRNA Site', *Chemistry & Biology*, 9: 455-63.

Lobritz, Michael A., Peter Belenky, Caroline B. M. Porter, Arnaud Gutierrez, Jason H. Yang, Eric G. Schwarz, Daniel J. Dwyer, Ahmad S. Khalil, and James J. Collins. 2015. 'Antibiotic efficacy is linked to bacterial cellular respiration', *Proceedings of the National Academy of Sciences*, 112: 8173-80.

Lou, Hubing, Min Chen, Susan S. Black, Simon R. Bushell, Matteo Ceccarelli, Tivadar Mach, Konstantinos Beis, Alison S. Low, Victoria A. Bamford, Ian R. Booth, Hagan Bayley, and James H. Naismith. 2011. 'Altered Antibiotic Transport in OmpC Mutants Isolated from a Series of Clinical Strains of Multi-Drug Resistant E. coli', *PLOS ONE*, 6: e25825.

Lovering, Andrew L., Susan S. Safadi, and Natalie C. J. Strynadka. 2012. 'Structural Perspective of Peptidoglycan Biosynthesis and Assembly', *Annual Review of Biochemistry*, 81: 451-78.

Lyczak, Jeffrey B., Carolyn L. Cannon, and Gerald B. Pier. 2000. 'Establishment of Pseudomonas aeruginosa infection: lessons from a versatile opportunist', *Microbes and Infection*, 2: 1051-60.

Malouin, F, S Chamberland, N Brochu, and T R Parr. 1991. 'Influence of growth media on Escherichia coli cell composition and ceftazidime susceptibility', *Antimicrobial agents and chemotherapy*, 35: 477-83.

Martínez-Solano, Laura, María D. Macia, Alicia Fajardo, Antonio Oliver, and Jose L. Martinez. 2008. 'Chronic Pseudomonas aeruginosa Infection in Chronic Obstructive Pulmonary Disease', *Clinical Infectious Diseases*, 47: 1526-33.

Masuda, N., E. Sakagawa, S. Ohya, N. Gotoh, H. Tsujimoto, and T. Nishino. 2000. 'Substrate specificities of MexAB-OprM, MexCD-OprJ, and MexXY-OprM efflux pumps in Pseudomonas aeruginosa', *Antimicrob Agents Chemother*, 44.

McCaffrey, C, A Bertasso, J Pace, and N H Georgopapadakou. 1992. 'Quinolone accumulation in Escherichia coli, Pseudomonas aeruginosa, and Staphylococcus aureus', *Antimicrobial agents and chemotherapy*, 36: 1601-05.

McMurry, L., and S. B. Levy. 1978. 'Two transport systems for tetracycline in sensitive Escherichia coli: critical role for an initial rapid uptake system insensitive to energy inhibitors', *Antimicrob. Agents Chemother.*, 14: 201.

McMurry, L., R. E. Petrucci, and S. B. Levy. 1980. 'Active efflux of tetracycline encoded by four genetically different tetracycline resistance determinants in Escherichia coli', *Proc. Natl. Acad. Sci. U. S. A.*, 77: 3974.

McMurry, L. M., J. C. Cullinane, and S. B. Levy. 1982. 'Transport of the lipophilic analog minocycline differs from that of tetracycline in susceptible and resistant Escherichia coli strains', *Antimicrob. Agents Chemother.*, 22: 791.

Meylan, Sylvain, Caroline B. M. Porter, Jason H. Yang, Peter Belenky, Arnaud Gutierrez, Michael A. Lobritz, Jihye Park, Sun H. Kim, Samuel M. Moskowitz, and James J. Collins. 2017. 'Carbon Sources Tune Antibiotic Susceptibility in Pseudomonas aeruginosa via Tricarboxylic Acid Cycle Control', *Cell Chemical Biology*, 24: 195-206.

Mingeot-Leclercq, Marie-Paule, and Jean-Luc Décout. 2016. 'Bacterial lipid membranes as promising targets to fight antimicrobial resistance, molecular foundations and illustration through the renewal of aminoglycoside antibiotics and emergence of amphiphilic aminoglycosides', *MedChemComm*, 7: 586-611.

Moradali, M. Fata, Shirin Ghods, and Bernd H. A. Rehm. 2017. 'Pseudomonas aeruginosa Lifestyle: A Paradigm for Adaptation, Survival, and Persistence', *Frontiers in cellular and infection microbiology*, 7: 39-39.

Morita, Yuji, Junko Tomida, and Yoshiaki Kawamura. 2014. 'Responses of Pseudomonas aeruginosa to antimicrobials', *Frontiers in microbiology*, 4: 422-22.

Mortimer, P. G. S., and L. J. V. Piddock. 1991. 'A comparison of methods used for measuring the accumulation of quinolones by Enterobacteriaceae, Pseudomonas aeruginosa and Staphylococcus aureus', *Journal of Antimicrobial Chemotherapy*, 28: 639-53.

Nadal Jimenez, Pol, Gudrun Koch, Jessica A. Thompson, Karina B. Xavier, Robbert H. Cool, and Wim J. Quax. 2012. 'The Multiple Signaling Systems Regulating Virulence in Pseudomonas aeruginosa', *Microbiology and Molecular Biology Reviews*, 76: 46-65.

Nakajima, Akira, Yohko Sugimoto, Hiroshi Yoneyama, and Taiji Nakae. 2002. 'High-Level Fluoroquinolone Resistance in Pseudomonas aeruginosa Due to Interplay of the MexAB-OprM Efflux Pump and the DNA Gyrase Mutation', *Microbiology and Immunology*, 46: 391-95.

Nalca, Yusuf, Lothar Jänsch, Florian Bredenbruch, Robert Geffers, Jan Buer, and Susanne Häussler. 2006. 'Quorum-Sensing Antagonistic Activities of Azithromycin in Pseudomonas aeruginosa PAO1: a Global Approach', *Antimicrobial agents and chemotherapy*, 50: 1680.

Nelson, David L., and Michael M. Cox. 2017. *Lehninger Principles of Biochemistry* (Seventh edition. New York : W.H. Freeman, 2017.).

Ning, Xinghai, Seungjun Lee, Zhirui Wang, Dongin Kim, Bryan Stubblefield, Eric Gilbert, and Niren Murthy. 2011. 'Maltodextrin-based imaging probes detect bacteria in vivo with high sensitivity and specificity', *Nature Materials*, 10: 602-07.

Noordman, Wouter H., and Dick B. Janssen. 2002. 'Rhamnolipid stimulates uptake of hydrophobic compounds by Pseudomonas aeruginosa', *Applied and Environmental Microbiology*, 68: 4502-08.

O'Sullivan, Mary E, Frédéric Poitevin, Raymond G Sierra, Cornelius Gati, E Han Dao, Yashas Rao, Fulya Aksit, Halilibrahim Ciftci, Nicholas Corsepius, Robert Greenhouse, Brandon Hayes, Mark S Hunter, Mengling Liang, Alex McGurk, Paul Mbgam, Trevor Obrinsky, Fátima Pardo-Avila, Matthew H Seaberg, Alan G Cheng, Anthony J Ricci, and Hasan DeMirci. 2018. 'Aminoglycoside ribosome interactions reveal novel conformational states at ambient temperature', *Nucleic acids research*, 46: 9793-804.

Oethinger, Margret, Winfried V. Kern, Angelika S. Jellen-Ritter, Laura M. McMurry, and Stuart B. Levy. 2000. 'Ineffectiveness of Topoisomerase Mutations in Mediating Clinically Significant Fluoroquinolone Resistance inEscherichia coli in the Absence of the AcrAB Efflux Pump', 44: 10-13.

Ogden, N. H., P. AbdelMalik, and J. Pulliam. 2017. 'Emerging infectious diseases: prediction and detection', *Can Commun Dis Rep*, 43: 206-11.

Olaitan, Abiola O., Serge Morand, and Jean-Marc Rolain. 2014. 'Mechanisms of polymyxin resistance: acquired and intrinsic resistance in bacteria', *Frontiers in microbiology*, 5: 643-43.

Opperman, Timothy, and Son Nguyen. 2015. 'Recent advances toward a molecular mechanism of efflux pump inhibition', 6.

Ovchinnikov, Yuri A., Galina S. Monastyrskaya, Sergei O. Guriev, Nadezhda F. Kalinina, Eugene D. Sverdlov, Alexander I. Gragerov, Irina A. Bass, Irina F. Kiver, Elena P. Moiseyeva, Vladimir N. Igumnov, Sofia Z. Mindlin, Vadim G. Nikiforov, and Roman B. Khesin. 1983. 'RNA polymerase rifampicin resistance mutations in Escherichia coli: Sequence changes and dominance', *Molecular and General Genetics MGG*, 190: 344-48.

Pang, Zheng, Renee Raudonis, Bernard R. Glick, Tong-Jun Lin, and Zhenyu Cheng. 2018. 'Antibiotic resistance in Pseudomonas aeruginosa: mechanisms and alternative therapeutic strategies', *Biotechnology Advances*.

Parenti, Francesco. 1986. 'Structure and mechanism of action of teicoplanin', *Journal of Hospital Infection*, 7: 79-83.

Pericolini, Eva, Bruna Colombari, Gianmarco Ferretti, Ramona Iseppi, Andrea Ardizzoni, Massimo Girardis, Arianna Sala, Samuele Peppoloni, and Elisabetta Blasi. 2018. 'Real-time monitoring of Pseudomonas aeruginosa biofilm formation on endotracheal tubes in vitro', *BMC Microbiology*, 18: 84.

Peterson, Ryan A., and Joseph E. Cavanaugh. 2019. 'Ordered quantile normalization: a semiparametric transformation built for the cross-validation era', *Journal of Applied Statistics*: 1-16.

Phelan, Vanessa V., Jinshu Fang, and Pieter C. Dorrestein. 2015. 'Mass Spectrometry Analysis of Pseudomonas aeruginosa Treated With Azithromycin', *Journal of the American Society for Mass Spectrometry*, 26: 873-77.

Phetsang, Wanida, Ruby Pelingon, Mark S. Butler, Sanjaya Kc, Miranda E. Pitt, Geraldine Kaeslin, Matthew A. Cooper, and Mark A. T. Blaskovich. 2016. 'Fluorescent Trimethoprim Conjugate Probes To Assess Drug Accumulation in Wild Type and Mutant Escherichia coli', *ACS Infectious Diseases*, 2: 688-701.

Piddock, L. J. 1991. 'Mechanism of quinolone uptake into bacterial cells', *J. Antimicrob. Chemother.*, 27: 399.

Piddock, L. J., and M. Zhu. 1991. 'Mechanism of action of sparfloxacin against and mechanism of resistance in Gram-negative and Gram-positive bacteria', *Antimicrob. Agents Chemother.*, 35: 2423.

Piddock, Laura J. V., Y.-F. Jin, V. Ricci, and Anne E. Asuquo. 1999. 'Quinolone accumulation by Pseudomonas aeruginosa, Staphylococcus aureus and Escherichia coli', *Journal of Antimicrobial Chemotherapy*, 43: 61-70.

Piddock, Laura J. V., and M. M. Johnson. 2002. 'Accumulation of 10 Fluoroquinolones by Wild-Type or Efflux Mutant Streptococcus pneumoniae', *Antimicrobial agents and chemotherapy*, 46: 813-20.

Piddock, Laura J. V. 2006. 'Multidrug-resistance efflux pumps ? not just for resistance', *Nature Reviews Microbiology*, 4: 629-36.

Pierson, Leland S., and Elizabeth A. Pierson. 2010. 'Metabolism and function of phenazines in bacteria: impacts on the behavior of bacteria in the environment and biotechnological processes', *Applied Microbiology and Biotechnology*, 86: 1659-70.

Pitt, James J. 2009. 'Principles and applications of liquid chromatography-mass spectrometry in clinical biochemistry', *The Clinical biochemist. Reviews*, 30: 19-34.

Poirel, Laurent, Aurélie Jayol, and Patrice Nordmann. 2017. 'Polymyxins: Antibacterial Activity, Susceptibility Testing, and Resistance Mechanisms Encoded by Plasmids or Chromosomes', *Clinical Microbiology Reviews*, 30: 557.

Poole, Keith. 2012. 'Stress responses as determinants of antimicrobial resistance in Gram-negative bacteria', *Trends in Microbiology*, 20: 227-34.

Price-Whelan, Alexa, Lars E. P. Dietrich, and Dianne K. Newman. 2007. 'Pyocyanin Alters Redox Homeostasis and Carbon Flux through Central Metabolic Pathways in Pseudomonas aeruginosa PA14', *Journal of bacteriology*, 189: 6372.

Prochnow, Hans, Verena Fetz, Sven-Kevin Hotop, Mariel A. García-Rivera, Axel Heumann, and Mark Brönstrup. 2018. 'Subcellular Quantification of Uptake in Gram-Negative Bacteria', *Analytical Chemistry*.

Qiu, Xing, Hulin Wu, and Rui Hu. 2013. 'The impact of quantile and rank normalization procedures on the testing power of gene differential expression analysis', *BMC Bioinformatics*, 14: 124.

Rahme, L. G., E. J. Stevens, S. F. Wolfort, J. Shao, R. G. Tompkins, and F. M. Ausubel. 1995. 'Common virulence factors for bacterial pathogenicity in plants and animals', *Science*, 268: 1899.

Ramirez, Maria S., and Marcelo E. Tolmasky. 2010. 'Aminoglycoside modifying enzymes', *Drug Resistance Updates*, 13: 151-71.

Rende-Fournier, R, R Leclercq, M Galimand, J Duval, and P Courvalin. 1993. 'Identification of the satA gene encoding a streptogramin A acetyltransferase in Enterococcus faecium BM4145', 37: 2119-25.

Ricci, Vito, and Laura Piddock. 2003. 'Accumulation of garenoxacin by Bacteroides fragilis compared with that of five fluoroquinolones', *Journal of Antimicrobial Chemotherapy*, 52: 605-09.

Rice, Kelly C., and Kenneth W. Bayles. 2003. 'Death's toolbox: examining the molecular components of bacterial programmed cell death', 50: 729-38.

Richter, Michelle F., Bryon S. Drown, Andrew P. Riley, Alfredo Garcia, Tomohiro Shirai, Riley L. Svec, and Paul J. Hergenrother. 2017. 'Predictive compound accumulation rules yield a broad-spectrum antibiotic', *Nature*, 545: 299.

Richter, Michelle F., and Paul J. Hergenrother. 2019. 'The challenge of converting Gram-positive-only compounds into broad-spectrum antibiotics', *Ann. N.Y. Acad. Sci.*, 1435: 18-38.

Romanowska, Julia, Nathalie Reuter, and Joanna Trylska. 2013. 'Comparing aminoglycoside binding sites in bacterial ribosomal RNA and aminoglycoside modifying enzymes', 81: 63-80.

Samra, Z., J. Krausz-Steinmetz, and D. Sompolinsky. 1978. 'Transport of tetracyclines through the bacterial cell membrane assayed by fluorescence: a study with susceptible and resistant strains of Staphylococcus aureus and Escherichia coli', *Microbios*, 21: 7.

Schrimpe-Rutledge, Alexandra C., Simona G. Codreanu, Stacy D. Sherrod, and John A. McLean. 2016. 'Untargeted Metabolomics Strategies—Challenges and Emerging Directions', *Journal of the American Society for Mass Spectrometry*, 27: 1897-905.

Schumacher, Anja, Rainer Trittler, Jürgen A. Bohnert, Klaus Kümmerer, Jean-Marie Pagès, and Winfried V. Kern. 2006. 'Intracellular accumulation of linezolid in Escherichia coli, Citrobacter freundii and Enterobacter aerogenes: role of enhanced efflux pump activity and inactivation', *Journal of Antimicrobial Chemotherapy*, 59: 1261-64.

Siriyong, Thanyaluck, Potjanee Srimanote, Sasitorn Chusri, Boon-ek Yingyongnarongkul, Channarong Suaisom, Varomyalin Tipmanee, and Supayang Piyawan Voravuthikunchai. 2017. 'Conessine as a novel inhibitor of multidrug efflux pump systems in Pseudomonas aeruginosa', *BMC Complementary and Alternative Medicine*, 17: 405.

Siuzdak, Gary. 2003. *The Expanding Role of Mass Spectrometry in Biotechnology* (MCC Press: San Diego, CA, USA).

Spangler, B., D. Dovala, W. S. Sawyer, K. V. Thompson, D. A. Six, F. Reck, and B. Y. Feng. 2018. 'Molecular probes for the determination of sub-cellular compound exposure profiles in Gram-negative bacteria', *ACS Infect. Dis.*

Stapleton, Paul D., and Peter W. Taylor. 2002. 'Methicillin resistance in Staphylococcus aureus: mechanisms and modulation', *Science progress*, 85: 57-72.

Stavenger, Robert A., and Mathias Winterhalter. 2014. 'TRANSLOCATION Project: How to Get Good Drugs into Bad Bugs', *Science Translational Medicine*, 6: 228ed7-28ed7.

Stone, M. Rhia L., Muriel Masi, Wanida Phetsang, Jean-Marie Pagès, Matthew A. Cooper, and Mark A. T. Blaskovich. 2019. 'Fluoroquinolone-derived fluorescent probes for studies of bacterial penetration and efflux', *MedChemComm*, 10: 901-06.

Subedi, Dinesh, Ajay Kumar Vijay, Gurjeet Singh Kohli, Scott A. Rice, and Mark Willcox. 2018. 'Association between possession of ExoU and antibiotic resistance in Pseudomonas aeruginosa', *PLOS ONE*, 13: e0204936.

Sun, Jingjing, Ziqing Deng, and Aixin Yan. 2014. 'Bacterial multidrug efflux pumps: Mechanisms, physiology and pharmacological exploitations', *Biochemical and Biophysical Research Communications*, 453: 254-67.

T., Thai, Salisbury BH., and Zito PM. 2020. 'Ciprofloxacin', StatPearls [Internet]. Accessed Jul 2020. Available from: https://www.ncbi.nlm.nih.gov/books/NBK535454/.

Tacconelli, Evelina, Elena Carrara, Alessia Savoldi, Stephan Harbarth, Marc Mendelson, Dominique L. Monnet, Céline Pulcini, Gunnar Kahlmeter, Jan Kluytmans, Yehuda Carmeli, Marc Ouellette, Kevin Outterson, Jean Patel, Marco Cavaleri, Edward M. Cox, Chris R. Houchens, M. Lindsay Grayson, Paul Hansen, Nalini Singh, Ursula Theuretzbacher, Nicola Magrini, Aaron Oladipo Aboderin, Seif Salem Al-Abri, Nordiah Awang Jalil, Nur Benzonana, Sanjay Bhattacharya, Adrian John Brink, Francesco Robert Burkert, Otto Cars, Giuseppe Cornaglia, Oliver James Dyar, Alex W. Friedrich, Ana C. Gales, Sumanth Gandra, Christian Georg Giske, Debra A. Goff, Herman Goossens, Thomas Gottlieb, Manuel Guzman Blanco, Waleria Hryniewicz, Deepthi Kattula, Timothy Jinks, Souha S. Kanj, Lawrence Kerr, Marie-Paule Kieny, Yang Soo Kim, Roman S. Kozlov, Jaime Labarca, Ramanan Laxminarayan, Karin Leder, Leonard Leibovici, Gabriel Levy-Hara, Jasper Littman, Surbhi Malhotra-Kumar, Vikas Manchanda, Lorenzo Moja, Babacar Ndoye, Angelo Pan, David L. Paterson, Mical Paul, Haibo Qiu, Pilar Ramon-Pardo, Jesús Rodríguez-Baño, Maurizio Sanguinetti, Sharmila Sengupta, Mike Sharland, Massinissa Si-Mehand, Lynn L. Silver, Wonkeung Song, Martin Steinbakk, Jens Thomsen, Guy E. Thwaites, Jos W. M. van der Meer, Nguyen Van Kinh, Silvio Vega, Maria Virginia Villegas, Agnes Wechsler-Fördös, Heiman Frank Louis Wertheim, Evelyn Wesangula, Neil Woodford, Fidan O. Yilmaz, and Anna Zorzet. 2018. 'Discovery, research, and development of new antibiotics: the WHO priority list of antibiotic-resistant bacteria and tuberculosis', *The Lancet Infectious Diseases*, 18: 318-27.

Tanimoto, K., H. Tomita, S. Fujimoto, K. Okuzumi, and Y. Ike. 2008. 'Fluoroquinolone enhances the mutation frequency for meropenem-selected carbapenem resistance in Pseudomonas aeruginosa, but use of the high-potency drug doripenem inhibits mutant formation', *Antimicrob Agents Chemother*, 52: 3795-800.

Tateda, Kazuhiro, Rachel Comte, Jean-Claude Pechere, Thilo Köhler, Keizo Yamaguchi, and Christian Van Delden. 2001. 'Azithromycin Inhibits Quorum Sensing in Pseudomonas aeruginosa', *Antimicrobial agents and chemotherapy*, 45: 1930.

Tegos, George P., Mark Haynes, J. Jacob Strouse, Mohiuddin Md T. Khan, Cristian G. Bologa, Tudor I. Oprea, and Larry A. Sklar. 2011. 'Microbial efflux pump inhibition: tactics and strategies', *Current pharmaceutical design*, 17: 1291-302.

Tian, H., D. A. Six, T. Krucker, J. A. Leeds, and N. Winograd. 2017. 'Subcellular chemical imaging of antibiotics in single bacteria using C60-secondary ion mass spectrometry', *Anal. Chem.*, 89: 5050.

Trancassini, M., M. I. Brenciaglia, M. C. Ghezzi, P. Cipriani, and F. Filadoro. 1992. 'Modification of Pseudomonas aeruginosa Virulence Factors by Sub-Inhibitory Concentrations of Antibiotics', *Journal of Chemotherapy*, 4: 78-81.

Van Acker, Heleen, and Tom Coenye. 2017. 'The Role of Reactive Oxygen Species in Antibiotic-Mediated Killing of Bacteria', *Trends in Microbiology*, 25: 456-66.

Verbrugghe, Elin, Alexander Van Parys, Roel Haesendonck, Bregje Leyman, Filip Boyen, Freddy Haesebrouck, and Frank Pasmans. 2016. 'Subtherapeutic tetracycline

concentrations aggravate Salmonella Typhimurium infection by increasing bacterial virulence', *Journal of Antimicrobial Chemotherapy*, 71: 2158-66.

Vergalli, Julia, Estelle Dumont, Bertrand Cinquin, Laure Maigre, Jelena Pajovic, Eric Bacqué, Michael Mourez, Matthieu Réfrégiers, and Jean-Marie Pagès. 2017. 'Fluoroquinolone structure and translocation flux across bacterial membrane', *Scientific Reports*, 7: 9821.

Vergalli, Julia, Estelle Dumont, Jelena Pajović, Bertrand Cinquin, Laure Maigre, Muriel Masi, Matthieu Réfrégiers, and Jean-Marie Pagés. 2018. 'Spectrofluorimetric quantification of antibiotic drug concentration in bacterial cells for the characterization of translocation across bacterial membranes', *Nature Protocols*, 13: 1348-61.

Villas-Bôas, S.G., U. Roessner, M.A.E. Hansen, J. Smedsgaard, and J. Nielsen. 2007. *Metabolome Analysis: An Introduction.*

Vincent, Isabel M., David E. Ehmann, Scott D. Mills, Manos Perros, and Michael P. Barrett. 2016. 'Untargeted Metabolomics To Ascertain Antibiotic Modes of Action', *Antimicrobial agents and chemotherapy*, 60: 2281-91.

Walsh, C. T., S. L. Fisher, I. S. Park, M. Prahalad, and Z. Wu. 1996. 'Bacterial resistance to vancomycin: five genes and one missing hydrogen bond tell the story', *Chemistry & Biology*, 3: 21-28.

Walsh, Christopher, and Timothy Wencewicz. 2016. *Antibiotics: Challenges, Mechanisms, Opportunities* (American Society of Microbiology).

Walters, Marshall C., Frank Roe, Amandine Bugnicourt, Michael J. Franklin, and Philip S. Stewart. 2003. 'Contributions of Antibiotic Penetration, Oxygen Limitation, and Low Metabolic Activity to Tolerance of Pseudomonas aeruginosa Biofilms to Ciprofloxacin and Tobramycin', *Antimicrobial agents and chemotherapy*, 47: 317-23.

Wang, Mingxun, Jeremy J. Carver, Vanessa V. Phelan, Laura M. Sanchez, Neha Garg, Yao Peng, Don Duy Nguyen, Jeramie Watrous, Clifford A. Kapono, Tal Luzzatto-Knaan, Carla Porto, Amina Bouslimani, Alexey V. Melnik, Michael J. Meehan, Wei-Ting Liu, Max Crüsemann, Paul D. Boudreau, Eduardo Esquenazi, Mario Sandoval-Calderón, Roland D. Kersten, Laura A. Pace, Robert A. Quinn, Katherine R. Duncan, Cheng-Chih Hsu, Dimitrios J. Floros, Ronnie G. Gavilan, Karin Kleigrewe, Trent Northen, Rachel J. Dutton, Delphine Parrot, Erin E. Carlson, Bertrand Aigle, Charlotte F. Michelsen, Lars Jelsbak, Christian Sohlenkamp, Pavel Pevzner, Anna Edlund, Jeffrey McLean, Jörn Piel, Brian T. Murphy, Lena Gerwick, Chih-Chuang Liaw, Yu-Liang Yang, Hans-Ulrich Humpf, Maria Maansson, Robert A. Keyzers, Amy C. Sims, Andrew R. Johnson, Ashley M. Sidebottom, Brian E. Sedio, Andreas Klitgaard, Charles B. Larson, Cristopher A. Boya P, Daniel Torres-Mendoza, David J. Gonzalez, Denise B. Silva, Lucas M. Marques, Daniel P. Demarque, Egle Pociute, Ellis C. O'Neill, Enora Briand, Eric J. N. Helfrich, Eve A. Granatosky, Evgenia Glukhov, Florian Ryffel, Hailey Houson, Hosein Mohimani, Jenan J. Kharbush, Yi Zeng, Julia A. Vorholt, Kenji L. Kurita, Pep Charusanti, Kerry L. McPhail, Kristian Fog Nielsen, Lisa Vuong, Maryam Elfeki, Matthew F. Traxler, Niclas Engene, Nobuhiro Koyama, Oliver B. Vining, Ralph Baric, Ricardo R. Silva, Samantha J. Mascuch, Sophie Tomasi, Stefan Jenkins, Venkat Macherla, Thomas Hoffman, Vinayak Agarwal, Philip G. Williams, Jingqui Dai, Ram Neupane, Joshua Gurr, Andrés M. C. Rodríguez, Anne Lamsa, Chen Zhang, Kathleen Dorrestein, Brendan M. Duggan, Jehad Almaliti, Pierre-Marie Allard, Prasad Phapale, Louis-Felix Nothias, Theodore Alexandrov, Marc Litaudon, Jean-Luc Wolfender, Jennifer E. Kyle, Thomas O. Metz, Tyler Peryea, Dac-Trung Nguyen, Danielle VanLeer, Paul Shinn, Ajit Jadhav, Rolf Müller, Katrina M. Waters, Wenyuan Shi, Xueting Liu, Lixin Zhang, Rob Knight, Paul R. Jensen, Bernhard Ø Palsson, Kit Pogliano, Roger G. Linington, Marcelino Gutiérrez, Norberto P. Lopes, William H. Gerwick, Bradley S. Moore, Pieter C. Dorrestein, and Nuno Bandeira. 2016. 'Sharing and community curation of mass spectrometry data with Global Natural Products Social Molecular Networking', *Nature Biotechnology*, 34: 828-37.

Wang, Yingyu, Xiaowei Li, Yang Wang, Stefan Schwarz, Jianzhong Shen, and Xi Xia. 2018. 'Intracellular Accumulation of Linezolid and Florfenicol in OptrA-Producing Enterococcus faecalis and Staphylococcus aureus', *Molecules*, 23: 3195.

Watson, J. Throck, and O. David Sparkman. 2007. *Introduction to Mass Spectrometry: Instrumentation, Applications and Strategies for Data Interpretation*.

Westfall, D. A., G. Krishnamoorthy, D. Wolloscheck, R. Sarkar, H. I. Zgurskaya, and V. V. Rybenkov. 2017. 'Bifurcation kinetics of drug uptake by Gram-negative bacteria', *PLOS ONE*, 12: e0184671.

WHO. 2017. "Prioritization of pathogens to guide discovery, research and development of new antibiotics for drug-resistant bacterial infections, including tuberculosis." In. Geneva, Switzerland: World Health Organization.

Widya, Marcella, William D. Pasutti, Meena Sachdeva, Robert L. Simmons, Pramila Tamrakar, Thomas Krucker, and David A. Six. 2019. 'Development and Optimization of a Higher-Throughput Bacterial Compound Accumulation Assay', *ACS Infectious Diseases*, 5: 394-405.

Wieling, J. 2002. 'LC-MS-MS experiences with internal standards', *Chromatographia*, 55: S107-S13.

Williams, K. J., G. A. Chung, and L. J. Piddock. 1998. 'Accumulation of norfloxacin by Mycobacterium aurum and Mycobacterium smegmatis', *Antimicrob. Agents Chemother.*, 42: 795.

Williams, K. J., and L. J. Piddock. 1998. 'Accumulation of rifampicin by Escherichia coli and Staphylococcus aureus', *J. Antimicrob. Chemother.*, 42: 597.

Wilson, Daniel N. 2013. 'Ribosome-targeting antibiotics and mechanisms of bacterial resistance', *Nature Reviews Microbiology*, 12: 35-48.

Wishart, David S, Yannick Djoumbou Feunang, Ana Marcu, An Chi Guo, Kevin Liang, Rosa Vázquez-Fresno, Tanvir Sajed, Daniel Johnson, Carin Li, Naama Karu, Zinat Sayeeda, Elvis Lo, Nazanin Assempour, Mark Berjanskii, Sandeep Singhal, David Arndt, Yonjie Liang, Hasan Badran, Jason Grant, Arnau Serra-Cayuela, Yifeng Liu, Rupa Mandal, Vanessa Neveu, Allison Pon, Craig Knox, Michael Wilson, Claudine Manach, and Augustin Scalbert. 2017. 'HMDB 4.0: the human metabolome database for 2018', *Nucleic acids research*, 46: D608-D17.

Witzgall, Florian, Tobias Depke, Michael Hoffmann, Martin Empting, Mark Brönstrup, Rolf Müller, and Wulf Blankenfeldt. 2018. 'The Alkylquinolone Repertoire of Pseudomonas aeruginosa is Linked to Structural Flexibility of the FabH-like 2-Heptyl-3-hydroxy-4(1H)-quinolone (PQS) Biosynthesis Enzyme PqsBC', *ChemBioChem*, 19: 1531-44.

Wolter, D. J., A. J. Schmidtke, N. D. Hanson, and P. D. Lister. 2007. 'Increased expression of ampC in Pseudomonas aeruginosa mutants selected with ciprofloxacin', *Antimicrob Agents Chemother*, 51: 2997-3000.

World Health Organization. 2001. "WHO global strategy for containment of antimicrobial resistance." In.: World Health Organization.

Wu, Yanxia, Marin Vulić, Iris Keren, and Kim Lewis. 2012. 'Role of Oxidative Stress in Persister Tolerance', *Antimicrobial agents and chemotherapy*, 56: 4922-26.

Wu, Yuan-Kun, Nai-Chen Cheng, and Chao-Min Cheng. 2019. 'Biofilms in Chronic Wounds: Pathogenesis and Diagnosis', *Trends in Biotechnology*, 37: 505-17.

Xiong, Lina, Dongjiang Liao, Xinpeng Lu, He Yan, Lei Shi, and Ziyao Mo. 2017. 'Proteomic analysis reveals that a global response is induced by subinhibitory concentrations of ampicillin', *Bioengineered*, 8: 732-41.

Yang, Jason H., Sarah N. Wright, Meagan Hamblin, Douglas McCloskey, Miguel A. Alcantar, Lars Schrübbers, Allison J. Lopatkin, Sangeeta Satish, Amir Nili, Bernhard O. Palsson, Graham C. Walker, and James J. Collins. 2019. 'A White-Box Machine Learning Approach for Revealing Antibiotic Mechanisms of Action', *Cell*, 177: 1649-61.e9.

Zampieri, Mattia, Michael Zimmermann, Manfred Claassen, and Uwe Sauer. 2017. 'Nontargeted Metabolomics Reveals the Multilevel Response to Antibiotic Perturbations', *Cell Reports*, 19: 1214-28.

Zampieri, Mattia, Balazs Szappanos, Maria Virginia Buchieri, Andrej Trauner, Ilaria Piazza, Paola Picotti, Sébastien Gagneux, Sonia Borrell, Brigitte Gicquel, Joel Lelievre, Balazs Papp, and Uwe Sauer. 2018. 'High-throughput metabolomic analysis predicts mode of action of uncharacterized antimicrobial compounds', *Science Translational Medicine*, 10.

Zgurskaya, Helen I., and Valentin V. Rybenkov. 2020. 'Permeability barriers of Gram-negative pathogens', *ANNALS OF THE NEW YORK ACADEMY OF SCIENCES*, 1459: 5-18.

Zhou, Ying, Camil Joubran, Lakshmi Miller-Vedam, Vincent Isabella, Asha Nayar, Sharon Tentarelli, and Alita Miller. 2015. 'Thinking Outside the "Bug": A Unique Assay To Measure Intracellular Drug Penetration in Gram-Negative Bacteria', *Analytical Chemistry*, 87: 3579-84.

Zimmermann, Willy, and Armel Rosselet. 1977. 'Function of the Outer Membrane of Escherichia coli as a Permeability Barrier to Beta-Lactam Antibiotics', *Antimicrobial agents and chemotherapy*, 12: 368-72.

PRELIMINARY PUBLICATION OF THE DISSERTATION

Partial results from this work were published in advance in the following articles:

Publications

1. Prochnow, H., Fetz, V., Hotop, S.-K., García-Rivera, M. A., Heumann, A., & Brönstrup, M. (2018): Subcellular Quantification of Uptake in Gram-Negative Bacteria. *Analytical Chemistry*. doi:10.1021/acs.analchem.8b03586

2. Richter, Robert; Kamal, Mohamed Ashraf M.; García-Rivera, Mariel A.; Kaspar, Jerome; Junk, Maximilian; Elgaher, Walid A. M.; et al. (2020): A Hydrogel-Based in Vitro Assay for the Fast Prediction of Antibiotic Accumulation in Gram-Negative Bacteria. *Materials Today Bio.* doi: 10.1016/j.mtbio.2020.100084

Poster contributions

García-Rivera M. A., Franke, R. Brönstrup, M. *The effect on P. aeruginosa secondary metabolome under antibiotic stress at sub-inhibitory concentrations.*1st Nordic Metabolomics Conference. 26-28th August 2018. Örebro, Sweden.

APPENDICES

I.   Standard curves for uptake studies

Table A1. Intensity in total counts of known concentrations of antibiotics used in uptake studies. Intensity values are the average of triplicates (n=3)

Concentration (µM)	Ciprofloxacin	Sulfamethoxazole	Novobiocin	Nalidixic acid
1.56	4.83E+06	2.72E+06	2.14E+06	1.48E+07
3.13	7.96E+06	4.99E+06	4.24E+06	2.63E+07
6.25	1.38E+07	9.44E+06	7.57E+06	5.07E+07
12.5	2.39E+07	1.77E+07	1.32E+07	9.37E+07
25	4.22E+07	3.32E+07	2.37E+07	1.65E+08
Slope	6.30E-07	7.70E-07	1.10E-06	1.56E-07
Intercept	-2.00E+00	-8.06E-01	-1.52E+00	-1.23E+00
R^2	0.99739	0.99915	0.99627	0.99581

Table S1 (continued). Intensity in total counts of known concentrations of antibiotics used in uptake studies. Intensity values are the average of triplicates (n=3)

Concentration (µM)	Lincomycin	Phosphomycin	Clindamycin	Tigecycline	Tetracycline
1.56	1.58E+07	2.03E+04	1.65E+07	3.85E+05	5.89E+06
3.13	2.83E+07	5.93E+04	3.07E+07	7.59E+05	1.12E+07
6.25	5.86E+07	1.28E+05	6.00E+07	1.78E+06	2.07E+07
12.5	1.04E+08	2.68E+05	1.12E+08	3.75E+06	4.03E+07
25	2.00E+08	4.93E+05	2.18E+08	7.96E+06	7.59E+07
Slope	1.28E-07	4.95E-05	1.17E-07	3.07E-06	3.35E-07
Intercept	-6.97E-01	1.02E-01	-5.03E-01	7.04E-01	-6.23E-01
R^2	0.99886	0.99657	0.99976	0.99938	0.99941

II. Extractables from filter-plate-based metabolomics workflow
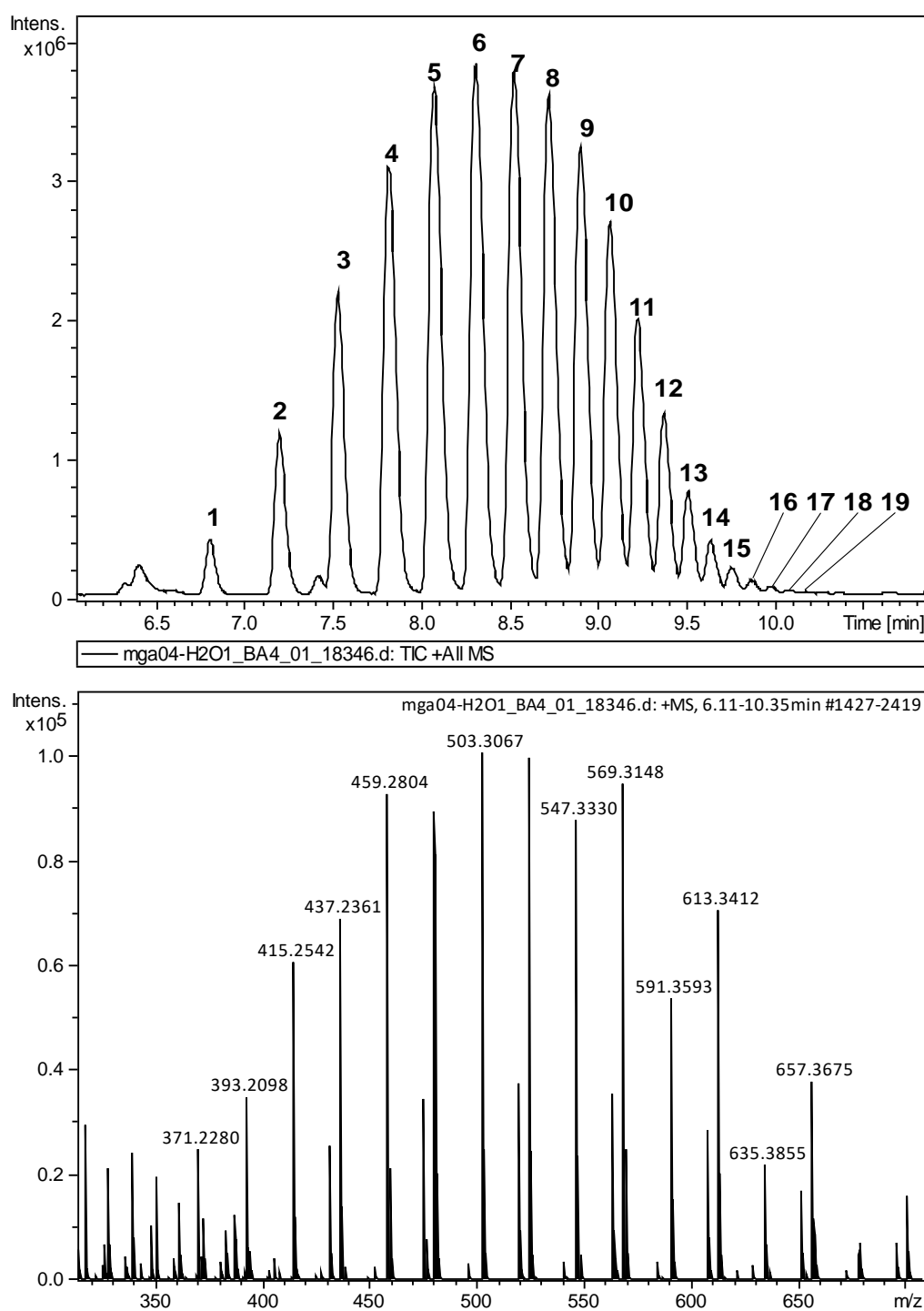
Figure A1. TIC of one untreated sample showing the 19 peaks coming from the filter plates (above), where the intrametabolome was extracted with 80% MeOH. Adjacent peaks from 1-9 have a difference in m/z values of 44.026 from the most abundant singly-charged ion, and from peaks 10-19 the m/z difference is 22.014, from the doubly-charged ions, shown in the average mass spectrum of the 19 peaks (below). Adjacent peaks with a difference in 44 Da show typical mass distribution of polyethylene glycol (PEG)

Table A2. Most abundant features found in the peaks coming from the filter plates. Intensity values are the average of all samples (n=48)

Peak	RT (min)	m/z	Adduct	Mean Log2 intensity	CV (%)
1	6.84	283.1753	[M+H]+	18.29	11%
1	6.84	300.2015	[M+NH4]+	16.38	12%
1	6.84	305.1572	[M+Na]+	19.31	10%
1	6.84	321.1300	[M+K]+	13.95	11%
2	7.22	327.2019	[M+H]+	19.98	10%
2	7.22	344.2281	[M+NH4]+	19.04	14%
2	7.22	349.1839	[M+Na]+	20.81	8%
2	7.22	365.1570	[M+K]+	15.97	8%
3	7.55	371.2278	[M+H]+	21.02	15%
3	7.55	388.2545	[M+NH4]+	20.24	13%
3	7.55	393.2097	[M+Na]+	21.71	10%
3	7.55	409.1829	[M+K]+	17.01	9%
4	7.83	415.2543	[M+H]+	21.75	13%
4	7.83	432.2808	[M+NH4]+	20.81	9%
4	7.83	437.2362	[M+Na]+	22.18	9%
4	7.83	453.2095	[M+K]+	17.41	8%
5	8.09	459.2808	[M+H]+	22.12	10%
5	8.09	476.3068	[M+NH4]+	21.03	6%
5	8.09	481.2628	[M+Na]+	22.36	8%
5	8.09	497.2361	[M+K]+	17.53	6%
6	8.32	503.3068	[M+H]+	22.18	10%
6	8.32	520.3360	[M+NH4]+	21.08	9%
6	8.32	525.2887	[M+Na]+	22.42	11%
6	8.32	541.2623	[M+K]+	17.64	6%
7	8.54	547.3332	[M+H]+	22.01	9%
7	8.54	564.3605	[M+NH4]+	20.99	10%
7	8.54	569.3151	[M+Na]+	22.33	10%
7	8.54	585.2882	[M+K]+	17.59	10%
8	8.73	591.3599	[M+H]+	21.36	11%
8	8.73	608.3856	[M+NH4]+	20.67	5%
8	8.73	613.3418	[M+Na]+	21.91	11%
8	8.73	629.3146	[M+K]+	17.32	6%
9	8.91	635.3857	[M+H]+	20.22	11%
9	8.91	652.4116	[M+NH4]+	19.97	11%
9	8.91	657.3676	[M+Na]+	21.10	12%
9	8.91	673.3414	[M+K]+	16.68	4%
10	9.08	340.2092	[M+2H]2+	20.59	11%
10	9.08	351.2002	[M+Na+H]2+	20.35	9%
10	9.08	362.1911	[M+2Na]2+	20.05	12%
10	9.08	370.1772	[M+Na+K]2+	15.76	12%
10	9.08	679.4122	[M+H]+	18.77	13%
10	9.08	696.4387	[M+NH4]+	18.89	5%
10	9.08	701.3942	[M+Na]+	20.04	12%
10	9.08	717.3682	[M+K]+	15.66	5%
11	9.24	362.2230	[M+2H]2+	20.15	13%
11	9.24	373.2139	[M+Na+H]2+	20.07	12%
11	9.24	384.2049	[M+2Na]2+	19.82	12%
11	9.24	392.1914	[M+Na+K]2+	15.64	4%
11	9.24	723.4372	[M+H]+	17.20	8%
11	9.24	740.4639	[M+NH4]+	17.58	12%
11	9.24	745.4193	[M+Na]+	18.71	12%
11	9.24	761.3929	[M+K]+	14.25	4%
12	9.38	384.2358	[M+2H]2+	19.45	5%
12	9.38	395.2266	[M+Na+H]2+	19.45	13%
12	9.38	406.2177	[M+2Na]2+	19.23	4%
12	9.38	414.2039	[M+Na+K]2+	15.10	8%
12	9.38	767.4635	[M+H]+	15.11	13%

12	9.38	784.4904	[M+NH4]+	15.76	5%
12	9.38	789.4457	[M+Na]+	17.01	5%
12	9.38	805.4185	[M+K]+	12.38	4%
13	9.52	406.2491	[M+2H]2+	18.56	9%
13	9.52	417.2399	[M+Na+H]2+	18.60	6%
13	9.52	428.2310	[M+2Na]2+	18.39	6%
13	9.52	436.2173	[M+Na+K]2+	14.22	5%
13	9.52	811.4900	[M+H]+	12.75	9%
13	9.52	828.5159	[M+NH4]+	13.49	7%
13	9.52	833.4720	[M+Na]+	14.74	8%
14	9.65	428.2618	[M+2H]2+	17.59	8%
14	9.65	439.2527	[M+Na+H]2+	17.61	12%
14	9.65	450.2436	[M+2Na]2+	17.41	9%
14	9.65	458.2307	[M+Na+K]2+	13.25	9%
14	9.65	877.4984	[M+Na]+	12.29	11%
15	9.76	450.2755	[M+2H]2+	16.57	11%
15	9.76	461.2662	[M+Na+H]2+	16.56	10%
15	9.76	472.2571	[M+2Na]2+	16.39	10%
15	9.76	480.2433	[M+Na+K]2+	12.17	13%
16	9.88	472.2888	[M+2H]2+	15.62	13%
16	9.88	483.2795	[M+Na+H]2+	15.55	13%
16	9.88	494.2702	[M+2Na]2+	15.40	13%
17	9.98	494.3010	[M+2H]2+	14.73	15%
17	9.98	505.2918	[M+Na+H]2+	14.60	14%
17	9.98	516.2827	[M+2Na]2+	14.50	15%
19	10.18	538.3279	[M+2H]2+	13.19	14%
19	10.18	560.3096	[M+2Na]2+	12.91	13%

III. Feature table - comparison between short and long exposure

Table A3. Feature table of identified metabolites in the metabolomics experiments under short exposure. Log2-fold-change values are calculated per antibiotic group against the untreated control group (n=3)

Feature name	RT (min)	m/z	Annotation	FC_SE_AZI	FC_SE_CIPRO	FC_SE_ERY	FC_SE_GENTA	FC_SE_LEVO	FC_SE_TOBRA
M79T2	1.56	79.0213	Glycin	-0.17	-0.01	-0.35	-0.06	-0.06	-0.38
M99T1_2	1.17	98.9841	D-Ribulose 1	-0.15	0.23	-0.01	-0.09	0.11	0.01
M101T2	1.56	101.0032	Inosine 5'-Diphosphate	0.23	-0.01	0.06	-0.11	0.01	-0.05
M104T1	1.18	104.0706	3-Amino-isobutanoate	-1.09	0.08	-0.54	-1.06	-0.03	-0.46
M114T6	6.12	114.0915	Agmatine sulfate	-0.27	-0.39	-0.19	-0.18	-0.38	-0.21
M132T2	2.01	132.1019	Leucine	-0.29	0.20	-0.08	-0.11	0.13	0.41
M136T6	6.12	136.0733	Adenine	-0.24	-0.31	-0.14	-0.17	-0.33	-0.20
M148T1_2	1.18	148.0604	N-Methyl-D-Aspartic acid	-1.96	-0.25	-0.87	-1.37	0.14	-0.25
M157T2_1	1.55	157.0351	Orotic acid	-0.38	-0.21	-0.57	-0.45	-0.44	-0.74
M166T3	3.49	166.0863	DL-normetanephrine	-0.61	0.58	-0.26	-0.42	0.02	-0.11
M182T2	2.02	182.0812	L-Tyrosine	-0.52	0.46	-0.09	-0.30	0.11	-0.05
M184T17	16.62	184.0757	Phosphocholine	-0.53	-0.97	-0.66	-1.01	-1.04	-1.00
M197T11	10.89	197.0710	1-Hydroxyphenazine	-1.20	-0.72	-1.15	-0.83	-0.92	-0.83
M211T6	6.40	211.0869	Pyocyanin	-1.58	-0.39	-1.46	-1.48	-1.39	-1.27
M224T11	10.55	224.0820	Phenazine-1-carboxamide	0.89	0.91	0.67	1.16	0.52	1.18
M225T11_1	11.38	225.0660	Phenazine-1-carboxylic acid	-1.00	-0.35	-1.52	-0.67	-2.08	-1.51
M233T11	11.35	233.1328	Melatonin	-0.18	0.21	-0.17	-0.23	-0.16	-0.13
M242T13	13.00	242.1543	C7:1-HQ	-0.81	-1.35	-0.84	-1.11	-1.41	-1.14
M244T13	13.06	244.1701	HHQ	-0.76	-1.09	-0.82	-1.01	-1.28	-0.99
M249T6	6.12	249.1575	Adenosine 3'	-0.29	-0.48	-0.18	-0.11	-0.45	-0.25
M255T18	18.43	255.2322	Palmitoleic acid	0.00	0.68	-0.30	-0.33	-0.77	-0.47
M256T14	13.95	256.1698	C8:1-HQ	-0.78	-1.27	-0.82	-1.07	-1.11	-0.97
M257T20	19.59	257.2479	Palmitate	0.31	0.94	0.08	0.11	-0.21	0.00
M258T14	13.98	258.1853	C8-HQ	-0.83	-1.17	-0.71	-0.93	-0.82	-0.71
M259T1_3	1.25	259.0925	5-Oxo-L-Proline	-2.64	-0.66	-1.40	-1.54	0.17	-0.46
M260T13_1	13.16	260.1650	PQS	-0.17	0.36	0.03	-0.13	0.01	0.01
M267T15	15.41	267.1721	SN-glycerol 3-phosphate	-0.01	0.16	-0.11	-0.17	-0.13	-0.02
M268T14	14.37	268.1699	C9:2-HQ	-0.49	-1.35	-0.62	-0.85	-1.02	-0.92
M270T15_1	14.52	270.1858	C9:1-HQ (I)	-0.57	2.78	-0.73	0.31	2.89	3.04
M272T14	13.55	272.1646	C8:1-QNO	-0.46	0.36	-0.27	-0.47	-0.08	-0.25
M274T14	14.03	274.1806	C8-QNO	-0.25	0.49	-0.01	-0.19	0.12	0.02
M277T1	1.25	277.1031	L-Glutamine	-2.63	-0.63	-1.36	-1.59	0.18	-0.47
M282T19_1	18.60	282.1368	Protoporphyrin	-0.50	0.14	-0.23	-0.43	0.18	-0.17
M282T19_3	19.23	282.2797	Petroselinic acid	0.69	0.73	0.56	0.69	0.85	0.97
M283T20	19.76	283.2636	Elaidic acid	-0.23	1.19	-0.51	-0.52	-0.23	-0.58
M284T15	14.80	284.2011	C10:1-HQ (I)	-0.79	-1.15	-1.01	-0.99	-1.08	-0.94
M284T20_2	20.46	284.2950	*C9:2-QNO [M+NH4]+	0.15	0.28	0.31	0.05	0.35	0.27
M286T14_1	14.19	286.1808	C9:1-QNO (I)	-0.52	-0.14	-0.30	-0.56	-0.40	-0.43
M288T21	20.85	288.1965	C9-PQS	-0.69	-0.23	-0.66	-0.81	-0.70	-0.71
M289T15_5	15.41	289.1541	C9-QNO	-0.03	0.18	-0.06	-0.16	-0.07	-0.06
M296T16_2	15.70	296.2014	C11:2-HQ (I)	0.02	-0.24	-0.21	-0.34	-0.35	-0.29
M298T17_1	16.62	298.2172	C11:1-HQ (I)	-0.47	-1.11	-0.56	-0.92	-0.92	-0.75
M298T16_1	15.52	298.2172	C11:1-HQ (II)	-0.59	-1.32	-0.67	-1.00	-1.06	-0.97
M300T17_2	16.65	300.2328	C11-HQ	-0.47	-0.90	-0.52	-0.73	-0.81	-0.67
M302T17_2	16.92	302.2117	Estradiol-17alpha	-0.02	-1.96	0.31	-0.10	-1.18	-0.17
M304T13	13.01	304.1911	C9:1-QNO (II)	-0.19	0.30	0.06	-0.14	-0.13	-0.02
M313T17	16.68	313.2740	*LPG (16:0) (fragment)	-0.34	2.39	-0.67	-0.70	1.01	-0.32
M329T21	20.85	329.2429	Docosahexaenoic acid	0.46	1.01	0.24	0.24	0.31	0.44
M338T22	21.89	338.3424	Erucic acid	1.63	0.98	1.79	1.29	2.00	3.40

M339T17_2	17.04	339.2896	*LPE (18:1) (fragment)	-0.24	0.65	0.06	-0.34	0.19	-0.06
M348T2	1.56	348.0704	Adenosine 5'-monophosphate	-1.00	0.04	-0.53	-0.67	0.35	-0.12
M359T16	15.87	359.2795	*Rha-C10-C10 (fragment)	0.81	-0.26	0.79	0.90	0.26	0.78
M359T17_3	16.66	359.2798	*Rha-C10-C10 (fragment)	1.62	0.06	1.56	1.62	1.05	1.56
M370T19_1	18.53	370.2747	C15:1-QNO	-0.40	0.25	-0.28	-0.27	-0.38	-0.28
M387T17	17.23	387.3108	*Rha-C10-C12 (fragment)	0.72	-0.11	0.62	0.71	0.49	1.05
M387T18	18.04	387.3111	*Rha-C10-C12 (fragment)	0.45	0.08	0.43	0.41	0.45	0.63
M397T20	20.42	397.3295	Vitamin D2	-0.17	0.08	-0.15	-0.16	-0.18	-0.09
M415T19_1	18.52	415.3421	*Rha-Rha-C12-C12 (fragment)	-0.44	-0.54	-0.33	-0.40	-0.22	-0.09
M429T18	17.67	429.3189	Cholesteryl acetate	-0.05	0.25	-0.06	-0.17	-0.25	-0.11
M436T17	16.70	436.2826	*LPE (16:0) [M-H2O+H]+	-0.60	2.97	-0.64	-0.80	1.49	-0.70
M452T15_2	15.32	452.2778	LPE (16:1)	-0.70	0.34	-0.27	-0.71	-0.05	-0.41
M454T17	16.68	454.2938	LPE (16:0)	-0.48	2.67	-0.44	-0.65	1.28	-0.49
M466T16	16.32	466.2930	LPE (17:1)	-0.76	1.54	-0.57	-0.79	0.35	-0.52
M474T15	15.32	474.2594	*LPE (16:1) [M+Na]+	-0.51	0.37	-0.20	-0.58	0.01	-0.32
M476T17	16.69	476.2754	*LPE (16:0) [M+Na]+	-0.59	2.17	-0.69	-0.96	0.94	-0.68
M480T17	17.05	480.3094	LPE (18:1)	-0.25	0.52	-0.04	-0.35	0.10	-0.08
M485T18_2	17.65	485.2877	LPG (16:0)	-0.72	0.20	-0.44	-0.74	-0.21	-0.28
M502T17	17.05	502.2912	*LPE (18:1) [M+Na]+	-0.04	0.40	0.00	-0.30	0.08	0.02
M505T17	16.64	505.3374	*Rha-C10-C10 [M+H]	1.76	-0.03	1.68	1.74	1.13	1.71
M511T18	18.12	511.3032	LPG (18:1)	-0.66	-0.37	-0.23	-0.56	-0.20	-0.16
M527T17	16.95	527.3260	Rha-C10-C10+Na	0.87	-1.39	-4.08	0.69	-2.21	0.81
M533T18_1	18.12	533.2853	*LPG (18:1) [M+Na]+	-0.18	-0.29	-0.20	-0.34	-0.04	0.00
M553T18_2	17.73	553.3395	Rha-C10-C12:1+Na	1.53	0.45	1.42	-0.59	-0.71	0.69
M559T15	14.90	559.3904	C9:1-HQ (I) [2M+H]+	-0.69	-1.03	-0.56	-0.95	-0.79	-0.87
M575T17	17.44	575.3170	*Rha-C10-C12:1 [M+Na]+	1.24	-0.05	0.83	0.91	0.73	1.12
M575T15	14.91	575.3854	*C9-QNO [2M+H]+	-0.33	0.67	0.07	-0.21	0.32	0.06
M651T16	15.87	651.3954	Rha-Rha-C10-C10	0.90	-0.34	0.80	0.94	0.29	0.81
M673T16_1	15.87	673.3777	Rha-Rha-C10-C10+Na	0.90	-0.29	0.78	0.91	0.28	0.79
M679T17_1	17.23	679.4270	Rha-Rha-C10-C12	0.81	-0.05	0.65	0.82	0.61	1.11
M699T17_2	16.64	699.3933	Rha-Rha-C10-C12:1+Na	0.91	-0.46	0.74	0.87	0.45	1.17
M701T17_3	17.23	701.4094	Rha-Rha-C10-C12+Na	0.75	-0.10	0.60	0.68	0.51	0.96
M707T19	18.52	707.4581	Rha-Rha-C12-C12	-0.49	-0.60	-0.34	-0.38	-0.24	-0.09
M727T18	17.92	727.4245	Rha-Rha-C12-C12:1+Na	0.10	-0.53	0.06	0.17	0.35	0.50
M729T19	18.52	729.4406	Rha-Rha-C12-C12+Na	-0.36	-0.54	-0.31	-0.33	-0.24	-0.08
M1032T17	16.66	1031.6504	*Rha-C10-C10+Na [2M+H]	3.31	-0.09	3.17	3.44	2.23	3.13

Table A4. Feature table of identified metabolites in the metabolomics experiments under long exposure. Log2-fold-change values are calculated per antibiotic group against the untreated control group (n=3)

Feature name	RT (min)	m/z	Annotation	FC_SE_AZI	FC_SE_CIPRO	FC_SE_ERY	FC_SE_GENTA	FC_SE_LEVO	FC_SE_TOBRA
M79T2	1.56	79.0213	Glycin	0.31	0.26	0.18	-0.14	-0.12	-0.10
M99T1_2	1.17	98.9841	D-Ribulose 1	-0.35	1.56	-0.22	-0.12	0.02	-0.17
M101T2	1.56	101.0032	Inosine 5'-Diphosphate	0.01	1.37	0.00	0.38	0.66	0.10
M104T1	1.18	104.0706	3-Amino-isobutanoate	-0.30	-0.14	-0.39	-0.47	-0.07	-0.42
M114T6	6.12	114.0915	Agmatine sulfate	0.49	0.33	0.29	-0.10	-0.11	-0.21
M132T2	2.01	132.1019	Leucine	0.07	0.86	0.05	0.11	0.06	0.07
M136T6	6.12	136.0733	Adenine	0.37	0.48	0.23	-0.05	-0.05	-0.16
M148T1_2	1.18	148.0604	N-Methyl-D-Aspartic acid	-0.70	0.61	-0.51	-0.39	0.19	-0.62
M157T2_1	1.55	157.0351	Orotic acid	0.18	0.00	-0.01	-0.18	-0.36	-0.77
M166T3	3.49	166.0863	DL-normetanephrine	-0.13	0.88	-0.05	-0.27	0.33	-0.35

M182T2	2.02	182.0812	L-Tyrosine	-0.01	0.66	0.01	-0.18	0.18	-0.29
M184T17	16.62	184.0757	Phosphocholine	0.18	-6.54	0.00	-0.51	-0.47	-0.55
M197T11	10.89	197.0710	1-Hydroxyphenazine	-0.18	-7.16	-0.97	-1.56	-1.34	-1.11
M211T6	6.40	211.0869	Pyocyanin	0.00	-2.75	-0.85	-1.16	-0.79	-0.78
M224T11	10.55	224.0820	Phenazine-1-carboxamide	-0.78	-4.22	-0.34	-0.56	-0.35	-0.06
M225T11_1	11.38	225.0660	Phenazine-1-carboxylic acid	-1.96	-7.19	-1.46	-3.62	-2.87	-2.25
M233T11	11.35	233.1328	Melatonin	-0.28	1.59	-0.16	-0.02	0.29	-0.18
M242T13	13.00	242.1543	C7:1-HQ	0.02	-1.84	-0.29	-0.86	-0.41	-0.64
M244T13	13.06	244.1701	HHQ	-0.01	-1.18	-0.31	-0.75	-0.29	-0.60
M249T6	6.12	249.1575	Adenosine 3'	0.66	-0.09	0.38	-0.10	-0.22	-0.21
M255T18	18.43	255.2322	Palmitoleic acid	0.34	0.69	0.29	0.41	-0.15	0.20
M256T14	13.95	256.1698	C8:1-HQ	-0.24	0.54	-0.33	-0.81	0.71	-0.63
M257T20	19.59	257.2479	Palmitate	0.26	1.68	0.24	0.64	0.66	0.37
M258T14	13.98	258.1853	C8-HQ	-0.24	0.55	-0.26	-0.71	0.60	-0.64
M259T1_3	1.25	259.0925	5-Oxo-L-Proline	-0.90	-0.06	-0.49	-0.37	0.33	-0.96
M260T13_1	13.16	260.1650	PQS	-0.25	-0.36	0.00	0.18	0.24	0.26
M267T15	15.41	267.1721	SN-glycerol 3-phosphate	-0.22	1.62	-0.06	0.08	0.29	0.00
M268T14	14.37	268.1699	C9:2-HQ	0.10	-1.92	-0.13	-0.75	-0.46	-0.53
M270T15_1	14.52	270.1858	C9:1-HQ (I)	-0.02	3.32	-0.13	-0.78	0.08	2.07
M272T14	13.55	272.1646	C8:1-QNO	-0.39	1.05	-0.03	-0.18	1.00	0.01
M274T14	14.03	274.1806	C8-QNO	-0.35	1.32	0.01	0.19	1.03	0.33
M277T1	1.25	277.1031	L-Glutamine	-0.93	-0.08	-0.50	-0.38	0.33	-0.97
M282T19_1	18.60	282.1368	Protoporphyrin	-0.03	-0.45	-0.33	-0.25	-0.40	-0.25
M282T19_3	19.23	282.2797	Petroselinic acid	0.01	2.01	1.32	-0.02	0.62	0.69
M283T20	19.76	283.2636	Elaidic acid	0.32	1.65	0.35	0.38	1.37	0.07
M284T15	14.80	284.2011	C10:1-HQ (I)	-0.57	0.40	-0.41	-0.69	0.65	-0.56
M284T20_2	20.46	284.2950	*C9:2-QNO [M+NH4]+	-0.10	1.78	0.34	0.11	0.57	0.36
M286T14_1	14.19	286.1808	C9:1-QNO (I)	-0.36	-0.55	0.03	-0.17	0.14	-0.13
M288T21	20.85	288.1965	C9-PQS	-0.58	0.89	-0.49	-0.35	-0.30	-0.47
M289T15_5	15.41	289.1541	C9-QNO	-0.21	1.66	-0.10	0.13	0.30	-0.02
M296T16_2	15.70	296.2014	C11:2-HQ (I)	0.44	0.10	0.17	-0.14	0.80	-0.13
M298T17_1	16.62	298.2172	C11:1-HQ (I)	0.15	-1.46	-0.01	-0.48	-0.26	-0.44
M298T16_1	15.52	298.2172	C11:1-HQ (II)	-0.11	-0.47	-0.11	-0.67	-0.06	-0.65
M300T17_2	16.65	300.2328	C11-HQ	-0.10	-1.48	-0.11	-0.41	-0.39	-0.35
M302T17_2	16.92	302.2117	Estradiol-17alpha	0.56	-2.85	0.52	0.32	-0.38	0.34
M304T13	13.01	304.1911	C9:1-QNO (II)	-0.40	-1.53	-0.13	-0.09	-0.14	-0.01
M313T17	16.68	313.2740	*LPG (16:0) (fragment)	-0.31	2.98	-0.14	-0.43	3.04	-0.36
M329T21	20.85	329.2429	Docosahexaenoic acid	0.37	1.97	0.40	1.12	1.08	0.56
M338T22	21.89	338.3424	Erucic acid	1.65	3.68	1.08	-0.15	2.98	1.47
M339T17_2	17.04	339.2896	*LPE (18:1) (fragment)	-0.37	1.31	-0.07	0.03	1.22	-0.07
M348T2	1.56	348.0704	Adenosine 5'-monophosphate	-0.39	0.49	-0.42	-0.36	0.25	-0.39
M359T16	15.87	359.2795	*Rha-C10-C10 (fragment)	-0.42	-4.14	0.01	0.03	0.16	0.13
M359T17_3	16.66	359.2798	*Rha-C10-C10 (fragment)	-0.19	-0.48	0.23	0.13	0.44	0.26
M370T19_1	18.53	370.2747	C15:1-QNO	-0.31	-0.66	0.07	0.06	0.23	0.17
M387T17	17.23	387.3108	*Rha-C10-C12 (fragment)	-0.41	-0.65	0.11	0.12	0.70	0.22
M387T18	18.04	387.3111	*Rha-C10-C12 (fragment)	-0.32	-0.45	0.15	-0.12	0.77	-0.02
M397T20	20.42	397.3295	Vitamin D2	-0.14	1.14	-0.13	0.00	0.17	-0.09
M415T19_1	18.52	415.3421	*Rha-Rha-C12-C12 (fragment)	-0.56	-2.80	0.17	-0.01	0.20	-0.07
M429T18	17.67	429.3189	Cholesteryl acetate	-0.12	1.56	-0.08	0.03	0.20	-0.09
M436T17	16.70	436.2826	*LPE (16:0) [M-H2O+H]+	-0.70	3.53	-0.29	-0.24	3.64	-0.19
M452T15_2	15.32	452.2778	LPE (16:1)	-0.37	0.24	-0.33	-0.57	-0.22	-0.60
M454T17	16.68	454.2938	LPE (16:0)	-0.50	3.27	-0.28	-0.18	3.29	-0.16
M466T16	16.32	466.2930	LPE (17:1)	-0.50	1.34	-0.25	-0.57	1.97	-0.63
M474T15	15.32	474.2594	*LPE (16:1) [M+Na]+	-0.35	0.52	-0.24	-0.44	0.56	-0.46
M476T17	16.69	476.2754	*LPE (16:0) [M+Na]+	-0.49	3.29	-0.24	-0.15	2.60	-0.13
M480T17	17.05	480.3094	LPE (18:1)	-0.42	1.31	-0.14	-0.03	1.06	-0.10
M485T18_2	17.65	485.2877	LPG (16:0)	0.00	0.23	-0.16	-0.35	0.13	-0.31
M502T17	17.05	502.2912	*LPE (18:1) [M+Na]+	-0.41	1.47	-0.04	0.03	0.91	-0.05
M505T17	16.64	505.3374	*Rha-C10-C10 [M+H]	-0.21	-1.97	0.29	0.13	0.40	0.28
M511T18	18.12	511.3032	LPG (18:1)	-0.22	-1.18	-0.31	-0.28	-0.42	-0.44

M527T17	16.95	527.3260	Rha-C10-C10+Na	-4.11	1.31	-1.88	-3.95	-1.86	-0.11
M533T18_1	18.12	533.2853	*LPG (18:1) [M+Na]+	-0.05	-0.04	-0.01	-0.05	-0.18	-0.20
M553T18_2	17.73	553.3395	Rha-C10-C12:1+Na	-0.35	-1.66	-0.96	-1.29	-0.17	0.10
M559T15	14.90	559.3904	C9:1-HQ (I) [2M+H]+	-0.26	-1.65	0.02	-0.41	-0.09	-0.30
M575T17	17.44	575.3170	*Rha-C10-C12:1 [M+Na]+	-0.20	-0.30	0.37	0.06	0.82	0.24
M575T15	14.91	575.3854	*C9-QNO [2M+H]+	-0.55	-0.56	0.20	0.47	0.27	0.47
M651T16	15.87	651.3954	Rha-Rha-C10-C10	-0.46	-5.55	0.02	0.03	0.15	0.17
M673T16_1	15.87	673.3777	Rha-Rha-C10-C10+Na	-0.49	-1.50	0.06	0.01	0.13	0.10
M679T17_1	17.23	679.4270	Rha-Rha-C10-C12	-0.40	-0.86	0.12	0.17	0.76	0.30
M699T17_2	16.64	699.3933	Rha-Rha-C10-C12:1+Na	-0.46	-0.93	0.14	0.27	0.14	0.31
M701T17_3	17.23	701.4094	Rha-Rha-C10-C12+Na	-0.40	-0.62	0.15	0.16	0.68	0.24
M707T19	18.52	707.4581	Rha-Rha-C12-C12	-0.58	-7.25	0.12	0.00	0.22	-0.07
M727T18	17.92	727.4245	Rha-Rha-C12-C12:1+Na	-0.48	-2.32	0.29	0.02	0.38	0.30
M729T19	18.52	729.4406	Rha-Rha-C12-C12+Na	-0.57	-1.80	0.19	0.05	0.21	-0.14
M1032T17	16.66	1031.6504	*Rha-C10-C10+Na [2M+H]	-0.18	-5.98	0.60	0.16	0.47	0.54

Table A5. Features responsive to the treatment with fluoroquinolone (Region 1,2 and 3). Log2-fold-change values are calculated per antibiotic group against the untreated control group (n=3)

Feature name	RT (min)	m/z	Annotation	FC_SE_CIPRO	FC_SE_LEVOO	FC_LE_CIPRO	FC_LE_LEVOO
M112T1_2	1.25	112.0504		0.78	0.48	1.39	0.49
M173T1_2	1.20	173.0922		5.11	0.00	6.61	0.83
M181T1	1.12	180.9038		0.32	0.41	1.19	0.05
M191T1	1.20	191.1026		5.47	0.00	6.47	1.09
M196T1	1.20	196.0949		4.07	0.74	5.42	2.34
M197T1_1	1.21	196.5966		5.98	0.00	7.01	1.42
M204T1	1.23	204.0868		4.92	0.00	3.73	0.63
M219T1_2	1.13	219.0267		2.32	-1.24	5.45	2.11
M232T1	1.26	231.6135		5.94	0.00	8.38	3.10
M237T13	13.44	237.1466		4.31	1.06	2.77	1.29
M243T1_1	1.27	242.5620		4.54	1.08	7.32	6.34
M244T1	1.22	244.0790		5.99	0.00	2.36	2.03
M246T15_1	15.32	245.6159		0.37	-0.02	0.47	0.49
M247T17_1	16.69	246.6239		2.13	0.90	3.17	2.49
M252T17	17.05	251.6430		0.62	0.30	1.41	1.21
M255T15	15.32	254.6213		0.52	-0.08	0.14	0.58
M256T17_1	16.70	255.6292		2.21	0.95	3.48	2.61
M256T17_2	16.71	256.1309		6.02	4.20	7.12	6.15
M259T5	5.25	259.0709		7.31	1.08	7.99	4.99
M259T17	16.71	259.1489		3.18	1.72	4.37	3.57
M260T17_1	17.05	259.6318		0.44	0.05	1.47	0.88
M267T17	16.71	267.1373		6.24	3.37	7.26	6.73
M268T5	5.26	268.0762		6.27	0.00	6.92	2.94
M268T3	2.73	268.0762		7.94	0.00	9.70	2.47
M269T17	17.05	268.6370		0.68	0.24	1.80	1.12
M272T14	13.55	272.1646	C8:1-QNO	0.36	-0.08	1.05	1.00
M274T14	14.03	274.1806	C8-QNO	0.49	0.12	1.32	1.03
M276T4	3.87	276.1079		3.11	-0.02	2.11	1.22
M279T1_1	1.27	278.7998		7.64	0.00	9.90	4.75
M279T1_2	1.27	279.1341		3.99	0.57	6.43	-0.42
M282T17_2	16.70	282.2796		5.97	3.85	6.27	6.73
M298T4	3.87	298.0899		4.43	0.06	2.16	1.88
M300T15	14.72	300.1963		0.56	0.01	1.58	1.27
M302T1	1.27	302.4789		8.85	0.00	11.27	6.87

M302T2	2.32	302.4790		9.79	0.00	11.97	8.02
M303T1_1	1.27	302.8131		7.66	0.00	10.09	5.20
M303T2_1	2.33	302.8133		8.52	0.00	10.78	6.30
M303T1_2	1.27	303.1473		5.10	0.00	8.17	0.00
M303T2_2	2.32	303.1474		6.15	0.00	8.84	1.04
M305T19	19.43	305.2547		1.34	-0.14	1.76	1.58
M313T17	16.68	313.2740	*LPG (16:0) (fragment)	2.39	1.01	2.98	3.04
M314T16_3	16.32	314.2774		4.21	2.65	4.54	4.85
M320T1	1.21	320.1453		7.11	0.00	8.38	4.56
M324T1	1.25	324.0591		0.41	0.32	1.27	0.53
M326T16	15.91	326.2118		0.79	0.01	1.58	1.67
M328T16	16.34	328.2277		0.45	-0.13	1.40	1.27
M339T17_2	17.04	339.2896	*LPE (18:1) (fragment)	0.65	0.19	1.31	1.22
M382T1	1.26	382.1769		4.40	0.00	7.11	0.00
M391T1	1.19	391.1822		4.30	0.98	5.55	2.46
M392T1	1.19	392.1851		5.44	0.00	6.63	1.40
M413T1_2	1.18	413.1642		7.13	2.17	8.48	5.37
M418T1_1	1.27	417.6958		6.44	0.00	8.84	1.59
M418T1_2	1.26	418.1974		3.75	0.00	7.26	0.00
M426T15	14.89	426.2618		4.59	3.30	4.80	4.85
M435T1_2	1.18	435.1461		3.69	0.00	5.74	0.82
M436T17	16.70	436.2826	*LPE (16:0) [M-H2O+H]+	2.97	1.49	3.53	3.64
M437T17	16.70	437.2863		5.80	3.99	6.11	6.40
M447T15	15.32	447.1821		0.46	-0.06	-0.60	0.57
M449T17	16.71	449.1978		3.41	2.08	4.50	3.82
M453T1	1.27	453.2141		7.12	0.00	9.51	3.36
M453T2	2.32	453.2145		7.62	0.00	9.86	2.13
M454T1	1.27	453.7154		4.93	0.00	8.19	0.77
M454T2	2.31	453.7157		5.04	0.00	8.30	0.72
M454T17	16.68	454.2938	LPE (16:0)	2.67	1.28	3.27	3.29
M457T17	16.70	457.3017		6.39	4.59	6.82	7.09
M462T17	17.05	462.2981		0.72	0.27	1.39	1.34
M465T17	16.70	465.2779		4.87	1.48	5.62	5.36
M466T17	16.71	465.7795		5.98	1.80	6.10	6.52
M466T16	16.32	466.2930	LPE (17:1)	1.54	0.35	1.34	1.97
M467T16	16.32	467.2965		4.32	1.72	0.45	4.77
M470T15	14.85	470.2883		5.28	2.76	0.00	5.75
M473T17	16.70	473.2668		3.76	1.84	4.60	4.31
M474T17_1	16.71	473.7687		4.96	2.83	5.76	5.47
M474T15	15.32	474.2594	*LPE (16:1) [M+Na]+	0.37	0.01	0.52	0.56
M474T17_2	16.71	474.2698		6.84	3.76	7.57	7.40
M475T17	17.05	475.2133		0.66	0.29	1.50	1.10
M476T17	16.69	476.2754	*LPE (16:0) [M+Na]+	2.17	0.94	3.29	2.60
M478T17_1	16.71	478.2824		4.30	2.76	5.40	4.61
M478T17_2	16.56	478.2927		3.31	0.00	5.59	6.43
M479T5	5.25	479.1871		4.04	1.21	5.00	2.80
M480T5	5.26	480.1905		6.48	0.00	6.64	2.42
M480T17	17.05	480.3094	LPE (18:1)	0.52	0.10	1.31	1.06
M482T19	19.19	482.3242		0.82	0.08	1.79	1.19
M486T17	16.70	486.2746		3.35	1.83	4.51	3.74
M488T6	5.62	488.1925		8.44	0.00	10.45	6.10
M488T16	16.33	488.2744		3.75	0.30	-0.93	3.86
M489T6_1	5.62	488.6941		7.23	0.00	9.23	2.10
M489T6_2	5.62	489.1953		4.66	0.00	7.16	0.00
M491T17_2	17.05	491.2934		4.22	3.12	0.43	4.95
M492T17	16.71	492.2427		5.35	3.63	6.99	5.66
M494T18	18.44	494.3244		1.45	0.37	2.24	2.17
M496T15_2	15.32	496.2410		0.30	-0.06	0.60	0.46
M497T3	2.71	497.1977		9.37	0.00	11.49	6.94
M498T3	2.73	498.2008		6.49	0.00	9.10	1.26

M498T17	16.70	498.2570		1.45	0.42	3.12	1.58
M499T17_1	16.68	498.7890		1.32	1.30	1.10	1.61
M499T6	5.62	499.1825		6.49	0.00	8.60	1.65
M499T17_3	16.87	499.2868		0.68	0.21	1.21	1.44
M500T6	5.62	499.6838		4.45	0.00	7.30	0.00
M500T17_1	17.05	499.7842		0.83	0.33	1.28	1.54
M501T5	5.26	501.1688		6.76	0.00	7.49	3.51
M502T17	17.05	502.2912	*LPE (18:1) [M+Na]+	0.40	0.08	1.47	0.91
M507T6	5.62	507.1660		7.36	0.00	9.28	3.14
M507T18	17.63	507.2700		0.12	-0.45	0.69	0.30
M508T6	5.62	507.6678		5.72	0.00	7.96	1.04
M510T6	5.62	510.1740		2.94	0.00	7.17	0.00
M516T18	18.44	516.3062		3.56	1.73	4.25	4.63
M518T6	5.62	518.1568		4.08	0.00	6.94	0.00
M518T17	17.05	518.2579		0.48	0.16	1.35	1.18
M519T3	2.72	519.1794		7.81	0.00	10.02	2.30
M532T25	25.24	532.4710		4.97	0.53	6.83	0.00
M537T24	24.13	537.3955		7.60	3.64	9.19	4.02
M538T24	24.13	538.3984		5.50	0.58	7.33	0.70
M583T14	14.48	583.2722		0.82	0.25	2.34	0.58
M585T17	16.66	584.8258		3.42	1.17	-0.51	4.54
M645T6	6.08	644.5846		2.59	0.00	5.14	0.00
M646T15	15.45	646.3568		3.91	2.25	3.11	4.29
M692T17	16.71	692.4216		3.91	0.00	0.92	5.19
M700T17_1	16.71	699.9098		7.95	4.54	8.39	8.67
M701T17_1	16.71	700.9129		6.16	1.21	6.01	6.88
M719T17	16.72	718.8826		5.13	0.00	4.62	5.74
M725T17	16.69	725.4322		6.06	5.18	3.95	6.61
M726T17_1	16.69	725.9336		6.48	5.54	3.31	7.03
M726T17_2	16.69	726.4345		4.90	3.68	0.00	5.45
M727T6	5.91	727.2829		6.76	0.00	8.54	2.33
M728T6	5.91	727.7843		6.04	0.00	7.85	1.02
M738T6	5.92	738.2732		4.01	0.00	6.29	0.00
M739T17_1	17.05	738.9333		2.25	1.44	-0.37	3.41
M739T17_2	17.05	739.4350		4.07	2.91	0.91	5.72
M746T6	5.92	746.2564		2.78	0.00	5.36	0.00
M831T17	16.72	831.0248		5.69	1.52	3.54	6.38
M832T17	16.72	831.5261		5.50	1.39	2.39	6.48
M908T17	16.70	907.5801		5.98	3.16	5.77	7.07
M909T17	16.70	908.5833		7.50	4.81	7.34	8.66
M910T17	16.70	909.5858		7.36	2.92	7.08	8.45
M911T17	16.71	910.5875		3.99	0.00	0.00	5.54
M919T17_1	16.71	918.5681		4.34	-0.57	-0.57	5.55
M919T17_3	16.71	919.0694		4.87	0.00	0.93	6.24
M927T17_1	16.71	926.5527		6.25	0.00	5.42	7.30
M927T17_2	16.71	927.0544		6.21	0.53	5.48	7.26
M928T17	16.71	927.5561		4.79	0.00	0.98	6.25
M930T17_1	16.71	929.5610		6.44	4.18	7.28	7.00
M930T17_2	16.71	930.0619		4.26	0.00	1.00	5.86
M931T17	16.71	930.5646		7.06	4.33	7.93	7.65
M932T17	16.71	931.5685		4.66	0.00	3.21	5.44
M934T17	16.70	933.5952		5.64	3.47	5.59	6.51
M935T17	16.70	934.5981		4.86	0.99	0.00	6.23
M946T17	16.72	945.5269		5.29	0.82	6.38	6.06
M952T17_1	16.72	951.5431		6.25	2.06	7.70	6.70
M952T17_2	16.69	952.0744		5.21	1.31	0.00	6.07
M953T17_1	16.69	952.5758		5.49	1.93	0.00	6.15
M953T17_2	16.69	953.0776		3.05	0.56	0.00	4.40
M959T17	16.67	958.6239		2.61	2.53	1.08	3.42
M960T17_1	17.05	959.6108		0.91	0.40	1.06	2.00

M962T17	17.05	961.6164		2.13	0.81	0.00	3.51
M981T17	16.67	980.6053		1.92	2.01	0.72	2.29
M982T17_1	17.05	981.5923		0.88	0.36	1.22	1.79
M982T17_2	16.68	981.6088		4.20	4.33	0.77	4.59
M1131T17	16.67	1130.6972		3.59	2.54	0.00	5.58
M1145T17	16.71	1145.2136		4.43	0.00	0.00	6.27
M1146T17_1	16.71	1145.7141		4.96	0.00	0.00	6.67
M1146T17_2	16.71	1146.2150		3.93	0.00	0.00	5.99
M1153T17	16.71	1153.1949		2.56	0.00	0.00	5.43
M1154T17_1	16.71	1153.6979		3.50	0.00	0.00	6.00
M1156T17	16.71	1156.2036		3.12	0.00	0.00	5.34
M1157T17	16.71	1156.7060		4.26	0.00	0.00	5.82
M1170T17	16.71	1169.8101		5.13	3.64	3.20	6.12
M1171T17_1	16.71	1170.8131		6.40	4.21	4.36	7.42
M1171T17_2	16.69	1171.2358		3.52	0.00	0.00	5.17
M1361T17	16.70	1360.8666		5.05	0.00	0.00	6.78
M1362T17	16.70	1361.8685		4.60	0.00	0.00	6.22

Table A6. Features responsive to the treatment at short-exposure (Region 4). Log2-fold-change values are calculated per antibiotic group against the untreated control group (n=3)

Feature name	RT (min)	m/z	Annotation
M111T16_1	15.87	111.0441	
M135T17	16.67	135.1169	
M137T17	17.44	137.1325	
M153T17	16.66	153.1275	
M161T17	17.44	161.1326	
M171T17	16.66	171.1381	
M179T17	17.44	179.1431	
M189T18	18.04	189.1487	
M189T17	16.66	189.1487	
M197T17	17.44	197.1537	
M199T18	18.04	199.1694	
M217T17	17.23	217.1800	
M241T12	12.26	240.6361	
M272T17	16.66	272.1462	
M281T17	16.66	281.1513	
M285T17_1	16.65	284.6706	
M285T17_2	17.44	285.1539	
M286T18	18.04	286.1619	
M293T17_1	16.66	292.6593	
M293T17_2	17.23	293.1234	
M294T17	17.44	294.1592	
M295T18_1	18.04	295.1670	
M302T17_1	16.65	301.6647	
M306T17_1	17.44	305.6671	
M307T18_1	18.04	306.6751	
M315T17	17.45	314.6723	
M338T16_1	15.87	337.6877	
M341T17_3	16.64	341.2687	
M345T16	15.87	345.1750	
M346T16_2	15.87	346.1780	
M351T17	17.23	351.2021	
M358T17	16.64	358.1830	
M359T17_1	16.62	358.6845	
M359T17_2	17.23	359.1908	
M359T17_3	16.66	359.2798	*Rha-C10-C10 (fragment)
M360T17_1	17.23	359.6925	

M367T17	16.62	367.1880	
M368T17	17.23	368.1959	
M369T18_2	18.04	369.3002	
M384T20_1	19.74	384.2262	
M387T17	17.23	387.3108	*Rha-C10-C12 (fragment)
M387T18	18.04	387.3111	*Rha-C10-C12 (fragment)
M469T16	15.87	469.3159	
M503T8_1	7.65	502.7621	
M503T8_2	7.66	503.0129	
M505T17	16.64	505.3374	*Rha-C10-C10 [M+H]
M516T17	16.64	516.3222	
M517T17	16.64	516.8238	
M522T17	16.64	522.3639	
M524T17_2	16.66	524.3111	
M525T17_1	16.65	524.8128	
M525T17_3	16.64	525.3140	
M527T1_1	1.27	526.6407	
M527T3	2.64	526.6411	
M528T17	16.66	528.3234	
M531T17	17.44	531.3530	
M533T18_2	18.04	533.3688	
M543T17	16.66	543.2874	
M548T17	17.44	548.3793	
M549T17	16.65	549.3014	
M551T17_2	17.44	551.3295	
M553T18_2	17.73	553.3395	Rha-C10-C12:1+Na
M554T17	17.45	554.3401	
M557T18	18.04	557.3570	
M569T17	17.44	569.3022	
M571T18	18.04	571.3196	
M575T17	17.44	575.3170	*Rha-C10-C12:1 [M+Na]+
M610T17	16.65	610.3479	
M611T17	16.63	610.8497	
M633T17_1	17.45	633.2751	
M668T16	15.88	668.4214	
M670T16	15.87	670.3694	
M671T16_2	15.87	671.3720	
M673T16_1	15.87	673.3777	Rha-Rha-C10-C10+Na
M678T17	16.63	678.4141	
M679T17_1	17.23	679.4270	Rha-Rha-C10-C12
M690T17	17.23	690.4112	
M691T17	17.23	690.9133	
M696T17	17.23	696.4533	
M699T17_2	16.64	699.3933	Rha-Rha-C10-C12:1+Na
M699T17_3	17.23	699.4037	
M701T17_2	16.62	701.3986	
M701T17_3	17.23	701.4094	Rha-Rha-C10-C12+Na
M717T17_3	17.23	717.3761	
M723T17	17.23	723.3906	
M751T17_1	16.66	750.9542	
M776T17	16.64	776.4765	
M777T17_2	16.64	777.4797	
M778T17	16.64	777.9805	
M819T18_1	18.04	818.5232	
M819T18_2	18.04	819.0249	
M863T17_1	16.63	862.5132	
M863T17_2	16.63	863.0145	
M882T17	16.65	882.0697	
M883T17	16.65	882.5713	
M985T17	16.65	984.6388	

M1010T17	16.64	1009.6682	
M1011T17	16.64	1010.6714	
M1029T17_1	16.64	1028.6424	
M1029T17_2	16.64	1029.1430	
M1030T17	16.64	1029.6448	
M1032T17	16.66	1031.6504	*Rha-C10-C10+Na [2M+H]
M1035T17	16.64	1034.6588	
M1038T17_1	17.23	1037.6101	
M1038T17_2	17.23	1038.1115	
M1048T17	16.64	1047.6171	
M1049T17	16.64	1048.6192	
M1054T17	16.64	1053.6310	
M1055T17	16.64	1054.6341	
M1084T17	17.44	1083.6813	
M1085T17	17.44	1084.6846	
M1110T18	18.04	1109.6947	
M1111T18	18.04	1110.6968	
M1204T17	16.63	1203.7229	
M1205T17	16.63	1204.7267	
M1380T17	17.23	1379.8293	
M1381T17	17.23	1380.8327	

Table A7. Features responsive to the treatment at short-exposure and long exposure (Region 5). Log2-fold-change values are calculated per antibiotic group against the untreated control group (n=3)

Feature name	RT (min)	m/z
M95T16	15.67	95.0856
M109T16	15.67	109.1012
M111T16_2	15.67	111.1169
M125T16	15.67	125.1324
M135T18	17.69	135.0804
M137T16	15.67	137.1325
M151T16_1	15.67	151.1119
M151T16_2	15.67	151.1480
M153T16_1	15.67	153.0911
M155T16	15.67	155.1067
M159T16	15.67	159.0932
M162T8	8.35	162.0549
M165T16	15.66	165.1275
M169T16	15.67	169.1224
M179T16	15.67	179.1431
M181T16	15.67	181.1226
M183T16	15.67	183.1380
M184T18	17.63	184.1118
M189T14	13.80	188.6119
M189T13	13.49	189.1639
M195T1	1.16	195.0028
M195T16	15.67	195.1381
M197T16	15.67	197.1537
M201T7	7.17	201.1472
M207T11	11.38	207.0554
M209T16	15.66	209.1538
M219T16	15.67	219.2109
M223T16	15.67	223.1694
M225T11_2	10.55	225.0854
M233T14	14.32	233.1901
M243T16	15.67	243.2109
M243T14	13.80	243.2109

M244T16	15.67	244.2143
M247T11	11.39	247.0479
M248T11	11.37	248.0514
M251T14_1	14.06	251.1619
M261T16	15.67	261.2215
M263T10	9.50	263.1179
M265T13	13.49	265.1776
M269T13	12.55	269.2112
M277T16	16.11	277.2163
M279T10	10.34	279.1127
M279T16_2	15.67	279.2323
M282T5	5.48	282.1643
M291T14	14.32	291.1933
M293T15_3	15.26	293.2477
M294T6	5.89	293.6731
M294T15_3	15.25	294.2511
M306T19	18.67	306.1703
M307T16	15.66	307.2109
M307T18_3	17.87	307.2247
M309T13_2	12.55	309.2037
M316T13	13.41	316.2272
M317T16_1	15.67	316.7179
M323T14	13.94	323.2195
M326T6	6.29	326.1895
M330T6	6.41	329.5177
M331T8	7.75	330.7183
M335T14_1	13.80	335.1895
M342T14	13.89	342.2432
M344T16_2	16.05	344.2585
M351T18_1	17.62	351.2509
M351T15	15.26	351.2510
M361T7	7.22	360.7057
M367T15	15.26	367.2247
M375T7	6.78	374.7032
M379T16_1	15.67	379.1802
M380T16	16.47	380.2951
M381T17	17.42	381.2614
M382T20	20.31	382.3112
M383T20_1	19.74	383.2231
M384T22	22.21	384.3265
M389T8	8.12	389.2183
M396T22	21.53	396.3263
M398T16	16.48	398.3058
M401T7	7.07	401.2760
M409T19	18.73	409.2926
M410T22	22.30	410.3422
M415T6	5.79	414.7141
M420T16	15.67	420.2059
M443T9	8.67	442.7532
M456T16	15.67	456.3450
M457T16	15.67	456.8466
M458T7_1	7.24	457.5970
M464T16	15.66	464.3339
M465T16_1	15.66	464.8356
M465T16_2	15.67	465.3370
M471T6	6.47	471.2744
M483T10_1	10.23	482.5894
M498T9	8.52	497.7880
M512T17	16.66	511.7966
M547T8_1	8.35	546.9671

M557T16	15.66	557.4568
M577T18	18.04	577.3329
M615T16	15.67	615.4604
M617T14	14.29	617.1796
M631T16	15.67	631.4334
M651T14	13.79	651.4801
M652T8	8.08	652.3303
M667T16	15.67	667.4007
M667T14	13.79	667.4458
M673T16_2	15.67	673.4183
M675T9_1	8.82	674.8140
M677T16	15.67	677.4298
M678T18	18.38	677.5019
M712T20	20.13	711.5830
M723T10	10.23	723.3803
M724T10_1	10.23	723.8816
M724T10_2	10.23	724.3835
M730T19_1	18.67	729.5337
M734T20	20.13	733.5646
M764T20	20.30	763.6143

IV. MS and MS/MS identification

2-Hydrophenazine (RT, MS, MS/MS):
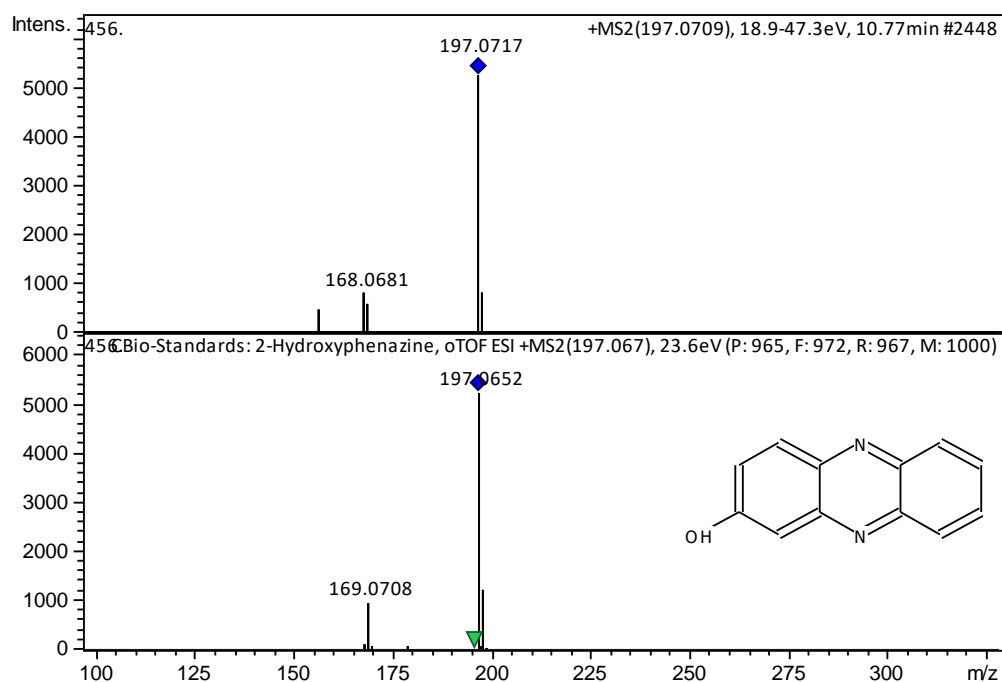
3-oxo-C12-HSL (RT, MS, MS/MS):
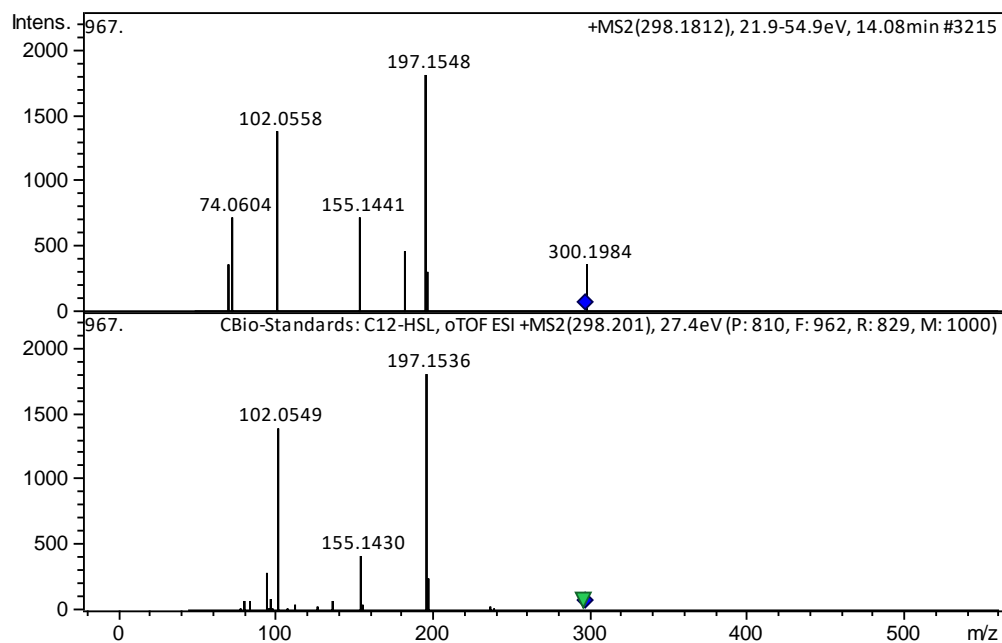
ADP and ADP [M+Na]+:
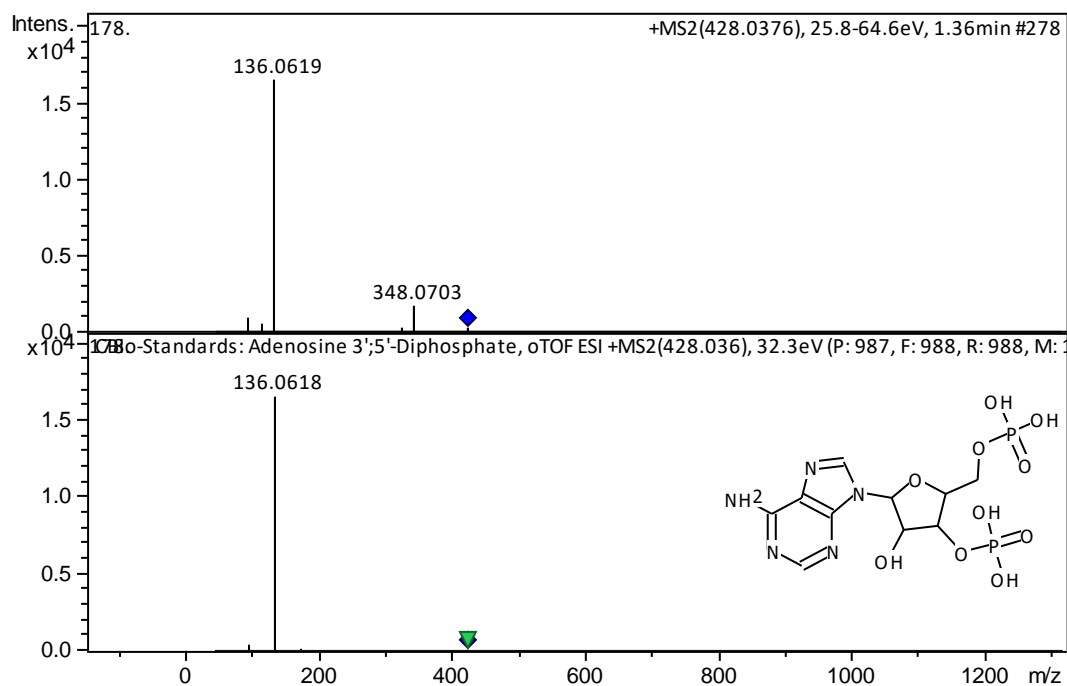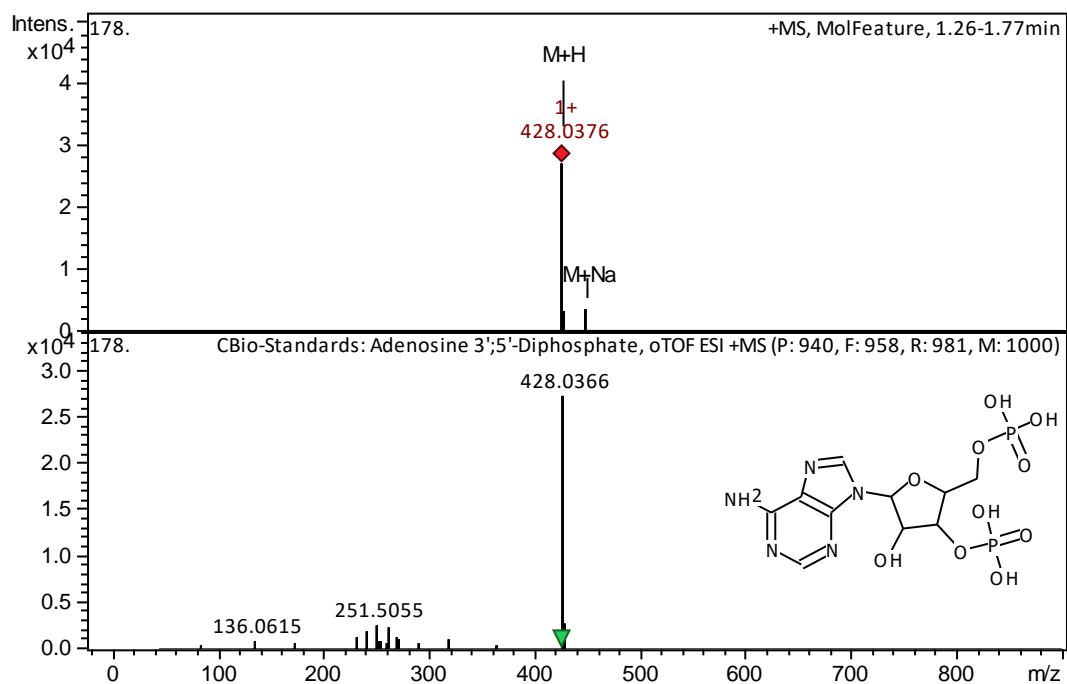
AMP (RT, MS, MS/MS):
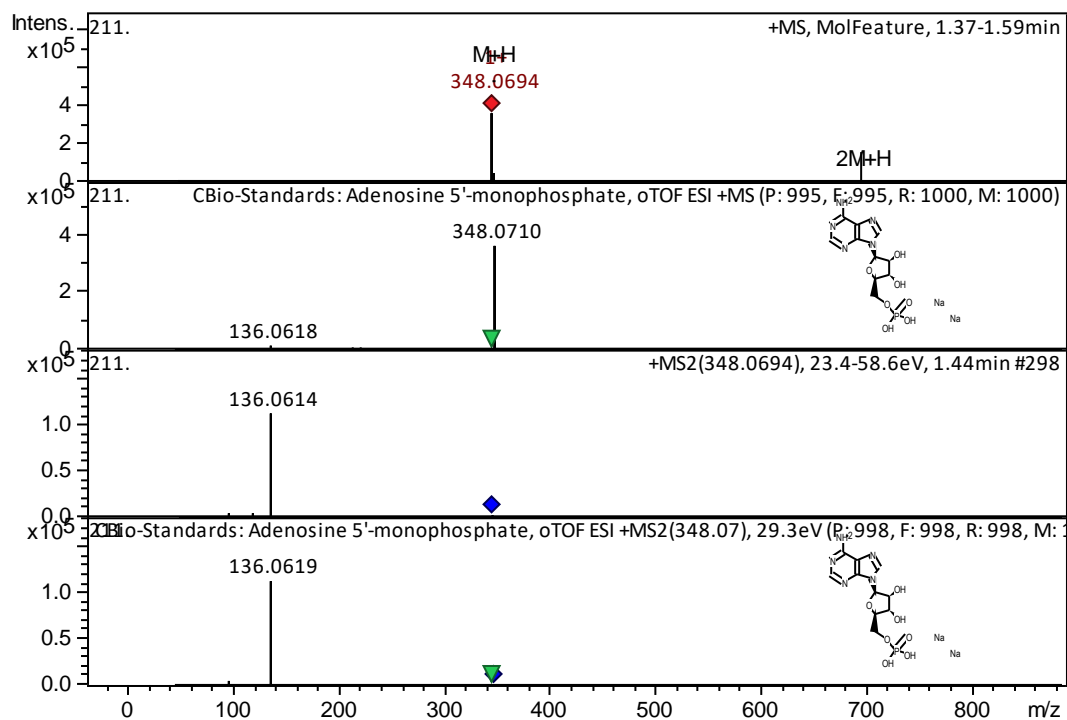
C7-QNO:
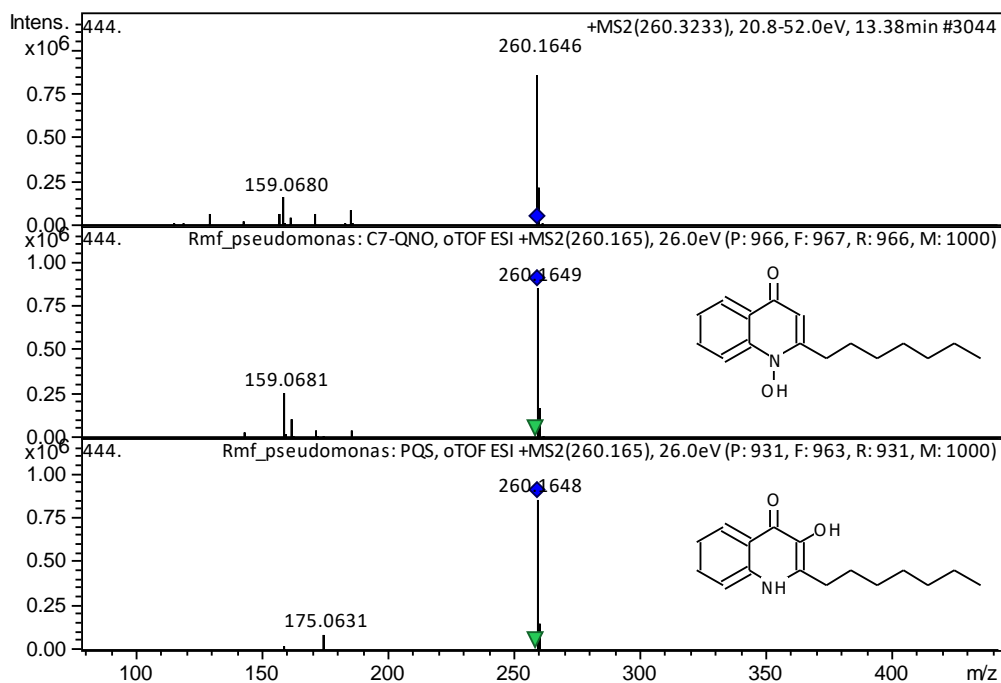
C7-PQS:
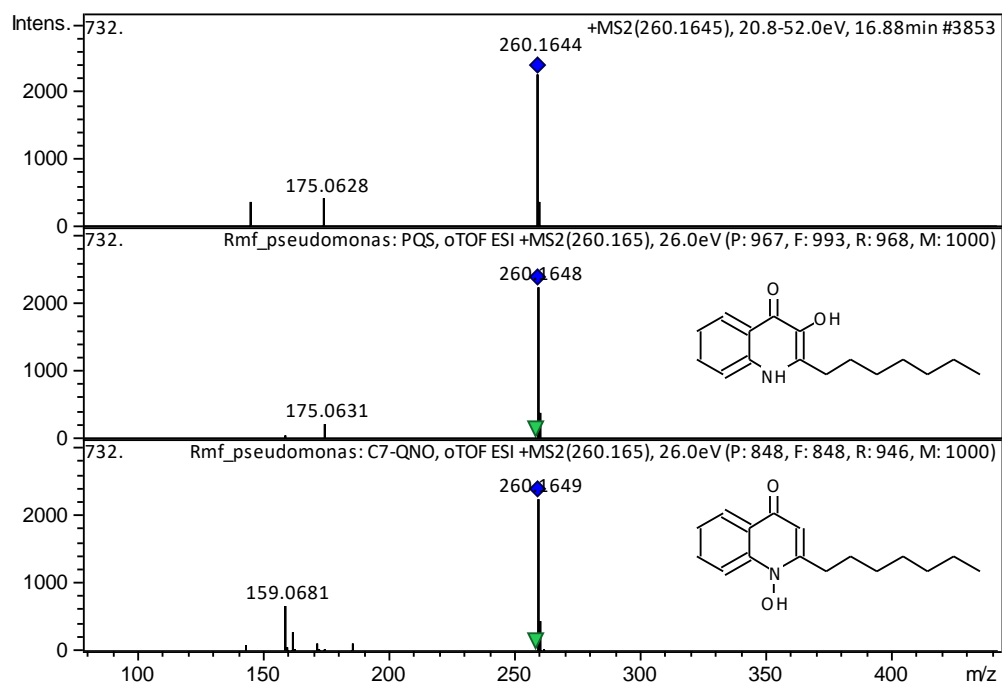
C7:1-PQS
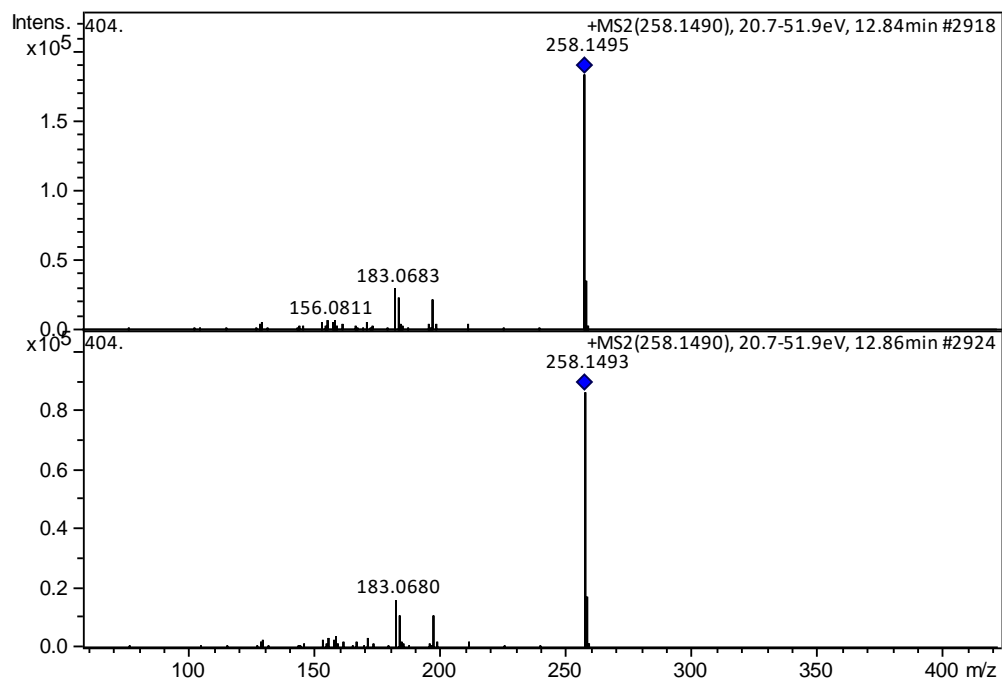
C8-QNO (RT, MS, MS/MS):
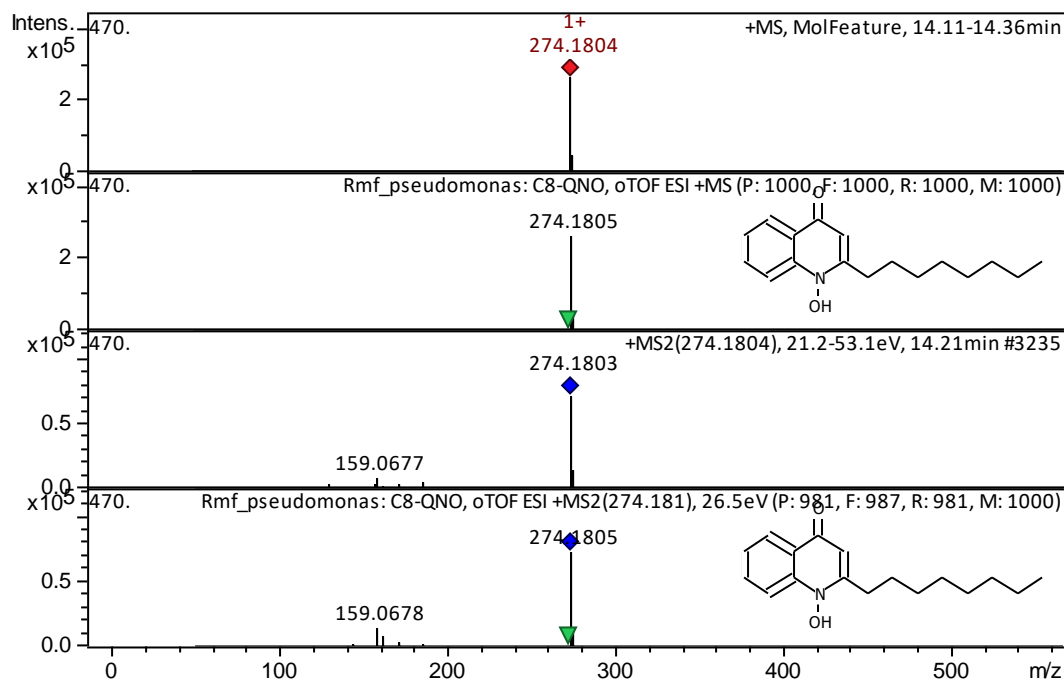
C6:-HQ (RT, MS, MS/MS):
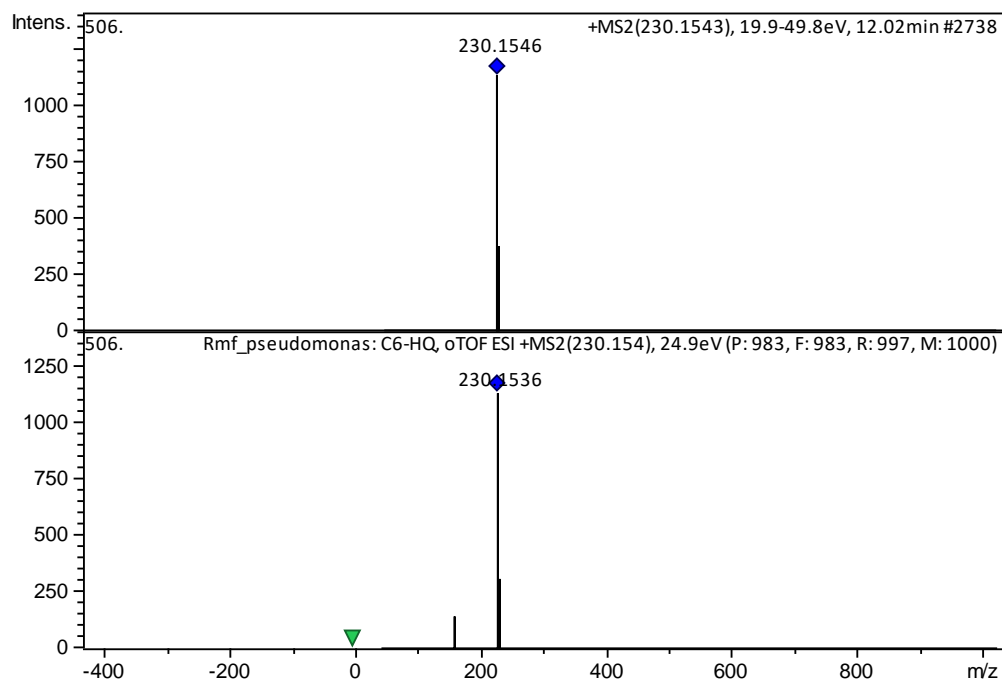
C7:1-HQ (RT, MS, MS/MS):
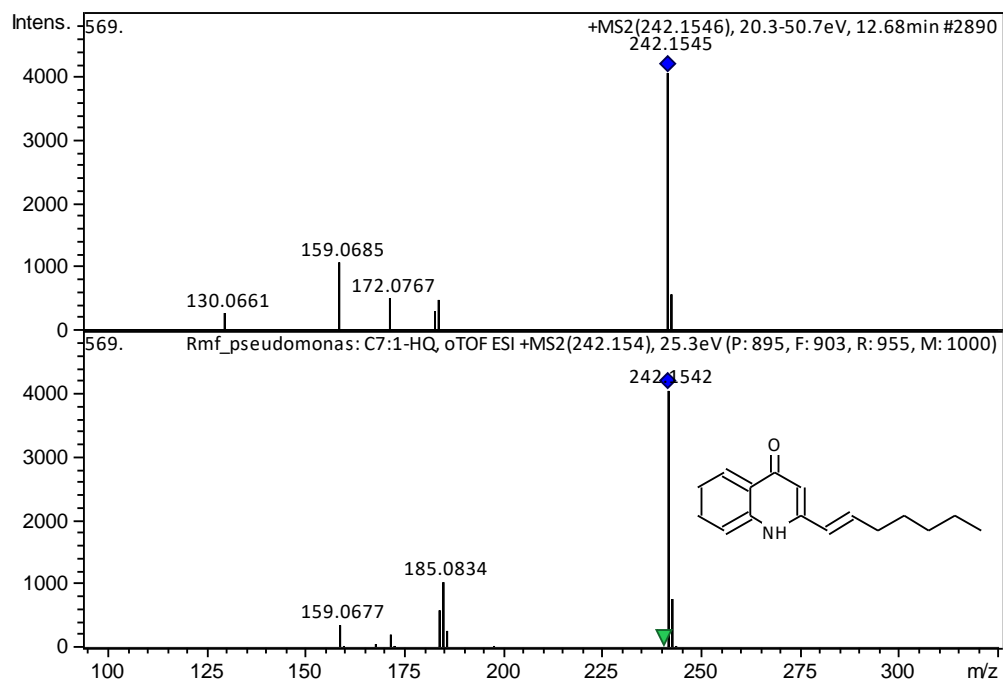
C9-QNO (RT, MS, MS/MS):
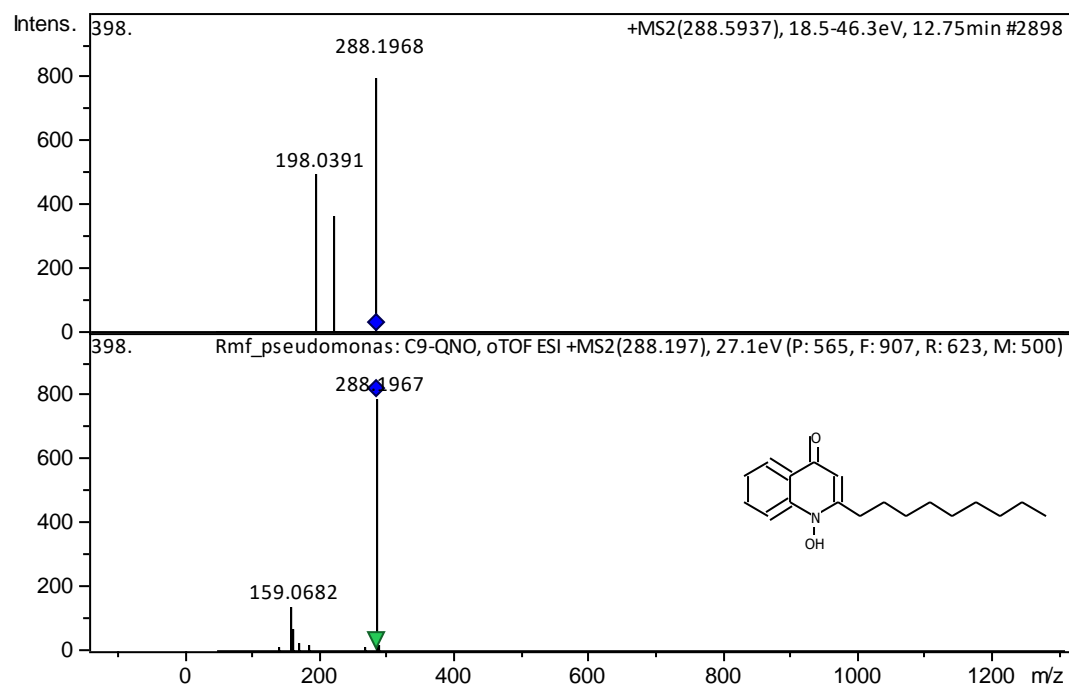
C9:1-HQ (RT, MS, MS/MS):
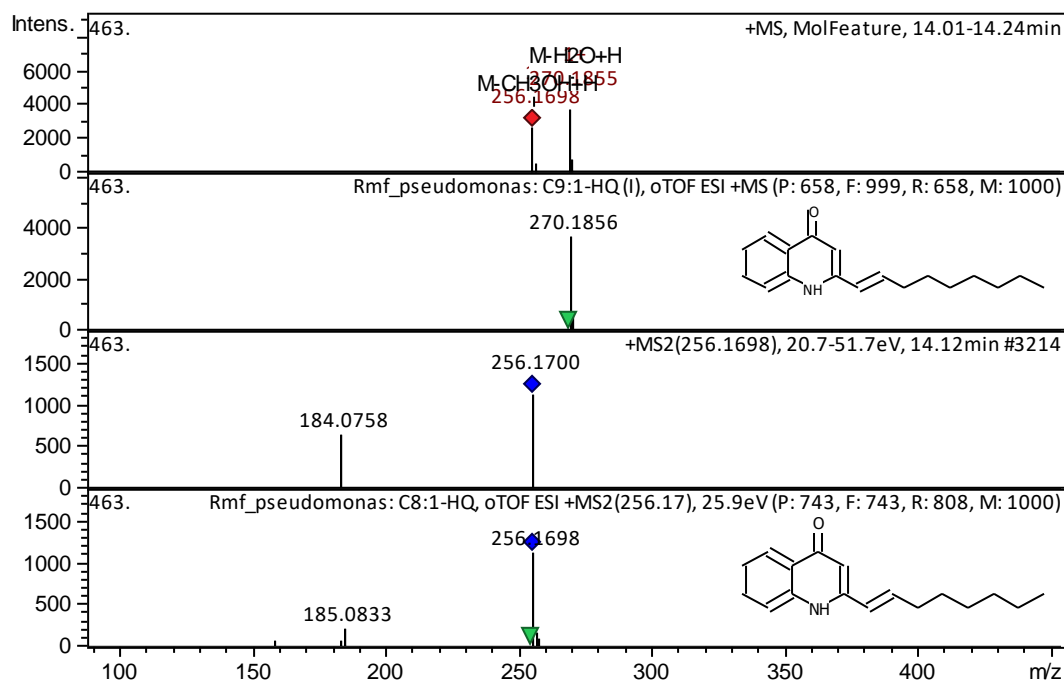
C9:1-QNO (RT, MS, MS/MS):
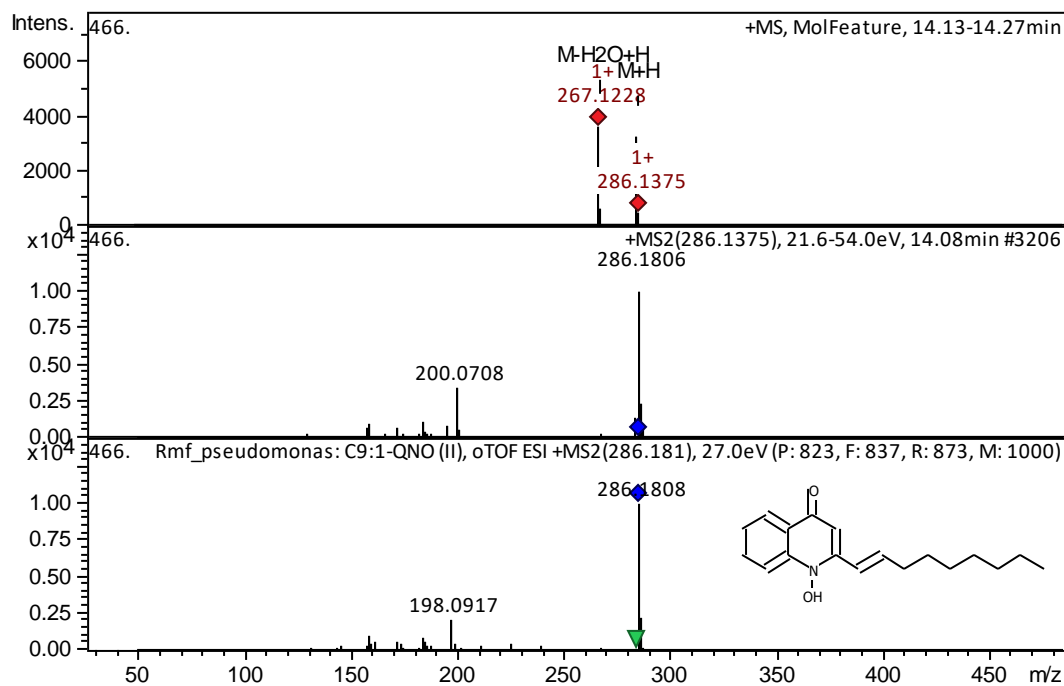
C11:0-PQS
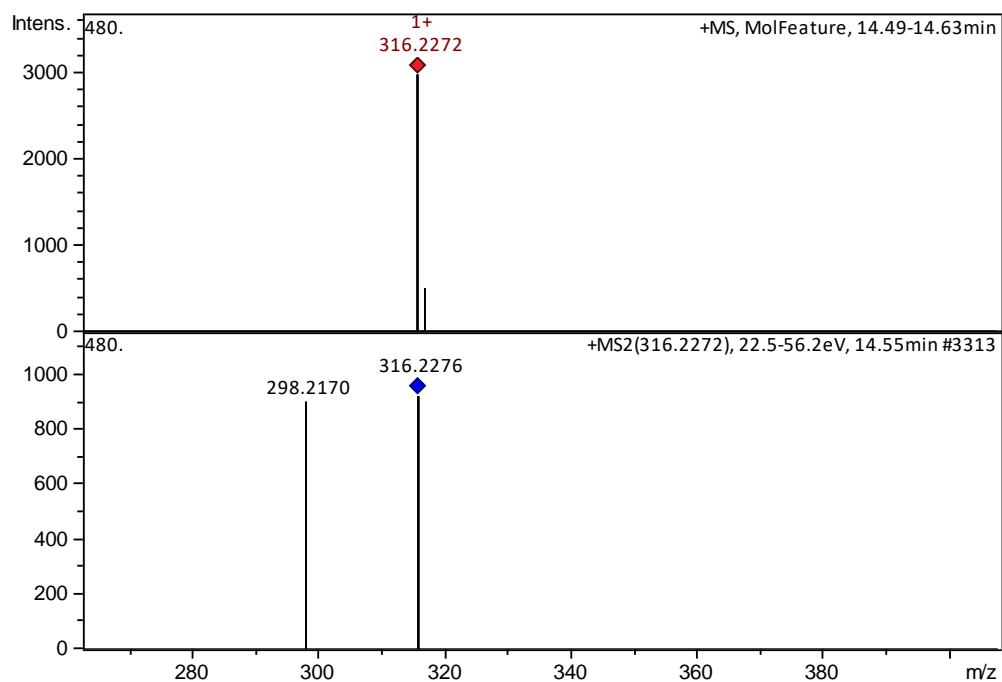
C11:0-PQS
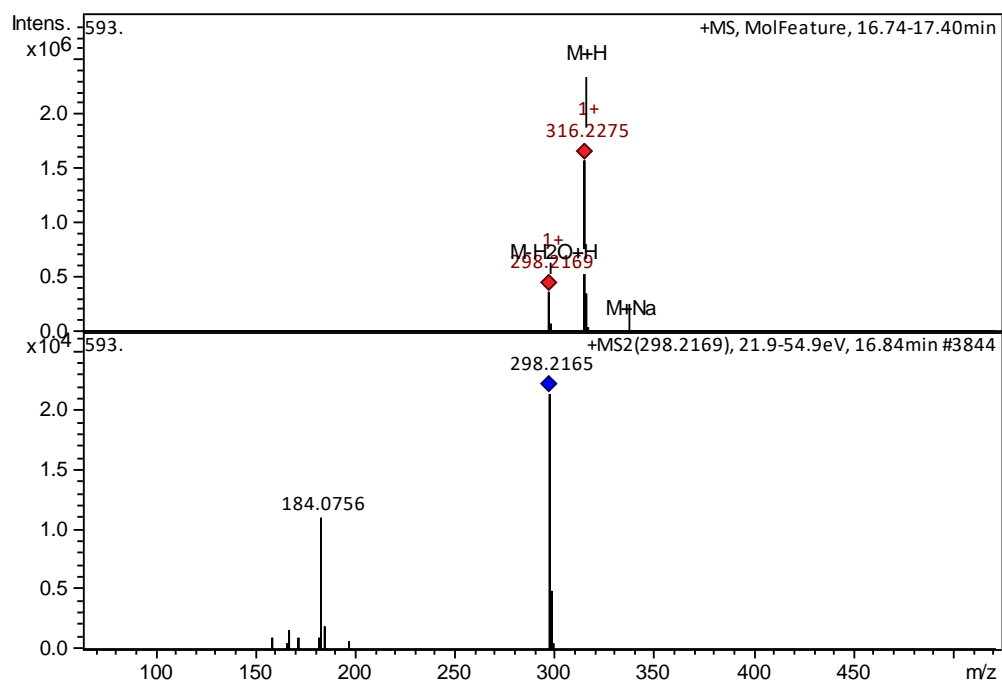
Not a AQ
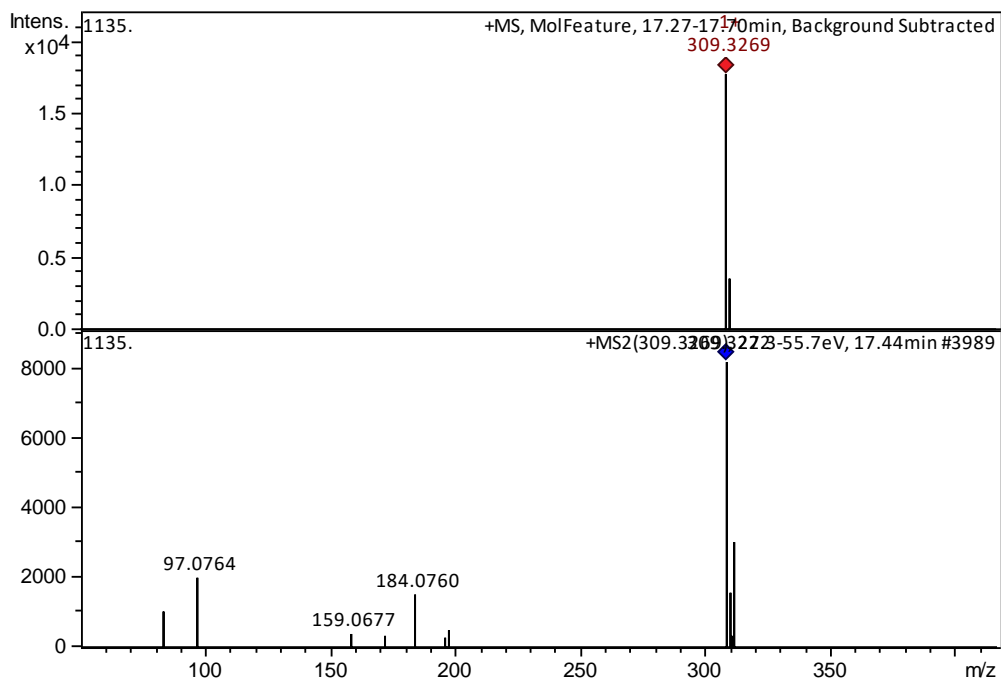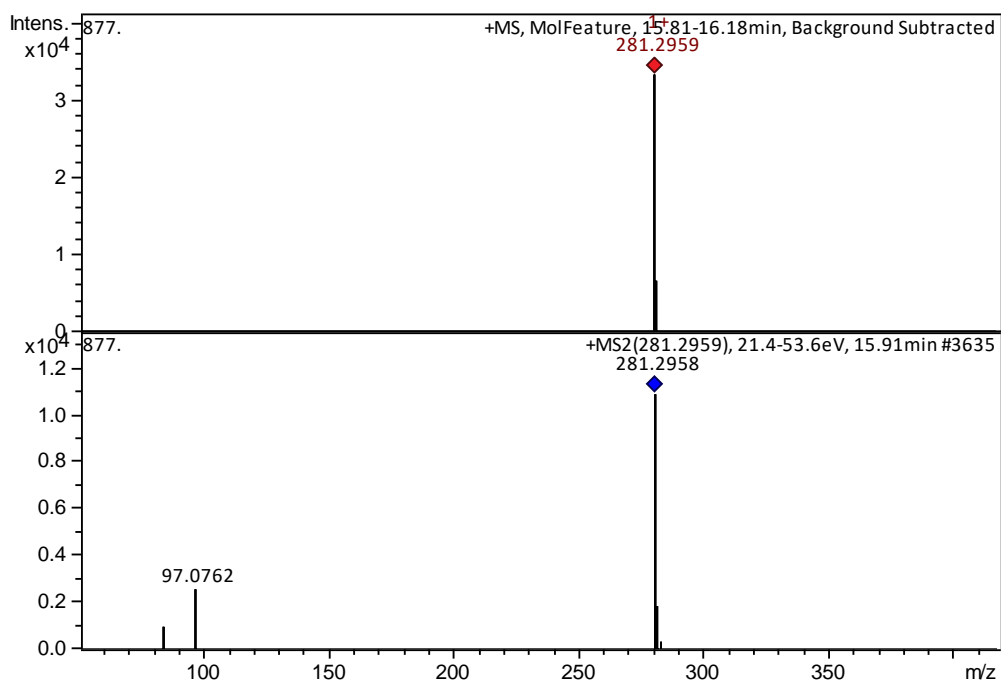
Ciprofloxacin
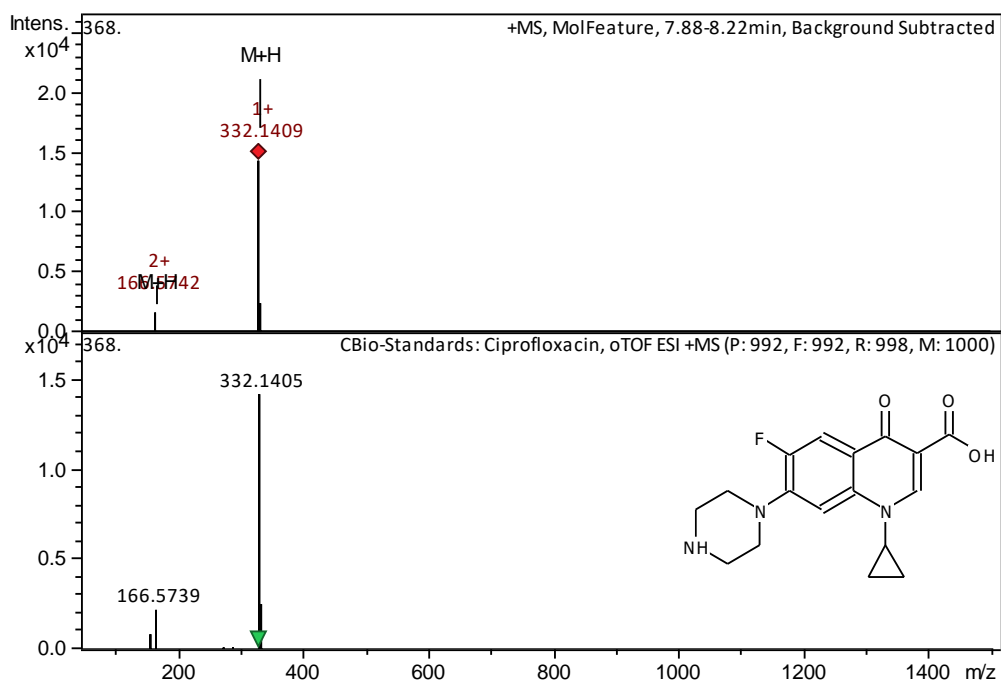
DHQ (RT, MS):
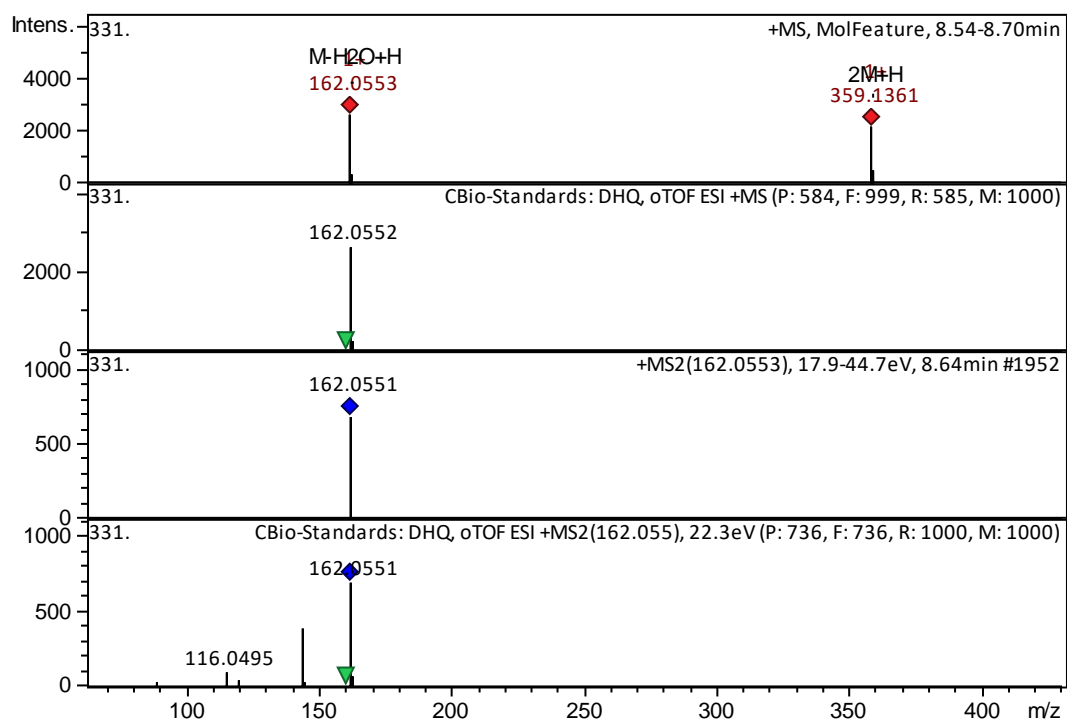
NAD (RT, MS, MS/MS):
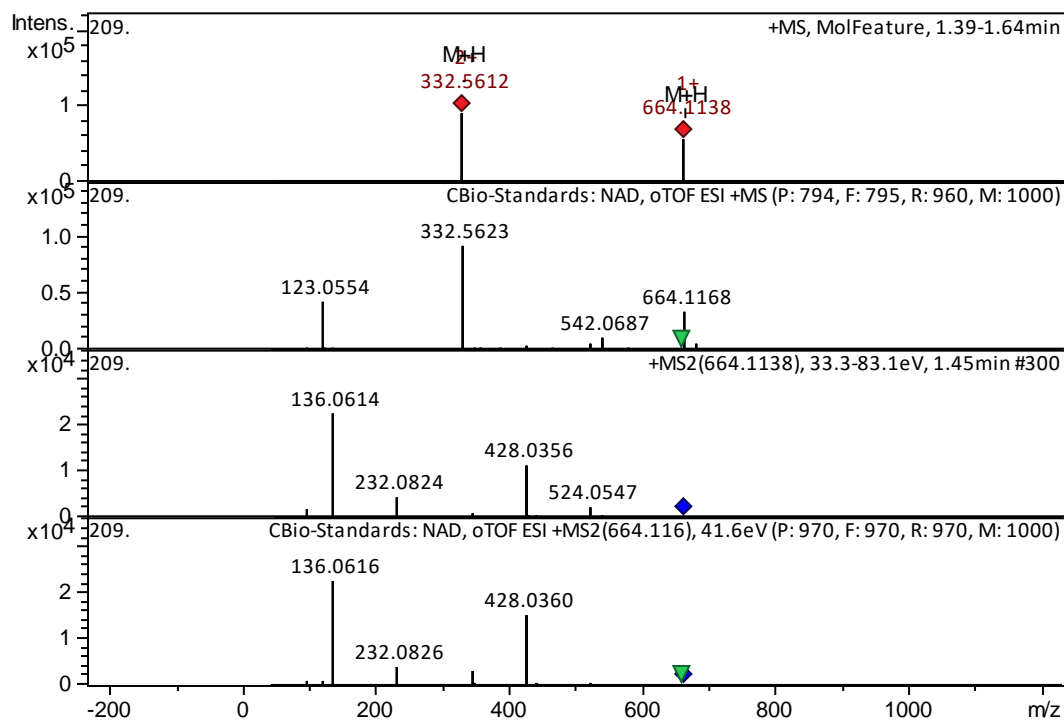
Ethanolamine phosphate (RT, MS, MS/MS)
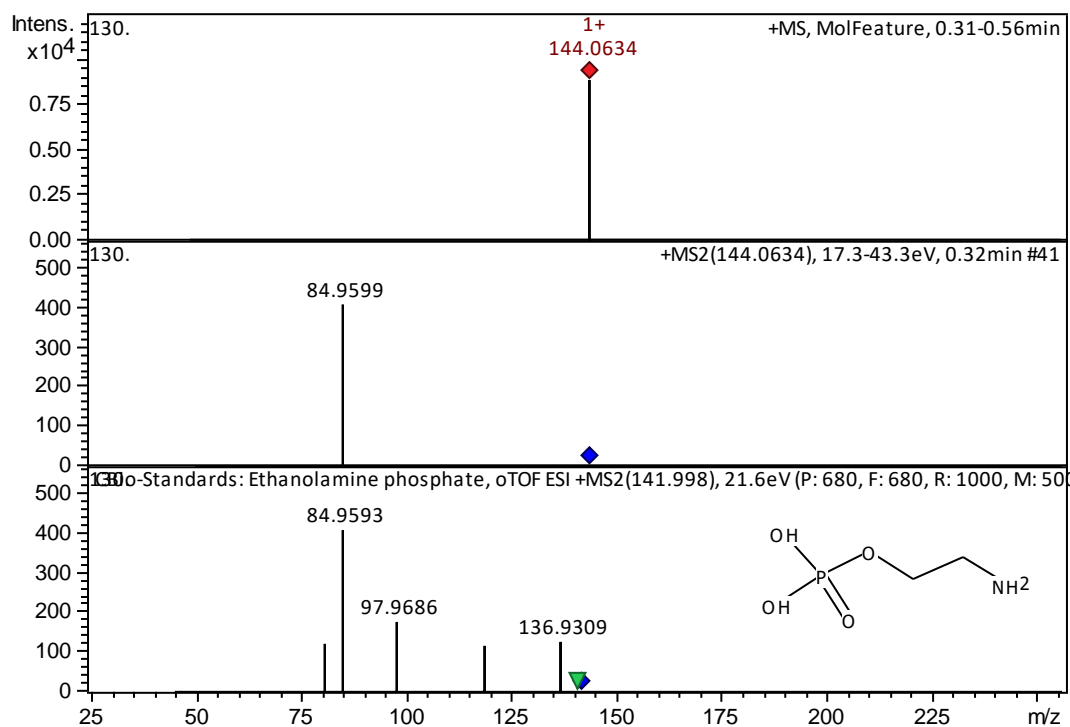
Erucic acid (RT, MS, MS/MS):
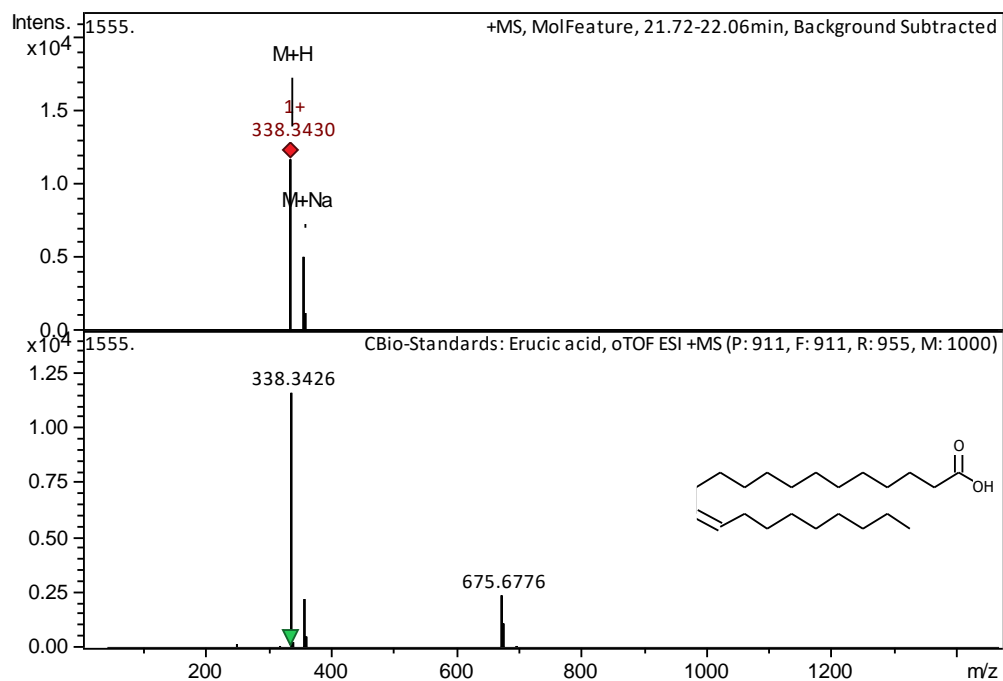
Glipizide (RT, MS, MS/MS):
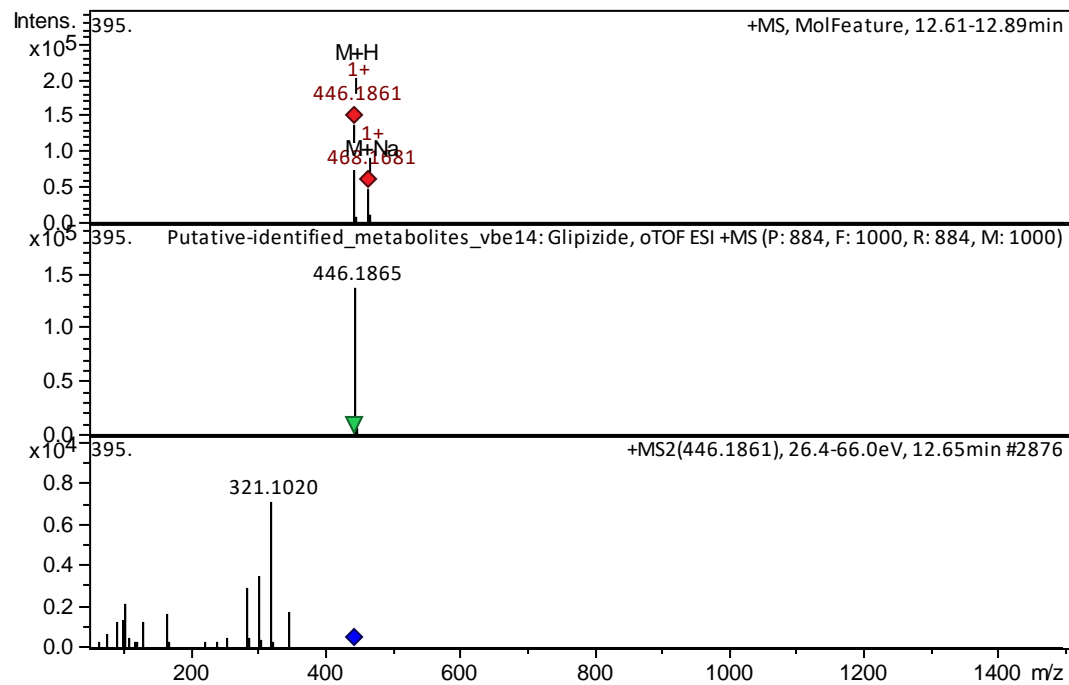
Gluthathion (RT, MS, MS/MS):
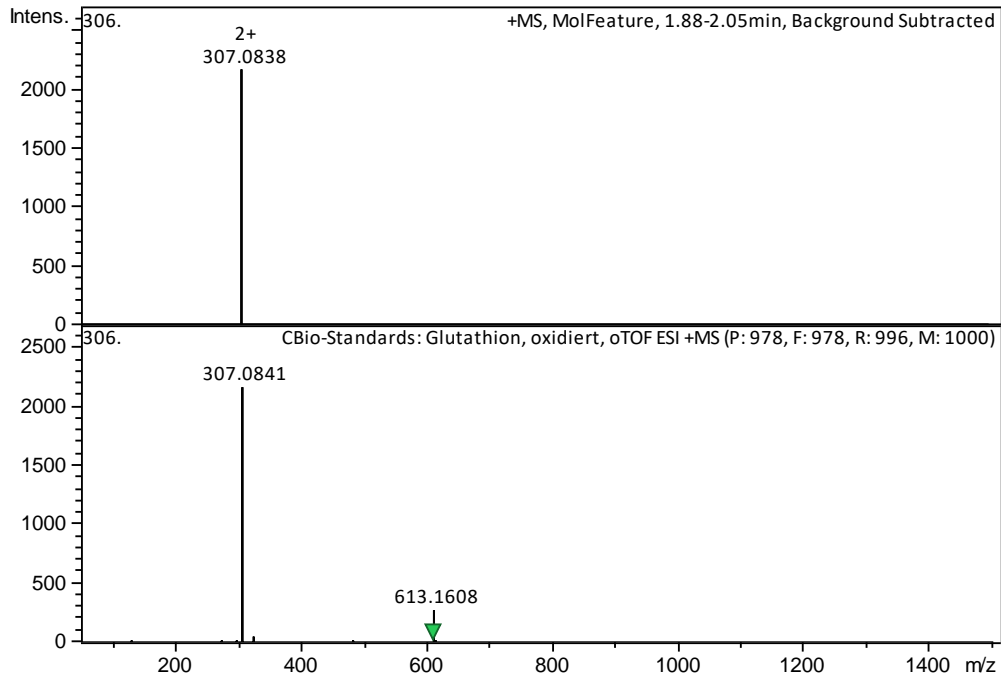
An AQ
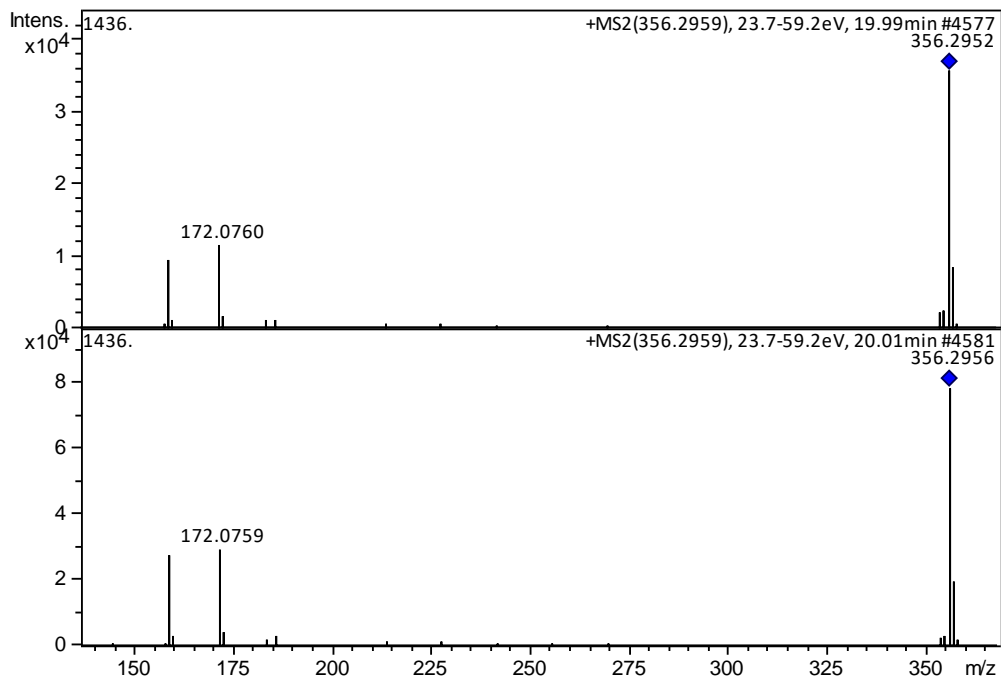
C15:1-HQ
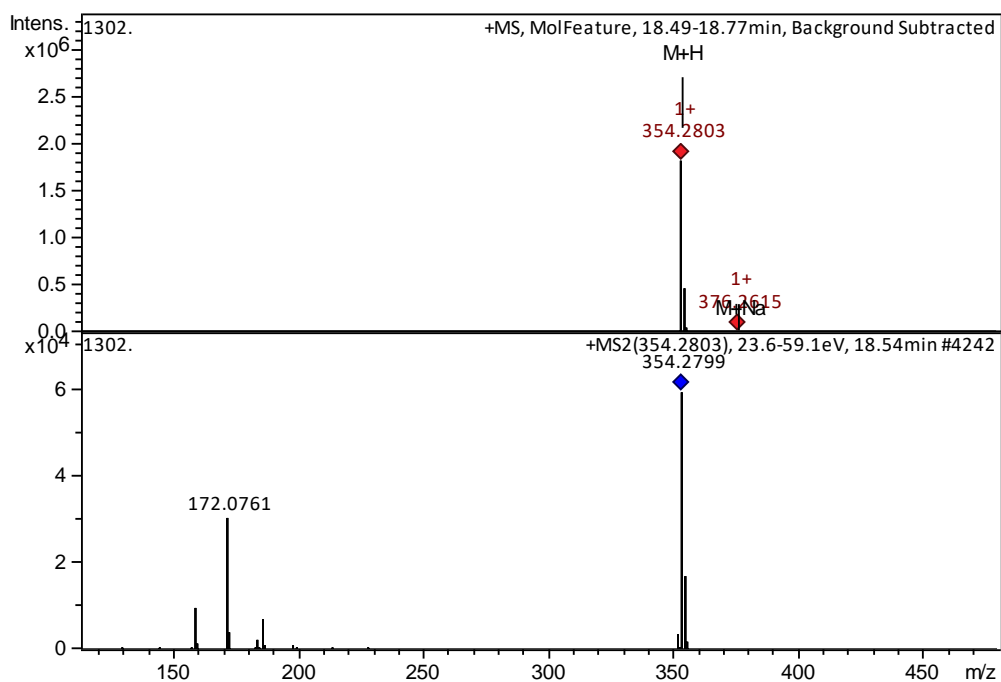
Rha-C10-C12:1+Na
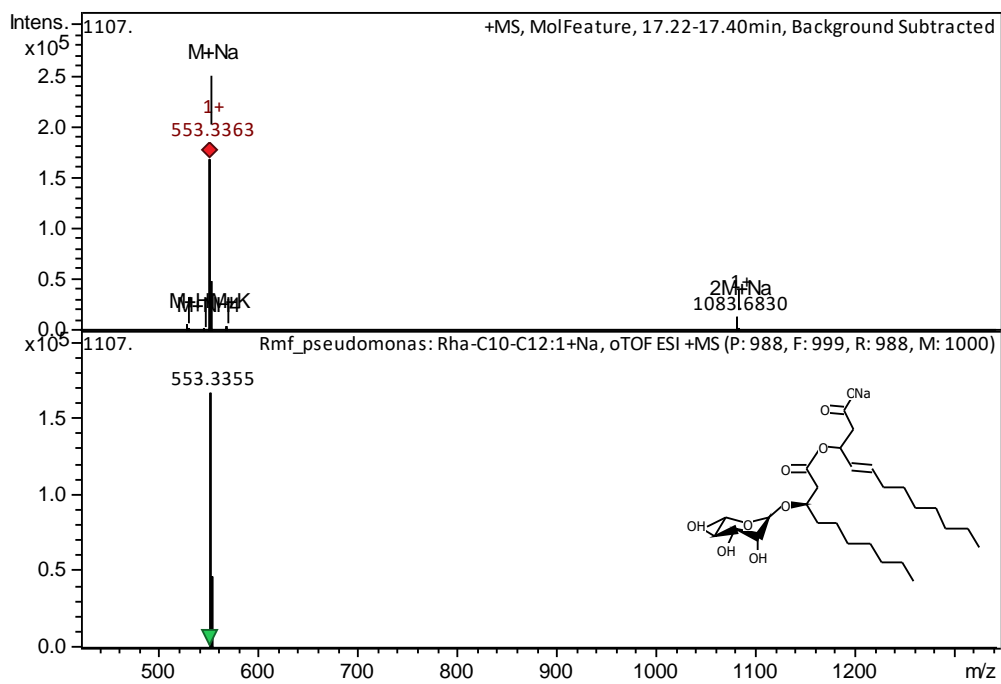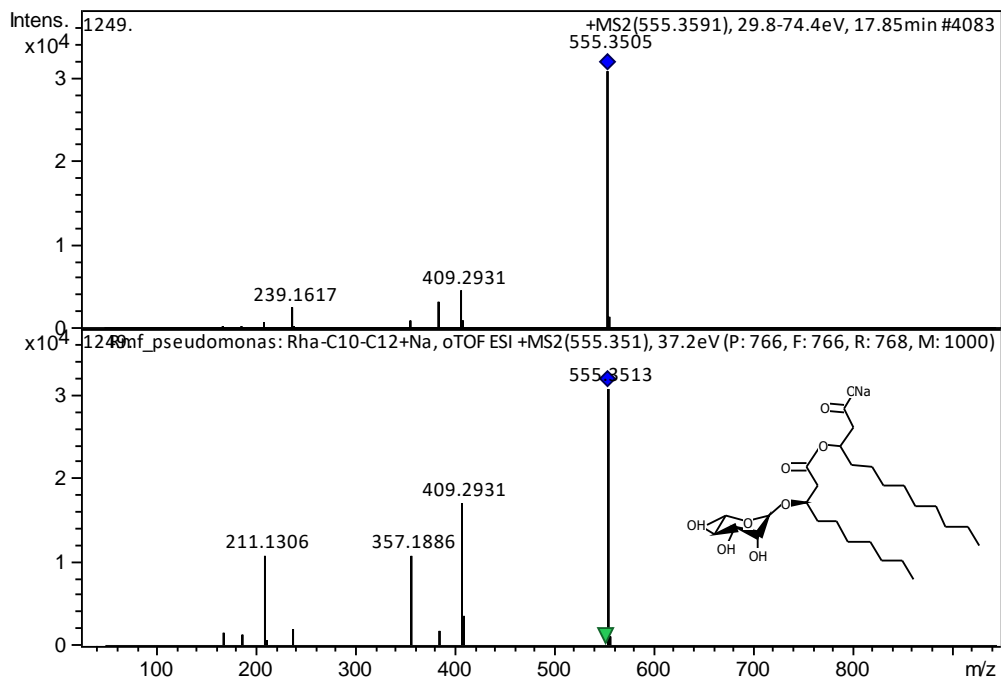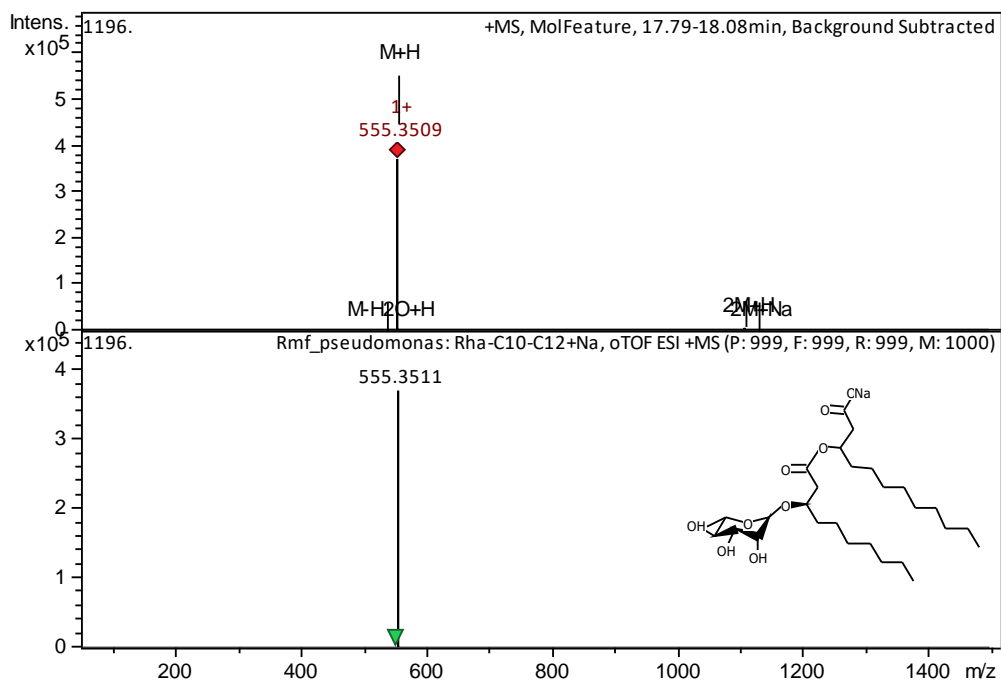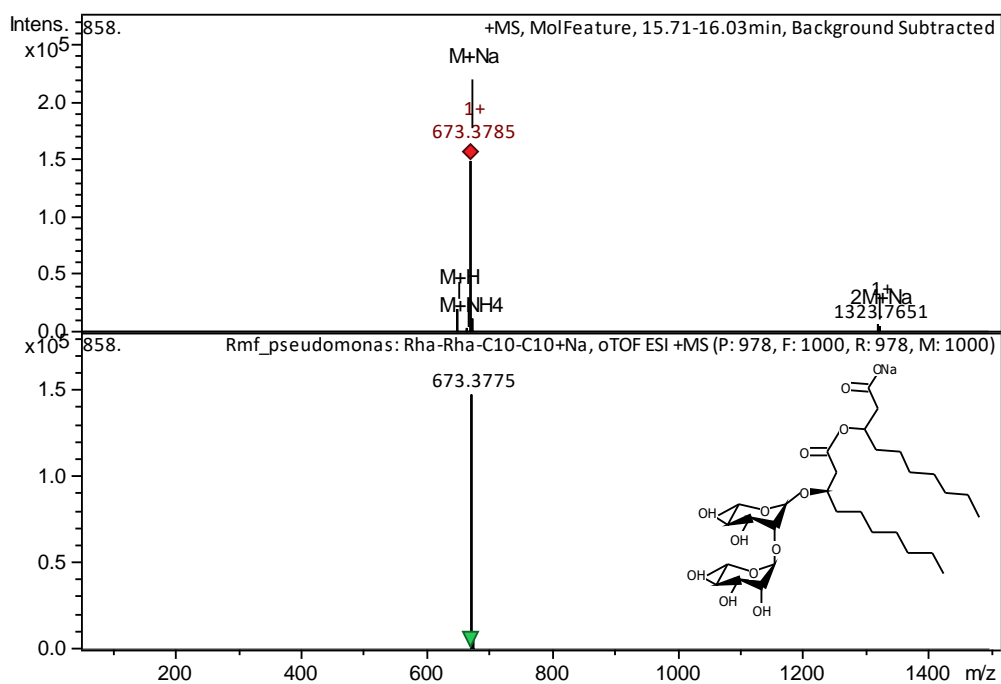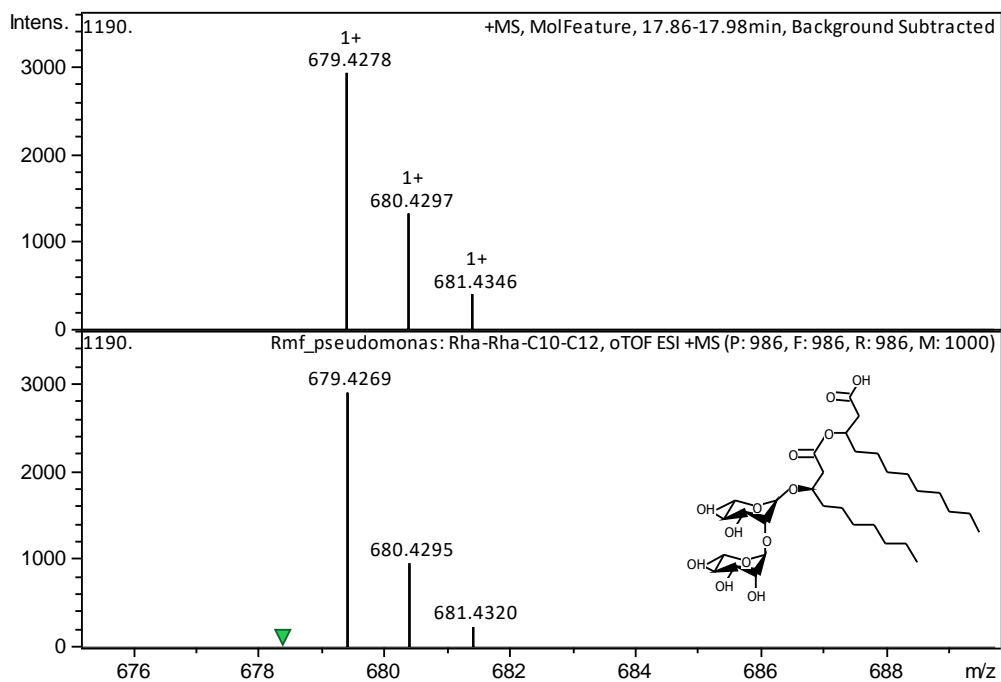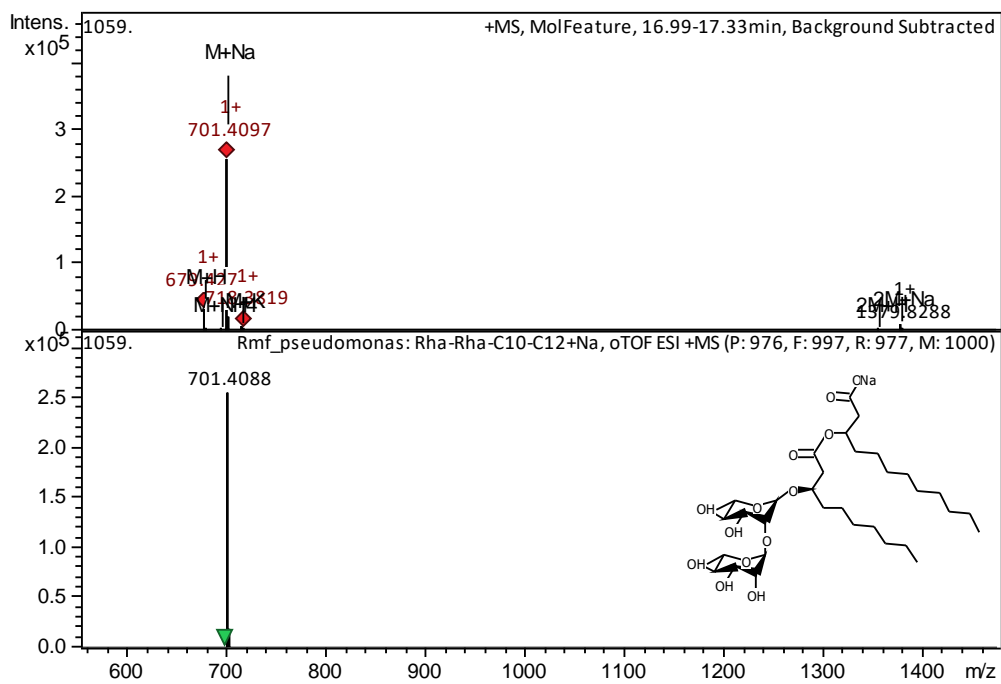
Hydroquinone:
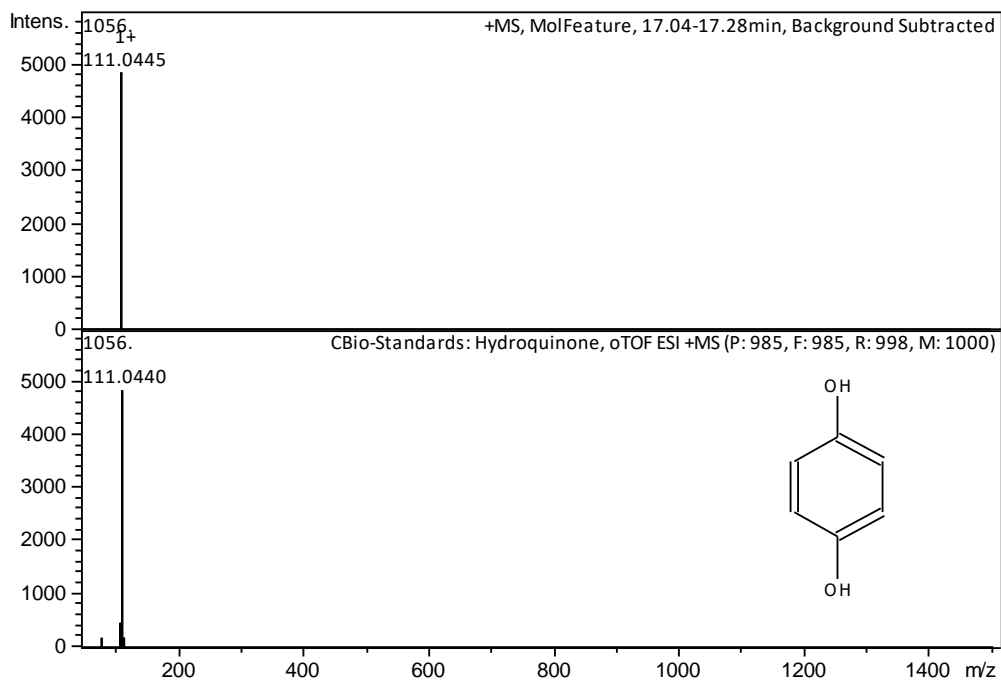
Pinolenic acid (RT, MS, MS/MS):
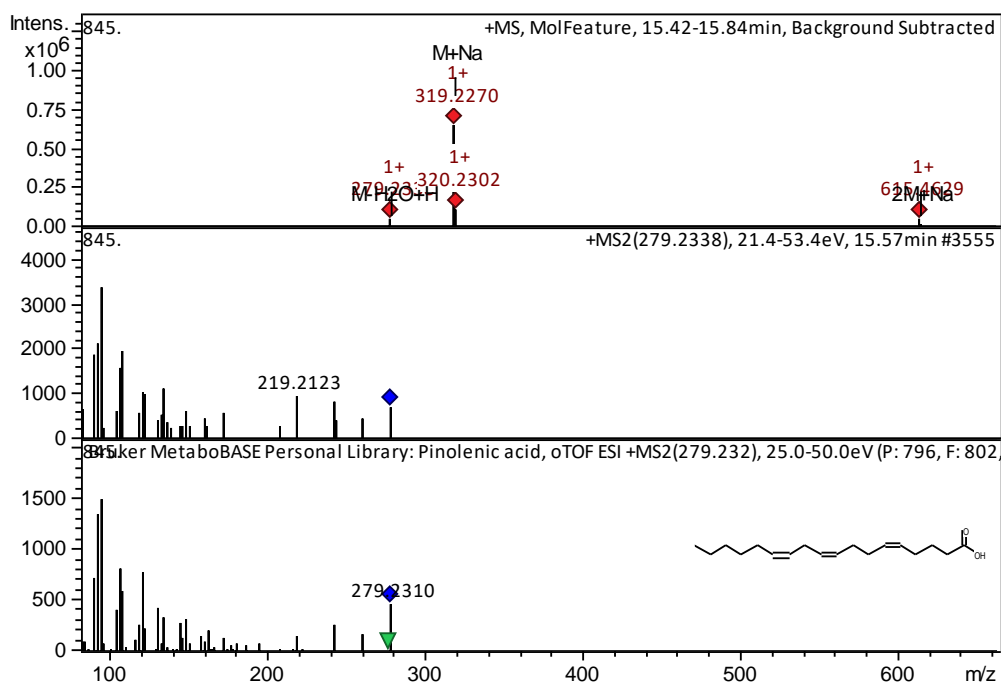
Palmitoleic acid (RT, MS):
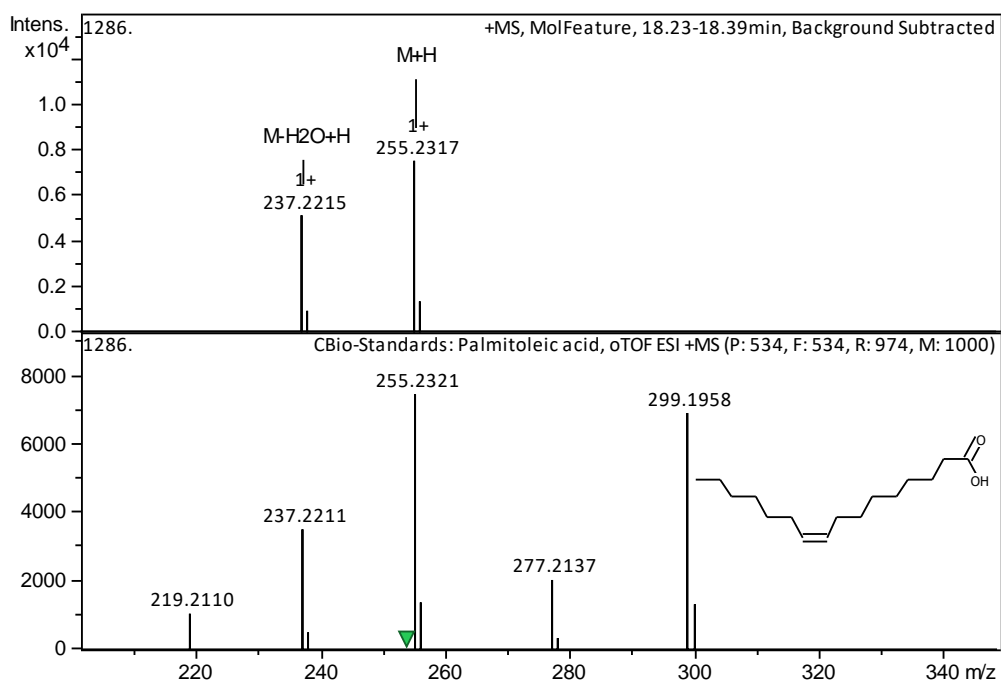
Tryptophan (RT, MS, MS/MS):

Glucose (RT, MS):

Intens. x10^4   191.   +MS, MolFeature, 1.13-1.32min, Background Subtracted

M+Na
1+
203.0529

M+K
1+
219.0267

Intens. x10^4   191.   Putative-identified_metabolites_vbe14: Glucose, oTOF ESI +MS (P: 765, F: 1000, R: 765, M: 1000)

203.0529

Glucose-phosphate (RT, MS)

Intens. x10^5   189.   +MS, MolFeature, 6.24-6.43min, Background Subtracted

M+Na
1+
261.1311

M+H
239.1490

Intens. x10^5   189.   CBio-Standards: D-Glucose-6-phosphate, oTOF ESI +MS (P: 720, F: 721, R: 988, M: 1000)

261.1308

84.9607
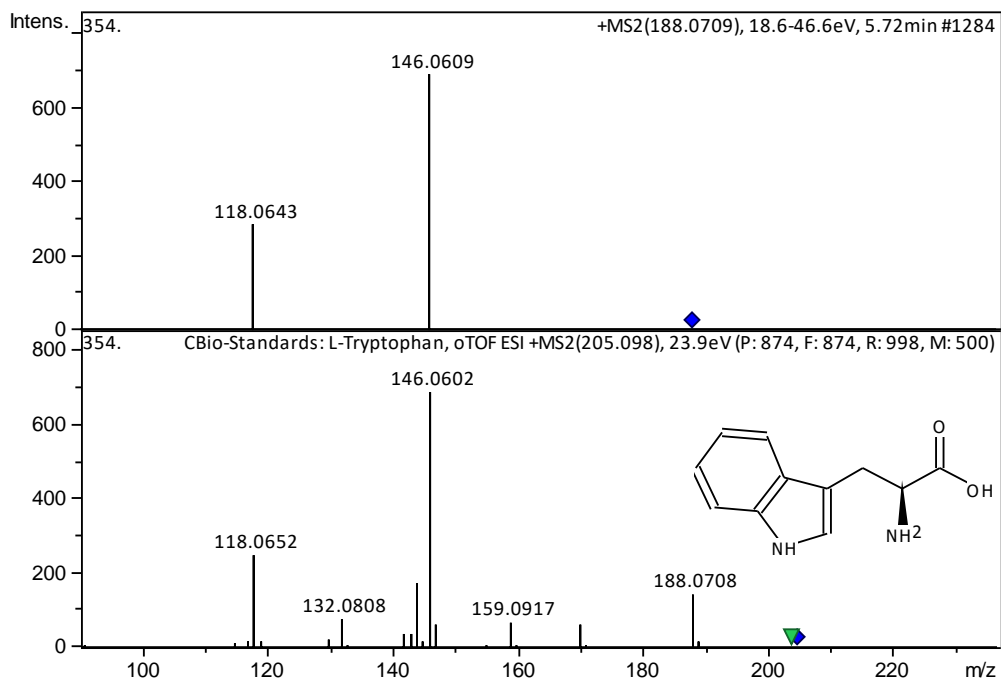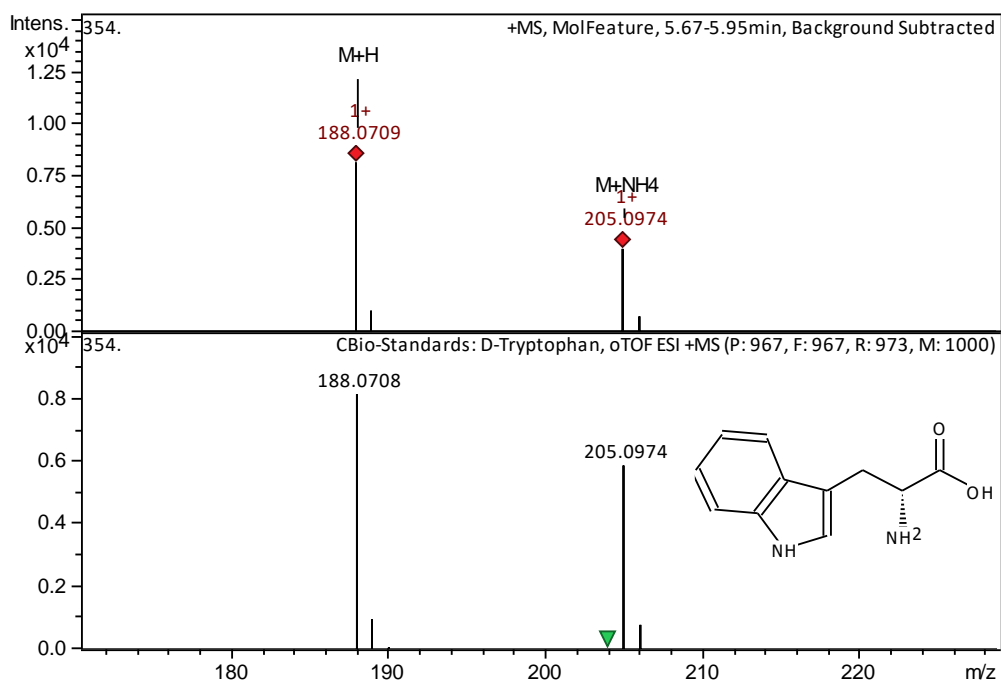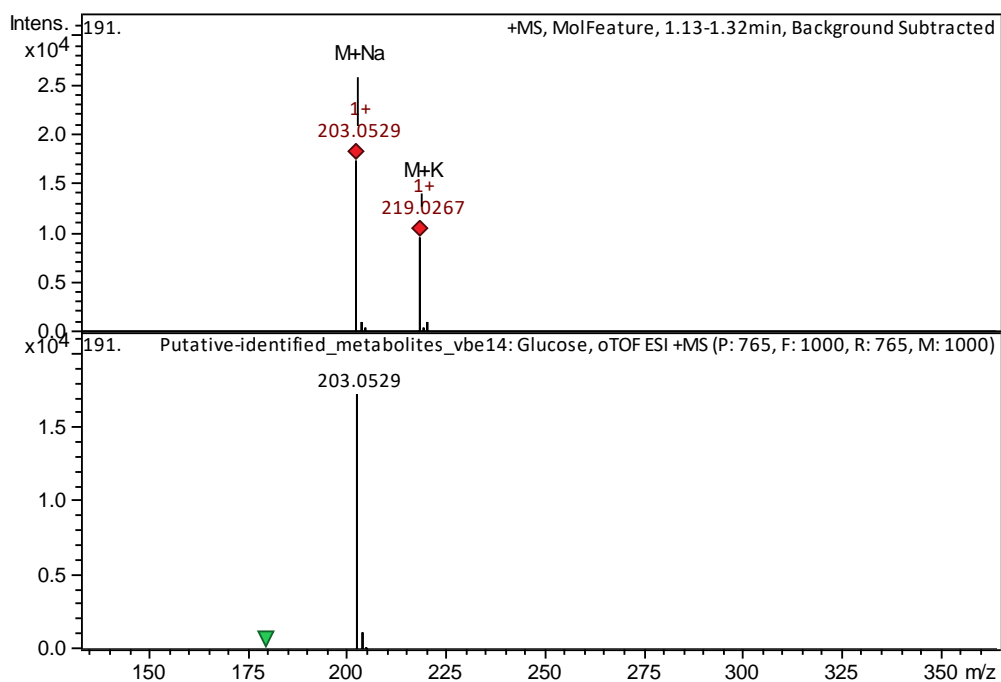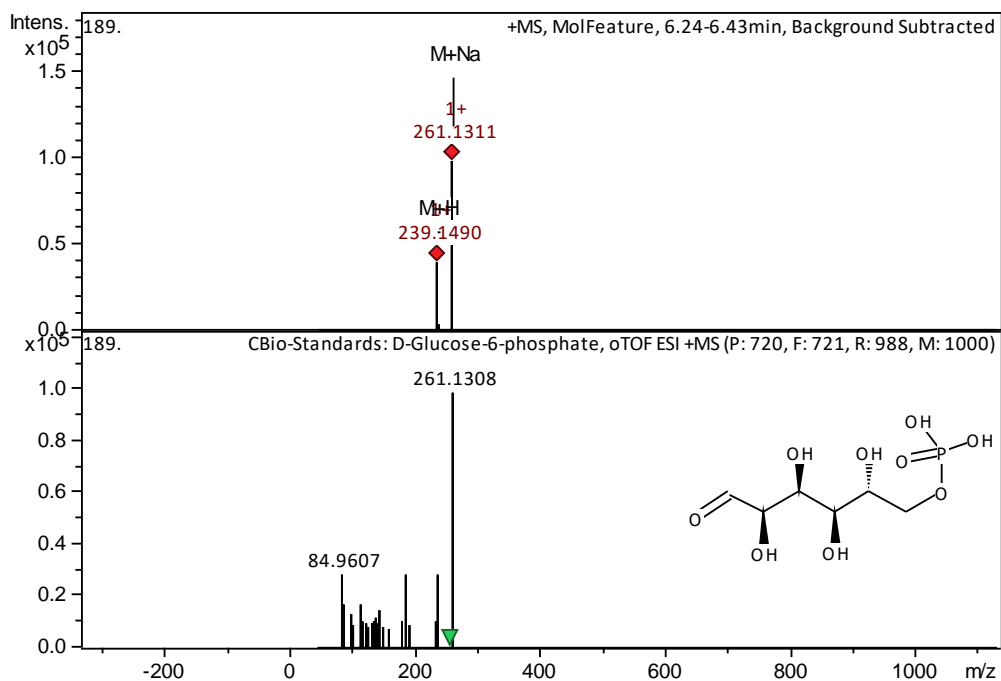
Glutamic acid (RT, MS, MS/MS):
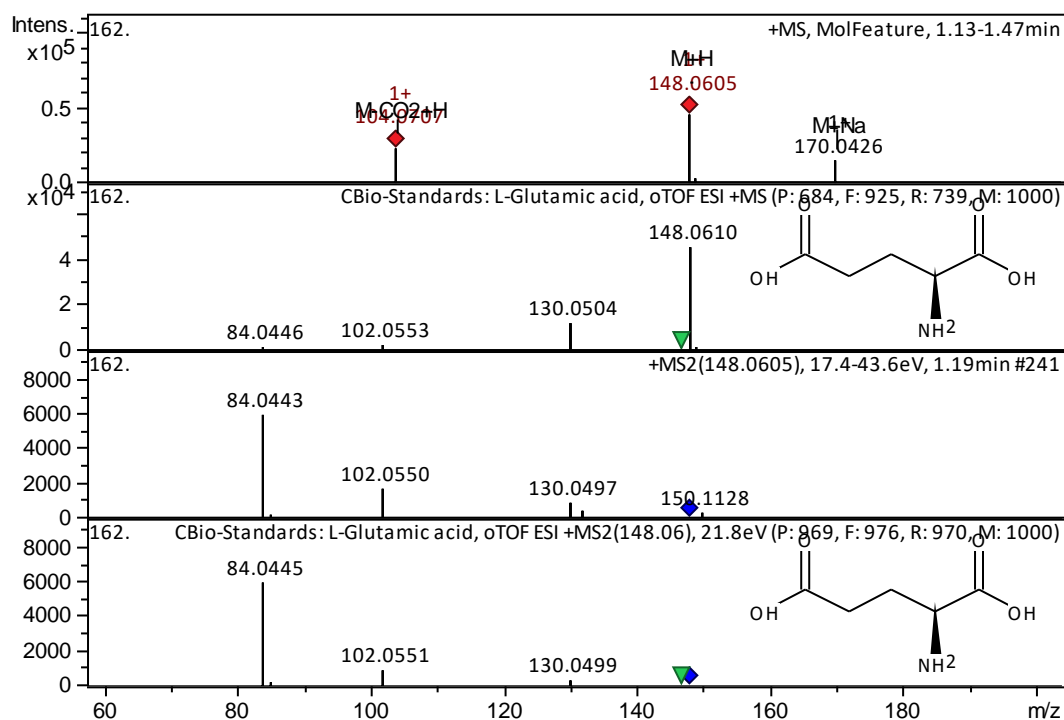
Hydroxy-phenazine-1-carboxilic acid (RT, MS):
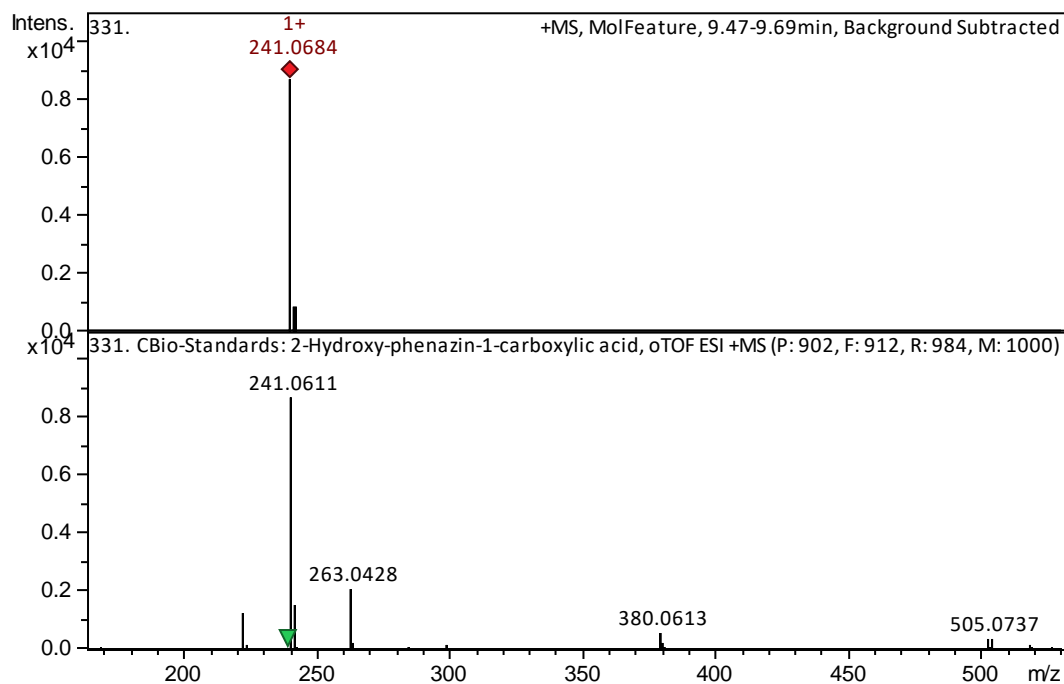
Phenazine-1-carboxamide (RT, MS, MS/MS):
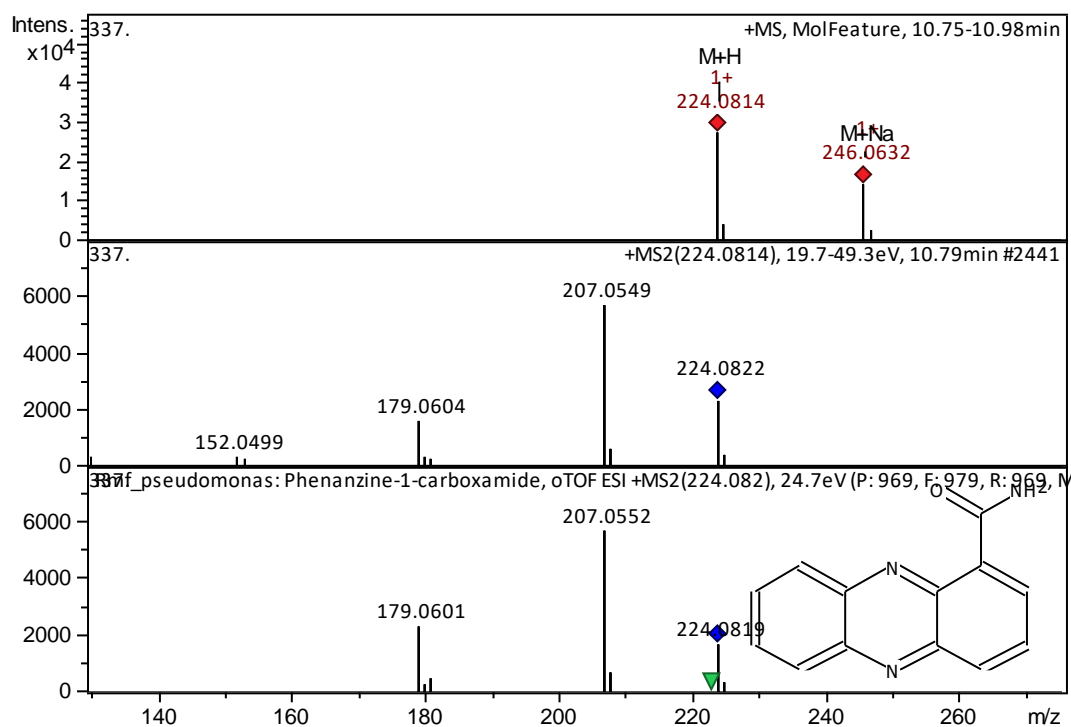
Phenazine (RT, MS):
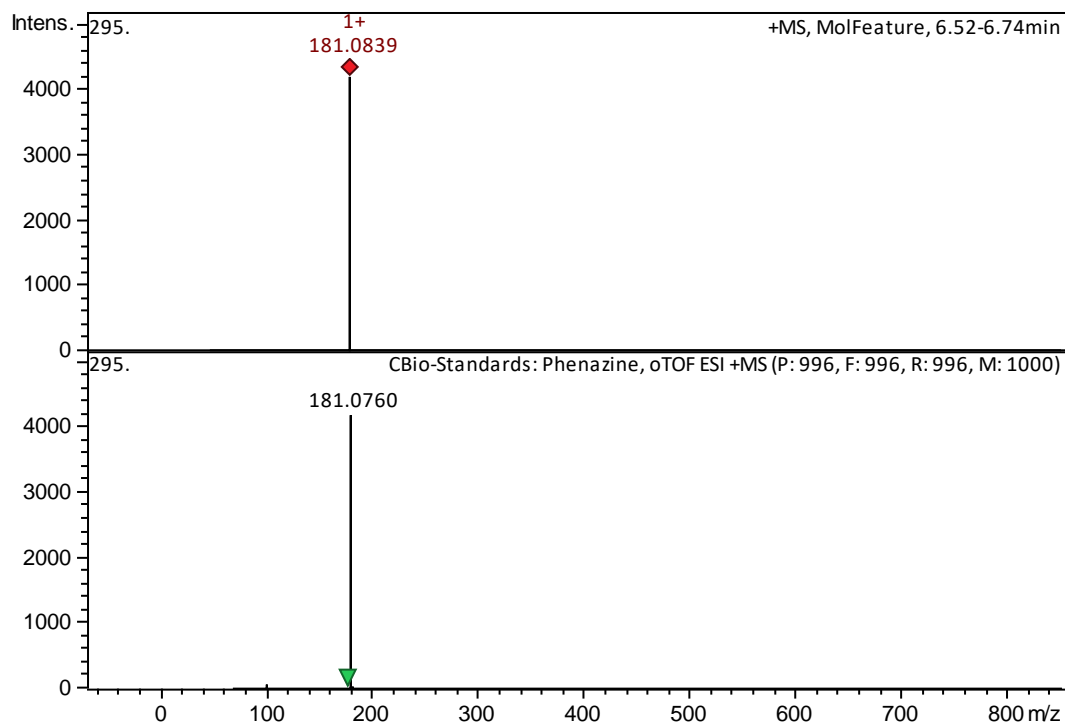
Pyochelin (RT, MS):

UDP-MurNAc-pentapeptide (RT, MS):

UDP-GlcNAc (RT, MS, MS/MS):

Intens.
x10^4

+MS, MolFeature, 1.21-1.49min

M+H
608.0885

CBio-Standards: Uridine 5'-Diphospho-N-acetylgalactosamine, oTOF ESI +MS (P: 480, F: 756, R: 635, M: 100

608.0890
204.0868
405.0101

+MS2(608.0886), 31.5-78.6eV, 1.30min #266

204.0866

CBio-Standards: Uridine 5'-Diphospho-N-acetylglucosamine, oTOF ESI +MS2(608.089), 39.3eV (P: 890, F: 89

138.0547

Spermidine (RT, MS, MS/MS):

Intens.
x10^4

+MS, MolFeature, 0.97-1.17min

1+
146.1656

CBio-Standards: Spermidine, oTOF ESI +MS (P: 785, F: 785, R: 1000, M: 1000)

146.1652
129.1386

+MS2(146.1656), 17.4-43.5eV, 1.00min #196

72.0807
112.1117
146.0826

Bruker MetaboBASE Personal Library: Spermidine, oTOF ESI +MS2(146.165), 10.0-25.0eV (P: 723, F: 821, R:

72.0812
84.0809
112.1121
146.1651

LPE 18:1 (RT, MS, MS/MS)

509.2883 C24H47O9P LPG 18:1; [M-H]- 18.00 min			

Analyte	Score	Fit	Prec. Ion
LPG 18:1; [M-H]-	977.99	995.78	509.2885

Precursor	ColEn. [eV]	Polarity
509.2883	30.4-30.4	NEGATIVE

Library: LipidBlast

m/z meas.: 509.2883 ± 5 ppm

Formula: $C_{24}H_{47}O_9P$

Name: LPG 18:1; [M-H]-

ColEn. [eV]: 30.4 ± 10 eV

Query
x10³ — 152.996, 227.032, 245.043, 281.248

☑ Synchronize y-axes
Spectral Library
x10³ — 152.996, 227.033, 245.043, 281.249

LPE 16:1 (RT, MS, MS/MS)

+MS, MolFeature, 15.67-15.84min, Background Subtracted

M+H
1+
483.2733

M-H2O+H
1+
465.2620

844. Putative-identified_metabolites_vbe14: LPG(16:1)9Z, oTOF ESI +MS (P: 724, F: 987, R: 725, M: 1000)

483.2721

LPE 16:0 (RT, MS, MS/MS)

483.2727 C22H45O9P LPG 16:0; [M-H]- 17.87 min		
Precursor	ColEn. [eV]	Polarity
483.2727	29.6-29.6	NEGATIVE

Library: LipidBlast

m/z meas.: 483.2727 ± 5 ppm

Formula: $C_{22}H_{45}O_9P$

Name: LPG 16:0; [M-H]-

ColEn. [eV]: 29.6 ± 10 eV

Analyte	Score	Fit	Prec. Ion
LPG 16:0; [M-H]-	961.76	985.78	483.2728

Query

x10³

152.996 227.033 255.233

☑ Synchronize y-axes

Spectral Library

x10³

152.996 227.033 245.043 255.233

LPE 16:0 (RT, MS, MS/MS)

Intens. 1235.   +MS, MolFeature, 17.93-18.13min, Background Subtracted

M+H

M-H2O+H
1+
467.2772

1+
485.2885

1235.   Putative-identified_metabolites_vbe14: LPG(16:0), oTOF ESI +MS (P: 627, F: 999, R: 628, M: 1000)

485.2875

PG 34:1 (RT, MS, MS/MS)

747.5182 C40H77O10P PG 34:1; PG...8:1; [M-H]- 13.00 min

Precursor		ColEn. [eV]	Polarity
	747.5182	39.9-39.9	NEGATIVE

Analyte	Score	Fit	Prec. Ion	ColEn. [eV]
PG 34:1; PG 16:0-18:1; [M-H	903.67	936.60	747.5176	
PG 34:1; PG 18:0-16:1; [M-H	37.16	700.13	747.5176	

Library: LipidBlast

m/z meas.: 747.5182 ± 5 mDa

Formula: $C_{40}H_{77}O_{10}P$

Name: PG 34:1; PG 16:0-18:1; [M-H]-

ColEn. [eV]: 39.9 ± 10 eV

Query

x10³
0.6
0.3
0.0
112.986 152.996 255.233 281.249

☑ Synchronize y-axes

Spectral Library

x10³
0.6
0.3
0.0
255.232 281.248 465.262 483.272 509.288

C9:1-PQS (RT, MS, MS/MS)

Intens.
x10⁶
286.1876   571.3546   856.5289   1426.8734   WT_MIC_1_GD5_01_28344.d: +MS, 14.41min #3290

x10⁶   286.1826   WT_MIC_1_GD5_01_28344.d: +MS2(286.1876), 18.4-46.1eV, 14.41min #3291

x10⁶   286.1815   WT_MIC_1_GD5_01_28344.d: +MS2(286.1876), 21.6-54.0eV, 14.41min #3292

x10⁶   286.1823   WT_MIC_1_GD5_01_28344.d: +MS2(571.3546), 30.3-75.7eV, 14.42min #3293

x10⁶   286.1820   WT_MIC_1_GD5_01_28344.d: +MS2(856.5289), 39.4-98.5eV, 14.42min #3294

x10⁶   286.1821   571.3558   WT_MIC_1_GD5_01_28344.d: +MS2(1426.8734), 44.0-110.0eV, 14.43min #3295

200   400   600   800   1000   1200   1400   m/z

Azithromycin C38H72N2O12 [M+2H]2+

mga06_SE_AZI1_BE5_01_21048.d: +MS, 9.11-9.32min #2120-2170

Compass IsotopePattern

$C_{38}H_{72}N_2O_{12}$

Chemical | M+H | z: 2

Building block: <none>

#	m/z	Abundance	Isotopomer
1	375.261539	100.000	^12C38^1H7
2	375.763197	43.139	^12C37^13C
3	376.264599	11.547	^12C 36 ^13
4	376.765962	2.306	^12C 35 ^13
5	377.267282	0.376	^12C 36 ^13
6	377.768581	0.052	^12C 35 ^13
7	378.269862	0.006	^12C 34 ^13

Resolution: 15000

FWHM: 0.025

Isotope threshold [%]: 0.001

Hill sorted sum formula: $C_{38}H_{74}N_2O_{12}$

Elemental composition: C 60.77% H 9.93% N 3.73% O 25.56%

Monoisotopic neutral mass: 748.508526

Nominal neutral mass: 748

Average neutral mass: 748.985964

Erythromycin $C_{37}H_{67}NO_{13}$

Lomefloxacin

+MS, MolFeature, 8.34-8.54min, Background Subtracted
1+
352.1471

+MS2(352.1471), 23.6-58.9eV, 8.45min #1874
308.1570
265.1144
352.1476
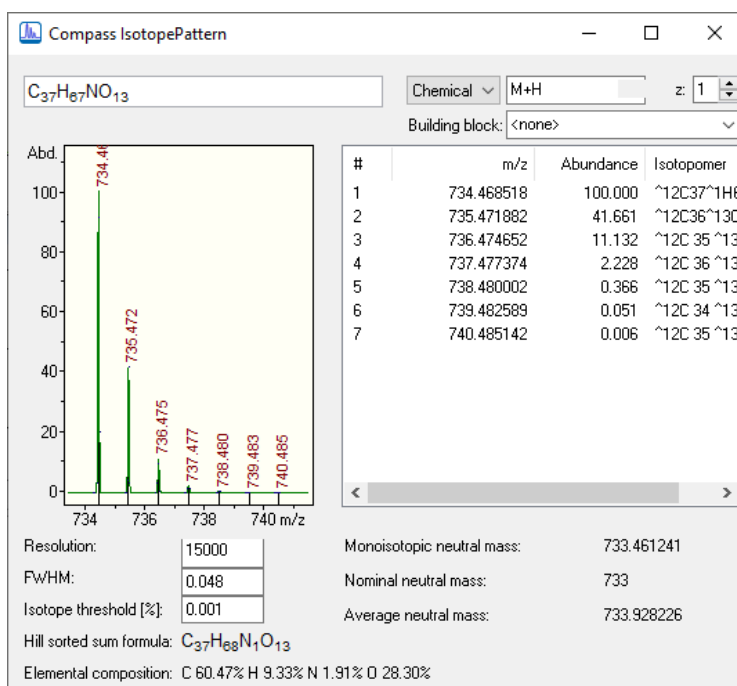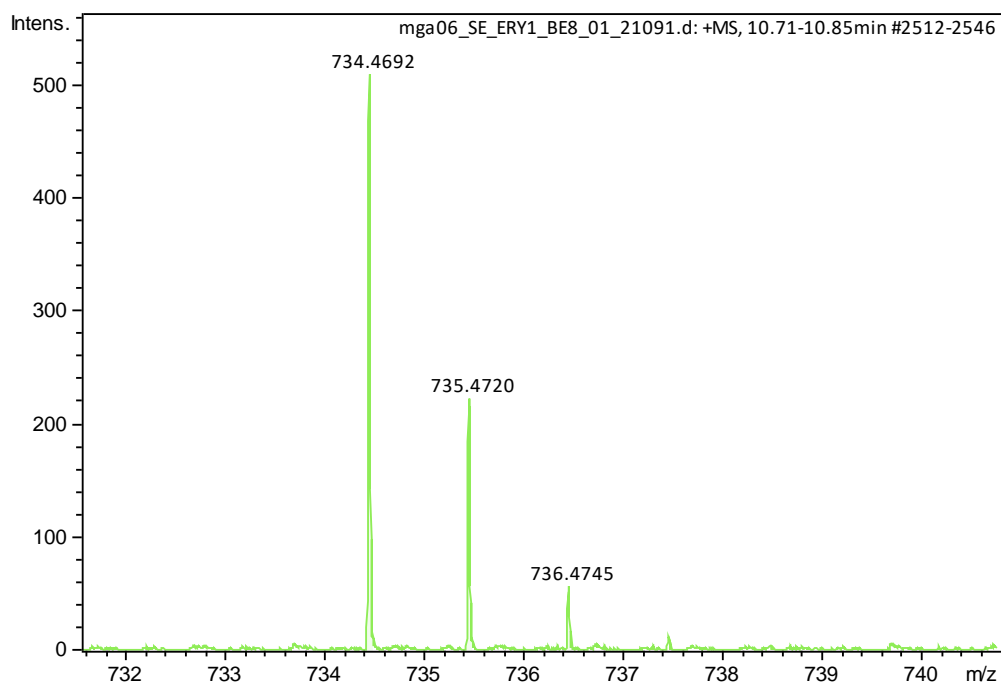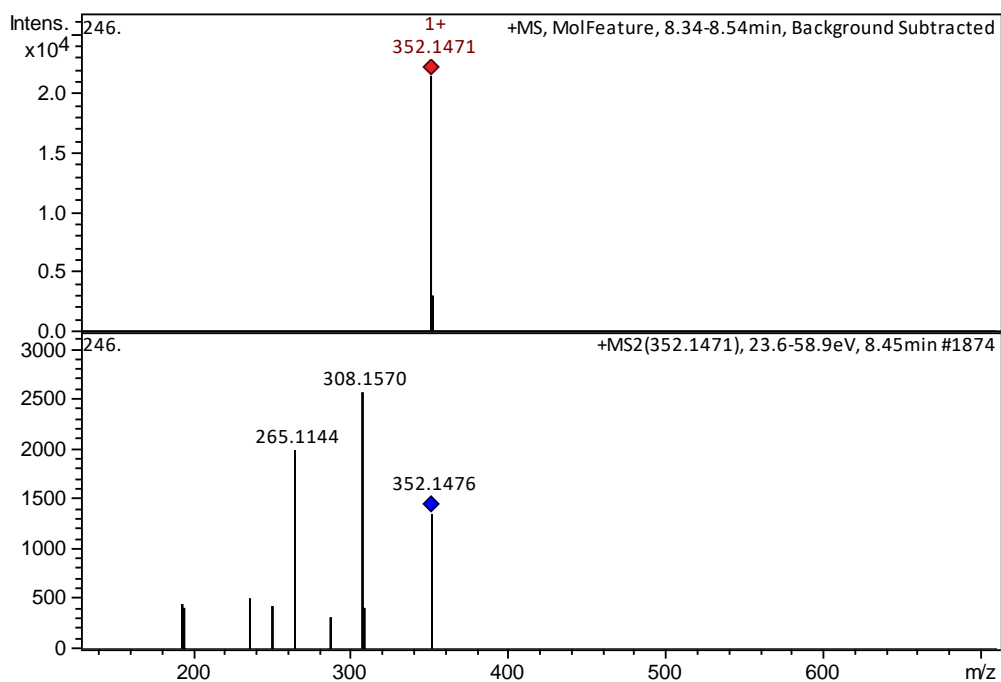
Compass LibraryEditor - [rmf_pseudomonas]

File Edit Compound Spectrum View Window Help

Compound:	34	Name:	Rha-Rha-C10-C12
Nominal mass:	678	CAS number:		InChl key:		InChl & SMILES...
Monoiso. mass:	678.419042	Chem. formula:	$C_{34}H_{62}O_{13}$	External DBs...
Average mass:	678.849611	Comment:	or isomer	Synonyms...

Mass Spectra   UV Spectra

Spectrum: 66

Acquisition Parameters   Spectrum Info   Mass List

ESI-TOF ESI +MS
ESI-TOF ESI +MS2(679.427), 42.2eV

Instrument type:	ESI-TOF	Ionization method:	ESI	Ion polarity:	pos.
MS/MS stage:	2	Precursor ions (m/z):	679.4269	Base peak (m/z):	153.1272
Trap drive:	0	Fragm. amplitude [V]:	0	Isolation width (m/z):	5.35885
Collision gas:			Collision gas pressure [hPa]:	0
Reagent ion:			Reagent gas pressure [hPa]:	0
Collision energy [eV]:	42.1769	Base peak intensity:	2288	Peak width (m/z):	0.012

Structure:

Abund.
153.1272
199.1687
129.0542
239.0912
275.1121
85.0278
387.3095

For Help, press F1   mga15   NUM

V.   GNPS clustering

Table A8. GNPS clustering information in positive mode

RTMean (s)	precursor mass m/z	Cluster_number	Compound_Name
1652.95	89.507	-1	
1653.03	113.964	-1	
564.99	120.070	-1	
1672.55	122.081	-1	
1648.62	124.087	-1	
1667.56	128.950	-1	
1670.27	145.930	-1	
63.41	146.165	-1	SPERMIDINE
71.44	148.061	-1	Spectral Match to L-Glutamic acid from NIST14
498.69	162.055	-1	Massbank:PB000618 1H-indole-3-carboxylic acid
479.33	182.051	-1	Spectral Match to L-Tyrosine from NIST14
482.08	183.092	-1	
739.32	185.097	-1	
667.52	186.131	-1	
430.89	195.088	-1	Massbank:EA030305 Caffeine|1,3,7-trimethyl-3,7-dihydro-1H-purine-2,6-dione|1,3,7-trimethylpurine-2,6-dione
1729.49	199.997	-1	
1643.12	202.181	-1	HIPPURATE
348.91	205.097	-1	Spectral Match to L-Tryptophan from NIST14
644.26	222.023	-1	
679.14	225.066	-1	phenazine-1-carboxylic acid
1556.27	226.952	-1	
437.72	229.097	-1	
649.63	230.118	-1	
1744.89	234.951	-1	
876.41	244.228	-1	
729.74	251.576	-1	
1073.01	264.167	-1	
809.49	267.123	-1	
543.94	275.031	-1	
441.36	275.114	-1	
621.14	279.113	-1	
1116.37	280.163	-1	
1108.63	282.138	-1	
1177.11	283.264	-1	
804.11	292.155	-1	
1100.05	293.171	-1	
1230.67	294.179	-1	
1185.94	296.237	-1	
1050.90	297.241	-1	
1028.80	298.347	-1	
786.42	300.160	-1	
833.76	302.175	-1	
773.95	302.176	-1	
841.23	302.193	-1	
109.66	302.478	-1	
764.01	304.190	-1	
715.02	307.022	-1	HPTzTn-COOH
852.01	308.162	-1	
866.51	312.195	-1	
965.15	319.224	-1	
729.65	321.102	-1	
697.13	325.067	-1	
707.04	325.069	-1	Pyochelin
1036.14	326.379	-1	
917.03	328.192	-1	
764.61	330.208	-1	
833.15	330.208	-1	
1081.95	407.249	-1	
1033.59	415.724	-1	

1035.83	425.215	-1	
832.01	429.218	-1	
1120.64	429.739	-1	
1146.53	430.296	-1	
391.11	432.027	-1	
1293.63	440.317	-1	
729.06	446.187	-1	Glipizide
428.36	457.113	-1	
1296.96	470.421	-1	
782.04	487.333	-1	
1296.37	492.403	-1	
761.17	515.292	-1	
80.47	519.179	-1	
339.12	525.183	-1	
1252.18	537.376	-1	
841.75	547.354	-1	
1148.01	559.132	-1	
1187.65	573.399	-1	
1265.65	577.408	-1	
847.35	583.257	-1	
798.88	583.257	-1	
323.94	597.678	-1	
1216.29	599.388	-1	
878.97	616.176	-1	Spectral Match to Hemin cation from NIST14
913.66	624.389	-1	
1325.26	645.490	-1	
977.45	655.446	-1	
1017.18	683.479	-1	
370.36	693.766	-1	
1456.75	708.511	-1	
740.88	729.239	-1	
387.66	730.242	-1	
1104.65	751.437	-1	
413.13	786.166	-1	
1035.48	827.439	-1	
896.43	903.367	-1	
1019.31	907.579	-1	Spectral Match to 1-Hexadecanoyl-sn-glycero-3-phosphoethanolamine from NIST14
1271.38	1079.600	-1	
1074.18	1087.710	-1	
913.99	452.278	1	
910.19	452.278	1	
1010.18	454.293	1	Spectral Match to 1-Palmitoyl-2-hydroxy-sn-glycero-3-phosphoethanolamine from NIST14
1005.44	454.294	1	Spectral Match to 1-Palmitoyl-2-hydroxy-sn-glycero-3-phosphoethanolamine from NIST14
1028.77	480.309	1	Spectral Match to 1-(9Z-Octadecenoyl)-sn-glycero-3-phosphoethanolamine from NIST14
1098.25	494.326	1	
1253.97	689.516	1	PE(16:0/16:1); [M+H]+ C37H73N1O8P1
1226.02	690.507	1	
898.28	716.522	1	
974.94	716.523	1	
784.01	718.539	1	
1117.71	718.539	1	Spectral Match to 1-Hexadecanoyl-2-(9Z-octadecenoyl)-sn-glycero-3-phosphoethanolamine from NIST14
1079.18	718.540	1	
1167.20	749.537	1	
76.72	259.093	2	
76.50	277.104	2	Spectral Match to L-.gamma.-Glutamyl-L-glutamic Acid from NIST14
82.28	406.145	2	
109.12	535.187	2	
98.69	535.188	2	
146.55	664.231	2	
146.44	664.232	2	
66.51	362.927	3	
1536.69	401.938	3	
820.43	430.915	3	
66.41	430.915	3	
1309.95	469.387	3	

1522.74	469.925	3	
1501.73	498.903	3	
1546.49	508.935	3	
1513.35	537.912	3	
1299.41	565.407	3	
1381.71	566.889	3	
1186.17	568.478	3	
1264.43	569.315	3	
1566.51	576.923	3	
1514.21	605.900	3	
1371.84	634.876	3	
1494.37	673.888	3	
1454.71	685.436	3	
1303.90	689.517	3	
1513.00	701.443	3	
1398.43	702.864	3	
1556.11	712.899	3	
1500.13	741.875	3	
1404.51	770.852	3	
1540.11	780.885	3	
1485.86	809.863	3	
1382.47	838.839	3	MS_Contaminant_Sodium_Formate_Cluster
1476.41	877.848	3	
1375.20	906.828	3	MS_Contaminant_Sodium_Formate_Cluster
1516.61	945.838	3	
1358.99	1215.770	3	
659.19	216.139	4	
769.93	242.155	4	
778.71	244.173	4	mixedMS2: 2-(hept-1-en-1-yl)quinolin-4-ol (Series 2 HAQ C7:1) and 2-heptylquinolin-4-ol (Series 1 HAQ C7)
785.28	245.172	4	
734.26	246.150	4	
833.83	256.170	4	
834.26	256.170	4	
969.83	256.292	4	
1167.23	257.248	4	
776.12	258.154	4	
764.35	259.151	4	
833.49	259.169	4	
1042.70	260.165	4	
753.19	260.167	4	
784.84	260.172	4	
791.65	261.169	4	
1135.40	261.169	4	
848.48	268.170	4	
840.47	270.184	4	2-(2-nonen-1-yl)-4-Quinolinol
864.65	270.189	4	2-(2-nonen-1-yl)-4-Quinolinol
895.52	271.181	4	
892.44	272.165	4	
937.25	272.204	4	mixedMS2: 2-(non-1-en-1-yl)quinolin-4-ol (Series 2 HAQ C9:1) and 2-nonylquinolin-4-ol (Series 1 HAQ C9 aka HNQ)
1016.66	273.194	4	
780.09	274.170	4	
825.50	274.182	4	4-hydroxy-2-octylquinoline 1-oxide:Series 4 HAQ C8
725.57	275.118	4	
656.64	276.160	4	
714.22	276.160	4	
883.00	276.160	4	
1124.50	277.175	4	
1127.46	278.183	4	
1151.77	279.191	4	
954.91	281.296	4	
864.40	284.183	4	
1037.82	285.169	4	
890.02	286.188	4	
861.11	287.185	4	

1059.44	287.190	4	
871.61	288.197	4	
1068.38	288.197	4	2-nonylquinoline-3,4-diol:Series 3 HAQ C9
888.98	288.204	4	
768.38	289.199	4	
945.05	289.200	4	
812.77	290.176	4	
925.87	294.185	4	
963.58	296.201	4	
934.75	296.202	4	
956.36	298.218	4	2-(undec-1-en-1-yl)quinolin-4-ol:Series 2 HAQ C11:1
1135.18	299.211	4	
913.86	300.197	4	
1002.48	300.234	4	
1119.83	301.231	4	
820.68	302.176	4	
915.90	302.211	4	
958.22	304.191	4	
1044.99	309.327	4	
920.94	310.205	4	
921.14	311.255	4	
803.60	312.197	4	
951.83	312.200	4	
973.86	313.222	4	
1069.36	314.212	4	
921.76	314.213	4	
937.91	314.218	4	C11-PQS, C11:db-UQNO
943.41	315.216	4	
904.60	316.192	4	
955.17	316.233	4	
997.57	317.229	4	
1006.21	324.233	4	
1021.91	326.248	4	
1018.35	328.241	4	
996.37	330.207	4	
824.14	330.207	4	
1049.01	332.223	4	
872.80	332.223	4	
1014.66	339.290	4	
986.73	340.227	4	
974.73	340.227	4	
1050.74	341.266	4	
1031.07	342.246	4	
1020.82	343.241	4	
1091.59	344.259	4	
1113.12	352.264	4	
1121.37	354.280	4	
1197.41	356.295	4	
904.31	358.238	4	
979.04	360.254	4	
1076.84	368.259	4	
1155.83	370.275	4	
1107.16	370.275	4	
1191.45	372.290	4	
1192.29	372.290	4	
1215.74	380.295	4	
1212.53	382.311	4	
1212.80	382.311	4	
1169.75	396.290	4	
1201.18	398.306	4	
1201.60	398.306	4	
78.78	324.060	6	
81.50	348.070	6	Spectral Match to Adenosine 5'-monophosphate from NIST14
77.87	428.037	6	Spectral Match to Adenosine 5'-diphosphate from NIST14
81.39	664.115	6	Spectral Match to .beta.-Nicotinamide adenine dinucleotide from NIST14
81.94	664.147	6	Spectral Match to .beta.-Nicotinamide adenine dinucleotide from NIST14

780.27	304.192	7	
988.42	328.199	7	
971.62	330.207	7	
1208.19	412.285	7	
1228.23	414.301	7	
1032.56	474.322	7	
888.47	539.364	7	
889.74	541.379	7	
891.64	543.394	7	
994.93	557.374	7	
891.89	559.389	7	
888.07	561.345	7	
889.03	561.345	7	
863.60	571.354	7	
1155.88	573.370	7	
892.81	575.385	7	
895.97	576.391	7	
864.54	856.528	7	
893.66	862.575	7	
865.62	1427.880	7	
751.01	228.196	8	MUCIC ACID
934.84	279.232	8	Spectral Match to 9(10)-EpOME from NIST14
824.22	297.243	8	Spectral Match to 9(10)-EpOME from NIST14
1308.33	338.342	8	Spectral Match to 13-Docosenamide, (Z)- from NIST14
1185.49	573.434	8	
1148.09	575.105	8	
1148.84	575.106	8	
818.99	496.245	9	
821.04	496.247	9	
790.55	519.319	9	
788.84	519.323	9	
793.48	520.314	9	
790.09	778.481	9	
790.63	1296.800	9	
992.61	527.319	10	
1060.43	543.322	10	
1061.94	543.322	10	
1038.53	553.335	10	
1077.67	553.343	10	
1071.69	555.351	10	
1074.28	555.351	10	
1101.84	555.360	10	
1086.57	569.338	10	
1139.02	571.354	10	
1115.86	581.367	10	
1150.05	583.382	10	
1156.74	597.370	10	
947.87	673.377	10	Rha-C10-C10 Na+
947.81	673.378	10	Rha-C10-C10 Na+
1026.89	701.409	10	
1067.94	727.425	10	
1104.69	729.440	10	
1104.01	729.440	10	
365.91	359.644	11	
351.38	367.641	11	
350.92	367.641	11	
697.71	226.181	13	
698.14	244.191	13	
969.94	359.280	13	Rhamnolipid C10-C10 base lipid no sugar
1039.25	385.295	13	
1051.16	387.311	13	
1104.64	415.342	13	
676.90	232.134	14	
679.67	233.133	14	
680.61	264.175	14	MoNA:976720 Nortriptyline (INN)
682.48	265.174	14	

885.54	306.185	14	
695.12	272.129	15	
830.12	300.160	15	
799.22	159.068	17	
459.80	176.071	17	
1157.19	291.191	18	
807.34	302.176	18	
910.24	474.260	19	
1014.51	476.275	19	Spectral Match to 1-Palmitoyl-2-hydroxy-sn-glycero-3-phosphoethanolamine from NIST14
1029.35	502.291	19	Spectral Match to 1-(9Z-Octadecenoyl)-sn-glycero-3-phosphoethanolamine from NIST14
946.74	505.254	19	
1049.90	507.270	19	
1225.51	712.490	19	
1008.96	738.506	19	
1184.34	740.520	19	
1232.97	740.521	19	
1275.75	741.522	19	
1205.87	769.497	19	
1198.38	769.501	19	
1197.31	771.515	19	
1165.45	771.520	19	
79.63	242.562	20	
538.92	282.122	20	
511.66	294.761	20	
534.22	295.432	20	
318.33	304.078	20	
93.78	306.075	20	
97.94	307.083	20	Spectral Match to Glutathione, oxidized from NIST14
115.16	307.084	20	Spectral Match to Glutathione, oxidized from NIST14
81.52	308.091	20	GLUTATHIONE REDUCED
511.42	441.637	20	
534.21	442.644	20	
534.56	454.644	20	
820.57	326.175	21	
820.75	326.176	21	
1140.28	282.222	22	
1139.72	282.222	22	
77.24	299.085	23	
78.62	301.115	23	
62.76	110.009	24	
63.07	128.019	24	
60.97	129.139	24	
63.96	151.035	24	
981.71	521.318	25	
1251.41	547.333	25	
1048.82	549.347	25	
876.28	302.176	26	
818.81	342.171	26	
746.40	344.187	26	
1684.49	139.965	27	
1660.88	141.959	27	
1659.69	158.003	27	
1511.93	158.003	27	
1668.72	158.963	27	
1742.56	159.969	27	
1766.14	174.972	27	
1434.44	176.017	27	
1597.70	182.980	27	
1664.14	184.970	27	
1763.78	186.956	27	
1674.80	186.957	27	
1458.25	786.533	28	
1456.46	786.534	28	
100.38	332.562	29	Spectral Match to .beta.-Nicotinamide adenine dinucleotide from NIST14
81.76	332.562	29	Spectral Match to .beta.-Nicotinamide adenine dinucleotide from NIST14
995.65	597.441	30	

996.24	599.457	30	
928.89	611.421	30	
995.37	615.451	30	
942.72	627.416	30	
993.23	631.447	30	
993.90	631.447	30	
930.96	940.619	30	
1670.18	130.008	31	
1540.93	132.062	31	
959.81	132.064	31	
1026.89	132.066	31	
1735.34	133.070	31	
779.63	328.189	32	
780.23	328.191	32	
1073.48	577.332	33	
1073.58	577.333	33	
766.63	274.145	35	
870.61	302.176	35	
788.49	172.076	36	
787.55	186.091	36	
1690.01	97.514	38	
1690.39	97.969	38	
1657.41	98.512	38	
1646.51	99.512	38	
1561.03	122.089	40	
1464.86	124.087	40	
1498.80	144.982	40	
1502.04	146.987	40	
1602.13	148.112	40	
1209.18	436.399	41	
1192.58	524.452	41	
885.47	608.183	42	
905.13	624.178	42	
390.24	364.618	46	
381.23	365.626	46	
648.63	197.071	48	
660.88	207.056	48	
389.63	211.087	48	Spectral Match to Pyocyanin from NIST14
631.84	224.082	48	
632.97	224.083	48	
698.10	226.180	48	
1690.19	150.057	49	
1686.13	172.058	49	
1282.51	939.596	50	
1271.01	1011.620	50	
1385.72	1199.770	50	
181.38	166.087	54	L-phenylalanine
739.46	231.103	54	MassbankEU:SM854403 Naproxen|2-(6-methoxynaphthalen-2-yl)propanoic acid
740.60	250.076	54	
739.90	250.076	54	
870.12	184.076	55	
846.71	198.091	55	
443.46	291.146	56	Massbank:EA019905 Trimethoprim|2,4-Diamino-5-(3,4,5-trimethoxybenzyl)pyrimidine|5-[(3,4,5-trimethoxyphenyl)methyl]pyrimidine-2,4-diamine
444.47	292.149	56	
791.59	341.197	59	
809.87	397.259	59	
1111.54	657.437	59	
336.08	488.192	61	
133.43	497.197	61	
948.81	651.395	62	
1029.20	679.426	62	
1685.51	110.009	63	
1700.15	110.009	63	
753.47	284.166	65	
817.59	310.181	65	

Table A9. GNPS clustering information in negative mode

RTMean (s)	precursor mass m/z	Cluster_number	Compound_Name
790.57	169.091	-1	
801.57	170.086	-1	
87.88	191.046	-1	Citric acid
1641.85	248.986	-1	
75.36	251.020	-1	
76.97	253.038	-1	
71.54	268.828	-1	
837.49	274.171	-1	
831.14	293.203	-1	
812.88	298.173	-1	
829.48	302.203	-1	
1026.48	311.196	-1	5,6,2'-Trimethoxyflavone
867.26	313.266	-1	
1009.70	314.240	-1	
1090.01	325.212	-1	2,4-dihydroxyheptadec-16-ynyl acetate
1264.35	381.203	-1	
861.14	393.258	-1	
852.25	395.274	-1	
435.49	455.129	-1	
796.72	485.351	-1	
89.03	495.217	-1	
773.20	513.310	-1	
802.84	517.341	-1	
857.55	545.374	-1	
312.98	621.205	-1	
1003.46	649.415	-1	
1003.09	653.473	-1	
1126.17	653.546	-1	
1149.05	705.578	-1	
418.63	784.196	-1	FAD
1306.60	792.944	-1	
1179.11	841.466	-1	
1292.36	859.586	-1	
1092.26	1355.910	-1	
792.58	240.165	1	
795.24	242.181	1	
928.51	257.168	1	
927.91	258.175	1	
876.64	267.189	1	
891.89	268.197	1	
909.51	270.213	1	
927.88	274.171	1	
1034.38	285.200	1	
974.86	286.208	1	
953.16	294.214	1	
976.76	296.229	1	
1020.32	298.245	1	
1017.91	298.245	1	
1032.91	302.203	1	
1047.52	322.245	1	
1055.53	324.261	1	
1125.44	326.277	1	
1127.47	326.277	1	
1069.65	328.220	1	
1069.76	328.220	1	
1147.67	352.293	1	
770.57	255.147	2	

771.86	256.160	2
771.53	256.160	2
801.50	258.176	2
826.39	270.176	2
856.21	272.192	2
855.62	272.193	2
873.26	284.192	2
909.27	286.208	2
941.57	293.205	2
903.27	298.208	2
901.07	298.208	2
962.44	300.224	2
796.19	302.203	2
949.09	310.210	2
961.60	312.224	2
1013.36	314.240	2
984.63	326.237	2
899.04	330.235	2
1018.77	338.241	2
1056.05	340.256	2
1118.00	342.272	2
882.30	352.182	2
914.87	354.197	2
1138.64	368.288	2
984.82	380.213	2
1014.00	382.229	2
1045.06	408.245	2
904.97	537.384	2
884.49	553.380	2
908.23	555.396	2
876.78	569.375	2
854.76	569.376	2
1186.52	571.390	2
910.55	573.407	2
935.28	597.407	2
901.94	597.408	2
1020.69	597.480	2
977.27	599.423	2
1012.88	601.438	2
933.50	609.409	2
1019.99	613.476	2
939.26	621.409	2
946.77	623.427	2
968.85	625.440	2
1017.30	629.471	2
1013.66	629.472	2
1047.56	681.507	2
881.60	854.561	2
912.36	860.608	2
1049.65	647.499	3
1049.86	649.514	3
1049.51	665.509	3
1045.15	681.505	3
1198.70	653.447	4
1196.96	655.461	4
1197.91	655.463	4
1187.86	727.485	4
1359.80	915.650	4
1347.77	987.676	4
1489.91	462.989	5

1498.61	530.979	5	
1465.55	598.971	5	
1460.98	666.958	5	
1473.42	734.949	5	
1466.53	802.939	5	
902.79	450.294	6	
968.00	452.310	6	Spectral Match to 1-Palmitoyl-2-hydroxy-sn-glycero-3-phosphoethanolamine from NIST14
990.48	478.327	6	Spectral Match to 1-(9Z-Octadecenoyl)-sn-glycero-3-phosphoethanolamine from NIST14
969.85	481.290	6	
1056.54	483.306	6	
1090.30	509.322	6	
898.06	518.284	6	
973.05	520.300	6	
994.62	546.317	6	
1041.66	551.296	6	
1091.51	577.313	6	
896.82	586.275	6	
1080.88	645.304	6	
1233.95	688.535	6	
1264.35	714.551	6	
1187.94	716.567	6	Spectral Match to 1-Oleoyl-2-palmitoyl-sn-glycero-3-phosphoethanolamine from NIST14
1000.22	717.410	6	
977.58	717.451	6	PE(16:0/18:1); [M-H]- C39H75N1O8P1
1053.21	743.427	6	
1053.60	743.428	6	
1090.56	745.444	6	
1113.75	745.488	6	
1110.36	745.495	6	
1131.14	747.563	6	[2,3-dihydroxypropoxy][3-(hexadecanoyloxy)-2-[octadec-9-enoyloxy]propoxy]phosphinic acid
1087.07	747.568	6	
1079.08	748.569	6	PG(16:0/18:1); [M-H]- C40H76O10P1
1238.58	756.527	6	
1177.90	773.475	6	
1178.98	773.476	6	
1179.54	773.478	6	
1260.65	782.542	6	
1289.30	784.558	6	
1000.97	785.401	6	
1090.57	813.435	6	
1093.72	813.435	6	
1258.86	850.534	6	
1275.03	852.554	6	
763.77	512.193	7	
764.07	580.182	7	
1342.81	316.974	8	
1467.83	452.958	8	
1455.91	588.932	8	
78.09	565.083	9	ReSpect:PT203680 Uridine-5'-diphospho-glucose disodium salt|UDPG|UDP-Glc|UDP-glucose|Uridine-5'-diphospho-glucose|UDP-glucopyranoside|[[(2R,3S,4R,5R)-5-(2,4-dioxopyrimidin-1-yl)-3,4-dihydroxyoxolan-2-yl]methoxy-hydrox
327.56	595.702	9	
78.05	606.113	9	ReSpect:PT203700 Uridine-5'-diphospho-N-acetylglucosamine sodium salt|UDPAG|UDP-GlcNAc|UDP-N-acetylglucosamine|[(2R,3R,4R,5S,6R)-3-acetamido-4,5-dihydroxy-6-(hydroxymethyl)oxan-2-yl] [[(2R,3S,4R,5R)-5-(2,4-dioxopyrim
1062.33	503.356	10	
1115.49	529.373	10	
1153.96	531.389	10	
1200.58	557.406	10	
1237.86	559.421	10	
1063.47	571.347	10	

1066.00	571.348	10	
1115.87	597.364	10	
1117.05	597.364	10	
1154.34	599.379	10	
1157.09	599.380	10	
1063.62	639.336	10	
1062.65	639.338	10	
999.42	649.421	10	
1116.74	665.356	10	
1155.02	667.369	10	
1154.72	667.370	10	
1052.15	675.438	10	
1089.61	677.453	10	
1133.45	703.470	10	
1124.35	703.470	10	
1177.91	705.486	10	
1177.06	705.488	10	
1063.84	1007.710	10	
1156.76	1063.770	10	
1511.03	355.987	11	
1468.43	423.977	11	
1427.72	489.310	11	
1456.22	491.968	11	
1470.77	559.958	11	
1457.99	627.948	11	
1480.52	695.933	11	
1469.03	763.933	11	
82.87	426.053	12	ADENOSINE 5'-DIPHOSPHATE
105.60	662.143	12	ReSpect:PT203860 beta-Nicotinamide adenine dinucleotide hydrate|beta-NAD|beta-DPN|Diphosphopyridine nucleotide|Coenzyme1|Cozymase|Nadide|[(2R,3S,4R,5R)-5-(6-aminopurin-9-yl)-3,4-dihydroxyoxolan-2-yl]methyl [[(2R,3S,4R
86.55	742.112	12	BETA-NICOTINAMIDE ADENINE DINUCLEOTIDE PHOSPHATE
81.99	322.072	13	CMP
87.27	323.056	13	URIDINE MONOPHOSPHATE
85.10	323.056	13	URIDINE MONOPHOSPHATE
88.07	346.085	13	2'-DEOXYGUANOSINE 5'-MONOPHOSPHATE
844.23	282.177	14	
839.20	324.188	14	
785.80	326.204	14	
1198.01	701.469	15	
1359.73	961.659	15	
75.18	193.061	17	D-sorbosonic acid
73.92	195.076	17	Spectral Match to D-Gluconic acid from NIST14
1452.28	831.858	18	
1429.16	831.925	18	
82.18	275.115	19	
84.09	275.115	19	
763.12	444.203	20	
760.15	444.203	20	

VI.   CluMSID clustering

Table A10. CluMSID clustering information in positive mode

RT (s)	m/z	Cluster_ID	Neutral Losses Cluster
161.57	106.9920	1	25
125.60	130.0073	1	17
201.47	130.0093	1	53
236.08	130.0082	1	2
313.84	130.0095	1	53
342.08	130.0070	1	17
415.19	130.0074	1	17
425.08	130.0097	1	53
460.44	130.0077	1	17
520.05	130.0072	1	17
522.64	130.0095	1	53
522.90	130.0057	1	50
565.86	130.0063	1	50
574.97	130.0113	1	13
603.04	130.0083	1	17
625.14	130.0091	1	2
675.09	130.0083	1	214
768.79	130.0091	1	53
477.60	132.0076	1	160
186.82	132.0623	1	73
247.80	132.0609	1	62
314.23	132.0618	1	73
393.87	132.0637	1	4
45.23	132.0639	1	4
473.18	132.0623	1	73
541.65	132.0624	1	73
612.15	132.0624	1	73
756.30	132.0644	1	4
123.28	132.0657	1	1
131.85	132.0686	1	11
137.34	132.0705	1	55
1670.25	132.0657	1	1
184.49	132.0687	1	11
223.84	132.0705	1	55
237.51	132.0680	1	7
267.32	132.0689	1	11
286.10	132.0714	1	78
357.18	132.0659	1	1
37.65	132.0678	1	7
394.92	132.0688	1	11
447.97	132.0675	1	7
46.26	132.0687	1	11
475.52	132.0686	1	11
496.34	132.0662	1	1
509.12	132.0703	1	66
529.41	132.0693	1	11
557.52	132.0700	1	180
598.62	132.0693	1	180
618.64	132.0656	1	1
631.38	132.0677	1	7
634.52	132.0694	1	11
690.08	132.0664	1	1
726.62	132.0686	1	7
746.67	132.0658	1	14
770.74	132.0676	1	7

797.39	132.0658	1	1
902.98	132.0660	1	1
116.66	132.1020	1	25
144.76	132.0031	1	56
1662.31	132.0032	1	2
275.65	132.0028	1	56
302.78	132.0039	1	48
318.91	132.0027	1	56
337.13	132.0050	1	48
376.42	132.0029	1	56
518.49	132.0005	1	131
593.16	132.0035	1	56
615.52	132.0019	1	56
98.59	132.0042	1	48
134.98	133.9777	1	54
242.06	133.9781	1	84
337.90	133.9801	1	110
531.22	134.0716	1	173
183.44	134.9432	1	71
362.63	136.0732	1	121
72.68	148.0609	1	25
306.03	150.0758	1	14
320.21	150.0780	1	67
466.94	150.0774	1	71
261.06	154.0446	1	92
186.57	154.0476	1	72
255.34	154.0484	1	86
49.38	154.0507	1	18
347.95	172.0574	1	47
376.16	172.0610	1	89
471.87	172.0615	1	89
520.55	172.0582	1	47
521.87	172.0564	1	169
529.91	172.0601	1	47
576.27	172.0608	1	89
616.95	172.0562	1	169
660.52	172.0576	1	47
796.87	172.0590	1	255
561.69	174.1848	1	182
76.72	259.0925	1	37
76.46	277.1029	1	37
366.01	359.6438	1	123
377.85	365.6249	1	124
350.16	367.6417	1	115
340.77	376.6455	1	112
84.52	406.1370	1	43
81.41	406.1453	1	37
109.77	535.1878	1	37
147.75	664.2321	1	59
367.57	718.2780	1	108
385.26	730.2422	1	128
178.89	110.0090	2	2
250.66	110.0100	2	90
273.32	110.0089	2	2
137.85	113.9633	2	17
1651.68	113.9636	2	2
306.67	113.9637	2	17
543.98	113.9637	2	2
60.04	113.9639	2	2
641.55	113.9649	2	53

693.85	113.9615	2	50
771.90	113.9633	2	17
257.16	113.9651	2	2
301.73	113.9655	2	53
361.08	114.0914	2	32
613.96	114.0899	2	196
622.67	114.0918	2	32
655.59	114.0923	2	202
1671.67	116.9770	2	435
244.15	156.9616	2	87
132.65	158.0060	2	13
181.88	158.0050	2	53
195.98	158.0065	2	13
228.52	158.0051	2	53
278.26	158.0064	2	13
431.57	158.0062	2	13
45.23	158.0066	2	13
495.42	158.0054	2	53
533.83	158.0052	2	53
596.81	158.0057	2	53
1677.38	158.9621	2	2
182.93	158.9646	2	69
222.28	158.9633	2	82
279.18	158.9633	2	82
339.46	158.9579	2	111
348.59	158.9610	2	116
449.52	158.9633	2	82
478.37	158.9626	2	82
530.97	158.9631	2	82
593.42	158.9602	2	185
128.22	158.0050	2	53
139.16	158.0012	2	50
165.73	157.9999	2	16
1669.07	158.0029	2	2
169.36	158.0034	2	2
211.09	158.0005	2	16
243.24	157.9997	2	16
283.48	157.9982	2	95
315.02	158.0049	2	53
322.17	158.0010	2	50
344.56	157.9996	2	16
453.42	158.0010	2	50
46.52	158.0008	2	16
505.99	158.0000	2	16
540.86	158.0011	2	50
570.54	158.0032	2	17
624.63	158.0041	2	2
514.97	159.0655	2	168
275.14	159.9712	2	68
60.30	159.9694	2	23
426.64	160.0763	2	9
175.62	174.9744	2	67
281.92	174.9732	2	71
373.81	174.9741	2	67
656.10	175.1227	2	203
200.93	176.9811	2	32
353.27	186.9592	2	117
721.17	235.1674	2	229
907.64	267.1730	2	281
1654.79	87.0039	2	432

1652.07	89.5066	2	430
70.06	96.9220	2	30
546.84	97.5151	2	175
214.72	97.9698	2	80
260.02	97.9683	2	91
36.08	97.9708	2	12
58.75	97.9687	2	20
1651.43	98.5121	2	26
1658.68	98.5116	2	96
1674.78	98.5093	2	433
320.35	98.5126	2	26
329.84	98.5115	2	96
380.05	98.5130	2	26
415.45	98.5124	2	26
482.68	98.5115	2	96
525.24	98.5133	2	26
626.70	98.5114	2	96
637.38	98.5134	2	159
693.60	98.5126	2	26
735.21	98.5126	2	26
88.41	98.5127	2	26
72.68	98.9844	2	32
1643.89	99.5121	2	430
288.97	99.5310	2	96
475.25	99.5315	2	159
253.27	120.0126	3	53
279.83	120.0097	3	50
294.97	120.0125	3	53
31.91	120.0106	3	2
457.33	120.0109	3	2
465.90	120.0089	3	16
496.86	120.0114	3	2
557.78	120.0126	3	53
586.66	120.0109	3	17
337.39	120.0447	3	109
659.47	121.5477	3	205
1589.30	121.9682	3	424
132.38	122.0793	3	6
1665.69	122.0812	3	3
1675.56	122.0824	3	9
244.66	122.0772	3	88
245.45	122.0807	3	3
247.54	122.0834	3	9
324.64	122.0823	3	9
34.13	122.0812	3	3
340.51	122.0810	3	3
36.08	122.0796	3	6
376.93	122.0846	3	130
38.05	122.0825	3	9
481.24	122.0829	3	9
548.15	122.0817	3	9
97.81	122.0824	3	9
98.84	122.0810	3	3
1524.56	122.0970	3	161
1610.62	122.0967	3	161
1642.86	122.0966	3	161
109.12	123.0554	3	49
451.73	124.0841	3	150
525.51	124.0842	3	150
574.45	124.0838	3	150

598.11	124.0822	3	151
663.13	124.0842	3	150
851.46	124.0840	3	16
1041.52	124.0898	3	60
1280.49	124.0910	3	398
1324.13	124.0906	3	406
1340.24	124.0891	3	60
1382.35	124.0852	3	50
1538.33	124.0879	3	53
206.41	124.0873	3	77
297.05	124.0886	3	77
331.65	124.0856	3	106
429.90	124.0887	3	142
506.11	124.0905	3	164
558.82	124.0926	3	181
573.67	124.0904	3	183
596.03	124.0855	3	50
612.66	124.0924	3	195
636.61	124.0900	3	60
646.22	124.0892	3	142
688.14	124.0899	3	60
834.96	124.0874	3	2
841.60	124.0898	3	60
846.26	124.0890	3	53
919.73	124.0858	3	50
922.96	124.0892	3	53
961.07	124.0900	3	13
976.67	124.0893	3	53
211.59	124.9732	3	78
1588.28	125.0925	3	423
191.53	125.9836	3	16
250.15	125.9849	3	50
294.18	125.9842	3	50
165.47	125.9889	3	60
166.25	125.9858	3	17
1679.45	125.9876	3	53
177.07	125.9882	3	53
251.70	125.9867	3	2
302.52	125.9860	3	17
332.96	125.9869	3	2
34.25	125.9870	3	2
350.41	125.9860	3	17
376.67	125.9873	3	2
450.03	125.9870	3	2
50.43	125.9858	3	17
91.54	125.9870	3	2
58.22	126.9719	3	21
286.61	128.9522	3	8
104.83	141.9594	3	46
1654.14	141.9585	3	2
1668.03	141.9614	3	8
1668.55	141.9630	3	117
1669.46	141.9565	3	5
215.64	141.9569	3	5
237.38	141.9585	3	2
249.36	141.9555	3	5
260.28	141.9566	3	5
261.85	141.9611	3	8
28.53	141.9568	3	5
35.29	141.9611	3	8

50.55	141.9585	3	2
97.55	141.9573	3	5
506.50	144.0633	3	47
559.08	143.9972	3	21
687.61	143.9973	3	21
632.82	145.1043	3	189
1672.97	145.9293	3	434
239.98	146.0815	3	85
333.21	146.0810	3	107
231.52	150.0756	3	6
246.77	150.0772	3	67
39.22	150.0779	3	14
41.17	150.0752	3	14
62.64	164.9703	3	25
118.86	165.0550	3	51
429.76	167.0525	3	144
702.96	169.0514	3	223
188.40	172.0572	3	74
249.89	172.0608	3	89
266.42	172.0585	3	47
52.50	172.0621	3	19
98.34	172.0582	3	47
168.20	173.0785	3	63
345.20	181.0840	3	113
699.59	181.0758	3	221
478.89	181.9876	3	158
236.60	182.9856	3	2
309.80	182.9856	3	2
117.44	184.9692	3	15
220.97	184.9700	3	15
300.96	184.9687	3	15
39.99	184.9698	3	15
398.82	184.9712	3	15
517.97	185.1150	3	167
648.30	186.1311	3	17
1675.04	186.9532	3	16
1668.69	186.9565	3	22
1679.18	186.9598	3	117
273.70	186.9566	3	22
559.34	186.9591	3	117
59.79	186.9564	3	22
528.35	188.1077	3	172
773.47	201.0912	3	51
652.21	213.1466	3	201
1456.16	786.5306	3	414
488.77	215.1404	4	67
55.36	216.9399	4	6
327.51	217.1054	4	105
581.20	234.2064	4	187
125.86	234.9482	4	52
149.31	234.9522	4	32
205.62	234.9523	4	32
236.34	234.9487	4	83
258.46	234.9515	4	32
270.97	234.9484	4	93
278.01	234.9548	4	94
359.51	234.9546	4	114
46.53	234.9516	4	3
213.16	234.9553	4	65
37.26	234.9557	4	10

214.97	236.9396	4	81
196.24	236.9511	4	75
403.50	251.0471	4	137
646.73	256.1337	4	193
508.60	257.1035	4	49
401.94	257.9681	4	53
451.86	257.9696	4	2
534.09	273.1675	4	174
606.42	274.1446	4	193
440.17	275.1142	4	3
213.95	276.1078	4	79
441.98	276.1215	4	15
611.89	276.1598	4	194
672.49	276.1597	4	14
62.39	110.0091	5	2
62.64	128.0196	5	21
64.07	151.0358	5	2
139.41	116.9785	6	57
61.09	146.1654	6	24
432.36	294.1970	6	146
417.53	318.2033	6	141
62.90	82.5373	7	26
1270.09	1011.6161	8	396
1271.38	1027.5905	8	397
1236.52	1027.6123	8	380
1384.42	1199.7741	8	409
1258.64	158.9624	8	390
1274.24	158.9626	8	390
1349.59	158.9627	8	390
1403.14	158.9627	8	390
1426.01	158.9617	8	390
1561.08	158.9617	8	390
1604.88	158.9628	8	390
1366.49	158.9668	8	382
1426.01	158.9654	8	382
1508.71	158.9666	8	382
1565.88	197.9745	8	237
1525.34	197.9769	8	382
68.37	216.9235	8	27
1005.92	226.1599	8	305
1011.63	226.9521	8	27
1082.37	226.9530	8	27
1153.61	226.9498	8	27
1245.64	226.9475	8	384
1294.53	226.9529	8	27
1432.50	226.9489	8	27
1480.89	226.9474	8	384
1560.69	226.9475	8	384
1580.73	226.9537	8	27
66.29	226.9525	8	27
1217.91	226.9555	8	375
1449.65	226.9551	8	375
1592.15	226.9560	8	375
1637.65	236.9858	8	429
1177.51	265.9619	8	27
1225.59	265.9622	8	27
1296.87	265.9643	8	27
1392.48	265.9644	8	27
1420.82	265.9586	8	384
1439.91	265.9607	8	27

1531.19	265.9645	8	27
1541.97	265.9584	8	384
1618.41	265.9645	8	27
1238.08	265.9674	8	375
1484.02	265.9659	8	375
1222.47	294.9402	8	27
1479.85	294.9392	8	27
1525.08	294.9403	8	27
1578.12	294.9408	8	27
1637.52	294.9391	8	27
1478.54	304.9725	8	411
1511.30	304.9691	8	411
1635.32	304.9712	8	411
1516.74	304.9765	8	375
1562.00	304.9754	8	375
1308.95	360.3234	8	405
988.50	362.2108	8	307
1227.40	362.9230	8	28
1284.90	362.9246	8	28
1352.71	362.9240	8	28
1423.80	362.9223	8	28
1304.53	362.9279	8	28
1334.79	362.9313	8	28
1423.68	362.9304	8	28
1540.92	362.9290	8	28
1589.04	362.9288	8	28
1604.89	362.9253	8	28
1641.82	362.9252	8	28
1210.24	363.3105	8	370
1016.57	364.2265	8	315
1441.08	399.3124	8	412
1473.86	399.3080	8	336
1503.25	399.3043	8	418
1451.47	401.9340	8	28
1594.49	401.9346	8	28
1481.66	401.9368	8	28
1535.48	401.9355	8	28
1563.94	401.9408	8	28
1054.80	429.3202	8	329
1288.93	430.9102	8	28
1297.64	430.9148	8	28
1376.62	430.9102	8	28
1470.22	430.9086	8	28
1553.41	430.9075	8	28
1610.22	430.9149	8	28
1610.87	430.9074	8	28
1327.26	430.9207	8	28
1412.75	430.9197	8	28
1462.92	430.9185	8	28
1546.91	430.9160	8	28
66.03	430.9152	8	28
1209.22	441.3554	8	369
1529.74	443.3335	8	420
1077.43	443.3362	8	337
1311.67	469.3866	8	401
1512.08	469.9210	8	28
1575.24	469.9211	8	28
1639.21	469.9225	8	28
1426.78	469.9288	8	28
1433.67	469.9256	8	28

1465.80	469.9292	8	28
1508.19	469.9292	8	28
1554.71	469.9288	8	28
1297.38	470.4212	8	297
1199.10	485.3820	8	369
1078.99	487.3610	8	338
1190.38	489.3564	8	263
1090.81	498.2867	8	340
1433.27	498.8941	8	28
1242.24	498.9048	8	28
1288.02	498.9017	8	28
1334.79	498.9030	8	28
1337.66	498.8967	8	28
1390.40	498.8993	8	28
1398.71	498.9045	8	28
1506.63	498.9021	8	28
1573.69	498.8990	8	28
1609.56	498.8955	8	28
1641.29	498.9009	8	28
1066.24	501.0871	8	335
1590.08	507.3251	8	425
1273.47	513.4124	8	399
1316.89	513.4128	8	399
1262.41	527.3905	8	393
1373.76	537.9119	8	28
1415.22	537.9116	8	28
1444.20	537.9065	8	28
1563.29	537.9118	8	28
1635.83	537.9103	8	28
1267.23	557.4390	8	389
1318.43	557.4387	8	389
1148.41	559.1315	8	356
1350.63	566.8822	8	28
1590.34	566.8846	8	28
1183.49	566.8891	8	28
1237.83	566.8885	8	28
1295.94	566.8922	8	28
1388.06	566.8929	8	28
1642.33	566.8873	8	28
1434.83	566.8954	8	28
1187.52	568.4793	8	213
1263.96	569.3130	8	394
1186.10	573.4350	8	368
1148.27	575.1051	8	357
1590.85	576.9161	8	28
1473.60	576.9256	8	28
1073.40	577.3327	8	296
1262.55	601.4643	8	391
1321.55	601.4648	8	391
1436.39	605.8995	8	28
1562.26	605.8985	8	28
1220.00	633.1503	8	376
1263.19	634.8746	8	28
1365.96	634.8758	8	28
1397.40	634.8804	8	28
1257.09	645.4905	8	389
1324.67	645.4913	8	389
1220.90	649.1243	8	376
1339.71	673.8826	8	28
1448.86	673.8893	8	28

1501.94	673.8857	8	28
1534.43	673.8905	8	28
1625.17	673.8907	8	28
1459.30	685.4252	8	415
1453.30	685.4351	8	413
1254.35	689.5174	8	388
1329.07	689.5165	8	388
1111.48	695.3933	8	348
1323.88	702.8608	8	28
1380.91	702.8613	8	28
1334.53	702.8709	8	28
1268.00	703.4961	8	395
1171.54	705.5115	8	363
1250.58	733.5436	8	386
1333.48	733.5421	8	386
1426.13	741.8742	8	28
1581.50	741.8675	8	28
1603.07	745.5936	8	427
1338.17	770.8445	8	28
1249.28	770.8471	8	28
1292.70	770.8466	8	28
1359.73	770.8550	8	28
1384.67	770.8485	8	28
1246.16	777.5669	8	385
1164.26	793.5632	8	360
1402.09	809.8544	8	28
1212.45	883.5332	8	374
1212.85	899.5074	8	373
1282.18	939.5947	8	374
1282.56	955.5675	8	400
1245.39	955.5901	8	379
70.20	164.9299	9	31
72.80	203.0529	9	34
68.50	232.8972	9	27
66.81	242.9263	9	27
69.55	112.8958	10	29
73.20	104.0708	11	21
72.54	239.0140	12	33
1069.10	749.4066	12	296
1105.74	751.4326	12	345
74.63	115.0368	13	35
458.10	460.2669	13	156
74.36	219.0478	14	36
76.33	299.0847	15	37
143.59	193.0682	16	58
375.91	298.0995	16	129
78.02	324.0591	16	38
106.14	332.5619	16	40
91.16	348.0628	16	45
406.11	348.0701	16	38
81.16	348.0700	16	38
84.27	348.0777	16	42
427.68	349.1844	16	143
412.59	412.5597	16	139
78.02	428.0364	16	39
389.82	432.0264	16	132
109.12	664.1161	16	41
412.33	786.1651	16	138
412.85	808.1452	16	138
119.89	136.0758	17	49

115.50	182.0814	17	25
347.03	188.0710	17	51
677.17	191.0860	17	76
348.06	205.0975	17	21
676.65	233.1336	17	169
569.51	263.1186	17	184
616.32	263.1175	17	184
683.71	264.1674	17	217
676.40	264.1759	17	213
688.26	264.1022	17	165
680.82	265.1725	17	216
554.92	291.1118	17	109
685.28	336.1962	17	141
931.04	336.1951	17	264
1263.45	547.3314	17	394
1048.55	549.3501	17	270
311.10	679.2904	18	98
361.47	679.2888	18	120
85.68	679.2883	18	44
364.18	679.7871	18	122
197.29	103.0536	19	76
170.93	120.0100	19	50
162.61	120.0809	19	49
163.91	120.0827	19	61
146.18	122.0831	19	9
171.71	122.0799	19	64
1481.40	133.9579	19	417
1507.80	136.1122	19	161
1542.48	136.1105	19	421
1242.53	138.1028	19	378
1242.77	138.1010	19	381
1348.30	138.1022	19	407
1386.50	138.1011	19	410
1399.76	138.1026	19	407
1445.50	138.1018	19	407
1528.18	138.1015	19	419
1535.74	138.1027	19	378
1626.73	138.1020	19	407
167.04	166.0821	19	62
198.33	166.0848	19	4
160.02	166.0866	19	25
173.80	166.0904	19	66
181.11	166.0886	19	68
183.18	166.9598	19	70
979.40	212.1447	19	305
525.78	321.1014	19	170
729.24	321.1027	19	170
731.32	347.0825	19	234
591.08	379.1081	19	191
629.56	393.1212	19	198
731.85	446.1811	19	235
728.73	446.1878	19	232
305.90	479.1886	20	97
323.60	597.6782	20	102
324.90	608.6685	20	103
325.16	617.1508	20	104
348.58	693.7651	21	100
358.21	693.7712	21	119
325.93	694.2684	21	99
371.99	694.2681	21	127

948.72	338.2324	22	297
949.50	354.1822	22	296
766.97	413.2534	22	211
317.35	727.2060	22	101
431.32	138.0659	23	109
428.21	195.0883	23	2
432.11	195.0860	23	145
433.67	195.0941	23	147
1678.15	195.9123	23	434
601.62	197.0713	23	51
648.31	197.0708	23	109
400.65	197.0782	23	135
320.47	207.9863	23	2
406.37	120.0445	24	109
407.40	138.0550	24	14
844.20	170.0975	24	268
876.59	266.2103	24	280
619.69	279.1130	24	32
337.65	525.1827	24	108
355.10	686.7594	25	118
368.61	475.4962	26	125
370.44	704.7582	27	126
480.47	183.0919	28	161
484.11	183.0876	28	163
389.96	211.0822	28	51
392.56	211.0798	28	134
383.71	211.0873	28	131
435.22	211.0873	28	131
573.55	211.0871	28	131
437.83	229.0979	28	25
1643.12	202.1801	29	219
391.52	243.1828	29	133
403.50	285.0993	30	49
414.40	285.0967	30	140
539.30	315.1103	30	22
401.68	305.1566	31	136
549.20	243.0882	32	49
501.82	359.1348	32	166
454.47	377.1459	32	154
413.64	439.1013	32	49
426.91	457.1124	32	3
649.60	230.1176	33	148
439.64	261.0987	33	149
454.99	289.1626	33	155
447.19	291.1386	33	152
438.35	291.1461	33	148
443.81	291.1513	33	151
448.48	393.2103	34	153
788.54	159.0678	35	109
895.18	159.0693	35	109
458.63	176.0706	35	25
876.06	184.0765	35	109
960.67	184.0767	35	109
789.05	186.0911	35	131
863.58	198.0919	35	224
658.45	216.1379	35	204
755.13	242.1544	35	219
781.02	244.1701	35	219
801.42	244.2643	35	257
785.43	245.1668	35	250

733.41	246.1492	35	219
833.27	256.1700	35	219
1167.64	257.2474	35	361
612.40	257.9685	35	144
763.99	258.1438	35	246
744.59	258.1499	35	219
816.24	258.1498	35	219
831.58	258.1861	35	219
956.00	259.1594	35	248
824.70	259.1705	35	241
1000.85	260.1645	35	219
1097.05	260.1630	35	219
1194.93	260.1611	35	208
644.92	260.1648	35	3
662.60	260.1608	35	208
708.95	260.1638	35	219
781.53	260.1646	35	219
980.96	260.1616	35	208
1045.42	260.1674	35	197
1168.95	260.1682	35	197
626.18	260.1683	35	197
702.45	260.1670	35	197
754.73	260.1675	35	197
786.47	260.1709	35	252
791.14	260.1705	35	252
904.01	260.1654	35	219
937.02	260.1665	35	219
798.17	261.1586	35	256
788.80	261.1683	35	246
580.68	262.2384	35	94
839.51	268.1707	35	219
842.11	268.1727	35	248
944.30	269.2101	35	295
857.21	270.1803	35	276
851.35	270.1868	35	219
871.00	270.1919	35	252
1060.90	272.1653	35	219
810.41	272.1654	35	219
889.71	272.2088	35	282
891.27	272.2044	35	265
1061.30	273.1735	35	219
830.15	274.1817	35	219
840.54	274.1755	35	246
842.64	274.1842	35	265
844.70	274.1888	35	269
714.67	276.1598	35	32
867.74	276.1605	35	219
1077.83	277.1756	35	269
1139.17	277.1751	35	269
1182.33	277.1752	35	269
1126.16	278.1832	35	269
1143.33	279.1907	35	269
1188.95	279.1908	35	269
1178.30	283.2636	35	264
752.92	284.1655	35	219
818.47	284.1658	35	219
904.80	284.1659	35	219
883.21	284.2025	35	219
940.80	284.2028	35	219
1223.25	284.2953	35	377

670.79	285.1341	35	211
811.70	285.1341	35	211
1084.07	285.1732	35	219
1162.44	285.1726	35	219
984.08	285.1739	35	219
1108.61	286.1808	35	219
1185.06	286.1823	35	219
673.27	286.1818	35	212
711.54	286.1791	35	226
765.42	286.1789	35	6
781.53	286.1802	35	219
845.75	286.1819	35	219
938.06	286.1822	35	219
859.81	286.1860	35	252
862.94	286.1934	35	24
866.06	286.1894	35	269
934.55	286.2182	35	264
549.19	287.1140	35	176
856.68	287.1783	35	274
1130.20	287.1884	35	219
1189.72	287.1886	35	219
863.20	287.1864	35	243
1141.38	287.6898	35	354
1045.29	288.1933	35	243
1202.46	288.1924	35	243
1231.58	288.1895	35	276
982.26	288.1931	35	243
893.36	288.2091	35	24
808.06	288.2901	35	6
1045.69	288.1994	35	265
1080.81	288.1961	35	219
1085.10	288.2001	35	265
1191.28	288.1999	35	265
1245.12	288.1968	35	219
682.91	288.1964	35	3
758.00	288.1969	35	219
814.56	288.1971	35	219
881.39	288.1980	35	219
893.36	288.2009	35	265
965.36	288.2009	35	265
1643.63	288.9212	35	431
908.17	289.1553	35	141
1208.69	289.1964	35	276
755.78	289.2006	35	243
893.62	289.2027	35	243
690.86	290.2702	35	94
1149.43	291.1909	35	269
937.80	296.2030	35	219
943.26	296.1967	35	276
1051.41	297.2415	35	327
1054.26	297.2405	35	327
960.43	298.2184	35	264
972.65	298.2244	35	282
1025.66	298.3482	35	319
1156.73	299.1888	35	219
883.73	300.1905	35	276
995.53	300.2354	35	264
1217.26	300.1964	35	219
899.86	300.1976	35	219
977.84	301.1431	35	304

1167.39	301.2120	35	282
1241.47	301.2035	35	306
655.84	302.1745	35	3
726.11	302.1757	35	71
793.23	302.1758	35	219
859.41	302.1764	35	219
945.87	302.1772	35	219
928.31	302.2132	35	264
784.13	304.1840	35	216
697.63	304.1910	35	14
778.15	304.1909	35	14
814.57	304.1917	35	14
959.91	304.1927	35	219
965.10	304.1942	35	67
836.39	310.1813	35	219
895.70	310.1794	35	219
906.09	310.1866	35	285
984.09	310.2178	35	219
884.89	311.1278	35	281
1101.07	311.2562	35	343
1046.21	312.2335	35	264
977.07	312.2345	35	264
980.19	312.2307	35	306
1048.56	312.1973	35	219
853.69	312.1971	35	219
910.51	312.1981	35	219
918.05	313.1947	35	274
1009.02	314.2144	35	264
1010.33	314.2113	35	306
1238.34	314.2105	35	306
767.23	314.2099	35	226
814.44	314.2126	35	14
877.23	314.2128	35	264
879.57	314.2136	35	264
939.37	314.2139	35	264
931.57	314.2204	35	282
962.77	314.2169	35	265
1047.25	314.2496	35	264
966.15	315.2101	35	274
930.01	315.2161	35	292
820.02	316.1919	35	262
992.41	316.2227	35	292
859.54	316.2289	35	264
940.40	316.2310	35	265
987.33	316.2295	35	264
994.23	316.2320	35	265
990.85	316.2378	35	308
998.64	319.2252	35	313
999.69	324.2338	35	264
1024.62	324.2413	35	282
820.16	326.1764	35	219
951.84	326.2131	35	219
1018.26	326.2499	35	264
1071.96	326.2485	35	264
779.19	328.1913	35	219
978.63	328.2233	35	292
1009.16	328.2286	35	264
973.42	328.2292	35	264
1097.71	328.2643	35	131
1102.62	328.2711	35	344

753.17	330.2067	35	6
834.31	330.2078	35	14
944.82	330.2089	35	264
985.13	330.2080	35	51
1042.56	330.2443	35	264
1049.32	332.2236	35	264
880.35	332.2242	35	32
913.62	334.1795	35	287
984.22	340.2294	35	264
1043.08	342.2448	35	264
1061.81	342.2359	35	292
898.30	342.2449	35	264
1020.99	343.2401	35	317
1019.95	343.2558	35	265
1095.23	344.2521	35	292
1089.91	344.2598	35	71
1122.13	353.2669	35	346
1119.53	354.2726	35	346
1114.86	354.2805	35	281
1205.06	356.2889	35	372
1201.04	356.2951	35	299
915.71	358.2395	35	32
978.89	360.2558	35	71
1077.69	368.2603	35	71
1142.94	369.2979	35	350
1107.06	370.2746	35	71
1153.35	370.2745	35	359
1191.03	372.2902	35	299
1211.81	382.3109	35	281
1005.14	386.2701	35	32
1228.97	414.3008	35	219
1294.26	440.3160	35	285
791.66	519.3110	35	254
788.28	519.3222	35	253
887.36	539.3661	35	270
889.57	541.3818	35	270
890.87	559.3928	35	270
861.10	571.3558	35	270
1154.77	573.3700	35	270
896.23	575.3768	35	284
892.31	575.3881	35	270
996.05	599.4589	35	312
928.44	611.4236	35	291
930.52	627.4186	35	291
992.66	631.4494	35	309
789.05	778.4803	35	253
863.71	856.5321	35	277
892.83	862.5796	35	283
465.13	437.2364	36	157
483.05	248.0910	37	162
493.88	229.0722	38	49
497.12	162.0551	39	165
767.36	274.1442	39	248
527.59	339.0445	40	171
551.54	229.1419	41	177
555.46	229.1353	41	179
551.80	207.1595	42	178
1200.89	407.3370	42	370
1208.95	436.3997	42	213
1193.10	451.3647	42	370

1200.64	480.4269	42	213
1196.22	481.3497	42	371
1193.62	524.4520	42	213
583.56	320.1118	43	188
581.21	320.1155	43	186
589.40	343.1729	44	190
632.43	207.0549	45	199
680.43	207.0555	45	109
630.36	224.0817	45	49
633.49	224.0833	45	21
682.65	225.0607	45	218
679.26	225.0665	45	14
600.18	269.0560	45	67
606.16	387.2015	46	192
632.95	469.1378	47	200
660.78	226.6207	48	206
695.16	272.1289	49	219
786.98	282.1464	49	251
662.08	300.1601	49	207
807.80	300.1601	49	219
856.30	300.1608	49	219
668.83	163.1155	50	209
669.63	363.1781	51	210
809.75	267.1235	52	260
670.92	341.1966	52	211
809.37	341.1970	52	211
680.04	247.0482	53	215
710.50	353.1581	54	220
717.92	397.1848	55	225
700.10	399.2004	55	222
744.85	178.1225	56	241
743.80	185.0906	56	240
704.53	185.0964	56	224
739.38	185.0959	56	224
743.03	231.0948	56	152
738.86	231.1014	56	25
740.68	250.0746	56	239
739.90	253.0834	56	237
715.58	239.2483	57	227
719.35	223.0639	58	228
721.43	230.1543	59	230
723.50	451.2311	60	231
729.76	468.1701	61	232
730.28	251.5763	62	233
733.92	441.2117	63	236
739.63	275.0650	64	238
752.66	381.1885	65	242
856.68	451.1958	65	267
853.81	453.2109	65	273
759.43	149.0238	66	109
759.17	177.0552	66	76
1251.87	393.2985	66	387
762.03	245.0732	67	245
759.44	245.0796	67	244
765.67	435.2356	68	247
783.09	583.2555	69	249
1127.33	256.2637	70	281
771.66	274.2741	70	71
781.01	318.3011	70	94
773.99	230.2479	71	14

805.07	611.2469	72	258
809.11	419.2423	73	259
812.22	435.2160	74	261
875.68	244.2281	75	21
824.96	279.2330	75	264
934.55	279.2339	75	264
824.45	297.2438	75	263
947.69	359.2815	75	263
992.40	359.2812	75	263
1180.38	383.3143	75	367
1052.45	385.2941	75	263
1480.10	385.2907	75	416
1027.48	387.3123	75	263
1073.01	387.3116	75	263
976.28	395.2092	75	303
1069.62	413.3265	75	263
1104.83	415.3425	75	263
911.15	452.2799	75	286
912.32	474.2607	75	288
1038.64	480.3111	75	286
1044.64	480.3032	75	325
975.51	489.2126	75	302
1041.91	502.2934	75	288
949.76	651.3983	75	298
1027.74	679.4299	75	298
824.19	337.2364	76	10
844.45	407.1698	77	266
861.62	308.1635	78	271
853.82	291.1945	79	272
887.10	561.3477	79	270
888.92	563.3638	79	270
856.16	324.1585	80	275
866.58	495.2224	81	278
870.21	435.2006	82	279
915.32	256.3013	83	281
917.00	200.2018	84	289
926.10	320.1999	85	290
995.79	322.2150	85	311
938.58	319.2191	86	294
934.04	319.2268	86	67
934.81	615.4629	86	293
995.00	1031.6605	87	310
1039.95	1083.6847	87	323
1036.06	381.2628	87	296
1081.08	407.2785	87	296
991.36	527.3224	87	296
1038.40	553.3373	87	296
947.95	673.3807	87	296
996.30	699.3944	87	296
952.37	281.2964	88	299
967.96	335.1269	89	300
972.39	411.0959	90	301
1008.77	639.3311	91	314
1017.09	454.2955	92	286
1018.78	476.2776	92	288
1065.73	485.1136	92	334
1059.59	507.2707	92	332
1021.50	507.3318	92	318
1019.68	348.2315	93	316
1074.05	1087.7122	94	298

1115.37	409.2939	94	296
1061.29	543.3227	94	333
1076.92	553.3447	94	333
1078.73	553.3421	94	333
1072.75	555.3518	94	296
1092.11	555.3613	94	270
1130.72	555.3585	94	270
1133.58	555.3571	94	270
1188.16	555.3588	94	270
1084.47	569.3390	94	333
1138.53	571.3536	94	71
1156.99	597.3691	94	14
1025.93	701.4112	94	296
1031.89	701.4008	94	320
1151.53	325.2718	95	358
1031.38	326.3799	95	264
1036.32	326.3755	95	322
1403.40	326.3752	95	322
1176.74	327.2277	95	365
1242.27	329.2417	95	383
1032.41	561.3977	96	321
1220.14	397.3297	97	369
1200.13	398.3057	97	71
1044.12	399.2191	97	324
1102.36	399.3086	97	336
1097.96	350.2461	98	341
1051.28	351.2525	98	326
1308.70	338.3416	99	404
1051.68	341.2677	99	328
1056.35	473.3464	100	330
1057.38	517.3723	101	331
1107.96	581.3672	102	296
1150.23	583.3811	102	296
1068.20	727.4249	102	296
1103.93	729.4407	102	296
1080.29	415.2138	103	339
1233.67	353.3029	104	329
1101.85	355.2825	104	342
1592.41	355.2850	104	426
1107.05	469.3151	105	347
1111.22	679.4193	106	349
1254.75	413.2666	107	219
1124.45	413.3243	107	263
1122.12	457.3511	108	351
1134.37	379.2824	109	352
1139.83	282.2222	110	353
1142.68	282.2190	110	355
1383.12	422.3789	110	408
1167.90	749.5383	111	362
1174.54	661.4865	112	364
1179.87	617.4605	113	366
1192.08	529.4087	114	369
1603.32	129.9845	115	428
1366.21	129.9879	115	46
1469.17	129.9895	115	8
1476.48	129.9863	115	5
1479.33	129.9877	115	46
1515.84	129.9898	115	8
1560.42	129.9886	115	46
1572.13	129.9854	115	5

1576.29	129.9910	115	422
1617.37	129.9895	115	8
1632.96	129.9857	115	5
1635.58	129.9877	115	46
1355.31	131.9611	115	54
1395.72	131.9632	115	73
1403.66	131.9612	115	54
1473.34	131.9615	115	54
1530.00	131.9591	115	417
1547.16	131.9640	115	73
1550.30	131.9613	115	54
1583.06	131.9596	115	417
1585.93	131.9632	115	73
1622.58	131.9619	115	54
1430.94	144.9794	115	16
1479.72	144.9805	115	50
1486.09	144.9836	115	2
1547.04	144.9792	115	16
1608.27	144.9789	115	16
1411.20	144.9854	115	13
1497.79	144.9854	115	13
1597.88	144.9852	115	13
1366.09	146.9804	115	144
1375.05	146.9827	115	13
1469.95	146.9780	115	16
1492.08	146.9810	115	2
1538.21	146.9786	115	50
1545.10	146.9812	115	2
1556.27	146.9831	115	13
1612.43	146.9790	115	50
1244.09	147.0921	115	161
1591.25	186.0074	115	50
1261.50	483.3658	116	392
1311.16	425.3604	117	402
1295.56	492.4023	118	297
1308.82	381.3341	119	403
1670.37	236.9399	120	2

Table A11. CluMSID clustering information in negative mode

RT (s)	m/z	Cluster_ID	Neutral Losses Cluster
36.28	148.0872	1	1
48.69	148.0844	1	3
237.30	148.0868	1	1
149.55	148.0892	1	25
190.32	148.0891	1	25
225.36	148.0890	1	25
261.70	148.0905	1	25
266.78	148.0845	1	3
342.45	148.0846	1	3
340.77	194.0934	1	40
385.01	148.0898	1	25
372.60	148.0875	1	1
375.96	148.0915	1	46
412.30	148.0843	1	3
411.42	148.0860	1	1
459.00	148.0876	1	1
480.46	148.0893	1	25
462.36	148.0822	1	30

513.31	148.0912	1	46
504.25	148.0844	1	3
557.88	148.0874	1	1
581.47	148.0824	1	30
599.55	148.0888	1	25
603.20	148.0847	1	3
606.55	148.0918	1	46
614.29	146.9865	1	56
623.34	148.0862	1	1
632.39	195.0831	1	58
648.44	148.0893	1	25
643.63	148.0835	1	3
664.07	148.0869	1	1
702.05	148.0849	1	3
716.65	148.0868	1	1
760.32	148.0851	1	3
1434.77	148.0865	1	1
1461.62	148.0898	1	25
1466.51	148.0838	1	3
1469.86	194.0945	1	151
1487.82	148.0863	1	1
1487.97	191.0349	1	14
1506.78	191.1347	1	155
1509.10	148.0826	1	30
1511.43	148.0890	1	25
1653.42	146.9641	1	157
1661.16	145.9563	1	159
1671.37	148.0873	1	1
1676.92	194.0938	1	40
44.02	174.9822	2	2
204.58	174.9817	2	2
166.54	174.9845	2	14
146.84	174.9799	2	3
192.37	174.9879	2	28
260.67	174.9844	2	14
269.48	174.9790	2	3
294.12	174.9772	2	30
307.64	174.9798	2	3
360.04	174.9846	2	14
387.06	174.9874	2	28
378.30	174.9798	2	3
420.33	174.9822	2	2
419.82	175.0875	2	1
456.67	174.9860	2	46
470.25	174.9788	2	3
473.76	174.0820	2	53
483.31	174.9816	2	2
509.95	174.9875	2	28
516.67	173.1089	2	54
569.80	174.9825	2	2
576.80	173.1448	2	40
647.79	174.9793	2	3
672.98	174.9847	2	14
677.36	174.9827	2	2
692.11	173.1445	2	40
808.33	174.9840	2	14
1667.86	174.9824	2	2
1677.94	174.9795	2	3
54.67	206.9983	3	2
336.10	206.9960	3	3

365.60	206.9994	3	2
1662.32	206.9990	3	2
63.24	159.0044	4	2
64.27	272.9872	4	4
66.60	248.9877	5	5
67.63	316.9770	5	6
610.93	452.9587	5	55
625.67	261.1312	5	57
687.44	520.9454	5	55
698.83	339.2114	5	62
699.86	385.2190	5	63
707.60	384.9690	5	55
823.07	316.9765	5	6
845.28	316.9732	5	83
864.40	316.9767	5	6
899.03	518.2876	5	68
918.13	316.9770	5	6
989.68	113.0101	5	104
1099.48	316.9783	5	6
1053.51	811.4251	5	117
1066.94	639.3427	5	121
1076.49	248.9880	5	5
1075.98	250.1727	5	122
1083.72	599.3993	5	123
1127.38	113.0089	5	3
1137.45	384.9685	5	55
1265.06	113.0120	5	2
1287.53	113.0103	5	104
1164.33	316.9803	5	55
1173.37	588.9399	5	130
1174.39	384.9667	5	55
1205.77	113.0084	5	3
1196.87	655.4672	5	133
1197.89	701.4761	5	134
1199.20	653.4506	5	135
1200.22	569.3802	5	136
1206.93	385.3278	5	128
1207.96	453.3176	5	128
1248.27	113.0132	5	14
1265.05	417.2571	5	55
1374.81	248.9875	5	5
1350.14	180.9992	5	5
1371.45	316.9770	5	6
1354.67	180.9978	5	145
1390.59	248.9911	5	6
1397.68	452.9595	5	55
1375.83	588.9388	5	130
1394.97	316.9812	5	55
1379.19	181.0022	5	75
1408.40	288.0011	5	6
1385.92	520.9444	5	55
1409.58	316.9728	5	83
1437.62	355.9899	5	55
1451.04	248.9829	5	83
1425.71	627.9464	5	130
1418.48	287.9982	5	5
1421.84	220.0108	5	5
1427.54	491.9659	5	55
1431.92	113.0066	5	30
1436.31	316.9788	5	6

1443.02	287.9942	5	83
1445.35	559.9614	5	130
1447.69	462.9902	5	55
1448.71	763.9291	5	130
1449.74	559.9550	5	55
1454.77	248.9947	5	55
1454.40	113.0162	5	148
1466.14	113.0104	5	104
1467.16	316.9709	5	83
1471.17	113.0072	5	149
1477.75	287.9973	5	5
1475.56	180.9962	5	145
1477.89	491.9735	5	130
1516.47	113.0087	5	3
1510.13	180.9945	5	153
1494.68	248.9937	5	55
1495.70	288.0035	5	55
1496.72	588.9446	5	130
1575.21	113.0120	5	2
1507.94	423.9757	5	55
1500.71	220.0116	5	5
1503.42	113.0183	5	154
1508.59	113.0161	5	148
1505.75	181.0022	5	75
1513.48	598.9816	5	130
1554.92	248.9835	5	83
1524.71	316.9727	5	83
1519.17	248.9897	5	6
1520.19	316.9812	5	55
1522.52	520.9445	5	55
1523.55	491.9640	5	55
1526.90	180.9968	5	145
1529.24	287.9948	5	83
1578.57	113.0098	5	104
1539.29	288.0023	5	55
1543.67	180.9997	5	5
1548.34	113.0139	5	14
1546.01	248.9930	5	55
1552.72	181.0025	5	75
1553.75	452.9609	5	55
1603.60	248.9919	5	55
1560.47	316.9742	5	83
1563.83	248.9890	5	6
1573.53	113.0081	5	3
1569.52	316.9711	5	83
1575.58	180.9953	5	145
1570.55	287.9990	5	6
1586.31	180.9967	5	145
1590.70	559.9588	5	130
1597.40	180.9999	5	5
1608.77	113.0134	5	14
1597.41	588.9453	5	130
1603.09	316.9708	5	83
1606.45	316.9811	5	55
1614.17	220.0121	5	5
1620.88	384.9668	5	55
1624.24	695.9387	5	130
1636.64	248.9876	5	5
1633.93	113.0089	5	3
1634.30	180.9959	5	145

1637.66	248.9834	5	83
1643.36	316.9773	5	6
1644.38	452.9568	5	55
69.96	92.9538	6	7
70.99	268.8288	6	8
73.32	195.0772	7	9
75.37	96.9953	7	10
76.68	606.1163	7	11
77.71	193.0615	7	12
78.74	253.0392	7	13
82.75	426.0547	7	15
82.10	322.0737	7	16
87.13	323.0576	7	17
88.44	346.0865	7	15
104.58	662.1463	7	19
97.20	184.0636	7	20
110.27	547.1145	7	21
126.03	918.8250	7	22
130.05	678.1398	7	23
154.22	321.0784	7	26
160.20	323.0459	7	27
245.86	524.6658	7	29
311.14	621.2073	7	32
312.17	1243.4119	7	33
322.66	702.2399	7	34
341.42	595.7043	7	39
373.63	906.9456	7	45
417.12	784.2020	7	49
414.78	403.5895	7	50
420.84	806.1852	7	51
436.25	455.1323	7	52
697.52	716.5721	7	59
728.40	747.5663	7	60
720.00	747.5725	7	60
777.10	747.5726	7	60
821.76	747.5577	7	60
896.98	450.2968	7	93
915.80	747.5669	7	60
965.81	452.3139	7	93
972.89	747.5717	7	60
976.90	481.2944	7	103
994.36	478.3304	7	93
988.66	747.5625	7	60
996.40	546.3199	7	68
1003.12	717.4158	7	106
1119.64	747.5639	7	60
1058.68	483.3092	7	103
1052.48	743.4341	7	106
1083.72	747.5738	7	60
1093.94	509.3264	7	103
1093.28	716.5760	7	59
1091.08	745.4498	7	106
1092.11	813.4412	7	124
1140.80	771.4656	7	106
1162.28	747.5749	7	60
1144.17	716.5788	7	59
1180.09	773.4828	7	106
1184.09	253.2456	7	131
1183.44	747.5812	7	60
1184.47	321.2354	7	90

1224.38	688.5394	7	59
1224.24	747.5768	7	60
1221.39	747.5555	7	60
1231.47	756.5320	7	138
1247.90	714.5566	7	59
1248.92	782.5478	7	138
1248.27	850.5407	7	139
1252.93	255.2608	7	140
1263.00	281.2773	7	141
1264.03	349.2669	7	90
1279.79	716.5730	7	59
1277.46	784.5638	7	138
1278.48	852.5565	7	139
1297.60	716.5602	7	142
1476.58	688.6259	7	152
1492.33	747.5672	7	60
1549.36	747.5612	7	60
1643.86	747.5672	7	60
1645.68	716.5707	7	59
74.35	146.0716	8	2
81.73	275.1163	8	14
332.74	523.2047	8	36
363.27	732.3073	8	42
366.91	714.2982	8	43
382.68	728.2743	8	47
397.41	726.2617	8	48
91.14	191.0461	9	18
324.86	274.1215	9	35
999.39	649.4253	9	105
1051.46	675.4431	9	105
1063.21	503.3604	9	118
1064.24	571.3513	9	119
1063.58	1007.7169	9	120
1090.06	677.4587	9	105
1114.60	529.3772	9	118
1116.28	597.3685	9	119
1129.20	703.4747	9	105
1153.88	531.3933	9	118
1154.91	599.3844	9	119
1155.93	667.3757	9	121
1177.38	705.4916	9	105
1202.55	557.4084	9	118
143.48	180.0920	10	24
292.07	164.0966	11	31
330.04	1251.4661	12	37
331.72	1413.5262	13	38
358.88	665.3391	14	41
367.94	1384.5883	15	44
575.78	187.1238	16	18
679.70	241.1329	17	5
712.26	242.2036	17	64
762.00	444.2052	17	67
763.67	512.1965	17	68
764.70	580.1872	17	69
835.20	312.2267	17	81
852.13	313.2673	17	82
867.76	381.2568	17	86
687.58	230.1456	18	61
745.85	244.1621	18	65
750.23	284.1939	18	65

771.04	256.1621	18	61
770.38	286.2103	18	70
773.74	513.3134	18	71
787.17	285.2361	18	73
791.55	240.1671	18	74
794.54	242.1827	18	66
796.08	302.2054	18	70
801.25	258.1777	18	65
802.28	517.3448	18	76
803.30	170.0870	18	77
826.43	270.1777	18	65
827.46	282.1777	18	78
851.49	272.1935	18	70
872.29	284.1940	18	65
848.64	557.3773	18	84
874.48	569.3784	18	84
854.33	328.2208	18	70
857.69	545.3774	18	84
877.85	267.1910	18	87
888.58	268.1988	18	88
881.72	553.3832	18	89
881.71	352.1833	18	90
882.23	854.5663	18	91
899.69	330.2373	18	94
900.35	298.2104	18	70
904.73	537.3878	18	89
905.76	304.1765	18	95
908.74	286.2100	18	80
908.09	270.2145	18	96
910.28	573.4106	18	97
912.46	860.6144	18	98
914.77	354.1967	18	75
933.90	310.2110	18	99
931.57	298.2104	18	70
939.31	621.4119	18	97
935.95	597.4124	18	97
940.48	293.2070	18	87
952.37	312.2266	18	80
946.02	623.4305	18	97
954.05	294.2157	18	99
969.02	625.4449	18	97
953.91	296.2309	18	100
963.98	300.2267	18	94
973.54	286.2104	18	80
984.65	380.2165	18	86
1005.97	296.2316	18	100
1002.09	326.2425	18	94
1004.42	310.2477	18	107
1012.82	314.2430	18	94
1013.85	629.4774	18	108
1013.20	382.2333	18	109
1019.54	298.2460	18	110
1018.89	597.4845	18	111
1019.92	338.2431	18	80
1027.29	286.2108	18	80
1032.33	297.2723	18	112
1034.52	285.2022	18	100
1039.04	288.1895	18	113
1043.06	340.2590	18	94
1045.11	681.5104	18	114

1048.10	324.2642	18	115
1049.12	649.5200	18	116
1050.15	665.5166	18	116
1083.86	340.2586	18	94
1117.96	342.2749	18	127
1121.98	324.2638	18	115
1125.33	326.2784	18	129
1139.78	368.2907	18	127
1147.16	352.2952	18	129
748.04	258.1775	19	66
830.82	302.2051	19	80
836.50	274.1726	19	65
938.28	258.1783	19	66
927.18	274.1730	19	65
968.50	258.1752	19	102
1032.98	302.2055	19	80
1128.69	330.2379	19	126
766.01	457.2782	20	19
831.47	293.2049	20	79
782.78	328.2215	21	72
786.14	326.2064	21	72
839.21	324.1905	21	72
1070.44	328.2224	21	107
1111.89	328.2235	21	126
789.50	169.0921	22	1
790.53	229.1145	22	25
793.89	297.1040	22	75
852.14	395.2755	23	85
1362.04	473.3187	23	146
861.70	393.2600	24	63
885.59	424.2797	25	92
958.44	265.1766	26	101
1107.37	293.2087	26	125
1124.03	357.2961	27	128
1194.16	339.2640	28	132
1218.04	100.9594	29	137
1328.84	100.9592	29	143
1328.85	100.9603	29	53
1362.41	100.9615	29	147
1475.56	100.9568	29	150
1536.96	134.9188	29	156
1651.09	116.9542	29	137
1302.65	698.9593	30	144
1650.72	190.9545	31	2
1662.47	235.9533	31	158

VII.   Annotation table - sub-MIC ciprolfoxacin concentrations

Table A12. Annotation table of metabolomics experiments upon treatment at sub-MIC and MIC concentrations. *:Putative label, AA: amino acids, AQ: alkylquinolones, FA: fatty acids, Glu: glutamate-related, Gluc:glucose, HSL: homoserine lactones, Nuc: nucleotides, Phen: phenazines, Phenyl: phenylalanine, PhosLip: phospholipids, Rha: rhamnolipids, UDP: uridine phosphate-related

Feature name	RT (min)	m/z	GNPS_Cluster	CluMSID_Cluster	NeutralLosses_Cluster	Manual_Cluster	Manual_Class	Annotation
M116T1_2	1.24	116.0707	-1	NA	NA	AA	AA	D-Proline
M146T1_4	1.00	146.1654	-1	6	24	AA	AA	Sperminide
M182T2	1.91	182.0809	5	17	25	AA	AA	L-Tyrosine
M188T6	5.85	188.0709	-1	17	51		AA	Tryptophan [M-H2O+H]+
M205T6	5.85	205.0975	-1	17	21		AA	Tryptophan
M159T13	13.15	159.0681	5	35	109	AQ	AQ	
M162T8	8.31	162.0552	-1	39	165		AQ	DHQ
M184T15_1	14.82	184.0757	5	35	109	AQ	AQ	
M184T16	16.04	184.0758	5	35	109	AQ	AQ	
M186T13_2	13.15	186.0917	5	35	131	AQ	AQ	*C3:1-HQ
M188T9	8.82	188.1072	-1	3	172		AQ	*C3-HQ
M198T14	14.40	198.0914	5	35	224	AQ	AQ	
M216T11	11.00	216.1393	NA	35	204	AQ	AQ	C5-HQ
M230T12_2	12.06	230.1543	-1	59	230		AQ	C6-HQ
M242T13	12.97	242.1548	1	35	219	AQ	AQ	C7:1-HQ
M244T13_1	13.04	244.1708	1	35	219	AQ	AQ	C7-HQ
M246T12	12.24	246.1496	NA	35	219	AQ	AQ	
M254T14	14.40	254.1537	NA	NA	NA	AQ	AQ	C9:1-PQS [M-CH3OH+H]+
M256T14_2	13.93	256.1701	1	35	219	AQ	AQ	C8:1-HQ
M258T13_1	12.68	258.1497	1	35	219	AQ	AQ	
M258T14	13.96	258.1859	1	35	219	AQ	AQ	C8-HQ [M+K]+
M259T14_1	13.77	259.1695	NA	35	241	AQ	AQ	
M260T13_1	13.17	260.1230	1	NA	NA	AQ	AQ	
M260T13_2	13.18	260.1675	NA	NA	NA	AQ	AQ	C7-PQS
M260T12_5	11.72	260.2223	1	NA	NA	AQ	AQ	
M261T13_8	13.15	261.1687	1	35	246	AQ	AQ	
M266T13	13.03	266.1520	-1	NA	NA	AQ	AQ	C7-HQ [M+Na]+
M267T11_2	11.17	267.1230	NA	NA	NA		AQ	*C9:1-QNO (II)
M267T14	13.50	267.1231	NA	52	260	AQ	AQ	C9:1-QNO (II) [M-H2O]+
M268T14_2	14.32	268.1702	1	35	219	AQ	AQ	C9:2-HQ
M269T16	15.74	269.2088	-1	35	295	AQ	AQ	
M270T19	19.22	270.1855	1	NA	NA	AQ	AQ	
M270T14_1	14.45	270.1860	1	35	219	AQ	AQ	C9:1-HQ (I)
M272T12_2	11.61	272.1285	-1	49	219	AQ	AQ	
M272T18	17.69	272.1649	27	35	219	AQ	AQ	
M272T14_1	13.55	272.1654	1	35	219	AQ	AQ	C8:1-QNO
M272T15_1	14.84	272.2020	1	NA	NA	AQ	AQ	C9-HQ
M273T18_2	17.91	273.1724	6	35	219	AQ	AQ	
M274T14_2	14.01	274.1811	1	35	219	AQ	AQ	C8-QNO
M276T14_1	14.49	276.1601	NA	35	219	AQ	AQ	
M277T20	19.70	277.1751	27	35	269	AQ	AQ	
M277T18	17.96	277.1752	27	35	269	AQ	AQ	
M278T19	18.82	278.1831	27	35	269	AQ	AQ	
M279T19_2	19.08	279.1904	27	35	269	AQ	AQ	
M281T16_3	15.93	281.2953	1	88	299	AQ	AQ	
M282T13_1	13.05	282.1259	NA	NA	NA	AQ	AQ	C7-HQ [M+K]+
M282T13_2	13.17	282.1469	-1	49	251	AQ	AQ	C7-QNO [M+Na]+

M284T16_1	15.52	284.1646	1	35	219	AQ	AQ	*C9:2-QNO
M284T13	12.59	284.1651	63	35	219	AQ	AQ	*C9:2-PQS
M284T14	13.80	284.1652	1	35	219	AQ	AQ	C8-HQ
M284T16_2	15.70	284.2015	1	35	219	AQ	AQ	*C10:1-HQ (II)
M284T15	14.74	284.2017	1	35	219	AQ	AQ	*C10:1-HQ (I)
M284T20_2	20.38	284.2950	51	35	377	AQ	AQ	
M285T11_1	11.18	285.1337	-1	35	211	AQ	AQ	
M285T19	19.39	285.1724	NA	35	219	AQ	AQ	
M285T18	18.12	285.1729	1	35	219	AQ	AQ	
M285T20	20.40	285.2976	1	NA	NA	AQ	AQ	
M286T27_1	26.77	286.1803	NA	NA	NA		AQ	*C9:1-PQS (26 min)
M286T24	24.07	286.1804	NA	NA	NA		AQ	*C9:1-PQS (24 min)
M286T21_2	21.40	286.1806	NA	NA	NA		AQ	*C9:1-PQS (21 min)
M286T19_2	18.53	286.1807	1	35	219	AQ	AQ	C9:1-PQS
M286T16_1	15.65	286.1808	1	35	219	AQ	AQ	*C9:1-PQS
M286T14_2	13.97	286.1813	1	35	219	AQ	AQ	C9:1-QNO (II)
M286T16_2	15.73	286.2170	NA	35	264	AQ	AQ	
M287T9	9.19	287.1140	-1	35	176	AQ	AQ	
M287T19_3	19.13	287.1880	1	35	219	AQ	AQ	
M287T11_2	11.47	287.2694	1	NA	NA	AQ	AQ	
M288T19	19.26	287.6900	1	35	354	AQ	AQ	
M288T18	17.78	288.1966	NA	35	219	AQ	AQ	
M288T15_2	15.49	288.1967	NA	35	219	AQ	AQ	C9-QNO
M288T20	19.52	288.1969	NA	35	219	AQ	AQ	
M288T21	21.15	288.1970	NA	35	219	AQ	AQ	
M288T13	13.39	288.2901	1	35	6	AQ	AQ	
M289T27	27.39	288.9218	NA	35	431	AQ	AQ	
M289T15_6	15.15	289.1547	1	35	141	AQ	AQ	
M292T15_1	14.82	292.1674	NA	NA	NA	AQ	AQ	C9:1-HQ (I) [M+Na]+
M294T16_1	15.81	294.1270	1	NA	NA	AQ	AQ	
M294T15	14.82	294.1829	NA	NA	NA	AQ	AQ	C9-HQ [M+Na]+
M296T14	14.01	296.1620	NA	NA	NA		AQ	*C8-QNO [M+Na]+
M296T16	15.67	296.2017	1	35	219	AQ	AQ	C11:2-HQ (I)
M297T18_2	17.54	297.2406	52	35	327	AQ	AQ	
M298T13_1	13.18	298.1209	NA	NA	NA	AQ	AQ	C7-PQS [M+K]
M298T16_2	15.91	298.2174	1	35	264	AQ	AQ	C11:1-HQ (I)
M298T17_3	17.19	298.3475	5	35	319	AQ	AQ	
M299T19	19.30	299.1885	6	35	219	AQ	AQ	
M300T14	13.53	300.1599	63	49	219	AQ	AQ	
M300T19	19.46	300.1960	6	35	219	AQ	AQ	
M300T15_2	15.02	300.1967	1	35	219	AQ	AQ	
M300T17_2	16.61	300.2331	1	35	264	AQ	AQ	C11-HQ
M301T16	16.19	301.1413	-1	35	304	AQ	AQ	
M302T12	12.29	302.1757	-1	35	71	AQ	AQ	
M302T13_3	13.27	302.1757	55	35	219	AQ	AQ	
M302T14	14.17	302.1757	55	35	219	AQ	AQ	
M302T16	15.78	302.1758	NA	35	219	AQ	AQ	
M302T15	15.40	302.2122	1	35	264	AQ	AQ	*C10-QNO
M304T13_1	13.18	304.1286	NA	NA	NA	AQ	AQ	C7-PQS [M+2Na-H]+
M304T16_1	16.04	304.1914	3	35	219	AQ	AQ	
M304T13_2	13.05	304.1916	1	35	14	AQ	AQ	
M308T14	14.20	308.1625	-1	78	271	AQ	AQ	C9:1-QNO [M+Na]+
M309T17_2	17.41	309.3268	1	NA	NA	AQ	AQ	
M310T14_2	14.43	310.1781	1	35	219	AQ	AQ	C9-PQS [M+Na]+
M310T16	16.40	310.2168	1	35	219	AQ	AQ	
M311T15_1	14.69	311.1269	-1	35	281	AQ	AQ	
M311T18_2	18.37	311.2561	-1	35	343	AQ	AQ	
M311T15_3	15.19	311.2585	1	NA	NA	AQ	AQ	
M312T18	17.52	312.1963	1	35	219	AQ	AQ	*C11:2-PQS
M312T15_2	15.23	312.1967	1	35	219	AQ	AQ	*C11:2-QNO

M312T17_1	17.44	312.2325	NA	35	264	AQ	AQ	
M312T16_1	16.32	312.2330	1	35	264	AQ	AQ	*C12:1-HQ
M314T21	20.64	314.2119	67	35	306	AQ	AQ	
M314T16_2	15.79	314.2122	1	35	264	AQ	AQ	C11:1-QNO
M314T14	13.62	314.2124	1	35	14	AQ	AQ	*C11:1-QNO
M314T17_1	17.46	314.2482	NA	35	264	AQ	AQ	
M315T16_3	15.75	315.2155	1	35	292	AQ	AQ	
M316T14_1	13.67	316.1915	NA	35	262	AQ	AQ	
M316T14_2	14.32	316.2275	1	35	264	AQ	AQ	*C11:0-PQS
M316T17_2	16.54	316.2284	1	35	264	AQ	AQ	*C11:0-QNO
M320T15	15.47	320.1988	NA	85	290	AQ	AQ	C11:1-HQ (I) [M+Na]+
M324T17_1	16.69	324.2329	1	35	264	AQ	AQ	*C13:2-HQ
M326T14_1	13.70	326.1756	1	35	219	AQ	AQ	
M326T16_1	15.86	326.2118	1	35	219	AQ	AQ	*C12:2-PQS
M326T18_1	17.57	326.2485	1	35	264	AQ	AQ	*C13:1-HQ
M328T16_1	16.06	328.1909	1	NA	NA	AQ	AQ	
M328T13_2	12.98	328.1914	NA	35	219	AQ	AQ	
M328T16_2	16.30	328.2277	1	35	264	AQ	AQ	C12:1-QNO
M328T18	18.32	328.2643	1	35	131	AQ	AQ	C13:0-HQ
M330T16_1	16.43	330.2070	NA	35	51	AQ	AQ	
M330T13	12.55	330.2072	NA	35	6	AQ	AQ	
M330T14	13.93	330.2072	1	35	14	AQ	AQ	
M332T18	17.51	332.2225	3	35	264	AQ	AQ	
M332T15_2	14.69	332.2230	1	35	32	AQ	AQ	
M334T18_1	17.52	334.1781	NA	NA	NA		AQ	*C11:2-PQS [M+Na]+
M334T15_1	15.23	334.1783	-1	35	287	AQ	AQ	*C11:2-HQ [M+Na]+
M334T16	16.32	334.2142	NA	NA	NA		AQ	*C12:1-QNO [M+Na]+
M338T17_2	16.54	338.2090	NA	NA	NA		AQ	*C11:0-QNO [M+Na]+
M339T17_2	17.36	339.2896	1	NA	NA	AQ	AQ	
M340T17_1	16.50	340.2281	1	35	264	AQ	AQ	*C13:2-PQS
M340T18_2	17.97	340.2928	1	NA	NA	AQ	AQ	
M342T15_2	14.97	342.2433	1	35	264	AQ	AQ	*C13:1-PQS
M342T17_2	17.39	342.2438	1	35	264	AQ	AQ	C13:1-QNO
M344T18_1	18.21	344.2595	1	35	71	AQ	AQ	C13:0-QNO
M346T15_1	14.69	346.1364	1	NA	NA	AQ	AQ	
M353T19	18.56	353.2665	1	35	346	AQ	AQ	
M354T19	18.61	354.2800	1	35	281	AQ	AQ	*C15:1-HQ
M356T21	21.36	356.2859	1	NA	NA	AQ	AQ	*C15:0-HQ
M356T19	18.58	356.2860	1	NA	NA	AQ	AQ	
M358T18	17.98	358.2381	1	NA	NA	AQ	AQ	*C13:2-PQS [M+NH4]+
M358T15	15.26	358.2383	1	35	32	AQ	AQ	*C13:2-QNO
M360T16	16.32	360.2537	NA	35	71	AQ	AQ	
M360T17_3	16.55	360.2831	1	NA	NA	AQ	AQ	
M364T15_2	14.98	364.2246	NA	NA	NA		AQ	*C13:1-PQS [M+Na]+
M368T18	17.96	368.2588	1	35	71	AQ	AQ	*C15:2-QNO
M369T19_2	18.92	369.2981	-1	35	350	AQ	AQ	
M370T16	16.48	370.2746	NA	NA	NA		AQ	*C15:1-PQS
M370T18_3	18.48	370.2750	NA	35	71	AQ	AQ	C15:1-QNO
M370T19_2	19.49	370.3014	1	NA	NA	AQ	AQ	*C16:0-HQ
M372T20	19.88	372.2903	1	35	299	AQ	AQ	*C15:0-QNO
M376T19_1	18.61	376.2615	-1	NA	NA		AQ	*C15:1-HQ [M+Na]+
M381T20	20.22	381.2981	1	NA	NA	AQ	AQ	
M382T20	20.25	382.3110	1	35	281	AQ	AQ	*C17:1-HQ
M386T17_2	16.74	386.2698	NA	35	32	AQ	AQ	
M392T19	18.61	392.2357	NA	NA	NA		AQ	*C15:1-HQ [M+K]+
M398T20_1	20.04	398.3060	1	97	71	AQ	AQ	*C17:1-QNO
M404T20	20.25	404.2929	-1	NA	NA		AQ	*C17:1-HQ [M+Na]+
M414T20	20.48	414.3006	NA	35	219	AQ	AQ	
M487T13	13.03	487.3328	NA	NA	NA	AQ	AQ	C7-HQ [2M+H]2+
M509T13	13.03	509.3144	NA	NA	NA	AQ	AQ	C7-HQ [2M+Na]+

M519T13	13.20	519.3225	NA	35	253	AQ	AQ	C7-PQS [2M+H]+
M541T13	13.15	541.3040	NA	NA	NA	AQ	AQ	C7-QNO [2M+Na]+
M543T15	14.84	543.3926	13	NA	NA		AQ	*C9-HQ [2M+H]+
M547T14	14.04	547.3533	NA	NA	NA		AQ	*C8-QNO [2M+H]+
M559T15	14.84	559.3896	13	35	270	AQ	AQ	
M571T14	14.40	571.3539	1	35	270	AQ	AQ	C9:1-PQS (I) [2M+H]+
M575T15	14.89	575.3852	1	35	270	AQ	AQ	*C9-QNO [2M+H]+
M593T14	14.40	593.3350	NA	NA	NA	AQ	AQ	C9:1-QNO(I) [2M+Na]+
M597T15_1	14.89	597.3663	NA	NA	NA	AQ	AQ	C9-PQS [2M+Na]+
M597T17_2	16.59	597.4411	1	NA	NA	AQ	AQ	
M611T15_3	15.49	611.4216	1	35	291	AQ	AQ	
M627T15	15.50	627.4158	1	35	291	AQ	AQ	*C11:1-PQS [2M+H]+
M631T16	15.53	631.4296	1	NA	NA	AQ	AQ	*C11:0-PQS [2M+H]+
M649T17	17.01	649.4727	1	NA	NA	AQ	AQ	C12:0-HQ [2M+Na]+
M667T17	16.99	667.4825	1	NA	NA	AQ	AQ	
M683T17	16.95	683.4787	1	NA	NA	AQ	AQ	*C13:1-PQS [2M+H]+
M708T19	18.60	707.5523	NA	NA	NA		AQ	*C15:1-HQ [2M+H]+
M730T19	18.61	729.5362	NA	NA	NA		AQ	*C15:1-HQ [2M+Na]+
M752T13	13.02	752.4767	NA	NA	NA	AQ	AQ	C7-HQ [3M+Na]+
M778T13	13.15	778.4802	-1	35	253	AQ	AQ	C7-PQS [3M+H]+
M857T14	14.40	856.5268	NA	35	277	AQ	AQ	
M181T18	17.91	181.1589	NA	NA	NA		FA	*Omega-hydroxydodecanoic acid (frag.)
M183T16_3	16.41	183.1749	NA	NA	NA		FA	*Lauric acid [M+H-H20]+
M199T18	17.91	199.1693	-1	NA	NA		FA	*Omega-hydroxydodecanoic acid [M-H2O+H]+
M199T17	17.15	199.1695	NA	NA	NA		FA	*Omega-hydroxydodecanoic acid [M-H2O+H]+
M201T16	16.40	201.1852	NA	NA	NA		FA	*Lauric acid
M217T18	17.91	217.1801	NA	NA	NA		FA	*Omega-hydroxydodecanoic acid
M219T18	18.32	219.2113	NA	NA	NA		FA	Palmitoleic acid (frag.)
M227T15	14.62	227.2009	NA	NA	NA		FA	*Myristoleic acid
M229T18	18.01	229.2163	NA	NA	NA		FA	*Myristic acid
M237T19	18.66	237.2312	NA	NA	NA		FA	Palmitoleic acid [M-H2O+H]+
M239T19	19.47	239.2370	NA	NA	NA		FA	Palmitate [M-H2O+H]+
M245T16	16.40	245.1489	NA	NA	NA		FA	*Lauric acid [M+2Na-H]+
M255T18	18.32	255.2318	-1	NA	NA		FA	Palmitoleic acid
M257T19_1	19.47	257.2475	NA	35	361	AQ	FA	Palmitate
M265T20	19.63	265.2527	NA	NA	NA		FA	Elaidic acid [M-H2O+H]+
M279T19_3	19.47	279.2297	NA	NA	NA		FA	Palmitate [M+Na]+
M279T16_2	15.57	279.2324	50	75	264	Lipid	FA	Pinoleic acid
M282T19_3	19.02	282.2791	NA	NA	NA		FA	*Petroselinic acid
M283T20	19.64	283.2634	NA	35	264		FA	Elaidic acid
M295T19	19.47	295.1949	NA	NA	NA		FA	Palmitate [M+K]+
M299T18_2	18.32	299.1947	NA	NA	NA		FA	Palmitoleic acid (adduct)
M301T19	19.47	301.2119	6	35	282	AQ	FA	Palmitate [2Na-H]+
M305T20	19.63	305.2453	NA	NA	NA		FA	Elaidic acid [M+Na]+
M319T16_2	15.57	319.2251	-1	86	67		FA	Pinoleic acid [M+Na]+
M321T20	19.65	321.2099	NA	NA	NA		FA	Elaidic acid [M+K]+
M327T20_1	19.63	327.2274	-1	95	365		FA	Elaidic acid [M+2Na-H]+
M338T22	21.83	338.3420	-1	99	404		FA	Erucic acid
M343T20	19.63	343.2017	NA	NA	NA		FA	Elaidic acid [M+Na+K-H]+
M360T22	21.83	360.3237	-1	8	405		FA	Erucic acid [M+Na]+
M376T22	21.83	376.2976	NA	NA	NA		FA	Erucic acid [M+K]+
M615T16_2	15.58	615.4593	NA	86	293		FA	Pinoleic acid [2M+Na]+
M130T1_2	1.18	130.0500	NA	NA	NA	Glu	Glu	L-Glutamic acid [M-H2O+H]+
M132T15	14.70	132.0658	-1	1	1	Glu	Glu	
M132T28_2	27.93	132.0659	NA	1	1	Glu	Glu	
M132T13	13.06	132.0660	NA	1	14	Glu	Glu	
M135T2	2.47	134.9422	-1	1	71	Glu	Glu	
M135T4	3.84	134.9422	-1	1	71	Glu	Glu	
M136T6	6.05	136.0735	-1	1	121	Glu	Glu	
M148T1_2	1.19	148.0607	21	1	25	Glu	Glu	L-Glutamic acid

M162T1_1	1.33	162.0756	NA	NA	NA		Glu	*N-methyl-L-glutamate
M174T9	9.40	174.1856	-1	1	182	Glu	Glu	
M186T1_1	1.17	186.0165	NA	NA	NA	Glu	Glu	L-Glutamic acid [M+K]+
M223T1	1.37	222.5492	NA	NA	NA	Glu	Glu	
M230T1_2	1.34	230.1130	NA	NA	NA		Glu	
M259T1_3	1.24	259.0929	21	1	37	Glu	Glu	Glu Glu [M+H-H2O]+
M274T1_2	1.36	274.1023	NA	NA	NA	Glu	Glu	
M277T1_3	1.25	277.1037	21	1	37	Glu	Glu	Glu Glu
M299T1_5	1.24	299.0854	-1	15	37	Glu	Glu	Glu Glu [M+Na]+
M321T1_4	1.24	321.0671	NA	NA	NA	Glu	Glu	*Glu Glu [M+2Na-H]
M333T2	2.41	332.6199	21	NA	NA	Glu	Glu	
M360T6_1	6.13	359.6440	-1	1	123	Glu	Glu	
M366T6_1	6.45	365.6256	-1	1	124	Glu	Glu	
M368T6_1	5.87	367.6414	33	1	115	Glu	Glu	
M377T6	5.73	376.6464	NA	1	112	Glu	Glu	
M388T1_3	1.35	388.1344	NA	NA	NA	Glu	Glu	
M397T4	3.56	397.1406	21	NA	NA	Glu	Glu	
M406T1	1.35	406.1455	21	1	37	Glu	Glu	
M428T1_2	1.34	428.1270	NA	NA	NA	Glu	Glu	
M535T1_2	1.34	535.1872	21	1	37	Glu	Glu	
M535T2	1.81	535.1892	21	1	37	Glu	Glu	
M664T1_2	1.34	664.2285	21	NA	NA	Glu	Glu	
M664T2	2.42	664.2316	21	1	59	Glu	Glu	
M718T6	6.12	718.2791	-1	1	108	Glu	Glu	
M793T4	3.56	793.2732	21	NA	NA	Glu	Glu	
M811T1	1.33	811.2705	NA	NA	NA	Glu	Glu	
M203T1_2	1.21	203.0529	-1	9	34		Gluc	Glucose
M219T1_2	1.07	219.0268	NA	NA	NA		Gluc	Glucose [M+K]
M243T1_1	1.30	242.5616	7	NA	NA	Glutathion	Glutathion	
M306T1_3	1.29	306.0753	7	NA	NA	Glutathion	Glutathion	
M307T1_3	1.34	307.0829	7	NA	NA	Glutathion	Glutathion	Glutathion oxidized [M+2H]2+
M484T1	1.29	484.1158	NA	NA	NA		Glutathion	*Glutathion oxidized (fragment)
M613T1	1.29	613.1574	NA	NA	NA		Glutathion	*Gluthation oxidized
M194T5	4.96	194.0790	-1	NA	NA		HSL	*C4-HSL
M298T14_3	14.11	298.2017	NA	NA	NA		HSL	3-oxo-C12-HSL
M320T14	14.11	320.1838	-1	NA	NA		HSL	*3-oxo-C12-HSL [M+Na]+
M336T14	14.11	336.1574	NA	NA	NA		HSL	*3-oxo-C12-HSL [M+K]+
M617T14_2	14.10	617.3771	NA	NA	NA		HSL	*3-oxo-C12-HSL [2M+Na]+
M279T14_2	13.76	279.2324	-1	75	264	Lipid	Lipid	
M297T14_3	13.75	297.2430	50	75	263	Lipid	Lipid	
M359T17_2	16.55	359.2796	80	75	263	Lipid	Lipid	
M383T20_2	19.70	383.3140	39	75	367	Lipid	Lipid	
M385T17	17.34	385.2939	-1	75	263	Lipid	Lipid	
M387T18	17.90	387.3112	80	75	263	Lipid	Lipid	
M415T19	18.92	415.3419	80	75	263	Lipid	Lipid	
M485T18	17.78	485.1133	-1	92	334	Lipid	Lipid	
M507T17_1	17.49	507.2702	77	92	332	Lipid	Lipid	
M507T17_2	17.03	507.3297	-1	92	318	Lipid	Lipid	
M575T19	19.16	575.1054	20	8	357	Lipid	Lipid	
M651T16	15.52	651.4025	24	75	298	Lipid	Lipid	
M718T16	16.45	717.5269	20	NA	NA	Lipid	Lipid	
M739T17_1	16.69	738.5053	36	NA	NA	Lipid	Lipid	
M741T17	16.67	740.5205	36	NA	NA	Lipid	Lipid	
M186T1_2	1.24	186.0757	NA	NA	NA		Nuc	*N-acetylglucosamine
M193T2	2.27	193.0684	-1	16	58	Nuc	Nuc	
M204T1_2	1.24	204.0866	NA	NA	NA		Nuc	*N-acetylglucosamine
M208T9	9.15	208.0971	NA	NA	NA		Nuc	*N-acetyl-L-phenylalanine
M243T9	9.20	243.0874	5	32	49	Nuc	Nuc	Lumichrome
M298T6	6.27	298.0973	-1	16	129	Nuc	Nuc	MTA
M332T2	1.87	332.0761	NA	NA	NA	Nuc	Nuc	DAMP

M333T1_1	1.37	332.5620	-1	16	40	Nuc	Nuc	NAD [M+2H]2+
M348T1_2	1.34	348.0704	NA	16	38	Nuc	Nuc	AMP
M348T7	6.91	348.0711	-1	16	38	Nuc	Nuc	
M349T7_2	7.15	349.1836	-1	16	143	Nuc	Nuc	
M359T8	8.40	359.1354	-1	32	166	Nuc	Nuc	
M364T1_2	1.37	364.0650	-1	NA	NA	Nuc	Nuc	GMP
M373T1_1	1.34	372.5447	NA	NA	NA	Nuc	Nuc	NADP+ [M+2H]2+
M394T7_1	6.94	393.5869	NA	NA	NA	Nuc	Nuc	FAD [M+2H]2+
M405T7	6.94	404.5727	NA	NA	NA	Nuc	Nuc	FAD [M+H+Na]2+
M413T7_1	6.91	412.5599	-1	16	139	Nuc	Nuc	FAD [M+H+K]2+
M428T1_1	1.28	428.0366	71	16	39	Nuc	Nuc	ADP
M439T7	6.94	439.1021	-1	32	49	Nuc	Nuc	FAD (fragment)
M450T1_1	1.27	450.0186	-1	NA	NA	Nuc	Nuc	ADP [M+Na]+
M457T7	7.17	457.1122	-1	32	3	Nuc	Nuc	FMN
M479T7	7.17	479.0940	NA	NA	NA	Nuc	Nuc	FMN [M+Na]+
M664T1_1	1.34	664.1148	21	16	41	Nuc	Nuc	NAD
M744T1	1.32	744.0804	NA	NA	NA	Nuc	Nuc	NADP+
M786T7	6.94	786.1650	-1	16	138	Nuc	Nuc	FAD
M808T7	6.94	808.1464	-1	16	138	Nuc	Nuc	FAD [M+Na]+
M824T7	6.94	824.1124	NA	NA	NA	Nuc	Nuc	FAD [M+K]+
M830T7	6.91	830.1285	NA	NA	NA	Nuc	Nuc	FAD [M+2Na-H]
M179T11_2	10.55	179.0606	-1	NA	NA		Phen	*Phenazine-1-carboxylic acid [M+H-HCOOH]+
M179T11_1	11.34	179.0606	-1	NA	NA		Phen	*Phenazine-1-carboxylic acid [M+H-HCOOH]+
M181T12_2	11.65	181.0762	-1	3	221		Phen	*Phenazine
M183T8	8.08	183.0920	5	28	161	Phen	Phen	
M195T10	9.55	195.0879	NA	NA	NA		Phen	*Phenazine-methosulfate
M197T11	10.81	197.0712	5	23	51		Phen	1-Hydroxyphenazine
M206T11_1	10.54	206.0536	NA	NA	NA	Phen	Phen	Phenazine-2-carboxamide [M+H-H20]+
M206T11_2	10.54	206.0717	NA	NA	NA	Phen	Phen	Phenazine-1-carboxamide [M+H-H20]+
M207T11_2	11.33	207.0555	35	45	199	Phen	Phen	Phenazine-1-carboxylic acid [M+H-H2O]+
M208T11_2	10.83	208.0589	-1	NA	NA		Phen	1-Hydroxyphenazine [M+K]+
M211T7	7.19	211.0871	5	28	131	Phen	Phen	Pyocyanin
M224T11	10.55	224.0823	35	45	49	Phen	Phen	Phenazine-1-carboxamide
M225T11_1	11.35	225.0661	35	45	14	Phen	Phen	Phenazine-1-carboxylic acid
M229T7	7.36	229.0977	-1	28	25	Phen	Phen	
M233T6_1	6.49	233.0687	-1	NA	NA	Phen	Phen	Pyocyanin [M+Na]+
M241T10_1	10.42	241.0608	NA	NA	NA		Phen	2-Hydroxyphenazine-1-carboxilic acid
M244T11	11.33	244.0407	NA	NA	NA	Phen	Phen	Phenazine-1-carboxylic acid [2M+H+K]2+
M246T11_1	10.55	246.0644	-1	NA	NA	Phen	Phen	Phenazine-1-carboxamide [M+Na]+
M247T11_1	11.33	247.0481	-1	53	215	Phen	Phen	Phenazine-1-carboxylic acid [M+Na]+
M262T11_1	10.55	262.0377	NA	NA	NA	Phen	Phen	Phenazine-1-carboxamide [M+K]+
M263T10_1	10.45	263.0423	NA	NA	NA		Phen	2-Hydroxyphenazine-1-carboxilic acid [M+Na]+
M269T11	11.33	269.0296	NA	NA	NA	Phen	Phen	Phenazine-1-carboxylic acid [M+2Na-H]+
M269T10	10.09	269.0562	-1	45	67	Phen	Phen	Phenazine-1,6-dicarboxylic acid
M308T11	10.55	308.0357	NA	NA	NA	Phen	Phen	Phenazine-1-carboxamide [M+K+HCOOH]+
M309T11_1	11.35	309.0184	NA	NA	NA		Phen	*Phenazine-1-carboxylic acid [M+K+HCOOH]+
M325T12_2	11.85	325.0683	-1	NA	NA	Phen	Phen	Pyochelin
M356T11	11.32	356.0706	NA	NA	NA		Phen	*Phenazine-1-carboxylic acid [3M+H+K]2+
M443T6	6.49	443.1479	-1	NA	NA	Phen	Phen	Pyocyanin [2M+Na]+
M469T11	10.56	469.1383	-1	47	200	Phen	Phen	Phenazine-1-carboxamide [2M+Na]+
M103T3	2.86	103.0543	-1	19	76	Phenyl	Phenyl	
M120T3	3.19	120.0810	5	NA	NA		Phenyl	*Phenylalanine (fragment)
M166T3	2.78	166.0866	5	19	25	Phenyl	Phenyl	L-Phenylalanine
M170T14_2	14.09	170.0967	NA	24	268		Phenyl	Diphenylamine
M212T16_2	16.32	212.1434	-1	19	305	Phenyl	Phenyl	
M321T9	8.79	321.1021	-1	19	170	Phenyl	Phenyl	
M321T12_2	12.18	321.1025	45	19	170	Phenyl	Phenyl	
M379T10	9.85	379.1076	45	19	191	Phenyl	Phenyl	
M393T11	10.50	393.1232	-1	19	198	Phenyl	Phenyl	
M260T17_1	17.36	259.6316	NA	NA	NA		PhosLip	*LPE 18:1 [M+K+H]+

M261T16_1	15.76	261.1139	NA	NA	NA	Lipid	PhosLip	*LPG (16:1/0:0) [M+K+H]2+
M313T17	17.43	313.2740	46	NA	NA	Lipid	PhosLip	LPE 16:1 (fragment)
M452T15	15.47	452.2780	20	75	286	Lipid	PhosLip	LPE 16:1
M454T17	16.97	454.2937	20	92	286	Lipid	PhosLip	LPE 16:0
M462T17	17.36	462.2980	NA	NA	NA		PhosLip	*LPE 18:1 [M+H-H2O]+
M465T16	15.87	465.2607	NA	NA	NA	Lipid	PhosLip	*LPG (16:1/0:0) [M-H2O+H]+
M466T16	16.17	466.2937	NA	NA	NA	Lipid	PhosLip	LPE 17:1
M467T18	17.50	467.2775	NA	NA	NA	Lipid	PhosLip	*LPG (16:0/0:0) [M-H2O+H]+
M474T15	15.18	474.2594	36	75	288	Lipid	PhosLip	*LPE 16:1 [M+Na]+
M476T17_1	16.97	476.2753	36	92	288	Lipid	PhosLip	*LPE 16:10[M+Na]+
M480T17_1	17.35	480.3096	20	75	286	Lipid	PhosLip	LPE 18:1
M483T18_neg	17.52	483.2717	NA	NA	NA		PhosLip	LPG 16:0 (neg)
M483T16	15.75	483.2726	NA	NA	NA	Lipid	PhosLip	*LPG (16:1/0:0)
M485T17	17.49	485.2884	20	NA	NA	Lipid	PhosLip	*LPG (16:0/0:0)
M493T19	18.55	493.2927	NA	NA	NA	Lipid	PhosLip	*LPG (18:1/0:0) [M-H2O+H]+
M502T17	17.36	502.2910	36	75	288	Lipid	PhosLip	LPE 18:1 [M+Na]+
M505T16	15.76	505.2543	77	NA	NA	Lipid	PhosLip	*LPG (16:1/0:0) [M+Na]+
M509T18_neg	18.14	509.2876	NA	NA	NA		PhosLip	LPG 18:1 (neg)
M511T19	18.53	511.3036	NA	NA	NA	Lipid	PhosLip	*LPG (18:1/0:0)
M518T17_1	17.36	518.2611	NA	NA	NA	Lipid	PhosLip	LPE 18:1 [M+K]+
M521T16_1	15.75	521.2201	NA	NA	NA	Lipid	PhosLip	*LPG (16:1/0:0) [M+K]+
M533T19	18.51	533.2854	29	NA	NA	Lipid	PhosLip	*LPG (18:1/0:0) [M+Na]+
M545T18_2	17.53	545.2239	NA	NA	NA	Lipid	PhosLip	*LPG (16:0/0:0) [M+Na+K-H]+
M691T27	27.44	690.5068	NA	NA	NA	Lipid	PhosLip	PE 32:1; PE 11:0-21:1 (27 min)
M712T27	27.40	712.4875	NA	NA	NA	Lipid	PhosLip	PE 32:1; PE 11:0-21:1 (27 min) [M+Na]+
M715T21_neg	21.13	714.5066	NA	NA	NA		PhosLip	PE 34:2; PE 16:1-18:1 (neg)
M715T27_neg	27.39	714.5069	NA	NA	NA		PhosLip	PE 34:2; PE 16:1-18:1 (neg)
M717T27	27.44	716.5221	NA	NA	NA	Lipid	PhosLip	PE 34:2; PE 16:1-18:1
M717T27_neg	27.39	716.5222	NA	NA	NA		PhosLip	PE 34:1; PE 16:0-18:1 (neg)
M717T15	15.37	716.5236	20	NA	NA	Lipid	PhosLip	PE 34:2; PE 16:1-18:1 (15 min)
M717T17_1	16.87	716.5236	20	NA	NA	Lipid	PhosLip	PE 34:2; PE 16:1-18:1 (17 min)
M719T15	15.36	718.5389	20	NA	NA	Lipid	PhosLip	PE 34:1; PE 16:0-18:1 (15 min)
M719T17_1	16.74	718.5390	20	NA	NA	Lipid	PhosLip	PE 34:1; PE 16:0-18:1 (17 min)
M719T18	17.78	718.5395	20	NA	NA	Lipid	PhosLip	PE 34:1; PE 16:0-18:1 (18 min)
M719T21	21.21	718.5416	20	NA	NA	Lipid	PhosLip	PE 34:1; PE 16:0-18:1 (21 min)
M739T27	27.41	738.5037	NA	NA	NA	Lipid	PhosLip	PE 34:2; PE 16:1-18:1 (27 min) [M+Na]+
M748T27_neg	27.39	747.5167	NA	NA	NA		PhosLip	PG 34:1; PG 16:0-18:1 (neg) [M-H]-
M748T13_neg	13.02	747.5169	NA	NA	NA		PhosLip	PG 34:1; PG 16:0-18:1 (neg) [M-H]-
M750T19	19.47	749.5360	20	111	362	Lipid	PhosLip	PG 34:1; PG 16:0-18:1
M908T17	16.97	907.5793	-1	NA	NA		PhosLip	*LPE 16:1 [2M+H]+
M930T17	16.97	929.5593	NA	NA	NA		PhosLip	*LPE 16:1 [2M+Na]+
M960T17_1	17.36	959.6114	NA	NA	NA		PhosLip	*LPE 18:1 [2M+H]+
M982T17_1	17.36	981.5926	NA	NA	NA		PhosLip	*LPE 18:1 [2M+Na]+
M1004T17_1	17.36	1003.5750	NA	NA	NA		PhosLip	*LPE 18:1 [2M+2Na-H]
M226T17	16.78	226.1593	69	8	305	Rha	Rha	
M227T20	19.54	226.9516	-1	8	27	Rha	Rha	
M227T21	20.74	226.9516	-1	8	27	Rha	Rha	
M227T27	27.35	226.9520	-1	8	27	Rha	Rha	
M227T23	23.18	226.9521	-1	8	27	Rha	Rha	
M237T27_2	27.28	236.9860	NA	8	429	Rha	Rha	
M264T17_2	16.56	264.1573	NA	NA	NA		Rha	*Rha-C10-C10+Na [M+2H]+
M266T27	27.28	265.9629	-1	8	27	Rha	Rha	
M295T27	27.34	294.9393	-1	8	27	Rha	Rha	
M351T17	17.15	351.2026	NA	NA	NA		Rha	*Rha-Rha-C10-C12 [M+H+Na]2+
M358T17_1	16.58	358.1826	NA	NA	NA		Rha	*Rha-Rha-C10-C12:1 [M+H+K]2+
M363T27	27.36	362.9269	-1	8	28	Rha	Rha	
M364T17_2	16.95	364.2253	-1	8	315	Rha	Rha	
M381T17	17.29	381.2618	-1	87	296	Rha	Rha	
M399T27	27.26	399.3084	2	NA	NA	Rha	Rha	
M402T27_1	27.28	401.9377	2	NA	NA	Rha	Rha	

M407T18_2	18.03	407.2775	NA	87	296	Rha	Rha	
M409T19	18.61	409.2929	NA	94	296	Rha	Rha	
M429T18_3	17.57	429.3195	2	8	329	Rha	Rha	
M431T27_2	27.36	430.9147	2	NA	NA	Rha	Rha	
M441T20	20.17	441.3562	5	8	369	Rha	Rha	
M443T18	18.13	443.3349	-1	8	337	Rha	Rha	
M469T22_2	21.91	469.3871	2	8	401	Rha	Rha	
M470T27	27.28	469.9252	2	8	28	Rha	Rha	
M470T22_2	21.62	470.4205	NA	8	297	Rha	Rha	
M485T20	20.01	485.3821	5	8	369	Rha	Rha	
M487T18	18.12	487.3610	-1	8	338	Rha	Rha	
M489T20	19.83	489.3557	-1	8	263	Rha	Rha	
M499T27_2	27.35	498.9020	2	8	28	Rha	Rha	
M501T18	17.78	501.0869	-1	8	335	Rha	Rha	
M501T19	18.92	501.3769	2	NA	NA	Rha	Rha	
M505T17	16.54	505.3370	NA	NA	NA		Rha	Rha-C10-C10
M507T26	25.86	507.3290	NA	8	425	Rha	Rha	
M513T22	21.96	513.4133	2	8	399	Rha	Rha	
M527T17	16.55	527.3199	2	87	296	Rha	Rha	Rha-C10-C10 [M+Na]+
M531T17	17.31	531.3530	NA	NA	NA		Rha	Rha-C10-C12:1+Na
M533T17_2	17.16	533.3688	NA	NA	NA		Rha	*Rha-Rha-C10-C12 [M+H-C6H16O4]+
M537T18	17.94	537.3480	NA	NA	NA		Rha	Rha-C10-C12+Na [M-H2O+H]+
M538T27	27.31	537.9126	2	8	28	Rha	Rha	
M543T17	16.54	543.2899	NA	NA	NA		Rha	Rha-C10-C10 [M+K]+
M543T18	17.69	543.3221	11	94	333	Rha	Rha	
M548T17_2	17.33	548.3790	NA	NA	NA		Rha	Rha-C10-C12:1+Na [M+NH4]+
M549T17_1	16.56	549.3011	NA	NA	NA		Rha	*Rha-C10-C10+Na [M+Na]+
M553T17	17.32	553.3354	NA	87	296	Rha	Rha	Rha-C10-C12:1
M553T18_2	17.96	553.3429	2	94	333	Rha	Rha	
M555T18_2	18.19	555.3574	2	94	270	Rha	Rha	Rha-C10-C12
M557T22	22.01	557.4391	2	8	389	Rha	Rha	
M557T21	21.15	557.4393	-1	8	389	Rha	Rha	
M559T19_1	19.15	559.1319	2	8	356	Rha	Rha	
M565T17	16.56	565.2762	NA	NA	NA		Rha	*Rha-C10-C10+Na [M+K]+
M567T27_2	27.34	566.8892	2	8	28	Rha	Rha	
M569T17	17.32	569.3057	NA	NA	NA		Rha	Rha-C10-C12:1+Na [M+K]+
M569T21	21.08	569.3140	-1	8	394	Rha	Rha	
M569T18	18.11	569.3380	11	94	333	Rha	Rha	
M571T19	19.00	571.3532	11	94	71	Rha	Rha	
M573T20	19.78	573.4344	NA	8	368	Rha	Rha	
M574T19	19.26	574.3724	NA	NA	NA	Rha	Rha	Rha-C10-C12+Na
M575T17_1	17.32	575.3168	66	NA	NA	Rha	Rha	Rha-C10-C12:1+Na
M577T18	17.91	577.3322	66	8	296	Rha	Rha	
M579T26	25.75	579.4959	2	NA	NA	Rha	Rha	
M583T19	19.18	583.3820	2	102	296	Rha	Rha	
M597T19_2	19.29	597.3691	11	94	14	Rha	Rha	
M601T21_3	21.05	601.4651	2	8	391	Rha	Rha	
M601T22	22.04	601.4652	2	8	391	Rha	Rha	
M606T27	27.28	605.8997	2	NA	NA	Rha	Rha	
M633T16_1	15.80	633.3852	NA	NA	NA		Rha	*Rha-Rha-C10-C10 [M-H2O+H]+
M635T27_2	27.36	634.8766	2	NA	NA	Rha	Rha	
M645T22	22.09	645.4913	2	8	389	Rha	Rha	
M651T17_1	16.54	651.3962	NA	NA	NA	Rha	Rha	Rha-Rha-C10-C10
M661T17_2	17.15	661.4162	NA	NA	NA		Rha	Rha-Rha-C10-C12 [M+H-H2O]+
M662T16	15.80	662.3799	NA	NA	NA		Rha	*Rha-Rha-C10-C10 [2M+Na+H]2+
M668T16	15.81	668.4219	NA	NA	NA		Rha	*Rha-Rha-C10-C10 [M+NH4]+
M670T16	15.81	670.3689	NA	NA	NA		Rha	*Rha-Rha-C10-C10 [2M+H+K]+
M673T16	15.81	673.3779	2	87	296	Rha	Rha	Rha-Rha-C10-C10+Na
M674T27	27.28	673.8870	NA	8	28	Rha	Rha	
M677T17	16.58	677.4097	NA	NA	NA		Rha	Rha-Rha-C10-C12:1

M679T19	18.53	679.4199	2	106	349	Rha	Rha	
M679T17	17.13	679.4290	24	75	298		Rha	Rha-Rha-C10-C12
M685T24	24.30	685.4367	2	8	413	Rha	Rha	
M690T22	22.17	689.5177	2	8	388	Rha	Rha	
M690T21	20.91	689.5179	-1	8	388	Rha	Rha	
M694T17_1	16.58	694.4367	NA	NA	NA		Rha	*Rha-Rha-C10-C12:1 [M+NH4]+
M695T16	15.81	695.3593	NA	NA	NA	Rha	Rha	*Rha-Rha-C10-C10 [M+2Na-H]+
M695T19	18.53	695.3934	-1	8	348	Rha	Rha	
M696T17	17.14	696.4530	NA	NA	NA		Rha	*Rha-Rha-C10-C12 [M+NH4]+
M699T17	16.58	699.3927	2	87	296	Rha	Rha	Rha-Rha-C10-C12:1 [M+Na]+
M701T17	17.14	701.4081	2	94	296	Rha	Rha	Rha-Rha-C10-C12 [M+Na]+
M701T24	24.29	701.4098	2	NA	NA	Rha	Rha	
M702T27	27.13	701.5686	2	NA	NA	Rha	Rha	
M703T27_2	27.36	702.8639	2	NA	NA	Rha	Rha	
M703T23	23.00	702.8651	2	8	28	Rha	Rha	
M703T21	21.13	703.4967	2	8	395	Rha	Rha	
M706T20	19.53	705.5124	NA	8	363	Rha	Rha	
M707T21	21.31	707.1690	2	NA	NA	Rha	Rha	
M715T17	16.60	715.3608	NA	NA	NA		Rha	*Rha-Rha-C10-C12:1 [M+K]+
M717T17_3	17.14	717.3778	NA	NA	NA		Rha	Rha-Rha-C10-C12 [M+K]+
M723T21	21.31	723.1425	2	NA	NA	Rha	Rha	
M723T17	17.14	723.3905	NA	NA	NA	Rha	Rha	*Rha-Rha-C10-C12 [M+2Na-H]+
M724T18	18.43	724.4836	NA	NA	NA		Rha	*Rha-C10-C10+Na [2M+Na]+
M727T18	17.81	727.4236	2	102	296	Rha	Rha	
M729T18_2	18.42	729.4395	2	102	296	Rha	Rha	Rha-Rha-C12-C12
M734T22	22.22	733.5436	2	8	386	Rha	Rha	
M739T17_2	17.13	739.3643	NA	NA	NA		Rha	*Rha-Rha-C10-C12 [M+Na+K-H]+
M742T27_2	27.31	741.8747	2	NA	NA	Rha	Rha	
M745T18	18.43	745.4103	NA	NA	NA		Rha	*Rha-C12-C12 [M+K]+
M746T27	26.74	745.5948	2	8	427	Rha	Rha	
M751T18	18.43	751.4287	-1	12	345	Rha	Rha	Rha-Rha-C12-C12+Na
M771T27_2	27.36	770.8514	2	NA	NA	Rha	Rha	
M778T21	20.79	777.5705	2	8	385	Rha	Rha	
M785T17	17.14	785.3610	NA	NA	NA		Rha	*Rha-Rha-C10-C12 [M+K+NaCOOH]+
M790T26	26.47	789.6218	2	NA	NA	Rha	Rha	
M794T19	19.40	793.5648	-1	8	360	Rha	Rha	
M810T27	27.28	809.8621	2	NA	NA	Rha	Rha	
M818T23	22.71	817.6099	2	NA	NA	Rha	Rha	
M838T19	19.36	837.5907	2	NA	NA	Rha	Rha	
M878T27	27.26	877.8496	2	NA	NA	Rha	Rha	
M900T20	20.22	899.5067	2	8	373	Rha	Rha	
M940T21	21.39	939.5962	2	8	374	Rha	Rha	
M956T21_1	21.39	955.5691	2	8	400	Rha	Rha	
M956T21_2	20.91	955.5911	NA	8	379	Rha	Rha	
M1012T21	21.21	1011.6170	2	8	396	Rha	Rha	
M1028T21	21.21	1027.5910	2	8	397	Rha	Rha	
M1032T17_1	16.55	1031.6484	-1	NA	NA		Rha	*Rha-C10-C10 [2M+Na]+
M1038T17_1	17.16	1037.6087	NA	NA	NA		Rha	*Rha-Rha-C10-C12 [3M+H+K]
M1048T17	16.55	1047.6171	NA	NA	NA		Rha	*Rha-C10-C10 [2M+K]+
M1054T17	16.56	1053.6308	NA	NA	NA		Rha	*Rha-C10-C10+Na [2M+H]+
M1070T17	16.54	1069.5969	NA	NA	NA		Rha	*Rha-C10-C10 [2M+Na+K-H]+
M1076T17	16.56	1075.6125	NA	NA	NA		Rha	*Rha-C10-C10+Na [2M+Na]+
M1084T17	17.32	1083.6803	-1	87	323	Rha	Rha	*Rha-C10-C12:1+Na [2M+Na]
M1088T18_2	17.91	1087.7110	-1	94	298	Rha	Rha	
M1110T18	17.91	1109.6930	NA	NA	NA		Rha	*Rha-C10-C12:1+Na [2M+H]+
M1132T18	17.91	1131.6750	NA	NA	NA		Rha	*Rha-C10-C12:1+Na [2M+Na]+
M1200T23	23.10	1199.7740	2	8	409	Rha	Rha	
M1216T23	23.10	1215.7470	2	NA	NA	Rha	Rha	
M1302T16	15.81	1301.7841	NA	NA	NA		Rha	*Rha-Rha-C10-C10 [2M+H]+
M1324T16	15.81	1323.7656	NA	NA	NA		Rha	*Rha-Rha-C10-C10 [2M+Na]+

M1340T16	15.82	1339.7324	NA	NA	NA		Rha	*Rha-Rha-C10-C10 [2M+K]+
M1346T16	15.81	1345.7465	NA	NA	NA		Rha	*Rha-Rha-C10-C10 [2M+2Na-H]+
M1380T17	17.16	1379.8279	NA	NA	NA		Rha	*Rha-Rha-C10-C12 [2M+Na]+
M1396T17_1	17.15	1395.7937	NA	NA	NA		Rha	*Rha-Rha-C10-C12 [2M+K]+
M1402T17	17.15	1401.8099	NA	NA	NA		Rha	*Rha-Rha-C10-C12 [2M+2Na]+
M1418T17_1	17.15	1417.7770	NA	NA	NA		Rha	*Rha-Rha-C10-C12 [2M+Na+K-H]+
M527T1_2	1.28	527.1413	NA	NA	NA		UDP	*UDP-MurNAc-tripeptide
M598T5_1	5.41	597.6783	-1	20	102		UDP	*UDP-MurNAc-pentapeptide [M+2H]2+
M598T5_2	5.42	598.1800	NA	NA	NA		UDP	*UDP-MurNAc-pentapeptide [M+2H]2+
M599T5	5.41	598.6807	NA	NA	NA		UDP	*UDP-MurNAc-pentapeptide [M+2H]2+
M608T1	1.24	608.0884	NA	NA	NA	Nuc	UDP	UDP-GlcNAc
M609T5_1	5.43	608.6684	-1	20	103		UDP	*UDP-MurNAc-pentapeptide [M+H+Na]2+
M617T5_1	5.41	616.6519	-1	NA	NA		UDP	*UDP-MurNAc-pentapeptide [M+H+K]2+
M620T5_1	5.42	619.6595	NA	NA	NA		UDP	*UDP-MurNAc-pentapeptide [M+2Na]2+
M628T5	5.41	627.6416	-1	NA	NA		UDP	*UDP-MurNAc-pentapeptide [M+Na+K]2+
M630T1	1.21	630.0706	NA	NA	NA	Nuc	UDP	UDP-GlcNAc [M+Na]+
M636T5_1	5.42	635.6247	NA	NA	NA		UDP	*UDP-MurNAc-pentapeptide [M+2K]2+
M702T1	1.28	702.0879	NA	NA	NA		UDP	*UDP-MurNAc
M1194T5	5.41	1194.3492	-1	NA	NA		UDP	*UDP-MurNAc-pentapeptide
M1217T5	5.41	1217.3305	NA	NA	NA		UDP	*UDP-MurNAc-pentapeptide [M+H+Na]+
M106T1	1.12	106.0862	NA	NA	NA			*Diethanolamine
M142T1	1.18	142.0266	NA	NA	NA			*Ethanolamine phosphate
M151T1_1	1.12	150.9789	NA	NA	NA			*Phosphoenolpyruvate
M138T7_2	7.20	138.0661	-1	23	109			Anthranilate
M120T7	6.83	120.0445	-1	3	109			Anthranilate [M-H2O+H]+
M391T21_1	20.92	391.2845	NA	NA	NA			Bis(2-ethylhexyl)Phthalate
M413T21	20.92	413.2670	-1	107	219			Bis(2-ethylhexyl)Phthalate+Na
M332T8	7.98	332.1410	-1	NA	NA			Ciprofloxacin
M167T8	7.98	166.5742	NA	NA	NA			Ciprofloxacin [M+2H]2+
M111T17_1	17.14	111.0442	NA	NA	NA			Hydroquinone
M187T1_2	1.13	187.0004	NA	NA	NA			L-2-Phosphoglyceric acid
M185T1_neg	1.27	184.9858	NA	NA	NA			L-2-Phosphoglyceric acid (neg)
M209T1_1	1.18	208.9823	NA	NA	NA			L-2-Phosphoglyceric acid [M+Na]+
M169T1_1	1.18	168.9900	NA	NA	NA			L-2-Phosphoglyceric acid [M-H2O+H]+
M191T1_1	1.19	190.9718	NA	NA	NA			L-2-Phosphoglyceric acid [M-H2O+Na]+
M265T9	9.19	265.0698	-1	NA	NA			Lumichrome [M+Na]+
M245T7_2	7.25	245.1861	-1	NA	NA			NH-Dval(Nme)-Val-Ome
M123T2	1.94	123.0442	NA	NA	NA			Nicotinamide
M118T1	1.32	118.0859	NA	NA	NA			N-methyl-a-aminoisobutiric acid
M99T1_2	1.16	98.9843	-1	2	32			Phosphoric acid

ACKNOWLEDGEMENTS

CURRICULUM VITAE

Mariel Anel García Rivera

Personal information

Date of birth: 05.03.1989

Place of birth: Mexico City

Education

03/2016 – present	**Helmholtz-Zentrum für Infektionsforschung (HZI)** **PhD in Chemical Biology** Braunschweig, Germany

- Expertise: Mass spectrometry, detection of small molecules, metabolomics, chemometrics, Data Mining
- PhD Thesis: "Antibiotic uptake in *Pseudomonas aeruginosa* and its consequences on the metabolome"
- Supervisor: Prof. Dr. rer. nat. Mark Brönstrup (Leibniz Universität Hannover and HZI)

09/2013 – 10/2015	**École Polytechnique Fédérale de Lausanne (EPFL)** **M.Sc. in Chemical Engineering and Biotechnology** Lausanne, Switzerland

- Expertise: Biotechnology, Process Development, Green Chemistry
- Master thesis: "Investigation of an integrated separation-racemization process for the production of enantiomerically pure mandelic acid"
- Supervisors: Hon.-Prof. Albert Renken (EPFL), Prof. Dr.-Ing. Andreas Seidel-Morgenstern (Max-Plank-Institute für Dynamik komplexer technischer Systeme, Magdeburg)

09/2006 – 04/2012	**Universidad Autónoma Metropolitana (UAM),** **B.Sc. in Chemical Engineering** Mexico City, Mexico

- Expertise: Process Development, Quality Systems, Environmental sustainability
- Bachelor thesis: The effect of hydraulic variables on the adsorption of phenol on activated coal
- Supervisors: Prof. Alejandro León Galicia (UAM), Prof. Alethia Vázquez Morillas (UAM)